On the Assessment of Nonlinear Ship Motions and Loads

Proefschrift

ter verkrijging van de graad van doctor
aan de Technische Universiteit Delft,
op gezag van de Rector Magnificus prof. dr. ir. J.T. Fokkema,
voorzitter van het College voor Promoties,
in het openbaar te verdedigen op maandag 25 februari 2002 om 13.30 uur
door

Louis Willem PASTOOR

maritiem ingenieur,
geboren te Assen.

Dit proefschrift is goedgekeurd door de promotor:

Prof. dr. ir. J.A. Pinkster

Samenstelling promotiecommissie:

Rector Magnificus,	voorzitter
Prof. dr. ir. J.A. Pinkster	Technische Universiteit Delft, promotor
Dr. ir. J.A. Keuning	Technische Universiteit Delft, toegevoegd promotor
Prof. dr. C. Guedes Soares	Technical University Portugal
Prof. dr. J. Juncher-Jensen	Technical University of Denmark
Prof. ir. J. Klein Woud	Technische Universiteit Delft
Dr. ir. L.J.M. Adegeest	AMARCON, Norway
Ir. E.M. Krikke	Koninklijke Marine, Den Haag

Pastoor, Louis Willem

ISBN 90-9015401-9

Delft University of Technology
Faculty of Design, Engineering and Production
Ship Hydromechanics Laboratory
Mekelweg 2
2628 CD Delft
The Netherlands

Contents

Summary

The behaviour of ships in a seaway is an important subject as the motions and loads have a strong impact on the safety, economics and operational performance of a vessel. With ships having novel hullforms, sailing at higher speeds and with offshore structures moving into deep and harsh waters, the need for hydrodynamic load and seakeeping analyses becomes even more and more important. Moreover, as the importance of safety and reliability increases not only the need for accurate predictions of motions and loads becomes more important but also the prediction of response statistics and their assessment. Only then, statements can be made about issues like safety, risk and performance reliability. While nonlinear ship hydrodynamic programs have been developed in the past, in order to enhance the accuracy of ship response predictions, their practical application is still a difficult task. Linear prediction tools benefit from easy assessment techniques like the frequency domain and linear spectral analytical methods. Nonlinear time domain codes are time-consuming and do not have straight forward assessment techniques. Still the need for nonlinear assessment techniques is imminent as linear prediction tools are not reliable when it comes to advanced vessels, higher speeds and severe operational conditions. This study therefore aims at the development of prediction and especially assessment techniques for nonlinear ship motions and loads.

Extreme response conditioning has been studied as a practical technique to calculate nonlinear extreme responses efficiently. On the assumption that a linear model is an appropriate identifier of extreme events an irregular incident wave is conditioned such that a prescribed linear extreme response occurs at a prescribed timestep and with a prescribed response profile. This profile is the so-called 'most likely response profile' around large response amplitudes. Subsequently this short conditioned incident wave sequence is simulated with a nonlinear program and the corresponding nonlinear extreme response is obtained. Different mathematical models to predict this most likely profile around large amplitudes have been evaluated. Two models take account of the systematic association between amplitudes and periods but it was shown that the third, simplest, model performed best for the case of large amplitudes. An important extension of the response conditioning technique was formulated in order to calculate nonlinear amplitude or extreme probability functions. By conducting a short series of conditioned

simulations for different prescribed extreme responses a functional relationship is obtained between the linear and nonlinear response values. This relationship is used to transform the linear amplitude or extreme probability function to the nonlinear probability function. This means an enormous reduction in computation time especially when calculating the nonlinear extreme probability function. In addition the response conditioning technique was formulated for directional seas as well.

A second technique, which has been studied, is the modelling of nonlinear ship responses by nonlinear approximate Volterra models. By doing so, a nonlinear ship motion and load program is only used to identify the Volterra kernels, after which the Volterra model is used to calculate response statistics in any sea state given. The basis of the two nonlinear approximate Volterra models, is to replace the higher order transfer functions by zero-memory operators and a linear transfer function. Consequently some nonlinear behaviour is omitted but easy identification and simulation procedures are obtained. A validation of the identification and simulation of both models showed good results.

The integration of the response conditioning technique and the Volterra modelling in long-term assessment procedures for the calculation of extreme responses and seakeeping performance is presented. Moreover a new seakeeping performance assessment technique is presented. This reliability based seakeeping assessment consists of a mission simulation approach and a probabilistic modelling of response criteria. By simulating a specified mission a large number of times the seakeeping performance of all responses and their combined result is obtained as a probability function. This gives the opportunity to study the performance uncertainty and specify a mission seakeeping performance reliability interval. In addition sensitivity factors and performance correlation factors are obtained. The sensitivity factors describe the influence of the individual responses on the total performance variance while the correlation factors are a quantification of the performance degradation correlation between mutual responses.

Several numerical case studies for different ships and responses prove that the response conditioning technique is an accurate technique and offers large computational savings. The Volterra modelling technique is also very fast but is not as accurate as the response conditioning technique. It does offer promising possibilities when applied in the reliability based seakeeping performance assessment technique. This new seakeeping assessment is a powerful tool to assist in the design process and the operation of ships as it gives more information about the seakeeping performance and the response relations compared to traditional approaches.

Modeltests have been conducted with a divided frigate hullform to study the response conditioning technique more extensively. The conditioned incident waves could well be generated and the synchronisation of the transient wave profile with the moving model could well be tuned by a control mechanism of the carriage. A series of conditioned tests in severe conditions with large amounts of green water were conducted and could very

well predict the bending moment amplitude probability function derived from irregular tests. A comparison with other existing techniques shows that the extrapolation by fitting some mathematical function is a critical approach as the tail of the response probability function can wrongly be predicted. And it is this tail that is of great importance when it comes to safety and reliability. The great advantage of the response conditioning technique is that it calculates the actual behaviour in these severe conditions, which define the tail.

Nomenclature

Co-ordinate systems

$Ox_0y_0z_0$	right-handed earth fixed co-ordinate system
$Gxyz$	steady moving right-handed co-ordinate

Greek symbols

α	Weibull scale parameter
α_s	wave spectrum factor
α^2	sensitivity factor
α_3	skew
α_4	kurtosis
β	Weibull slope parameter
β_s	wave spectrum factor
δ	random number between 0 and 1
$\delta(t)$	delta function
ε	spectral bandwidth parameter
ε_j	phase angle j^{th} harmonic component
$\varepsilon(t)$	instantaneous phase angle
γ	Weibull lower limit
γ_s	wave spectrum peak enhancement factor
γ_{jk}	hydrostatic correction factor at forward speed
Γ	waterline around ship
$\phi(\bar{x})$	perturbation potential
$\phi(t)$	instantaneous phase
$\Phi(\ )$	standard Gaussian distribution

$\Phi(\bar{x})$	steady part of total velocity potential= double-body flow potential
$\varphi(\bar{x},t)$	unsteady part of total velocity potential
φ_0	incident wave potential
$\varphi_{1..6}$	radiation potential
φ_7	diffraction potential
$\eta(t)$	normalised sine transform of spectral density
λ_{jk}	damping at infinite frequency
μ	wave heading
μ_{jk}	added mass at infinite frequency
ν	spectral width parameter
Σ	covariance matrix
ρ	density
$\rho(\ )$	correlation coefficient/function
σ	standard deviation
$\sigma(\bar{x})$	source strength
τ	time variable
ω	wave frequency/frequency
ω_e	encounter frequency
$\tilde{\omega}$	instantaneous frequency
$\bar{\omega}=(p,q,r)$	rotational velocities around body-fixed axes
$\bar{\omega}_1$	mean spectral frequency
ω_p	wave spectral peak frequency
ω_{upper}	maximum wave spectral frequency
ξ	complex body motions
$\zeta(t)$	wave elevation
ζ_a	wave amplitude
$\zeta_r(t)$	relative wave elevation
$\Psi(\bar{x},t)$	total velocity potential
$Z(\omega)$	wave elevation

Roman symbols

a	MLP amplitude
$a(\tau)$	impulse response function
a_{jk}	added mass coefficient

A	amplitude for cosine part of irregular response
$A_{1,2,3}(\omega)$	1st,2nd,3rd order frequency transfer function
b_{jk}	damping coefficient
B	amplitude for sine part of irregular response
$\overline{B}$	3 internal hull girder moments
$B_{1,2,3,4,5}(\omega)$	1st,2nd,3rd,4th,5th order frequency transfer function
$B_{0,2}(\omega)$	second order mean value transfer function
$B_{0,4}(\omega)$	fourth order mean value transfer function
c_j	jth harmonic complex amplitude
$c(\tau)$	impulse response function
D_1	travel distance until MLER event
D_2	distance from wavemaker to MLER event
D_3	run-length of shortest waves for MLER wave
$f(\ )$	probability density function
F	force
$F(\ )$	cumulative distribution function
g	gravitational acceleration
$g(\ )$	extreme probability function
$G(\ )$	extreme cumulative distribution function
$G(\overline{x},\overline{p})$	Green's function
$G(\omega)$	double-sided spectral density function
h	waterdepth
$h(\tau)$	impulse response function
$h(\ )$	function
H_s	significant wave height
$H\{\ \}$	Hilbert transform
$H_1(\omega_1)$	1st order frequency transfer function
$H_2(\omega_1,\omega_2)$	2nd order frequency transfer function
$H_3(\omega_1,\omega_2,\omega_3)$	3rd order frequency transfer function
$H_0(\omega)$	frequency transfer function
i	$\sqrt{-1}$
I	3x3 inertia matrix
k	wave number

$K_{jk}(\tau)$	impulse response function
L_c	loading condition
m	3x3 mass matrix
m_{jk}	mass and inertia elements of 6x6 mass/inertia matrix
m_j	jth spectral moment for j=0,1,2,4
m_j	m-terms for j=1..6
$\overline{n}$	normal vector
$n_{1..6}$	generalised normal vector, $n_{1,2,3} = \overline{n}$, $n_{4,5,6} = \overline{r} \times \overline{n}$
p	probability of occurrence
$p(\overline{x},t)$	pressure
P	seakeeping performance
$Q(\ )$	exceedance probability function
$\overline{Q}$	3 internal hull girder forces
$R(t)$	envelope
$R_{xy}(\tau)$	covariance function
S	surface area
S_f	free surface panel sheet inside vessel
$S(\omega)$	one-sided spectral density function
t	time variable
T	time duration / vessel draft
T_z	zero-crossing wave period
T_2	zero-crossing period
$T_{lifetime}$	lifetime of vessel in seconds
ΔT	time delay
U	forward velocity
U_a	Voltage amplitude
U_{wind}	wind velocity
$\overline{v} = (u, v, w)$	translational velocities of CoG
v_{cr}	critical slamming relative velocity
V_s	ship's speed
w	response weigh factor
$y(t)$	response
$\overline{y}$	mean response
y_a	response amplitude
Y_a	prescribed conditioned extreme

$\overline{Y}_n$	expected extreme in n cycles
$Y(\omega)$	response

Abbreviations

ASW	Anti Submarine Warfare
CoC	Coefficient of Contribution
CoG	Centre of Gravity
CoV	Coefficient of Variation
COFEA	Coefficient Of Floatation Extreme Aft
DMLER	Directional Most Likely Extreme Response
EMLER	Extended Most Likely Extreme Response
FORM	First Order Reliability Method
HSDHF	High Speed Displacement Hullforms
IACS	International Association of Classification Societies
ITTC	International Towing Tank Committee
LCB	Longitudinal Centre of Buoyancy
LCF	Longitudinal Centre of Floatation
LRFD	Load and Resistance Factor Design
LT	Long-Term
MISO	Multiple Input Single Output
MLER	Most Likely Extreme Response
MLP	Most Likely Profile
SDOF	Single Degree Of Freedom
ST	Short-Term
TEU	Twenty foot Equivalent Unit

1 Introduction

For many centuries ocean going vessels have been of vital importance first for the search for new trade in combination with the discovery of the world and later for the development of worldwide trade and transport, peace keeping and peace enforcing. For the safe operation of a vessel, its cargo and crew and a good performance both economical and operational, the prediction of the dynamic behaviour of ships in waves has become an important aspect in the design and operation of ships. With an increasing emphasis on safety and reliability, the continuous improvement of hullforms and the desire to operate in harsh environments the need for improved seakeeping prediction and assessment techniques is imminent.

This chapter summarises the state-of-the-art in ship motion and load assessment procedures and investigates the needs from a discussion of today's design and operational developments. This discussion sets the background to formulate the objectives for the Ph.D. research. Finally the contents and outline of the thesis are presented.

1.1 On the assessment of ship dynamic behaviour in waves

Ocean waves induce motions and loads on ships and floating offshore structures. Several important issues can be identified, which are affected by the motions and loads.

- Safety
  The safety of ship, cargo and crew is a key aspect when designing ship structures and during the planning of vessel voyages and offshore operations. The waves induce large forces and moments on the ship, which the structure must withstand. Secondly the motions must not cause dangerous situations, in which cargo can be lost, personnel can be injured or ships can even capsize.
- Economy
  Wave induced motions can cause downtime of an offshore structure or a scheduled round-trip-time cannot be made thus the economics are directly affected.

- Operational performance
  Other ocean activities can suffer from wave induced motions as well but are not directly expressed in economical terms, for example the seakeeping performance of an oil recovery vessel. Another example is a navy vessel. Their performance depends very much on the joint performance of personnel and equipment. Both exhibit performance degradation due to motions.

One of the objectives during the design and operation of ships and offshore structures is thus to improve the motion behaviour and take the loads and motions into account in a proper and reliable way for a sound structural design and safe operations. In order to do so several steps are identified. First one needs an operational scenario, i.e. route, period of year, loading condition, type of mission or voyage, speed profile. Next the environmental conditions have to be known, of which a wave database is most important. A number of options are possible. One can include seasonal or wave directional information, one can use a site-specific established database or a world wide average. Then the dynamic behaviour of the ship is to be calculated for all combinations of operational and environmental conditions. Together with the formulation of motion and load criteria an assessment can be made taking into account all relevant probability functions for all the variables present.

A complete hydrodynamic assessment is thus a labour intensive process in which many aspects are still subject of discussion and research. Moreover many variables are uncertain and thus need to be modelled as such, which implies a reliability based calculation scheme. It is not the aim of this thesis to deal with all these different aspects in depth. To confine the thesis to a limited number of key research subjects the following paragraph investigates the needs from a discussion on today's design and operational developments in combination with a discussion of ship motion and load prediction methods.

1.2 Motivation and objectives for present research

Although conventional hullforms have been dominating the seas, ship designers have put emphasis on advanced hullforms and futuristic designs and a significant number have been built, see examples given by Schönknecht and Laue (1990). The last decade has shown that the innovation of ship types and hullforms has been significant as an increasing number of advanced hullforms have been built. Some examples will be discussed.

The ferry market has demonstrated a scale increase of fast planning and semi-planing monohulls, see for instance the Aquastrada class of vessels from Rodriquez, which range from 100 to 150 meters with speeds over 40 knots. Furthermore the catamaran and wave-piercing catamaran have become widely used as ferry vessels, see for instance the designs from the Australia based company Incat. Another example is the semi-SWATH

Stena HSS. Besides a scale increase these vessels are operated in severe environmental conditions, like the North Sea. Another aspect of these vessels is their high speed, which is of great importance for the motion behaviour in waves. Significant nonlinear behaviour can occur especially for planning and semi-planing vessels, see Keuning (1994). Slamming and resulting peak accelerations influence the comfort on-board, the safety of the crew and passengers and the sustained speed. Considering these examples improved motion and load prediction and assessment techniques are very much in demand.

A scale increase is also seen in the fleet of containerships. Currently vessels over 7000 TEU are being built while 6 years ago the maximum was 4500. And the prospect is to build vessels well over 10.000 TEU in the future. Additionally these vessels operate at speeds of 25 knots or more and with their large bow flare and overhanging stems nonlinearities in hull girder loads will be considerable. Secondly these vessels are torsional sensitive inducing large deflections. These cause problems with respect to the deck cargo lashings and the cargo hatches, which have a weight restriction and thus need to be designed with great care.

Though navies have studied advanced hullforms and novel concepts for many years the backbone of navies is still the monohull displacement ship. But advanced concepts are candidates to be put in service as future surface combatants. See for instance Kapsenberg and Brouwer (1998). They undertook a major monohull parameter study with large hullform changes. One promising hullform was later selected for modeltesting and showed significant nonlinear behaviour for basic motions even in moderate sea states. Another navy example is the trimaran concept, see for instance Andrews (2001) and Van Griethuyzen (2001). After several years of conceptual studies in the UK, a trimaran was built. This demonstrator, named *Triton*, was launched by the Royal Navy in 2000, see RINA (2000), and this type is promoted as the future surface combatant.

Another industry branch which demands improved motion and load predictions and assessments is the offshore industry. In the last decade the offshore industry has paid more interest in the development of marginal oil fields for which the FPSO concept is most suitable. Even harsh environments like the Northern North Sea or West of Scotland are not avoided, see for example the FPSO for the Schiehallion field, MacGregor et al (1999). As these vessels are operated in severe conditions, always in head waves and without the possibility of avoiding bad weather the need to investigate the hull girder loads is of great importance.

These examples clearly stress the need for improved hydrodynamic capabilities. Moreover with the high operational speeds, strong 3 dimensional shaped hull geometries and enormous shipsize increases, the limit of linear prediction tools has been exceeded. The application of nonlinear ship motion and load programs is therefore imminent. In the following a summary is therefore given of the present linear and nonlinear numerical capabilities for predicting ship motions and loads.

Theoretical models for the motions of a ship in a seaway

The study of the behaviour of ships in a seaway has been of interest for decades. Of key importance was the linear spectral description of waves and ship responses, see Weinblum and St. Denis (1950). By calculation of the behaviour in regular waves it was possible to predict the behaviour in an irregular sea. With the development of strip theory, see for instance Korvin-Kroukovsky (1957), Gerritsma and Beukelman (1964) or the formulation by Salvesen et al (1970), the motions and loads of a ship could be calculated and assessed. Today linear strip theory is still the workhorse in engineering practice. Main problems of the strip theory are the two dimensional approach and the inconsistent forward speed formulation. Furthermore it is rather difficult to calculate pressure distributions over a hull surface, which hampers the transfer of pressures to a FE model. In order to overcome this a three dimensional forward speed method is desired. In principal two approaches can be followed: either a free surface Green function or a Rankine program can be used.

First efforts to apply a free surface Green function were done by Chang (1977), Inglis and Price (1981) and Guevel and Bougis (1982). The calculation of the free surface Green function is a difficult numerical task but has the advantage that only panels on the hull surface are required. Less computationally difficult is a time-domain approach, see King et al (1988). Overall the conclusion on these 3D methods is that they give a mixed improvement over strip theory. Possibly, poor improvements are caused by not taking care of the complete m-terms. However Beck and Magee (1990) did include the full m-terms but did not report much improvement. But this conclusion is not consistent as they used a Wigley, which is very slender. By using the zero-forward speed Green function and forward speed formulations an intermediate approach can be followed. See for instance Beck and Løken (1989). They substituted the zero-forward speed potentials directly into formulations for hydrodynamic forces from Salvesen et al (1970). Mixed improvements were obtained. Adegeest (1995) added another approach. He calculated the added mass and damping per strip of panels using a zero-forward speed 3D free surface Green function method and used these coefficients in the formulations from Salvesen et al (1970). An important disadvantage of the Green function approach is the fact that only the Kelvin free surface condition can be accounted for. Hence the slenderness restriction for strip theory is still applied.

The second possibility is to apply a Rankine panel program. Panels are distributed over the hull and part of the free surface. Main advantage over a free surface Green function approach is a consistent forward speed formulation with a free surface boundary condition derived from a linearisation around the steady base-flow around the hull. Most popular is to use the double-body flow as base flow, see the SWAN code developed by Nakos (1990) or Van 't Veer (1998). This approach gives good results for slender ships at high speed and blunt ships at low speed. It was shown that significant improvements can thus be obtained over methods using the Kelvin free surface condition. Bunnik (1999)

developed a model based on a linearisation around the nonlinear steady waves and obtained improved results over double-body linearised results. Still these developments assume small wave and motion amplitudes. In severe weather conditions this assumption is not valid and a nonlinear modelling is required.

Introducing nonlinearities can be done in many ways, because different nonlinear sources are identified. First a distinction is made between viscous and non-viscous models. It is well-known that viscous effects are important for the roll motions of ship but it is generally neglected for other modes. For practical use, viscous ship motion calculations are not possible yet and not likely in the near future. Thus our attention is focussed on the nonlinear potential flow problem. The most important sources of nonlinear behaviour are the

- Equations of motion,
- Body boundary condition,
- Free surface boundary condition,
- Hull geometry.

As the motion angles are still rather small the linearised equations of motion can be used but it is more appropriate to use Euler equations of motion. The body boundary condition is to be satisfied on the instantaneous positions of the hull leading to the so-called *exact-body condition*. In severe seas the wave steepness becomes larger and thus the nonlinearities in the free surface boundary condition become important. With a varying wetted surface and 3 dimensionally shaped surfaces strong nonlinearities are introduced.

A first attempt to cope with the varying wetted surface is to estimate this wetted surface by the instantaneous position and orientation of the vessel in the undisturbed waves. The integration of the incident wave pressure over this wetted surface gives a nonlinear Froude-Krylov and restoring force. By keeping the radiation and diffraction forces linearly dependent on the wave amplitudes a practical nonlinear program is obtained. Assuming that the incident waves and body motions are large but the radiated and diffracted waves are small the so-called weak-scatterer approach is obtained. Thus the incident waves may be steep and nonlinearities may be present, while the ship generated disturbances are linearised about the large amplitude motions and incident wave field. The final step is to solve the full nonlinear potential flow program.

The same subdivision, as for the linear programs, is seen for the nonlinear programs, i.e. strip theory, free surface Green function and Rankine panel programs. In addition mixed formulations are present. These utilise a Rankine panel formulation for the near field and a free surface Green function for the far field, which are matched at an intersection boundary.

One of the first successful attempts to calculate nonlinear motions and loads was presented by Jensen and Pedersen (1979). They formulated a second order frequency domain model based on the ordinary strip theory. They even modelled second order

Stokes' waves. This approach was applied to a variety of problems, like extreme bending moments, see Jensen and Pedersen (1981), wave-induced hull vibrations, Jensen and Dogliani (1995) and ship hull fatigue analyses, Jensen (1990). Satisfactory to good results are obtained with this method but for extreme situations the quadratic approach gives underestimated results as higher orders become more important. Widely applied are the time domain nonlinear strip theory programs see for instance, Fujino and Yoon (1986), Petersen and Marnæs (1989). An example, which is widely used to study the nonlinear roll behaviour of ships is the FREDYN program, see McTaggart and De Kat (2000).

Lin and Yue (1990) presented a nonlinear program using the free surface Green function. The original program satisfied the linearised free surface condition on the incident wave surface while the hydrodynamic and hydrostatic pressure were integrated over the instantaneous wetted surface as defined by the incident waves. The exact body boundary condition was used. The program was called LAMP (Large Amplitude Motion Program) and was later subdivided into a number of different versions, see Lin et al (1994).

The Rankine panel code SWAN, as developed by Nakos (1990), was extended to the time domain, see Nakos et al (1993). Later Kring et al (1996) added nonlinear Froude-Krylov and restoring forces. From 1996 this SWAN version was further developed at DNV and renamed WASIM, where it was made robust for the application in daily engineering practice, see Adegeest (2000) for a list of references. The weak-scatterer hypothesis was first introduced by Pawlowski (1992) and later implemented as a further extension of the SWAN code by Huang (1997). The final step is to satisfy the nonlinear free surface condition. Examples of this are shown, among others, by Beck et al(1993), Wang et al (1996) and Scorpio (1997). The regridding of the domain is computationally very expensive as influence coefficients need to be calculated every time step. Scorpio (1997) applies therefore a multi-pole accelerated approach. Distant influences may be accumulated into expansions before evaluation on a field or collocation point. Another effort to reduce the computation time of boundary integral equations are presented by Korsmeyer et al (1999). They utilise a so-called 'pre-corrected FFT' method. The near and far influence are computed separately by different algorithms. The summation of all influences is written in a convolution form, which allows the use of the Fast Fourier Transform. Large computational savings are obtained.

Besides difficulties like numerical stability, dispersion and damping more difficulties arise with advanced numerical programs. Fully nonlinear potential codes cannot cope with wave breaking, thus the simulation will stop if it occurs. Special care has to be taken if it occurs. Furthermore, the actual application to realistic ship dynamic problems requires more phenomena to be modelled correctly, issues like slamming, green water, anti-rolling fins and steering and control. Some can be accounted for in a modular way. For example, slamming can be added as a post-process calculation, see for instance Weems (1998).

For the practical application of nonlinear programs several issues are of importance. First of all the degree of mathematical modelling to adopt depends very much on the problem to be investigated. But additional aspects are of great importance as well. The computational costs should be limited, the program should be robust and should be well verified. In the light of these issues the application of fully nonlinear potential codes in the design phase of ships and offshore structures is not yet practical. Forward speed 3D programs with nonlinear Froude-Krylov and restoring forces are mature and practical applicable. Good examples are the WASIM and LAMP code, which have developed to mature programs with additional features covering issues like slamming, steering and anti-rolling fins. Still their computational costs are quite demanding especially when compared to the easy linear frequency domain techniques.

But even having a robust nonlinear program at one's disposal the assessment of an advanced hullforms or severe environmental conditions is not a straight forward procedure. The next section therefore discusses assessment strategies for two main subjects, i.e. global hull girder loads and seakeeping performance.

Hull girder loads for structural design

Traditionally the Rules from Classification Societies have been used to establish design values for the midship vertical hull girder bending moment. These Rules are simple formulas based on an empirical approach. Many problems are encountered in order to formulate rational design requirements. Guedes Soares (1996) discusses several aspects, which are of importance when formulating design rules. He states that even when following a direct calculation approach significant uncertainties have to be dealt with, i.e. uncertainties in the wave climate, the choice of theory to calculate transfer functions, the influence of nonlinearity and the effect of speed. Class Societies often adopt the North Atlantic as design wave climate, but Guedes Soares and Moan (1991) and Bitner-Gregersen et al (1995) showed that different trading routes can give significant different long-term response distributions. But even if a specific operational envelope is formulated it remains difficult to deal with the uncertainties of the wave databases. When different wave data sources are used for the same ocean area considerable different results can be obtained, see for instance Guedes Soares and Trovão (1991). Studies to compare linear prediction codes have demonstrated that large differences in long-term design values can be obtained, see Nitta et al (1992), illustrating the uncertainty of the prediction models. Moreover simple formulas to account for nonlinearity are utilised, but the IACS revision of 1993 does not even incorporate parameters like speed and ship length. As speed is an important parameter a well-defined probabilistic model is required to describe the voluntary and involuntary speed reductions as well as course changing.

Thus we can conclude that Rule based design values are easy and cheap to apply but are based on the experience with conventional ships. For novel concepts, new operational profiles and an increasing demand for safety and reliability the extrapolation of experience and Rule based design is critical or even impossible. Direct calculations and

or in combination with modeltesting is therefore required although there are lot of uncertainties, as discussed above, which have to be considered. Still the trend towards direct calculations and safe structural design is an ongoing process at Class Societies, see for instance Liu (1992) or Adegeest (2000).

Hull girder loads can become significantly nonlinear, even for conventional vessels, despite the fact that the basic motions are well predicted by linear theory. The use of a nonlinear approach to calculate hull girder loads is thus broadly required and not only for advanced vessels. The first problem is how accurate is the nonlinear code. A comparison of some programs was conducted by Watanabe and Guedes Soares (1999). Considerable differences were shown especially when elasticity was modelled in the calculations. But having adopted a nonlinear code how to establish loads for structural design? In fact a reliability approach taking account of the stochastic nature of the loads and the ultimate hull girder capacity is most appropriate, see for instance Friis-Hansen (1995). This implies that the lifetime distribution of the extreme hull girder load should be calculated, but that is a computationally intensive assignment. Simplifying the case is not only tempting but inevitable. The ISSC special committee, Jensen et al (2000), on extreme hull girder loading also stated that "it becomes very important to define reasonable critical wave episodes" and "it might be beneficial to introduce more advanced hydrodynamic procedures in the design calculations". Jensen and Pedersen (1979) presented a nonlinear frequency domain approach thus keeping computational costs low but this model is of second order only. One can use techniques to reduce the amount of calculations. For example one can omit those sea states which hardly contribute to the extreme loads, see for instance Larsen and Passano (1991). The lifetime expected extreme is calculated in a linear approach. Next the contribution from all sea states to the exceedance probability for this lifetime extreme is calculated. Thus the sensitivity of the short-term sea states is determined and thus only a small area of a scatter diagram is obtained, which is to be assessed with a nonlinear procedure. Sagli (2000) applied this approach and studied the vertical bending moments in the S-175 containership and concluded that the scatter diagram could be reduced to one sea state with an error of 10% in the expected lifetime extreme. By including 9 sea states the error was only 2%. Adegeest (1995) introduced a third order approximate Volterra model to simulate ship responses. This model is computationally very fast thus reducing computer time drastically. Only limited nonlinear computations are required to solve the Volterra model. Another approach is not to reduce the amount of calculations but conduct them in a linear frequency domain approach but with a nonlinear correction procedure, see for instance Guedes Soares and Schellin (1996). In order to drastically reduce the amount of nonlinear calculations one can rely on single design loads. A simple approach is to establish these by calculating expected extremes in a design storm or to use regular design waves. A more advanced method is proposed by Winterstein et al (1993). They used an inverse FORM to establish environmental contour lines which corresponds to certain probabilities of occurrence, e.g. the 100-year value. The great advantage is that the environmental conditions are decoupled from the response model. But this is also a critical aspect as the largest response does not necessarily have to occur in one of the conditions on the contour line

but within the this area. Torhaug (1996) studied several approaches to calculate extreme responses efficiently. By selecting only those wave histories, which differ not too much from their theoretical statistical properties, a few of these "design seastate histories" are used in a nonlinear simulation. Adegeest et al (1998) presented a technique to determine short wave trains, which induce prescribed most likely linear extreme response sequences. By simulating this wave train in a nonlinear program the corresponding nonlinear most likely extreme is obtained.

But to rely on single design loads is a critical or unreliable approach because these values do not give any information on the tail of the probability function. And it is this tail that overlaps with the tail of the capacity and thus defines the safety. Consequently a short nonlinear simulation with a fit technique is also disputable as this might not be sufficient to define the extreme probability function. Only in case the shape of the tail is known a priori a characteristic value is sufficient to apply in a LRFD approach. But calibrated LRFD methods are not yet available for ships. Consequently, the need to calculate the full extreme probability distribution is required and this enlarges the computational costs of a nonlinear assessment drastically. Thus the need for advanced techniques to reduce computational costs is indispensable, with the important precondition that the tail of the extreme probability function is actually calculated instead of estimated or fitted.

Seakeeping performance

Seakeeping performance is of importance in commercial shipping but it is even more important for the mission capability of navy vessels. Many seakeeping assessment studies are therefore dedicated to navy ships. The seakeeping performance assessment can be subdivided in different levels and different predictions methods are available.

The first motion prediction level is *designer's knowledge*, like the beneficial influence of a large waterplane coefficient for displacement type frigates. The first computational level are regression based programs. Based on systematic modeltest series prediction programs have been developed. For example based on the HSDHF series, Blok and Beukelman (1984), powering and seakeeping regression programs were developed at the MARIN. The next levels are direct computational programs ranging from linear strip theory to full nonlinear potential and beyond.

With regard to the assessment procedure different levels are identified as well. Starting with the evaluation of basic motions to derived quantities like relative motions or response statistics to full operability assessments. The ultimate assessment is to add an optimisation loop.

To illustrate this discussion the following figure is drawn. Three axes are shown listing prediction methods, assessment techniques and ship concepts with, more or less, increasing order of advancedness. From the previous discussion on today's ship concepts and needs we conclude that there is a desire to assess the operability of advanced

hullforms with nonlinear programs, but there's still a gap. A lot of attention is paid to the further development of the *Methods* axis with significant progress being made but the application of these tools for advanced ships is still not explored satisfactorily.

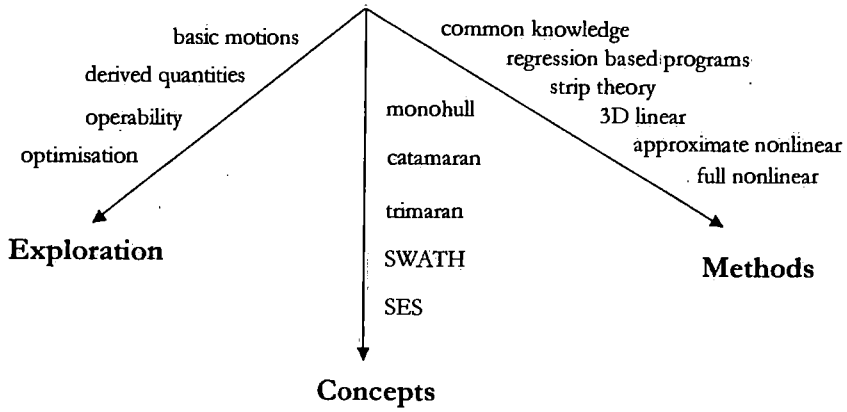

Figure 1 Seakeeping assessment levels

Our desire is thus to assess the seakeeping performance in a nonlinear way. But first a discussion is given on the operability or seakeeping performance assessment. When the operability or seakeeping performance is of interest we need to define first what is precisely meant by these terms. Operability or seakeeping performance is the ability of a ship to perform its mission or successfully carry out its voyage in a given wave environment. Different approaches have been presented in the past. A classical paper was presented by Bales (1980). He introduced a rank estimator based on an analysis of 20 hullforms. This rank estimator is a function of underwater coefficients and dimensionless particulars. But the most common approach is to use a linear ship motion program to calculate the response transfer functions. Together with a wave database the response characteristics can be calculated. Comparison of these values with response criteria define the operability of a response or system. Examples of this approach are given among others by Dallinga (1992) and McTaggart and Graham (1993). Further developments of the seakeeping performance assessment technique are mainly focussed on the integration in a design tool, see for instance Keane and Sandberg (1984) or Friits et al (1990) but these do not improve or alter the seakeeping calculation procedure but merely introduce a multi-level approach and an overall hydrodynamic assessment including resistance and propulsion, manoeuvring etcetera.

Among others, Lin et al (1994) and Kapsenberg and Brouwer (1998) concluded that advanced vessels can exhibit nonlinear behaviour even in moderate sea states. Thus the

need for a nonlinear seakeeping performance assessment is clear. But this is far from practical as the amount of nonlinear simulations to be conducted is too large, especially in a preliminary design phase where several hullforms are candidates and are to be assessed and in later design stages re-assessed.

With regard to the linear spectral seakeeping performance assessment approach several aspects are disputable. First of all, the seakeeping performance is in essence a stochastic variable, like hull girder loads, but it is not treated like that, instead the focus is on the expected value. The second aspect deals with the treatment of the response criteria. Without hesitation these are modelled as hard-clipped systems: either the system is available or not. But that is a rather crude approach, since the performance degradation due to motions is a gradual process. Additionally there is no general agreement on the absolute value of the criteria thus it would be more appropriate to model this uncertainty by specifying a criterion with an uncertainty distribution. The third aspect deals with the question how to use the results of a seakeeping performance assessment in the design process? If the performance is modelled as a stochastic variable the sensitivity due to all relevant responses can be quantified as well as the mutual correlations. By quantifying sensitivity factors and the mutual correlations, more information becomes available to support design decisions. Additionally the design of warship is increasingly relying on Simulation Based Design tools, see Wolf (2000). A mission simulation approach to assess the seakeeping performance fits this design approach well.

Problem definition and research objectives

The previous sections focussed on the issues of ship concepts, motion and load prediction methods and the assessment of hull girder loads and the seakeeping performance. Novel ship concepts have been built and severe environmental conditions are not avoided. This stresses the need for improved motion and load prediction and assessment techniques with emphasis on the application of a nonlinear approach. In the last decades nonlinear ship motion programs have been developed and robust versions are available. Still these demand considerable computer time. A straight forward application of nonlinear time domain codes is thus not practically feasible if a long-term assessment is required. An intelligent approach to apply these tools is thus required. Hull girder loads exhibit significant nonlinearities even for conventional ships. This subject deals with the question of structural safety, which implies that preferably the probability distribution of extreme hull girder loads is required. The conclusion is thus that the knowledge of expected extremes is not sufficient. This means that existing efficient procedures to calculate nonlinear extreme response statistics are not appropriate. The first question of this thesis is thus formulated as,

How to calculate nonlinear extreme response probability distributions in a practical way without large computational costs?

The second subject of interest in this thesis is the seakeeping performance. For many ships basic motions remain dominantly linear responses but advanced vessels can exhibit significant nonlinear behaviour even in moderate sea states. This demands a nonlinear seakeeping performance assessment procedure but following the standard approach is again hampered due to large computational costs. Thus the second question of the thesis reads as,

How to calculate the seakeeping performance with nonlinear modelling of the responses without large computational costs?

In the previous section some doubts were expressed regarding the standard procedure to calculate the seakeeping performance. First of all the seakeeping performance should be treated as a stochastic variable. Secondly, motion criteria are not hard-clipped systems but should account for gradual performance degradation and the procedure should quantify sensitivities and mutual correlations of the various responses and the total performance. The third question to answer in this thesis is thus,

How to formulate a seakeeping performance assessment procedure with stochastic treatment of the performance and taking account of gradual performance degradation?

Based on these questions the objectives of the thesis have been formulated. The first two questions demand the development of advanced techniques to calculate nonlinear ship response statistics efficiently and accurately. Secondly these techniques should be evaluated on their merits and it should be discussed how to implement these in existing assessment strategies for extreme hull girder loads and seakeeping performance. The third objective is to develop a seakeeping performance assessment method with stochastic treatment of the performance. This new approach should account for gradual performance degradation. The characteristics of this new method should be investigated and the differences with a standard approach should be presented.

As most of the analyses will be based on numerical case-studies a model experimental program is to be carried out for accurate and reliable validation.

How these objectives have been approached and how that is reflected in the present thesis is described in the next paragraph.

1.3 Contents and outline of the thesis

To reduce the computational effort in order to obtain nonlinear response statistics two techniques have been studied, developed and evaluated. The first method is described in chapter 1. This technique is based on the conditioning of an incident irregular wave train such that it induces a prescribed linear extreme response. First ideas and efforts were presented by Adegeest et al (1998) based on the work of Tromans et al (1991). By

simulating this short wave sequence in a nonlinear program the corresponding nonlinear extreme is obtained. Of key importance in this procedure is the prediction of the *Most Likely Profile* of the response around the linear extreme response. Three mathematical models are presented and evaluated. Both the accuracy of these models as well as the specific influence of the systematic association of amplitudes and periods is studied. In addition an extension to this technique is derived, which gives the opportunity to predict the full nonlinear amplitude or nonlinear extreme probability function based on a few short conditioned simulations. A second extension was formulated for the case of directional seas.

A second technique, to reduce computational efforts, is the approximate Volterra modelling technique, see Bendat (1990) and Adegeest (1995). In chapter 1 the general third order Volterra model is described together with two approximate models of 3rd and 5th order respectively. Both the identification process and the simulation of these models are described.

How the two techniques can be embedded in long-term assessments is discussed in chapter 1. Secondly the third objective is dealt with in this chapter. A reliability based seakeeping performance assessment is developed. Key elements of this approach are a probabilistic formulation of response criteria, a mission simulation approach and a reliability based post-processing of the mission simulation data.

The evaluation of the response conditioning technique and the Volterra modelling technique are the subjects for chapter 1. First the accuracy of the response conditioning technique and its extensions are investigated by two extensive case-studies. One concerns the vertical bending moment in a FPSO in head waves on the North Sea while the second concerns the vertical bending moment in a frigate in head waves sailing at 18 knots. For the FPSO 200 nonlinear simulations were conducted to obtain 200 hours of irregular data, while the frigate was simulated 100 times to get 100 hours. These datasets were used to investigate the extreme response and its stochastic nature. Furthermore an example is given of the application of the response conditioning technique for directional seas.

The Volterra modelling technique is investigated in-depth both on the identification side as well as the simulation accuracy. Stability, uniqueness and accuracy are criteria used to assess both approximate Volterra models. One the two models has subsequently be used in a reliability based seakeeping assessment of a navy frigate on a simplified Anti-Submarine Warfare mission. With this case the characteristics of this new seakeeping assessment technique are explored.

As the numerical cases of chapter 1 showed good and in some cases very good results a model experimental program should further verify the accuracy of the response conditioning technique. Moreover the feasibility as a test technique could be studied. Thus chapter 1 describes model experiments with a divided frigate to study the vertical

hull girder bending moments in head waves. A technique to generate response conditioned waves is described. These waves are to have prescribed profiles and should occur at a predefined position in the tank. A preliminary test program investigated the feasibility of this procedure. Regular wave experiments are described and the measured transfer functions are compared with linear predictions. Next, irregular wave experiments were carried out to obtain sufficient statistical information on the bending moment response. Subsequently response conditioned experiments are described and used to predict the nonlinear amplitude probability function. Two sea states were tested. In addition some extra analyses were conducted of the measurements and other existing techniques to calculate nonlinear response statistics were applied and the results were compared with the data.

The thesis ends with conclusions and recommendations for future research.

For the numerical case-studies a nonlinear program was required. As the focus of this thesis is on the application of nonlinear ship motion and loads programs the details of this and the development of a linear pre-process calculations are described in appendix A.

2 Time conditioning of ship responses

Considerable portions of an irregular sea state do not provide any information on the behaviour of a ship in extreme events. Nevertheless experiments and numerical simulations are often carried out for irregular seas to get extreme response statistics. In order to reduce the computational and experimental costs and to enhance accuracy it would be an interesting option to limit this effort by only simulating or testing the extreme events in a sea state with the preservation of probabilistic information. Based on this idea a response conditioning technique is presented in this chapter.

The basic principle of extreme response conditioning is to predict the incident wave, which induces a prescribed linear extreme response and use this in a short nonlinear simulation to obtain the nonlinear extreme. Thus the assumption is that the linear model is a good identifier for extreme events, which means that the nonlinear extreme is a correction of the linear extreme.

Of course many incident wave sequences can be constructed which induce a prescribed response, but in the present model the most likely profile is used. This aspect is dealt with in the first paragraph where three mathematical models are presented and evaluated for the most likely profile around large response amplitudes. Having established this it can be applied for the extreme response conditioning technique. The first objective for this technique is to calculate nonlinear expected extremes, which is described in the second paragraph. For the determination of nonlinear extreme or amplitude probability functions an extension of the response conditioning technique is proposed in the third paragraph. A special variation of the response conditioning technique is developed in the last paragraph where wave spreading is accounted for instead of a uni-directional sea.

2.1 Theoretical models for the most likely profile in time around a large response amplitude

A large response amplitude can occur in many response sequences. Upon averaging these sequences one obtains the most likely profile around this large amplitude. The objective of this paragraph is to get a formulation for the most likely profile without this time series averaging process. Consider the response sequence $y(t)$, which has a large amplitude at some time-step. The problem to solve is now to predict the most likely response value some small time-step τ away from the crest. With the probabilistic information of the response and the definition of conditional probabilities this can be solved. Three models are derived subsequently. Two have been presented in literature previously and a new model is given.

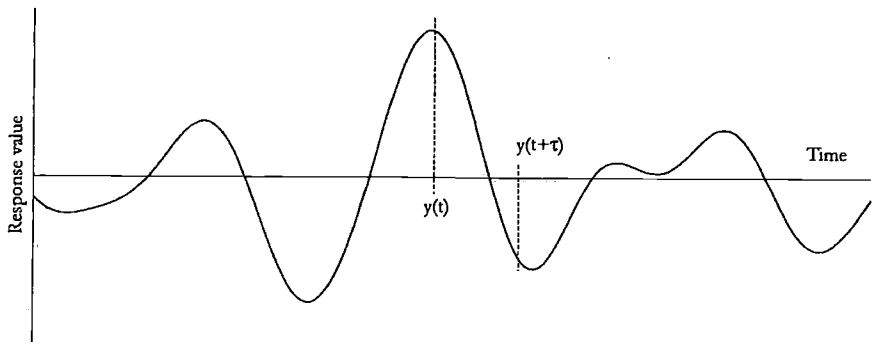

Figure 2 Ship response as a function of time

Tromans et al model

The first application of this technique was used to construct the most likely extreme storm wave of a given wave spectrum, see Tromans et al (1991). This most likely storm wave was used as a design wave for fixed offshore platforms. A short description of the model is given.

Consider an irregular response process $y(t)$ to be Gaussian distributed with zero mean and with variance σ_y^2. The response process is continuous in time and differentiable. Next a crest is assumed to occur at timestep t. In that case the time derivative of the response is zero. To formulate the most likely profile around a crest or trough the following conditional expectation has to be solved for,

$$E\left[y(t+\tau)\middle|y(t)=Y_a,\dot{y}(t)=0\right] \tag{2.1}$$

The conditional probability density function is derived in order to derive the formulation for the variance for the most likely profile as well.

$$f\left(y(t+\tau)\middle|y(t)=Y_a,\dot{y}(t)=0\right)=\frac{f\left(y(t+\tau),y(t),\dot{y}(t)\right)}{f\left(y(t),\dot{y}(t)\right)} \tag{2.2}$$

Because $y(t)$ and $\dot{y}(t)$ are both Gaussian distributed the two joint probability density functions are multi-variate Gaussian distributions and the resulting conditional distribution is then a Gaussian distribution as well,

$$f\left(y(t+\tau)\middle|\dot{y}(t),\ddot{y}(t)\right)=\frac{1}{\sigma\sqrt{2\pi}}e^{\frac{\left[y(t+\tau)-\rho(\tau)y(t)\right]^2}{2\sigma^2}} \tag{2.3}$$

where $\rho(\tau)$ is the autocorrelation function and the mean and variance are given by,

$$\begin{aligned}
&E\left[y(t+\tau)\middle|y(t)=Y_a,\dot{y}(t)=0\right]=Y_a\rho(\tau)\\
&E\left[\left[y(t+\tau)-Y_a\rho(\tau)\right]^2\middle|y(t)=Y_a,\dot{y}(t)=0\right]=\sigma_y^2\left(1-\rho^2(\tau)-\dot{\rho}^2(\tau)\frac{m_0}{m_1}\right)
\end{aligned} \tag{2.4}$$

Hence this derivation shows that the most likely profile around a crest or trough is simply the autocorrelation function scaled by the crest or trough value. Two important conclusions can be drawn from this result. First, the shape of the most likely profile is independent of the height of the crest. Secondly, the variance is also independent of the crest value, which means that the coefficient of variation becomes smaller for larger crests. This means that the larger the conditional amplitude the more accurate this formulation is, because the relative error becomes smaller.

Friis-Hansen & Nielsen model

The first conclusion of the above derivation is not in accordance with what is seen by the observation of ocean waves. It is well known that waves with large amplitudes tend to have long periods. This systematic association should preferably be taken into account in the formulation. Following this reasoning, Friis-Hansen and Nielsen (1996) proposed another solution to the same initial condition given by equation (2.1). They described the response process by an envelope process,

$$y(t) = R(t)\cos\phi(t) = R(t)\cos\left(\bar{\omega}_1 t + \varepsilon(t)\right) \tag{2.5}$$

with the envelope described by,

$$R(t) = \sqrt{y^2(t) + \hat{y}^2(t)} \tag{2.6}$$

where $\hat{y}(t)$ is the Hilbert transform of $y(t)$. Now a conditional probability density function is proposed as,

$$f\left(y(t+\tau)\middle|y(t), \hat{y}(t), \dot{y}(t), \dot{\hat{y}}(t)\right) = \frac{f\left(y(t+\tau), y(t), \dot{y}(t), \hat{y}(t), \dot{\hat{y}}(t)\right)}{f\left(y(t), \dot{y}(t), \hat{y}(t), \dot{\hat{y}}(t)\right)} \tag{2.7}$$

The Hilbert transforms of the $y(t)$ and $\dot{y}(t)$ read as,

$$\begin{aligned} H\{y(t)\} &= H\{R(t)\cos\phi(t)\} = R(t)\sin\phi(t) \\ H\{\dot{y}(t)\} &= H\{\dot{R}(t)\cos\phi(t) - R(t)\dot{\phi}(t)\sin\phi(t)\} = \dot{R}(t)\sin\phi(t) + R(t)\dot{\phi}(t)\cos\phi(t) \end{aligned} \tag{2.8}$$

and both are Gaussian distributed and hence the conditional distribution of equation (2.7) is a Gaussian distribution. On the condition of a crest at time-step t, conditions can be prescribed. From the derivation of the first model it is known that,

$$\begin{aligned} y(t) &= R(t) = Y_a \\ \dot{y}(t) &= \dot{R}(t) = 0 \end{aligned} \tag{2.9}$$

From this the conditions for the Hilbert transforms can be deduced as,

$$\begin{aligned} \hat{y}(t) &= 0 \\ \dot{\hat{y}}(t) &= R(t)\dot{\phi}(t) = Y_a\bar{\omega} \end{aligned} \tag{2.10}$$

Here an instantaneous frequency is introduced as the time derivative of the instantaneous phase,

$$\bar{\omega} = \dot{\phi}(t) \tag{2.11}$$

With these conditions, substituted in equation (2.7), the following prediction for the most likely profile around a crest is found,

$$E\left[y(t+\tau)\middle|y(t)=Y_a,\hat{y}(t)=0,\dot{y}(t)=0,\hat{\dot{y}}(t)=Y_a\tilde{\omega}\right]=$$
$$=\frac{Y_a}{m_0m_2-m_1^2}\int_0^\infty\left[(m_2-\omega m_1)-\tilde{\omega}(m_1-\omega m_0)\right]S_{yy}(\omega)\cos\omega\tau d\omega \tag{2.12}$$

While the variance reads as,

$$E\left[\left(y(t+\tau)-E\left[y(t+\tau)\middle|\ldots\right]^2\right)\middle|y(t)=Y_a,\hat{y}(t)=0,\dot{y}(t)=0,\hat{\dot{y}}(t)=Y_a\tilde{\omega}\right]=$$
$$=\frac{m_0}{m_0m_2-m_1^2}\left[-m_1^2+m_0m_2\left(1-\eta^2-\rho^2\right)+2m_0m_1\left(\eta\dot{\rho}+\dot{\eta}\rho\right)-m_0^2\left(\dot{\eta}^2+\dot{\rho}^2\right)\right] \tag{2.13}$$

With $\rho=\rho(\tau)$ and $\eta=\eta(\tau)$ given by,

$$\rho(\tau)=\frac{1}{m_0}\int_0^\infty S_{yy}(\omega)\cos\omega\tau d\omega$$
$$\eta(\tau)=\frac{1}{m_0}\int_0^\infty S_{yy}(\omega)\sin\omega\tau d\omega \tag{2.14}$$

When substituting the mean spectral frequency, $\bar{\omega}_1$, as an estimate of the instantaneous frequency the resulting most likely profile is equal to the result of equation (2.4).

Pastoor model

A third model for the most likely profile around a crest can be derived by conditioning on the second time derivative of the response as well, thus more information of the spectral bandwidth is used, as will be shown later. This model was published by Pastoor (2000A) and is subsequently described.

The conditional probability density function to be calculated is given by,

$$f\left(y(t+\tau)\middle|y(t),\dot{y}(t),\ddot{y}(t)\right)=\frac{f\left(y(t+\tau),y(t),\dot{y}(t),\ddot{y}(t)\right)}{f\left(y(t),\dot{y}(t),\ddot{y}(t)\right)} \tag{2.15}$$

This conditional probability function is a Gaussian distribution of which the most likely profile can be derived. In order to solve this function, three conditions have to be specified. For the elevation and the first derivative these are the same as previously given.

For the second derivative it is assumed that the response is sinusoidal shaped in the vicinity of the crest. The conditions are then formulated as,

$$\begin{aligned} y(t) &= Y_a \\ \dot{y}(t) &= 0 \\ \ddot{y}(t) &= -Y_a\tilde{\omega}^2 \end{aligned} \tag{2.16}$$

The same condition for the second derivative is obtained after differentiating the envelope process twice. Thus this condition is in accordance with the previous formulation (2.10).

The resulting most likely profile around a crest is then given by,

$$E\left[y(t+\tau)\middle|y(t)=Y_a,\dot{y}(t)=0,\ddot{y}(t)=-Y_a\tilde{\omega}^2\right]= \frac{Y_a\left(\rho(\tau)m_0m_4+\ddot{\rho}(\tau)m_0m_2-\tilde{\omega}^2\left(\rho(\tau)m_0m_2+\ddot{\rho}(\tau)m_0^2\right)\right)}{m_0m_4-m_2^2} \tag{2.17}$$

The variance of the conditional probability distribution is then,

$$E\left[\left(y(t+\tau)-E\left[y(t+\tau)\middle|\ldots\right]\right)^2\middle|y(t)=Y_a,\dot{y}(t)=0,\ddot{y}(t)=-Y_a\tilde{\omega}^2\right]= \frac{m_0}{m_2\left(m_0m_4-m_2^2\right)}\left[m_2m_4-m_2^3-m_0m_2m_4\rho^2-2m_0m_2^2\rho\ddot{\rho}-m_0^2m_4\dot{\rho}^2+m_0m_2^2\dot{\rho}^2-m_0^2m_2\ddot{\rho}^2\right] \tag{2.18}$$

For this model again the instantaneous frequency has to be specified. If the zero-upcrossing period is chosen,

$$\tilde{\omega}=\sqrt{\frac{m_2}{m_0}} \tag{2.19}$$

the first model, the Tromans formulation, is obtained again, as given by equation (2.4).

Joint distribution of wave period and amplitude

For the last two models an estimate of the instantaneous frequency is required. Many have addressed the problem of the joint distribution of wave amplitudes and period. See for instance Longuet-Higgins (1975), Longuet-Higgins (1983), Cavanié et al (1976) and

Lindgren and Rychlik (1983). Several studies compared these mathematical models with observed data and with parametric models, see for instance Srokosz and Challenor (1987), Sobey (1992), Myrhaug and Kvalsvold (1992) and Myrhaug and Rue (1998). One study, Tayfun (1993), studies the specific case of large amplitudes, which is most important for the present case. Tayfun (1993) proposed a simple formula for the mean zero-crossing period of large wave heights. Numerical simulations were carried out to verify this. The expected wave frequency for large wave heights is thus formulated as,

$$\tilde{\omega} = \frac{\omega_1}{1+\nu^2\left(1+\nu^2\right)^{-3/2}} \qquad \text{with} \quad \nu = \sqrt{\frac{m_0 m_2}{m_1^2} - 1} \tag{2.20}$$

Discretisation of the models

For the application of the three mathematical models it is of importance to obtain discretised formulations. Moreover the models are to be applied to ship responses for which we need to calculate with the encounter frequency, ω_e, instead of the wave frequency, ω. Use is made of the following formulations in order to discretise the theoretical models.

$$\begin{aligned} S_{yy}(\omega)d\omega &= \frac{1}{2}y_{a,j}^2 \\ \rho(\tau) &= \frac{1}{m_0}\int_0^\infty S_{yy}(\omega_e)\cos\omega_e\tau\, d\omega_e = \frac{1}{2m_0}\sum_{j=1}^{N} y_{a,j}^2\cos\omega_{e,j}\tau \\ \eta(\tau) &= \frac{1}{m_0}\int_0^\infty S_{yy}(\omega_e)\sin\omega_e\tau\, d\omega_e = \frac{1}{2m_0}\sum_{j=1}^{N} y_{a,j}^2\sin\omega_{e,j}\tau \end{aligned} \tag{2.21}$$

Moreover the spectral moments can be calculated using to the following equality,

$$\begin{aligned} S_{yy}(\omega)d\omega &= S_{yy}(\omega_e)d\omega_e \\ m_j &= \int_0^\infty \omega_e^j S_{yy}(\omega_e)d\omega_e = \int_0^\infty \omega_e^j S_{yy}(\omega)d\omega \end{aligned} \tag{2.22}$$

Tromans model:

$$y_{MLP}(t) = \frac{Y_a}{2m_0}\sum_{j=1}^{N} y_{a,j}^2\cos\omega_{e,j}t \tag{2.23}$$

Friis-Hansen & Nielsen model:

$$y_{MLP}(t)=\frac{Y_a}{2\left(m_0m_2-m_1^2\right)}\sum_{j=1}^{N}y_{a,j}^2\left[\left(m_2-\omega_{e,j}m_1\right)+\tilde{\omega}\left(\omega_{e,j}m_0-m_1\right)\right]\cos\omega_{e,j}t \quad (2.24)$$

Pastoor model:

$$y_{MLP}(t)=\frac{Y_a}{2\left(m_0m_4-m_2^2\right)}\sum_{j=1}^{N}\left[\left(m_4-\omega_{e,j}^2m_2\right)+\tilde{\omega}^2\left(\omega_{e,j}^2m_0-m_2\right)\right]y_{a,j}^2\cos\omega_{e,j}t \quad (2.25)$$

2.2 Evaluation of presented models

In order to evaluate the three models, as presented previously, a numerical study is conducted. Three sea states are modelled and long irregular simulations were carried out to deduce the average profile around large crests. These are compared with the three mathematical predictions. All sea states were modelled by the Modified Pierson-Moskowitz wave spectrum. The wave spectral zero-crossing periods and the frequency boundaries are described in Table 1. The last mathematical model described above needs fourth spectral moments, but this spectral integration is not convergent for the Pierson-Moskowitz spectrum. Several authors have discussed this issue. Medina et al (1985) recommended an approximate upper frequency limit of 4.4 [rad/s]. They based this conclusion on the measurement of spectra and spectral model accuracy. This upper limit can be formulated as a function of the spectral peak frequency,

$$\omega_{upper}=k_u\cdot\omega_p \quad (2.26)$$

When modelling the peak frequency as a function of wind speed,

$$\omega_p=\left(\frac{0.74}{1.25}\right)^{\frac{1}{4}}\frac{g}{U_{wind}} \quad (2.27)$$

the values of k_u range from 3.2 to 10.5 for windspeeds of 12 and 40 knots respectively. These values are in agreement with results from Bishop and Price (1978), who obtained experimentally values for k_u of 3.0 to 9.0. Based on these considerations Wang and Crouch (1993) proposed a maximum value of 10.0. In the present case this limit value was applied for the sea state with the largest period, 12 [s], and leads to the upper limit of 3.7 [rad/s].

T_z [s]	Frequency interval [rad/s]	Simulation time [hrs]
4.0	0.1 - 3.7	100
8.0	0.1 - 3.7	100
12.0	0.1 - 3.7	100

Table 1 Sea state properties

The irregular waves are formulated by a summation of regular wave components.

$$\zeta(t) = \sum_{j=1}^{N} \zeta_{a,j} \cos\left(\omega_j t + \varepsilon_j\right)$$

with

$N = 800$ (2.28)

Non-equidistant frequency intervals were used to circumvent repetition of the signal. These intervals were calculated by weighing the wave spectral density. The phase angles are randomly chosen between 0 and 2π.

For the 50%, 10% and 1% largest wave amplitudes the average profiles around the crests were derived. This variation in threshold value gives the possibility to study the profile shape in the limit case, namely the average profile around extreme amplitudes. For every crest the wave profile before and after the crest was normalised by the crest value. Thus if we write the wave sequence around a crest as $\zeta_j(t)$ and $t_{crest,j}$ is the timestep at which the crest occurs, the average profile and the variance are defined by,

$$\bar{\zeta}(t) = \frac{1}{N}\sum_{j=1}^{N} \frac{\zeta_j(t)}{\zeta_j(t_{crest})} \qquad \sigma_{\bar{\zeta}}^2(t) = \frac{1}{N}\sum_{j=1}^{N}\left(\frac{\zeta_j(t)}{\zeta_j(t_{crest})} - \bar{\zeta}(t)\right)^2$$

with

$N =$ *number of crests* (2.29)

From Figure 3 to Figure 8 the average wave profiles and the mathematical models are presented for the three wave spectra. For all the three spectra the shape of the average profiles is very much the same. Secondly the difference between the average profile around the 50% and 1% largest crests is small. The predictions by the Friis-Hansen-Nielsen model and the Pastoor model use the Tayfun formula, equation (2.20) for the instantaneous frequency. The models are compared with the average profile around the largest 1% crests. From these figure we can see that the Tromans model is closest to the 1% curve while the Friis-Hansen-Nielsen and Pastoor model are close together.

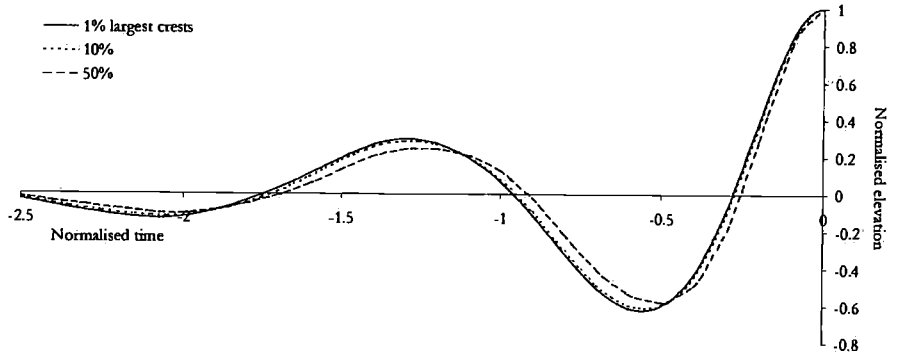

Figure 3 Mean profiles around wave crests Tz=4.0 [s]

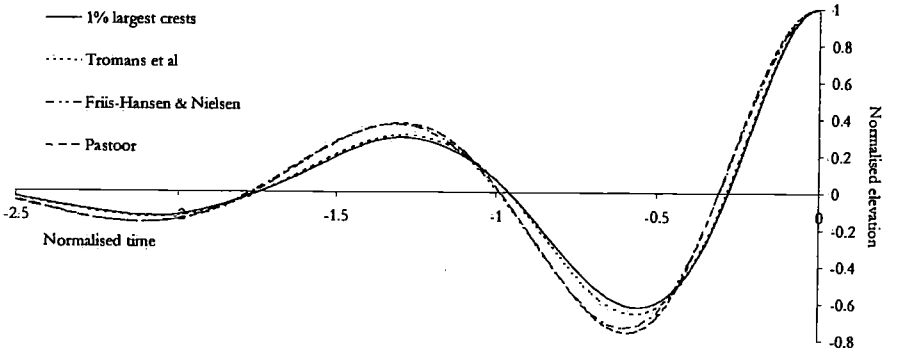

Figure 4 Mathematical models Tz=4.0

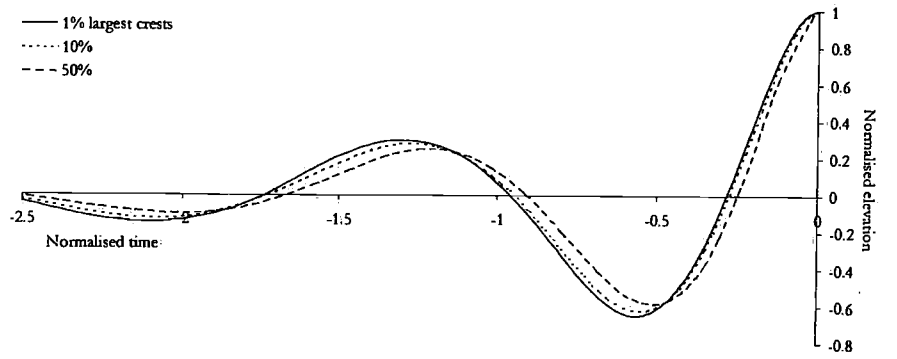

Figure 5 Mean profiles around wave crests Tz=8.0 [s]

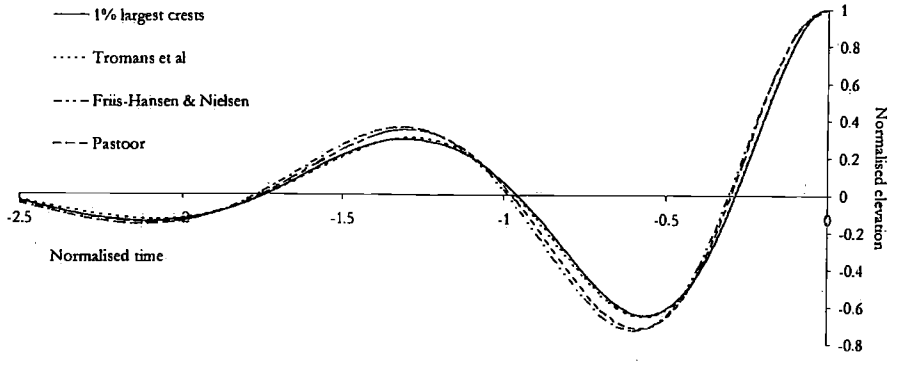

Figure 6 Mathematical models Tz=8.0 [s]

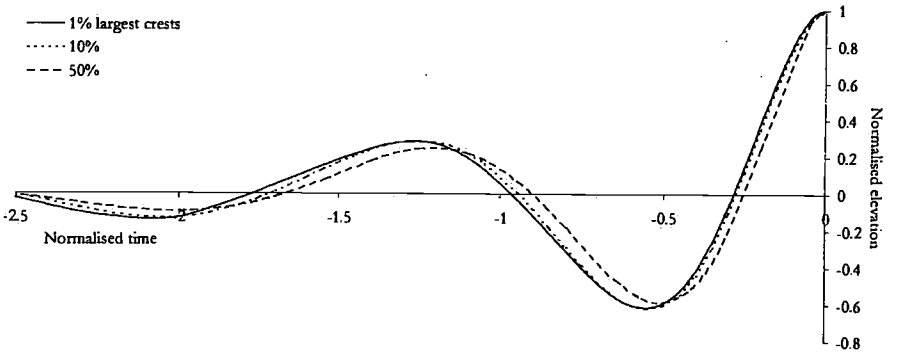

Figure 7 Mean profiles around wave crests Tz=12.0 [s]

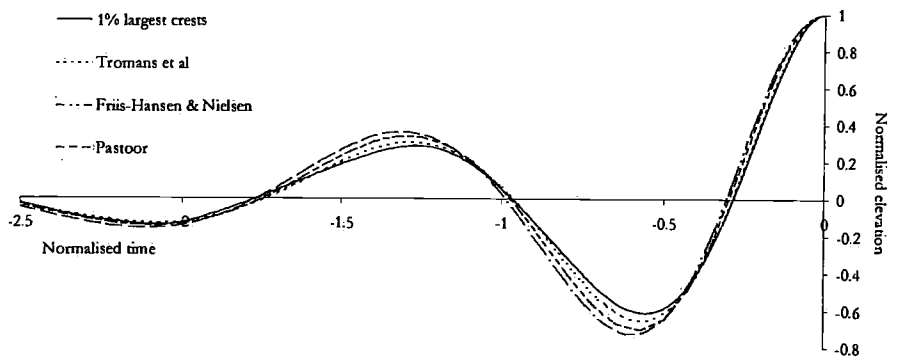

Figure 8 Mathematical models Tz=12.0 [s]

The curves with the standard deviations are again very similar for all three hence only the standard deviation for the spectrum with T_z=4.0 [s] is shown in Figure 9. The conclusion from this plot is that the uncertainty in the most likely profile shape is decreasing for larger crests.

The reliability of the calculated average profiles is investigated in a simple manner by calculating the 95% confidence interval using the calculated standard deviations.

$$\bar{\zeta}_{95\%}(t) = \bar{\zeta}(t) \pm k \cdot \frac{\sigma_{\bar{\zeta}}(t)}{\sqrt{N}} \qquad (2.30)$$

with $k = 1.96$

As the average profile for the 1% largest crests of the spectrum with a period of 12 [s] has the smallest number of crests this curve was used to calculate the 95% confidence interval. Figure 10 shows that the accuracy of the determined average profile is good. Of course the calculated standard deviation was used but it is not likely that this would change the curves significantly.

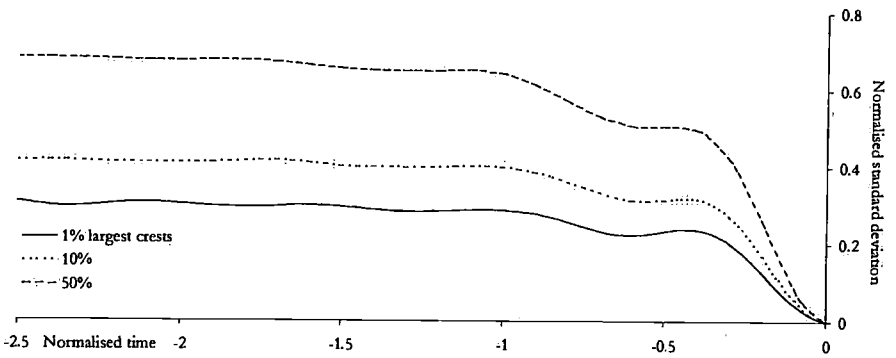

Figure 9 Standard deviation of mean profile around wave crests Tz=4.0 [s]

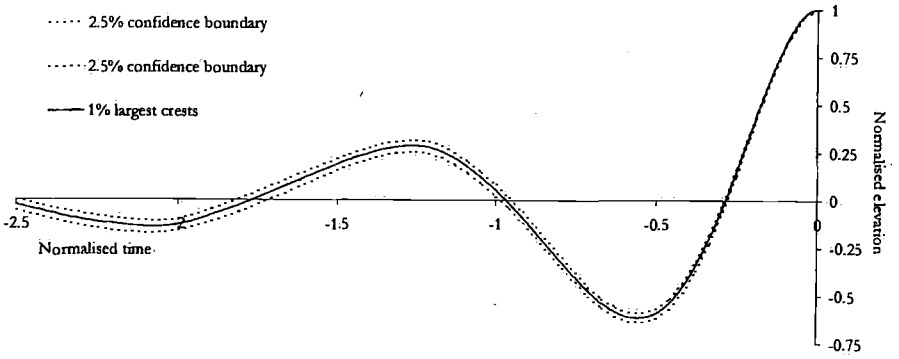

Figure 10 Confidence limit for mean profile around wave crests Tz=12.0 [s]

Envelope process

The previous analysis showed that both models with frequency dependency, the Friis-Hansen and Nielsen model and the Pastoor model, do not give improvements over the Tromans model. To study the instantaneous frequency in more detail an irregular wave is written as an envelope process.

$$\zeta(t) = \sum_{j=1}^{N} \zeta_{a,j} \cos\left(\omega_j t + \varepsilon_j\right) = R(t)\cos\phi(t)$$

with (2.31)

$$R(t)^2 = \sum_{j=1}^{N}\sum_{k=1}^{N} \zeta_{a,j}\zeta_{a,k} \cos\left(\left(\omega_j - \omega_k\right)t + \left(\varepsilon_j - \varepsilon_k\right)\right)$$

The instantaneous frequency is formulated as the time derivative of the phase angle as given by equation (2.11). For the Tromans formulation this model was applied and the instantaneous frequency was deduced. The following figure shows the instantaneous frequency for the spectrum with a period of 8.0 [s]. As can be seen the instantaneous frequency changes significantly over a short time period. When plotting the Tayfun approximation it is concluded that this formula does give a good estimate of the period around large crests as it is a good average of the instantaneous frequency around the crest.

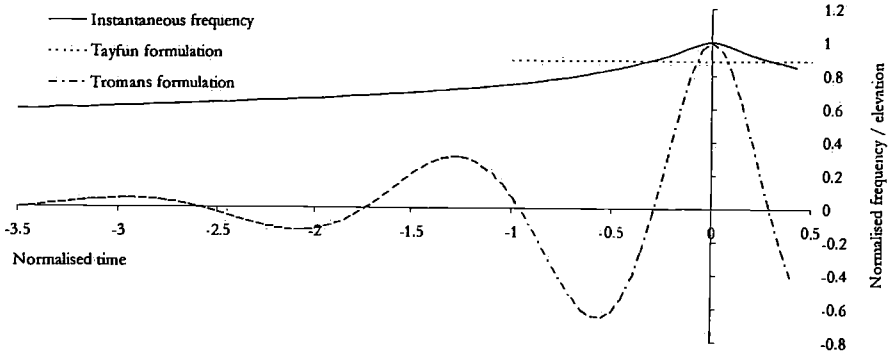

Figure 11 Instantaneous frequency of Tromans formulation

Two-peak spectrum

The three test spectra did not give significantly different results. The difference in spectral broadness was small. In order to investigate this aspect, a two-peak spectrum is tested as well. Two single wave spectra were simply summed together to obtain one two-peak spectrum. These were again of the modified Pierson-Moskowitz type with equal significant wave height and with a zero-crossing period of 5.0 [s] and 10.0 [s] respectively. The spectral shape of their summed result is pictured in the figure below.

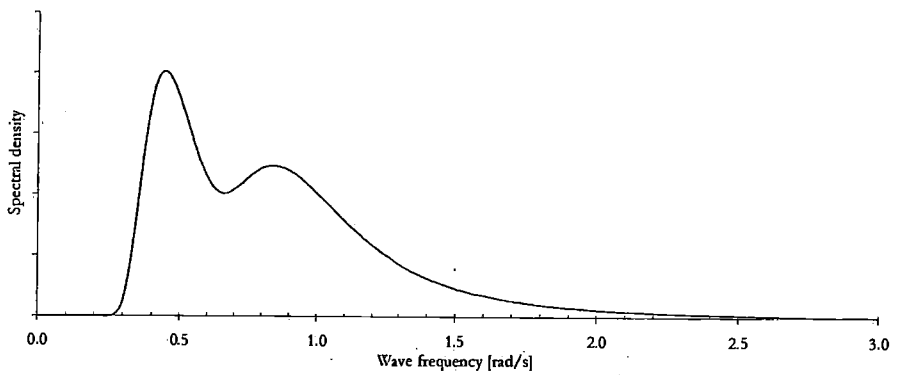

Figure 12 Two-peak wave spectrum

For this two peak spectrum a large simulation was conducted and the average profile around the 1% largest crests was derived. This is plotted together with the Tromans model for this spectrum and shown in the following figure. The Tromans model fits the data curve very well. Clearly is seen that the shape is considerably different compared to the mean profiles of the previous three spectra.

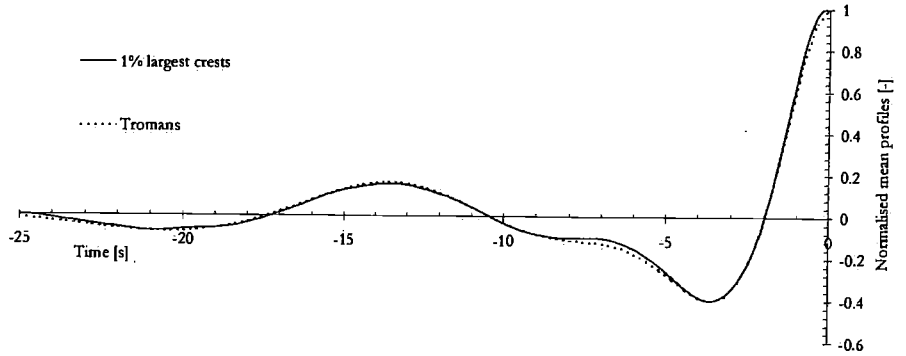

Figure 13 Mean profile around 1% largest crests for two-peak wave spectrum

Qualitative discussion on the mean profile around extremes

From the evaluation of the three models the Tromans model seems to be the best. It is most easy to apply and is accurate. This numerical evaluation study confirms thus the conclusions from Jonathan et al (1994). They analysed offshore wave measurements at the northern North Sea and concluded that the most probable shape for an extreme crest or trough is close to the correlation function for surface elevation. The most common way to deal with linear irregular waves is to sum harmonic components. A simple approach of modelling large crests is to let these harmonic components get into equal phase. But when the wave components are in-phase, extremely large crests are obtained, which do not have realistic occurrence probabilities. Secondly, no sound probabilistic formulation is used as basis for constructing these large waves. When comparing the Tromans wave with the wave with all harmonic components in-phase we get Figure 14.

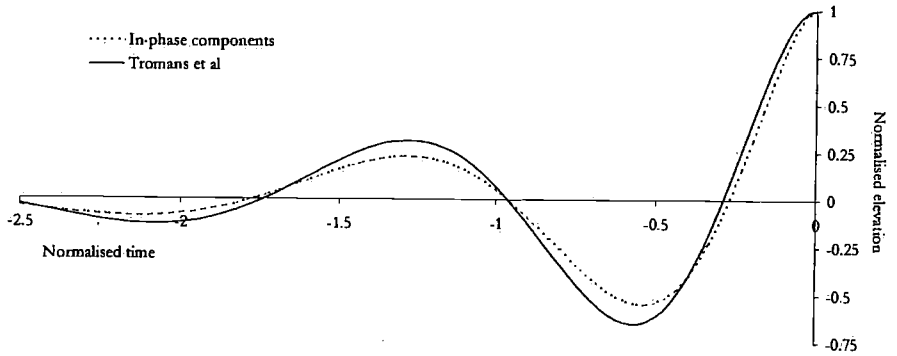

Figure 14 Comparison of in-phase wave components and Tromans et al

The two profiles are not the same and because the Tromans formulation gives good agreement with the numerical cases and offshore measurements it is concluded as being most accurate.

The paragraph is dedicated to the formulation of the most likely profile around a crest. If the variance of the profile shape is of interest or importance, another approach is necessary. One simple way to do so is to simulate linear time series and deduce large responses which are more or less equal to the desired value. By adjusting the wave phase angles the sequence can be reformulated such that the response value occurs after a arbitrary chosen time period. Another way is to fit the most likely profile into an irregular response sequence. This approach was presented by Taylor (1995). Select randomly a time-step from an irregular sequence. Subtract the most likely profile scaled by the response value in order to get a zero response value. Subtract then the slope of the most likely profile scaled by the slope at the selected time-step and finally add the most likely profile scaled by the desired response amplitude. In this way the profile in the vicinity of the crest looks very similar to the most likely profile and differs more away from the crest.

Too steep waves can easily be generated using one of the three models as the profile is simply scaled with a desired amplitude. A steepness check of the profile is therefore required. In case of too steep waves the Friis-Hansen or Pastoor model can be of use as a larger instantaneous period can be prescribed.

2.3 Response time conditioning: Most Likely Extreme Response (MLER)

The first application of conditioned waves was to calculate design loads for fixed offshore platforms, Tromans et al (1991). This design wave was conditioned on the expected largest wave amplitude, as the largest wave causes the largest load on a fixed platform. As presented above, Taylor et al (1995), applied the method in a slightly different way. They embedded the profile in a random sequence. Thus for every realisation a slightly different inswing was obtained. Upon conducting this procedure many times, sufficient data was obtained to get an estimate the extreme probability distribution. The same approach was followed by Harland et al (1996) to investigate the application to real problems. They showed that the probability distribution of extreme loads on fixed structures can be determined in this way and that the number of conditioned wave amplitudes and the number of simulations play a dominant role in both accuracy and simulation time. A further step in the application of the conditioned simulations was presented by Adegeest et al (1998). When dealing with floating structures the largest wave does not necessarily induce the largest load or response. Thus Adegeest et al (1998) formulated a conditioned response sequence for a given extreme response and calculated subsequently the incident wave causing this specific profile. By simulating this conditioned wave with a nonlinear program the corresponding nonlinear

extreme response is obtained. Examples were shown for the wave bending moment in a supply vessel and the relative wave motion on the side of the aft working deck. Adegeest et al (1998) compared this technique with other procedures and presented very good results.

Based on the approach of Adegeest (1998) a consistent formulation is given in this paragraph with one of the three models of the previous paragraph as predictor for the most likely profile around a large response amplitude. The formulation here is applicable to any combination of wave heading and forward speed.

Consider a linear ship response to an irregular uni-directional sea. The time domain response can then be written by,

$$y(t) = \sum_{j=1}^{N} \left| H_{y\zeta}(\omega_j) \right| \zeta_{a,j} \cos\left(\omega_{e,j} t + \varepsilon_{\zeta,j} + \varepsilon_{y\zeta,j}\right) \tag{2.32}$$

The three models for the most likely profile around a large response amplitude have been discretised and all are written in the following way,

$$y_{MLP}(t) = Y_a \sum_{j=1}^{N} a_j \cos \omega_{e,j} t \tag{2.33}$$

In order to force the extreme event at a desired time-step a time delay is introduced, ΔT . Phase angles are then defined by,

$$\varepsilon_{\Delta T,j} = -\Delta T \omega_{e,j} \tag{2.34}$$

and the most likely profile becomes,

$$y_{MLP}(t) = Y_a \sum_{j=1}^{N} a_j \cos\left(\omega_{e,j} t + \varepsilon_{\Delta T,j}\right) \tag{2.35}$$

By equating equation (2.32) and (2.35), the unknown incident wave amplitudes $\zeta_{a,j}$ and wave phase angles $\varepsilon_{\zeta,j}$ can be determined.

$$\zeta_{a,j} = \frac{Y_a a_j}{\left| H_{y\zeta}(\omega_j) \right|} \qquad \varepsilon_{\zeta,j} = \varepsilon_{\Delta T,j} - \varepsilon_{y\zeta,j} \tag{2.36}$$

Before applying these wave amplitudes and phases, the spatial wave should be evaluated on the steepness. There is no restriction embedded in the above formulations to generate too steep waves.

Most likely nonlinear extreme

If $f(y_a)$ is the amplitude probability density function of a response and $F(y_a)$ its cumulative distribution function, the cumulative distribution function of the extreme value to occur in n response cycles is,

$$\Pr\{y_a < Y_n\} = F(Y_n)^n = G(Y_n) \tag{2.37}$$

This formulation is valid under the assumption that the amplitudes are statistically independent. By differentiation the extreme response probability density function becomes,

$$g(Y_n) = n f(Y_n) F(Y_n)^{n-1} \tag{2.38}$$

With this result the expected extreme to occur in a specified time duration can be calculated. Commonly the *modal value approach* is used. This approach defines the extreme value as the value corresponding with the peak of the extreme response probability density function. This peak is defined by,

$$\frac{\partial g(Y_n)}{\partial Y_n} = 0 \tag{2.39}$$

For sufficiently large values this results in,

$$1 - F(Y_n) \approx \frac{1}{n} \tag{2.40}$$

The amplitudes of a stationary zero-mean Gaussian distributed response process are described by the Rice distribution, see Rice (1944,1945) and Cartwright and Longuet-Higgins (1956).

$$f(y_a) = \frac{\varepsilon}{\sqrt{2\pi m_0}} e^{-\frac{y_a^2}{2\varepsilon^2 m_0}} + \sqrt{1-\varepsilon^2}\,\frac{y_a}{m_0} e^{-\frac{y_a^2}{2m_0}} \cdot \Phi\left(\frac{\sqrt{1-\varepsilon^2}}{\varepsilon}\frac{y_a}{\sqrt{m_0}}\right)$$
$$\text{with } \Phi(u) = \frac{1}{\sqrt{2\pi}} \int_{-\infty}^{u} e^{-\frac{u^2}{2}} du \tag{2.41}$$

In case of a narrow-band response spectrum, $\varepsilon \to 0$, the amplitudes are Rayleigh distributed.

$$f(y_a) = \frac{y_a}{m_0} e^{-\frac{y_a^2}{2m_0}} \tag{2.42}$$

In general this function can be used for wave induced ship responses, especially when studying large amplitudes. Substitution of this probability function in equation (2.40) results in the so-called *Most Probable Maximum*,

$$\bar{Y}_n = \sqrt{2m_0 \ln(n)} \tag{2.43}$$

If the extreme probability density function $g(Y_n)$ is only slightly skewed this value is a good prediction of the expected extreme. If a more accurate value is required a *mean value approach* is required, given by the following integration,

$$\bar{Y}_n = \int_0^\infty y_a g(y_a) dy_a \tag{2.44}$$

An approximate formula is, see Barltrop (1991),

$$\bar{Y}_n = \sqrt{2m_0 \ln(n)} + \frac{0.5772\sqrt{m_0}}{\sqrt{2\ln(n)}} - \frac{\left(\pi^2/6 + 0.5772^2\right)\sqrt{m_0}}{2\left(2\ln(n)\right)^{3/2}} \tag{2.45}$$

Generally this *mean value* prediction of the most likely extreme response in a prescribed period of time is only a few percent larger than the *most probable maximum* for 1000 to1500 crests.

By prescribing one of these most likely extreme values in equation (2.36) the resulting wave amplitudes and phase angles can be used in a nonlinear simulation. A nonlinear simulation slightly longer than the time delay, ΔT, gives the corresponding most likely nonlinear extreme value. The basic assumption of this approach is that the nonlinear extreme is a correction of the linear extreme. Thus the linear model should be an appropriate identifier of extreme events.

Discussion

In case of following or stern quartering waves equal encounter frequencies can occur for different wave frequencies. This aspect poses no problem for the above technique by using the fundamental equality,

$$\frac{1}{2} y_{a,j}^2 = S_{rr}\left(\omega_{e,j}\right) d\omega_e = S_{rr}\left(\omega_j\right) d\omega \tag{2.46}$$

Thus the response spectrum on the basis of wave frequencies is used to calculate a series of response amplitudes. This also defines the wave frequencies for which the wave amplitudes and phases are determined from equation (2.36). Moreover this equality simplifies the calculation of response spectral moments.

What are the main advantages of this technique? Three important reasons can be given.

- the full wave spectrum is used,
- the full response transfer function is used,
- the inswing dynamics into the extreme event are incorporated,
- the method is computationally extremely fast.

The most important question to answer is how well does the method perform in comparison with other techniques? In chapter 1 this question is dealt with for different cases.

Is the linear model a good identifier of extreme responses? In many cases it is probably a good estimator but some responses are very strong or entirely nonlinear dominated responses. For example large horizontal amplitudes of a moored structure due to second order low frequency drift forces can never be calculated with this approach as this is fully second order dominated.

A problem that can occur is that too steep waves are generated. By simply calculating the response conditioned wave in the time domain and calculating the steepnesses this aspect can be checked. If too steep waves are obtained the Friis-Hansen and Nielsen or Pastoor model can be used with a sufficient large instantaneous frequency or the wave spectrum can be given a larger period.

If the uncertainty in the extreme profile is to be taken into account the number of simulations becomes significantly larger. One approach can be to derive extreme response profiles from linear simulations. Suppose the expected extreme in a 3-hours sea state is of interest. After a linear simulation of 3 hours the maximum responses in that period and the timestep at which it occurred are determined. The wave profile can be conditioned such that the extreme occurs after a prescribed time duration, T_{delay}, e.g. 30 [s]. When the timestep of the extreme event is given by $t_{\max}$ the conditioned wave amplitudes and frequencies are equal to the ones of the irregular simulation and the conditioned phases are calculated from the following equality,

$$\varepsilon'_{\zeta,j} = \omega_j \left(t_{\max} - T_{delay}\right) + \varepsilon_{\zeta,j} \tag{2.47}$$

An estimate of the extreme response probability function is obtained by conducting this procedure a number of times. Consequently the expected extreme is known as well.

2.4 Extended Most Likely Extreme Response (EMLER)

When the expected extreme is of interest the procedure as outlined above is applicable. But when the probability function of nonlinear amplitudes or nonlinear extremes is required an extended version of the MLER procedure can to be used. The basic idea of the MLER procedure is that a nonlinear large response amplitude is calculated as a correction of a linear large response. Consequently one can apply this procedure several times for different large linear response amplitudes. This results in a functional relationship between linear and nonlinear large amplitudes.

$$y_{a,nl} = h\left(y_{a,l}\right) \tag{2.48}$$

In the following figure a Rayleigh probability density function and an extreme probability function are sketched. A series of conditioned simulations are depicted by dotted lines.

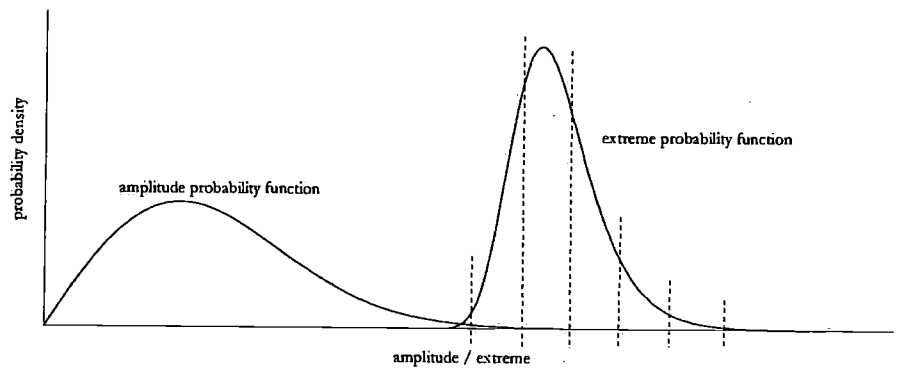

Figure 15 Amplitude and extreme probability functions

Having established this functional relationship the nonlinear amplitude or the nonlinear extreme probability function can be calculated by applying the fundamental transformation law of probability functions,

$$\left|f_x(x)\,dx\right| = \left|f_y(y)\,dy\right| \tag{2.49}$$

Hence the nonlinear amplitude and extreme probability functions can be determined under the condition that the functional relationship, (2.48), is a monotonously increasing function.

$$f_{nl}(y_{a,nl}) = f_l\left(h^{-1}(y_{a,nl})\right)\left|\frac{dh^{-1}(y_{a,l})}{dy_{a,nl}}\right|$$
$$g_{nl}(Y_{n,nl}) = g_l\left(h^{-1}(Y_{n,nl})\right)\left|\frac{dh^{-1}(Y_{n,l})}{dY_{n,nl}}\right| \qquad (2.50)$$

Here $f_l(\ )$ and $g_l(\ )$ are the linear probability functions as given by (2.41)/(2.42) and (2.38).

2.5 Directional Most Likely Extreme Response (DMLER)

A special case of the MLER technique is formulated in this paragraph for the application in a directional seaway. Again the procedure starts by describing the response process with a linear model and use this to specify the most likely response profile around a large response amplitude. With the linear transfer functions for all wave headings the conditioned incident wave profile can be determined.

A linear ship response is written as the superposition of a discrete number of independent wave headings M,

$$y(t) = \sum_{l=1}^{M} y_l(t) \qquad (2.51)$$

Consider a large response amplitude to occur at a prescribed time instance. This response is the result of all headings combined. Next we formulate for every heading the most likely response profile given a prescribed total response amplitude. This most likely response profile of heading l is then given by the following conditional expectation,

$$E\left[y_l(t+\tau)\middle|y(t)=Y_n, \dot{y}(t)=0\right] \qquad (2.52)$$

This can be determined from the conditional probability density function,

$$f\left(y_l(t+\tau)\middle|y(t),\dot{y}(t)\right) = \frac{f\left(y_l(t+\tau), y(t), \dot{y}(t)\right)}{f\left(y(t),\dot{y}(t)\right)} \qquad (2.53)$$

The derivation of this can be done in a similar way as for the other models. More details can be found in appendix A. The resulting conditional probability density function for the response profile due to direction l given a total response amplitude is,

$$f\left(y_l(t+\tau)\middle|y(t)=Y_n,\dot{y}(t)=0\right)=\frac{1}{\sigma_l^2(\tau)\sqrt{2\pi}}e^{\frac{(y_l(t+\tau)-\bar{y}_l(\tau))}{2\sigma_l^2(\tau)}}$$

with

$$\bar{y}_l(\tau)=Y_n\frac{m_{0,l}}{m_0}\rho_{ll}(\tau) \tag{2.54}$$

$$\sigma_l^2(\tau)=m_{0,l}-\frac{m_{0,l}^2}{m_0}\rho_{ll}^2(\tau)-\frac{m_{0,l}^2}{m_2}\dot{\rho}_{ll}^2(\tau)$$

When the coefficient of variation is studied,

$$CoV=\sqrt{\frac{m_0^2}{Y_n m_{0,l}\rho_{ll}^2(\tau)}-\frac{m_0}{Y_n^2}-\frac{m_2\dot{\rho}_{ll}^2(\tau)}{Y_n^2\rho_{ll}^2(\tau)}} \tag{2.55}$$

it is seen that a larger relative contribution of direction l to the total variance m_0 results in a smaller coefficient of variation.

The next step is to apply this formulation in a directional MLER approach. For this the linear response, as given by equation (2.51), is written as,

$$y(t)=\sum_{l=1}^{M}\sum_{j=1}^{N}\left|H_{y\zeta}(\omega_{j,l})\right|\zeta_{a,j,l}\cos\left(\omega_{e,j,l}t+\varepsilon_{\zeta,j,l}+\varepsilon_{y\zeta,j,l}\right) \tag{2.56}$$

Equation (2.54) can be discretised,

$$E\left[y_l(t+\tau)\middle|y(t)=Y_n,\dot{y}(t)=0\right]=Y_n\frac{m_{0,l}}{m_0}\rho_{ll}^2(\tau)=\frac{Y_n}{2m_0}\sum_{j=1}^{N}y_{a,j,l}^2\cos\left(\omega_{e,j,l}\tau\right) \tag{2.57}$$

Equally as done in the application to unidirectional seas a time delay is introduced, ΔT. In this way the conditioned extreme Y_n, will occur at this timestep after starting the simulation.

$$E\left[y_l(\Delta T+\tau)\middle|y(\Delta T)=Y_n,\dot{y}(\Delta T)=0\right]=\frac{Y_n}{2m_0}\sum_{j=1}^{N}y_{a,j,l}^2\cos\left(\omega_{e,j,l}\tau+\varepsilon_{\Delta T,j,l}\right) \qquad (2.58)$$

$$with\ \varepsilon_{\Delta T,j,l}=-\Delta T\omega_{e,j,l}$$

By equating (2.56) and (2.58) the unknown wave amplitudes and wave phase angles can be determined as,

$$\zeta_{a,j,l}=\frac{Y_n\cdot y_{a,j,l}^2}{2m_0\left|H_{y\zeta}\left(\omega_{j,l}\right)\right|} \qquad \varepsilon_{\zeta,j,l}=\varepsilon_{\Delta T,j,l}-\varepsilon_{y\zeta,j,l} \qquad (2.59)$$

Example of tri-directional conditioned wave profile

To demonstrate this theory an example is given for a conditioned wave. A modified Pierson-Moskowitz spectrum is modelled with a significant wave height of 5.0 meters and a period of 7.5 seconds both as a uni-directional and a tri-directional spectrum. The properties of these spectra are listed in the table below.

	Uni-directional		Tri-directional	
Direction [deg]	H_s [m]	T_z [s]	H_s [m]	T_z [s]
165.0	-	-	2.24	7.5
180.0	5.0	7.5	3.87	7.5
195.0	-	-	2.24	7.5

Table 2 Wave spectra for directional conditioned wave profile

A conditioned wave with an amplitude of 1.0 meter is modelled and the wave profiles are both shown in the following two figures. Figure 16 and Figure 17 clearly shows that the influence of directions 165.0 and 195.0 is quite large despite the fact that their individual weigh factors are only 0.2. As these figures do not have equal scales it is rather difficult to judge their shapes but it is likely that the directional conditioned wave profiles have wave segments which are too steep and a steepness check is quite laborious. It is therefore advised to use the directional variant with great care.

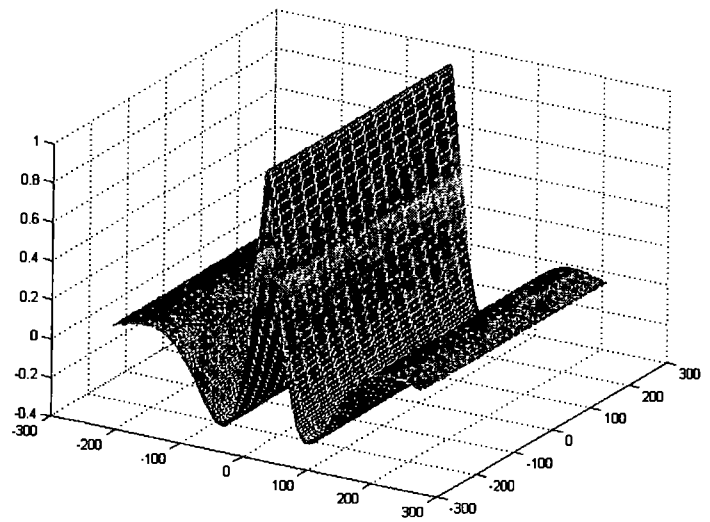

Figure 16 Uni-directional conditioned wave profile

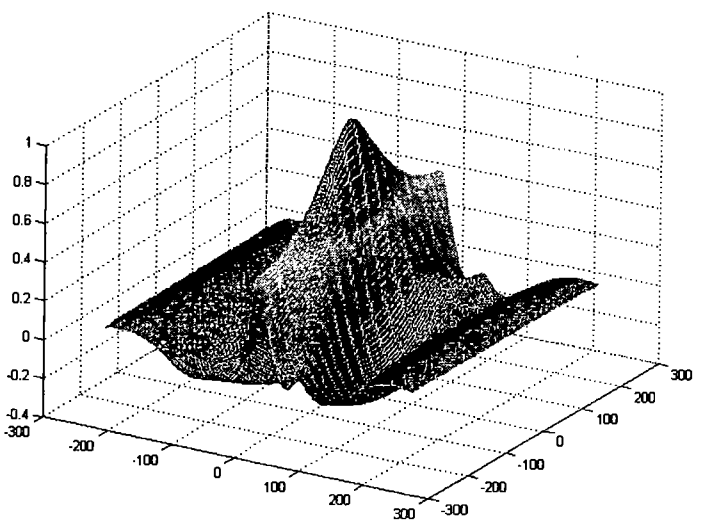

Figure 17 Tri-directional conditioned wave profile

3 Approximate Volterra modelling of nonlinear ship responses

In this chapter we study nonlinear ship responses, $y(t)$, induced by wave excitation, $\zeta(t)$, as a nonlinear time-invariant system. By varying the wave excitation the response sequence changes. Thus we can write the response as a function of the wave excitation, $y\{\zeta(t)\}$, which itself is a function of time. This formulation is called a functional. Original developments of functionals were done by Volterra (1880). In the 19th century he studied Taylor expansions of a function and these functional series have been named after him, the so-called *Volterra series*. The first order Volterra series is simply the linear, time-invariant system model as is widely used in engineering and science. The output $y(t)$ due to an input $x(t)$ is given by the convolution integral in the time domain or by multiplication in the frequency domain,

$$\begin{aligned} y(t) &= \int_{-\infty}^{\infty} h(\tau)x(t-\tau)d\tau \\ Y(\omega) &= H(\omega)X(\omega) \end{aligned} \tag{3.1}$$

The modelling of a nonlinear response by a higher order Volterra series is thus simply a generalisation of this linear model. In the naval architectural discipline linear transfer functions for ship motions and loads are widely used. In order to take nonlinear behaviour into account the extension to higher order Volterra series can thus be seen as a logical step. This chapter starts by giving a summary of previous work on the application of the Volterra modelling technique for ship responses. Next, the general third order Volterra model is described and transformed to an uncorrelated model. Two nonlinear approximate Volterra models are presented as simplifications of the general 3rd and 5th order Volterra model. The idea is to maintain a good prediction of the nonlinear behaviour but reduce the identification and simulation costs drastically.

3.1 Past research on Volterra modelling for ship motions and loads

One of the first studies on the application of Volterra series to ship responses was published by Vassilopoulos (1967). He discussed the application to the added resistance of ships in waves and the uncoupled roll motion of a ship. Dalzell (1975) studied the application to the ship resistance in waves and later Dalzell (1982) investigated the third order Volterra model for the modelling of nonlinear ship motions. A quadratic approach was presented by Juncher-Jensen and Pedersen (1979) to calculate wave induced bending moments. Pinkster (1980) applied second order transfer functions for the calculation of low frequency drift forces. Kim (1990) presented a method to predict the sway drift force and the yaw drift moment on large offshore structures. The method was based on a Volterra input-output model, for which he made use of the work of Dalzell. Kim and Yue (1991) studied the second order wave excitations on large bodies in waves. They used a second order Volterra series to calculate the statistical properties of these wave excitations. Paik (1997) studied the application of quadratic and cubic Volterra series to model the SDOF behaviour of offshore structures due to waves and current. O'Dea et al (1992) studied measurements of a standard ITTC hull form and modelled the responses by a third order Volterra functional expansion. With respect to the heave and pitch motion they concluded that cubic effects were the dominant nonlinearity. With the main contribution in the wave frequency band due to interaction of wave frequency triplets. Thus $H(\omega,\omega,-\omega)$ constitutes a dominant part of the response while the term $H(\omega,\omega,\omega)$ is rather small. Still the identification of the Volterra kernels, especially for cubic and higher order is difficult and impractical. Either a large amount of calculations with different frequency combinations or higher order spectral analyses is required. To simplify this the Volterra model can be reduced to approximate forms. Bendat (1990) introduced two simplifications of the general third order model. Adegeest (1995) applied one of these to the motions and hull girder loads of a Wigley with bow flare and obtained promising results. Moreover he presented another identification procedure for the determination of the kernels of the approximate model based on regular wave experiments.

3.2 The general uncorrelated third order Volterra model

A nonlinear dynamic system can be described by a higher order Volterra model. When the incident wave is modelled as an input signal and a ship response is the output the general third order model for is written in the time domain as,

$$
\begin{aligned}
y(t) &= y_1(t) + y_2(t) + y_3(t) \\
y_1(t) &= \int_{-\infty}^{\infty} h_1(\tau)\zeta(t-\tau)d\tau \\
y_2(t) &= \int_{-\infty}^{\infty}\int_{-\infty}^{\infty} h_2(\tau_1,\tau_2)\zeta(t-\tau_1)\zeta(t-\tau_2)d\tau_1 d\tau_2 \\
y_3(t) &= \int_{-\infty}^{\infty}\int_{-\infty}^{\infty} h_3(\tau_1,\tau_2,\tau_3)\zeta(t-\tau_1)\zeta(t-\tau_2)\zeta(t-\tau_3)d\tau_1 d\tau_2 d\tau_3
\end{aligned}
\tag{3.2}
$$

or in the frequency domain as,

$$
\begin{aligned}
Y(\omega) &= Y_1(\omega) + Y_2(\omega) + Y_3(\omega) \\
Y_1(\omega) &= H_1(\omega)Z(\omega) \\
Y_2(\omega) &= \frac{1}{2\pi}\int_{-\infty}^{\infty} H_2(\omega_1, \omega-\omega_1)Z(\omega_1)Z(\omega-\omega_1)d\omega_1 \\
Y_3(\omega) &= \frac{1}{4\pi^2}\int_{-\infty}^{\infty}\int_{-\infty}^{\infty} H_3(\omega_1,\omega_2-\omega_1,\omega-\omega_2)Z(\omega_1)Z(\omega_2-\omega_1)Z(\omega-\omega_2)d\omega_1 d\omega_2
\end{aligned}
\tag{3.3}
$$

Here the wave, the response and the transfer functions are related by the Fourier transform. The incident wave is a stationary, zero-mean and Gaussian distributed process and is modelled by a summation of harmonic components. It is easily seen that the third order response gives both third and first harmonic responses and is thus correlated with the first order output. The second order response is not correlated with the first or third order response as can be derived by calculating the covariance functions,

$$
E\left[y_1(t)\left(y_2(t+\tau)-\bar{y}_2\right)\right] = 0 \quad ; \quad E\left[\left(y_2(t)-\bar{y}_2\right)y_3(t+\tau)\right] = 0 \tag{3.4}
$$

The output autocovariance function can be calculated as a summation of the three orders and their correlated results.

$$
\begin{aligned}
E\left[y(t)y(t+\tau)\right] &= E\left[\left(y_1(t)+y_2(t)+y_3(t)\right)\left(y_1(t+\tau)+y_2(t+\tau)+y_3(t+\tau)\right)\right] \\
&= R_{y_1y_1}(\tau) + R_{y_2y_2}(\tau) + R_{y_3y_3}(\tau) + R_{y_1y_3}(\tau) + R_{y_3y_1}(\tau)
\end{aligned}
\tag{3.5}
$$

Taking the Fourier transform of the output autocovariance function the output spectral density is obtained with the use of the Wiener-Khintchine theorem, see appendix C.2,

$$
S_{yy}(\omega) = S_{y_1y_1}(\omega) + S_{y_2y_2}(\omega) + S_{y_3y_3}(\omega) + S_{y_1y_3}(\omega) + S^*_{y_1y_3}(\omega) \tag{3.6}
$$

In order to formulate a mutual uncorrelated model the correlation between the first and third order should be eliminated. The subsequent section does so by introducing an extra linear transfer function.

First the covariance function for the incident wave and the third order response is evaluated.

$$E\left[\zeta(t)y_3(t+\tau)\right]=$$
$$=\int_{-\infty}^{\infty}\int_{-\infty}^{\infty}\int_{-\infty}^{\infty}h_3(\tau_1,\tau_2,\tau_3)E\left[\zeta(t)\zeta(t+\tau-\tau_1)\zeta(t+\tau-\tau_2)\zeta(t+\tau-\tau_3)\right]d\tau_1 d\tau_2 d\tau_3 \quad (3.7)$$
$$=\int_{-\infty}^{\infty}c(\tau_1)R_{\zeta\zeta}(\tau-\tau_1)d\tau_1 \qquad with \quad c(\tau_1)=3\int_{-\infty}^{\infty}\int_{-\infty}^{\infty}h_3(\tau_1,\tau_2,\tau_3)R_{\zeta\zeta}(\tau_2-\tau_3)d\tau_2 d\tau_3$$

While the covariance function between the first and third order response is formulated as,

$$E\left[y_1(t)y_3(t+\tau)\right]=\int_{-\infty}^{\infty}\int_{-\infty}^{\infty}h_1(\tau_1)c(\tau_2)R_{\zeta\zeta}(\tau+\tau_1-\tau_2)d\tau_1 d\tau_2 \quad (3.8)$$

An uncorrelated model is proposed by introducing a linear transfer function, $D(\omega)$ or $d(\tau)$, on the incident wave, which is subtracted from the third order response and added to the first order response. Thus a revised first and third order output are obtained which should be uncorrelated. The revised third order response becomes,

$$y_c(t)=y_3(t)-\int_{-\infty}^{\infty}d(\tau)\zeta(t-\tau)d\tau \quad (3.9)$$

By imposing an uncorrelated response,

$$E\left[y_1(t)y_c(t+\tau)\right]=$$
$$\int_{-\infty}^{\infty}\int_{-\infty}^{\infty}h_1(\tau_1)c(\tau_2)R_{\zeta\zeta}(\tau+\tau_1-\tau_2)d\tau_1 d\tau_2-\int_{-\infty}^{\infty}\int_{-\infty}^{\infty}h_1(\tau_1)d(\tau_2)R_{\zeta\zeta}(\tau+\tau_1-\tau_2)d\tau_1 d\tau_2=0 \quad (3.10)$$

it is deduced that the introduced linear transfer function $d(\tau)$ should be equal to $c(\tau)$. Thus the general third order Volterra model is reformulated in a mutual uncorrelated model.

$$
\begin{aligned}
Y(\omega) &= Y_a(\omega) + Y_b(\omega) + Y_c(\omega) \\
Y_a(\omega) &= H_1(\omega) Z(\omega) + C(\omega) Z(\omega) \\
Y_b(\omega) &= \frac{1}{2\pi} \int_{-\infty}^{\infty} H_2(\omega_1, \omega - \omega_1) Z(\omega_1) Z(\omega - \omega_1) d\omega_1 \\
Y_c(\omega) &= \frac{1}{4\pi^2} \int_{-\infty}^{\infty} \int_{-\infty}^{\infty} H_3(\omega_1, \omega_2 - \omega_1, \omega - \omega_2) Z(\omega_1) Z(\omega_2 - \omega_1) Z(\omega - \omega_2) d\omega_1 d\omega_2 \\
&\quad - C(\omega) Z(\omega)
\end{aligned}
\tag{3.11}
$$

Where $C(\omega)$ is obtained by Fourier transformation of $c(\tau)$ and making use of the Wiener-Khintchine theorem thus resulting in,

$$
C(\omega) = 3 \int_{-\infty}^{\infty} H_3(\omega, -\omega_1, \omega_1) G_{\zeta\zeta}(\omega_1) d\omega_1 \tag{3.12}
$$

When calculating the output spectral density the result is uncorrelated being,

$$
S_{yy}(\omega) = S_{y_a y_a}(\omega) + S_{y_b y_b}(\omega) + S_{y_c y_c}(\omega) \tag{3.13}
$$

3.3 System identification and simulation of nonlinear approximate Volterra model I

The first nonlinear approximate Volterra model, which is described here, assumes that the higher order Volterra kernels can be represented by additive first order frequency response functions.

$$
\begin{aligned}
H_1(\omega) &= A_1(\omega) \\
H_2(\omega_1, \omega_2) &= A_2(\omega_1 + \omega_2) \\
H_3(\omega_1, \omega_2, \omega_3) &= A_3(\omega_1 + \omega_2 + \omega_3)
\end{aligned}
\tag{3.14}
$$

Upon substitution into equation (3.3) the response is given by,

$$
\begin{aligned}
Y_1(\omega) &= A_1(\omega) Z(\omega) \\
Y_2(\omega) &= \frac{A_2(\omega)}{2\pi} \int_{-\infty}^{\infty} Z(\omega_1) Z(\omega - \omega_1) d\omega_1 \\
Y_3(\omega) &= \frac{A_3(\omega)}{4\pi^2} \int_{-\infty}^{\infty} \int_{-\infty}^{\infty} Z(\omega_1) Z(\omega_2 - \omega_1) Z(\omega - \omega_2) d\omega_1 d\omega_2
\end{aligned}
\tag{3.15}
$$

The integrals have a simple interpretation, since the single integral in equation (3.15) is the Fourier transform of $\zeta^2(t)$ while the double integral is the Fourier integral of $\zeta^3(t)$, see appendix C.3 for proof. This nonlinear approximate Volterra model is pictured in the following figure.

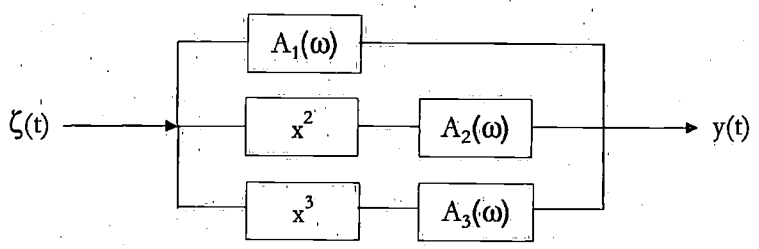

Figure 18 Nonlinear approximate Volterra model I

Identification

For identification of the unknown three Volterra kernels the mutually uncorrelated model is used. For this approximate model formula (3.12) becomes,

$$C(\omega) = 3\int_{-\infty}^{\infty} A_3(\omega) G_{\zeta\zeta}(\omega_1)\, d\omega_1 = 3A_3(\omega)\sigma_\zeta^2 \qquad (3.16)$$

and hence the model is simplified in a MISO model for which standard spectral analytical techniques can be used to solve the Volterra kernels.

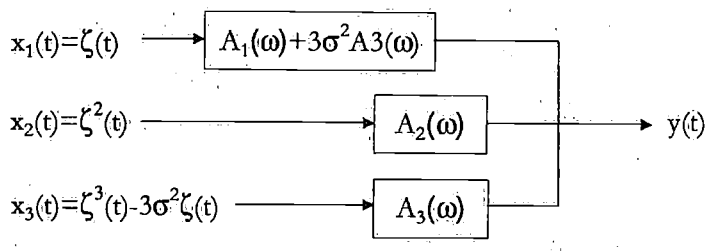

Figure 19 Model I uncorrelated MISO

By conducting an irregular wave simulation the three input and single output time series are required for identification of the kernels. By calculation of the input and output auto- and cross-spectral densities the kernels are given by,

$$H_0(\omega)=\frac{S_{x_1y}(\omega)}{S_{x_1x_1}(\omega)} \qquad A_2(\omega)=\frac{S_{x_2y}(\omega)}{S_{x_2x_2}(\omega)} \qquad A_3(\omega)=\frac{S_{x_3y}(\omega)}{S_{x_3x_3}(\omega)} \tag{3.17}$$

From this result the last kernel is determined by,

$$A_1(\omega)=H_0(\omega)-3\sigma_\zeta^2 A_3(\omega) \tag{3.18}$$

Simulation

Having finished the identification of the Volterra model it can be used to simulate the response in a seaway. Of course with the precondition that the model is derived for the specific case of heading, speed and loading condition. The time domain simulation of the approximate model I is done by Fourier transformation of the frequency domain Volterra transfer functions like,

$$a_j(\tau)=\frac{1}{2\pi}\int_{-\infty}^{\infty} A_j(\omega)e^{i\omega\tau}d\omega \qquad j=1,2,3 \tag{3.19}$$

It is important to notice here that impulse response functions should be calculated for positive and negative time-steps. While causality is often applicable in engineering cases it is not valid here. Consider for example the case that a wave front approaches the bow of the ship. Elsewhere on the vessel this can lead to motions while there is no wave elevation at the origin of the co-ordinate system.

By calculating an irregular wave as the summation of regular wave components like in equation (2.28) the nonlinear response is calculated as follows.

$$y(t) = y_1(t) + y_2(t) + y_3(t)$$

with

$$y_1(t) = \int_{-\infty}^{\infty} a_1(\tau)\zeta(t-\tau)d\tau \tag{3.20}$$

$$y_2(t) = \int_{-\infty}^{\infty} a_2(\tau)\zeta^2(t-\tau)d\tau$$

$$y_3(t) = \int_{-\infty}^{\infty} a_3(\tau)\zeta^3(t-\tau)d\tau$$

Of course the integrations are not performed from minus infinity to infinity but suitable integration limits are formulated depending on the response sequence in order to account properly for the memory effects.

3.4 System identification and simulation of nonlinear approximate Volterra model II

Another nonlinear approximate Volterra model is formulated by assuming that the higher order Volterra kernels can be replaced by products of linear transfer functions.

$$\begin{aligned}
&H_1(\omega) = B_1(\omega)\\
&H_2(\omega_1,\omega_2) = B_2(\omega_1)B_2(\omega_2)\\
&H_3(\omega_1,\omega_2,\omega_3) = B_3(\omega_1)B_3(\omega_2)B_3(\omega_3)\\
&H_4(\omega_1,\omega_2,\omega_3,\omega_4) = B_4(\omega_1)B_4(\omega_2)B_4(\omega_3)B_4(\omega_4)\\
&H_5(\omega_1,\omega_2,\omega_3,\omega_4,\omega_5) = B_5(\omega_1)B_5(\omega_2)B_5(\omega_3)B_5(\omega_4)B_5(\omega_5)
\end{aligned} \tag{3.21}$$

Substitution of this into equation (3.3) shows that this simplification is equal to a parallel linear transfer functions succeeded by zero-memory operators. Like for example the second order response,

$$\begin{aligned}
Y_2(\omega) &= \frac{1}{2\pi}\int_{-\infty}^{\infty} B_2(\omega_1)B_2(\omega-\omega_1)Z(\omega_1)Z(\omega-\omega_1)d\omega_1\\
&= \frac{1}{2\pi}\int_{-\infty}^{\infty} U_2(\omega_1)U_2(\omega-\omega_1)d\omega_1
\end{aligned} \tag{3.22}$$

Where the last integral is the Fourier transform of $u^2(t)$, as derived in appendix C.3. Thus the approximate Volterra model can be pictured by the model in Figure 20.

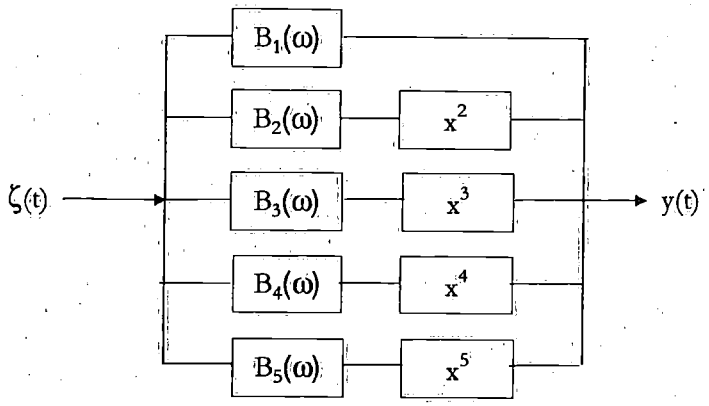

Figure 20 Nonlinear approximate Volterra model II

This second approximate model is extended to fifth order. This is done for two reasons. First of all the identification process, as will be shown subsequently, uses regular wave simulations, thereby harmonic analysis is used instead of higher order spectral analysis. Because of this it is easy to include higher order responses without difficulty. The second reason is that higher than third order might give more accuracy for strong nonlinear responses like hull girder loads.

Identification

The procedure to identify the five unknown transfer functions is based on regular wave simulations. This approach was first used by Adegeest (1995) for a third order model. The benefit of a regular wave identification scheme is that correlations are easily dealt with, regular wave simulations are quite fast and higher harmonics can be calculated quite accurately. If the model, as depicted in Figure 20, has a regular wave input like,

$$\zeta(t) = \zeta_a \cos \omega t \tag{3.23}$$

the response output is,

$$y(t) = \mathrm{Re}\left\{\bar{y} + y_1(t) + y_2(t) + y_3(t) + y_4(t) + y_5(t)\right\}$$

with

$$\bar{y} = \frac{1}{2}\zeta_a^2 \left|B_2(\omega)\right|^2 + \frac{3}{4}\zeta_2^4 \left|B_4(\omega)\right|^4$$

$$y_1(t) = \left[\zeta_a B_1(\omega) + \frac{3}{4}\zeta_a^3 B_3(\omega)\left|B_3(\omega)\right|^2 + \frac{5}{8}\zeta_a^5 B_5(\omega)\left|B_5(\omega)\right|^4\right] e^{i\omega t}$$

$$y_2(t) = \left[\frac{1}{2}\zeta_a^2 B_2^2(\omega) + \frac{1}{2}\zeta_a^4 B_4^2(\omega)\left|B_4(\omega)\right|^2\right] e^{i2\omega t} \qquad (3.24)$$

$$y_3(t) = \left[\frac{1}{4}\zeta_a^3 B_3^3(\omega) + \frac{5}{16}\zeta_a^5 B_5^3(\omega)\left|B_5(\omega)\right|^2\right] e^{i3\omega t}$$

$$y_4(t) = \frac{1}{8}\zeta_a^4 B_4^4(\omega) e^{i4\omega t}$$

$$y_5(t) = \frac{1}{16}\zeta_a^5 B_5^5(\omega) e^{i5\omega t}$$

From this it is seen that the response can be ordered by harmonic components like,

$$y(t) = \mathrm{Re}\left\{c_0 + c_1 e^{i\omega t} + c_2 e^{i2\omega t} + c_3 e^{i3\omega t} + c_4 e^{i4\omega t} + c_5 e^{i5\omega t}\right\} \qquad (3.25)$$

By conducting this harmonic analysis of the simulated output response the unknown transfer functions, $B_j(\omega)$ are determined by,

$$B_5(\omega) = \sqrt[5]{\frac{16c_5}{\zeta_a^5}}$$

$$B_4(\omega) = \sqrt[4]{\frac{8c_4}{\zeta_a^4}}$$

$$B_3(\omega) = \sqrt[3]{\frac{4c_3}{\zeta_a^3} - \frac{5}{4}\zeta_a^2 B_5^3(\omega)\left|B_5(\omega)\right|^2} \qquad (3.26)$$

$$B_2(\omega) = \sqrt{\frac{2c_2}{\zeta_a^2} - \zeta_a^2 B_4^2(\omega)\left|B_4(\omega)\right|^2}$$

$$B_1(\omega) = \frac{c_1}{\zeta_a} - \frac{3}{4}\zeta_a^2 B_3(\omega)\left|B_3(\omega)\right|^2 - \frac{5}{8}\zeta_a^4 B_5(\omega)\left|B_5(\omega)\right|^4$$

In this identification procedure no use is made of the mean value, c_0. Strictly speaking this should not be necessary as the second and fourth harmonic components fully determine the second and fourth order kernels. But the mean value information can be

used when the mean value is uncoupled from the second and fourth harmonic response and separate mean value response functions are defined:

$$\left|B_{0,2}(\omega)\right| \quad and \quad \left|B_{0,4}(\omega)\right| \tag{3.27}$$

But if a fourth order model is used, two simulations with different amplitudes are necessary to obtain unique solutions for these two transfer functions. To eliminate this problem a simple solution can be applied. The fourth order mean value response function is simply omitted and only the second order is used.

$$\left|B_{0,2}(\omega)\right| = \sqrt{\frac{2c_0}{\zeta_a^2}} \tag{3.28}$$

This alternative identification procedure has the benefit of using the mean value information, but it loses the fourth order contribution in the mean value if the simplified identification is used.

It is easily seen from equation (3.24) that a negative mean response cannot be simulated with the model. Thus the sign convention has to be changed if this situation occurs.

Simulation

The simulation of Model II is not done with convolution integrals but with summations of regular components. The irregular wave is defined by equation (2.28). For every frequency in the irregular wave the corresponding amplitude operator $\left|B_j(\omega)\right|$ and phase angle $\varepsilon_{B_j\zeta}$ are determined by interpolation in the known series of transfer function values. The response can now be calculated as follows,

$$y(t)=\sum_{j=1}^{N}\left[\frac{1}{2}\zeta_{a,j}^{2}\left|B_2(\omega_j)\right|^2+\frac{3}{8}\zeta_{a,j}^{4}\left|B_4(\omega_j)\right|^4+\left|B_1(\omega_j)\right|\zeta_{a,j}\cos\left(\omega_j t+\varepsilon_{\zeta,j}+\varepsilon_{B_1\zeta,j}\right)\right]+$$
$$\left[\sum_{j=1}^{N}\left|B_2(\omega_j)\right|\zeta_{a,j}\cos\left(\omega_j t+\varepsilon_{\zeta,j}+\varepsilon_{B_2\zeta,j}\right)\right]^2+$$
$$\left[\sum_{j=1}^{N}\left|B_3(\omega_j)\right|\zeta_{a,j}\cos\left(\omega_j t+\varepsilon_{\zeta,j}+\varepsilon_{B_3\zeta,j}\right)\right]^3+$$
$$\left[\sum_{j=1}^{N}\left|B_4(\omega_j)\right|\zeta_{a,j}\cos\left(\omega_j t+\varepsilon_{\zeta,j}+\varepsilon_{B_4\zeta,j}\right)\right]^4+$$
$$\left[\sum_{j=1}^{N}\left|B_5(\omega_j)\right|\zeta_{a,j}\cos\left(\omega_j t+\varepsilon_{\zeta,j}+\varepsilon_{B_5\zeta,j}\right)\right]^5 \tag{3.29}$$

Or if the alternative identification is used with a mean value response function the simulation becomes,

$$y(t)=\sum_{j=1}^{N}\left[\frac{1}{2}\zeta_{a,j}^{2}\left|B_{0,2}(\omega_j)\right|^2+\left|B_1(\omega_j)\right|\zeta_{a,j}\cos\left(\omega_j t+\varepsilon_{\zeta,j}+\varepsilon_{B_1\zeta,j}\right)\right]+...etc \tag{3.30}$$

4 Assessment of nonlinear ship responses

Assessment strategies for the calculation of extreme responses and the seakeeping performance are discussed by using the response conditioning technique from chapter 1 and the nonlinear approximate Volterra model of chapter 1. First a discussion is given of a standard linear approach for calculating extreme responses. Following along the lines of this approach for a nonlinear assessment the amount of nonlinear calculations would be too large even with the use of the techniques of the previous chapters. Thus the amount of calculations needs to be reduced. Here the *Coefficient of Contribution method* is discussed as a powerful reduction technique, which can be used in combination with the techniques of the previous chapters.

The second paragraph presents a reliability based seakeeping performance assessment method. The introduction of the thesis discussed several critical aspects of the standard linear seakeeping performance assessment technique. The seakeeping performance should be treated as a stochastic variable and the criteria should account for gradual performance degradation. This in turn gives the possibility to quantify the sensitivity of the performance due to all responses and to quantify the mutual correlations. These changes are dealt with in the second paragraph.

4.1 Long-term extreme response calculation procedures

A large number of stochastic variables are of importance for the calculation of a lifetime extreme response probability distribution of a ship or offshore structure. A short discussion is given of these stochastic variables and their integration to calculate the linear long-term extreme response distribution.

Two categories of variables are identified, namely environmental and operational aspects. The environmental variables are,

- Wave spectrum,

- Significant wave height and period,
- Wave direction,
- Energy spreading.

For a complete picture wind and current would have to be incorporated as well, but are not of interest regarding wave-induced responses. The environment is usually described by a discrete number of short-term sea states, characterised by a wave spectrum with an optional wave energy spreading function. This wave spectrum is formulated by a significant wave height and a wave period. The statistics of these two are usually given by a scatter diagram or by a mathematical function, like a Weibull function for the significant wave height with a conditional log-normal distribution for the wave period. Such wave databases can be formulated for a specific region or for a trade route and can additionally be specified for seasons and wave directions. The choice of wave database is quite important as significant uncertainties are present and different databases can result in considerable different results, see for instance Guedes Soares and Moan (1991).

The operational variables are;

- Course angle,
- Ship speed,
- Loading condition,

The combination of the ship's course and the wave direction determine the wave heading. This may very well be influenced by the captain in order to avoid excessive motions. For example the captain may change the course if excessive rolling occurs. The ship speed is also a stochastic variable depending on the ship condition, laden or ballast, and on weather conditions. Voluntary and involuntary speed reductions are both possible. Furthermore the loading condition determines the draft and the mass and inertia distributions of the vessel.

Probability distributions are required for all these stochastic variables. Some are conditional variables thus leading to conditional probability functions. For all combinations of wave heading, speed and loading condition the linear response transfer functions are to be calculated. Subsequently the short-term response statistics can be determined by calculating response spectra,

$$S_{yy}\left(\omega|H_s,T_z,\mu,V_s,L_c\right)=\left|H\left(\omega|\mu,V_s,L_c\right)\right|^2\cdot S_{\zeta\zeta}\left(\omega|H_s,T_z\right) \tag{4.1}$$

and response moments,

$$m_n=\int_0^\infty \omega_e^2 S_{yy}\left(\omega_e|H_s,T_z,\mu,V_s,L_c\right)d\omega_e=\int_0^\infty \omega_e^2 S_{yy}\left(\omega|H_s,T_z,\mu,V_s,L_c\right)d\omega \tag{4.2}$$

With the response spectral moments the response statistical quantities can be calculated, i.e. amplitude distributions and response periods. The amplitude distribution is given by

the Rayleigh function, $f(y_a)$, see equation (2.42). Strictly speaking the Rice distribution is correct but when extremes are of interest the tail of the probability function is of importance for which the difference is negligible.

Having established all short-term probability functions the long-term response amplitude distribution is calculated by summation of all short-term distributions taking account of all probabilities involved,

$$F_{LT}(y_a) = \int_{H_s}\int_{T_z}\int_{\mu}\int_{L_c}\int_{V_s} w_{H_s,T_z,\mu,L_c,V_s} F_{ST}(y_a|H_s,T_z,\mu,L_c,V_s) f(H_s,T_z) \\ f(\mu,V_s|H_s,T_z,L_c) f(L_c) dV_s d\mu dL_c dT_z dH_s \tag{4.3}$$

Here the term w_{H_s,T_z,μ,L_c,V_s} is a weigh factor, which represents the relative number of crests within each sea state and is given by,

$$w_{H_s,T_z,\mu,L_c,V_s} = \frac{\overline{T}_2}{T_2|H_s,T_z,\mu,L_c,V_s} \tag{4.4}$$

Where the term $\overline{T}_2$ is the average response period over the lifetime given by,

$$\frac{1}{\overline{T}_2} = \int_{H_s}\int_{T_z}\int_{\mu}\int_{L_c}\int_{V_s} \frac{1}{T_2|H_s,T_z,\mu,L_c,V_s} f(H_s,T_z) f(\mu,V_s|H_s,T_z,L_c) f(L_c) dV_s d\mu dL_c dT_z dH_s$$

with

$$T_2 = 2\pi\sqrt{\frac{m_0}{m_2}} \tag{4.5}$$

With establishing the long-term response amplitude distribution the lifetime extreme distribution can be obtained by applying order statistics as outlined in paragraph 2.3.

$$g_{LT}(y_a) = n_{LT} \cdot f_{LT}(y_a) \cdot \left[F_{LT}(y_a)\right]^{n_{LT}-1}$$

with (4.6)

$$n_{LT} = \frac{T_{lifetime}}{\overline{T}_2}$$

The next step is to calculate the nonlinear extreme distribution. Both the response conditioning technique from chapter 1 and the Volterra modelling of chapter 1 are presented as applicable to a short-term sea state. In case we follow the approach as presented above still a large amount of conditioned simulations have to be conducted in

order to transform the linear amplitude probability functions or every short-term sea state needs to be simulated with the nonlinear approximate Volterra model. But it is very well possible to reduce the amount of calculations because intuitively we know that many of the short-term sea states hardly contribute to the occurrence of extreme responses and may thus be omitted. In other words; the question under investigation case is if the following equality holds,

$$g_{LT}(y_a) \stackrel{?}{=} g'_{LT}(y_a) \tag{4.7}$$

Where the quotation mark designates the calculation for a reduced amount of sea states. It seems a very coarse simplification to reduce a full scatter diagram to only a handful sea states. Whether the equality of equation (4.7) holds, is discussed subsequently. First a simple numerical case is presented. No hard conclusions can be drawn from this example but the intention is to provide some understanding of the sensitivity. Instead of comparing the extreme response probability functions the expected extreme is calculated from these probability distributions.

Numerical example for the expected extreme wave due to two sea states

Consider the wave amplitude distribution resulting from two sea states. One sea state has a significant wave height H_s and the second sea state has a significant wave height of $C \cdot H_s$. Next the lifetime expected extreme wave amplitude is subject of investigation. Suppose,

- sea state #1 occurs 58400 times, which corresponds with 20 years x 365 days x 24 hours / 3 hours. Thus it is assumed that a short-term sea state lasts 3 hours. The average period is set to 7.5 [s].
- sea state #2 occurs only once, thus it has a return period of 20 years and lasts 3 hours as well. The average response period for this sea state is 12 [s].

The long-term extreme wave amplitude distribution is calculated by applying order statistics to the long-term amplitude distribution as calculated using equation (4.3). The simplified approach is to calculate the short-term response amplitude distribution for sea state #2 and apply order statistics to this probability function. From both estimates of the long-term extreme response distribution the expected extreme is determined and these two values are compared, where the full long-term assessment serves as benchmark. Some aspects are investigated and shown in two figures as described below.

Varying the coefficient C

By varying the coefficient C the error in the expected extreme is assessed and shown in the following figure. From this we see that even for a coefficient of $C = 1.45$ the error is less than -10%. Suppose this case concerns the extreme wave amplitude for a scatter diagram where sea states #2 has a significant wave height of 12.0 [m] (=20 years significant wave height). Then sea state #1 would have a significant wave height of 8.3

[m]. Thus the expected extreme for 58400 times a sea state with a significant wave height of 8.3 [m] and once a sea state with a significant wave height of 12.0 [m] can be simplified to the expected extreme in the single sea state with an error in the expected extreme less than 10%! But from the figure we can also see that the curve is rather steep for coefficients of 1.4 and smaller.

Varying the lifetime

By increasing the return period of sea state #2 the number of sea states #1 increases while sea state #2 still occurs only once. Again the error in the expected extreme is determined for three values of the coefficient C. The second figure shows that for larger return periods the error only slightly increases.

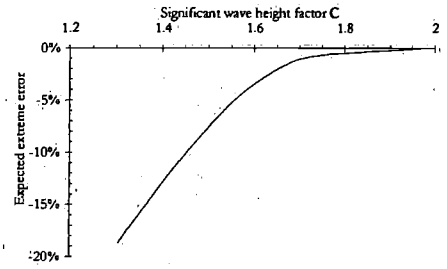

Figure 21 Variation of factor C

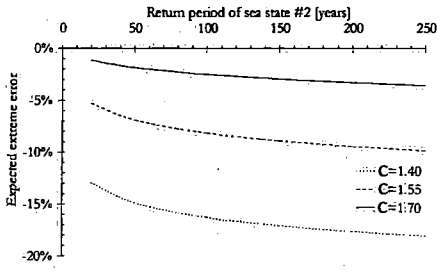

Figure 22 Variation of return period and factor C

But this simple numerical case cannot justify the reduction of a scatterdiagram to one or a few single sea states. Some other approaches are discussed hereafter.

Design extreme storm

To simplify the amount of nonlinear calculations one can model a design storm instead of a full nonlinear long-term assessment. This approach is a drastic simplification but plausible under the assumption that the maximum responses occur in the severest storm. This approach is common practice within the offshore discipline where the above assumption is valid as a large part of the offshore structures are bottom-fixed. For this the largest wave usually induces the largest load.

For such a design storm an expected significant wave height is required to occur in a prescribed number of years. For example the lifetime significant wave height is the expected significant wave height to occur in the lifetime of the vessel, e.g. *the 20-years significant wave height*. With a scatter diagram or a mathematical description of the wave environment this significant wave height can be determined.

But of course this extreme significant wave height is a stochastic variable. What is the influence of this variability on the response extreme distribution and secondly what is the

influence of the wave period? In order to assess this we need the joint distribution of the extreme response, the significant wave height and the wave period, $g(y_a, H_s, T_z)$. The resulting marginal distribution of the extreme response is,

$$g(y_a) = \int_0^\infty \int_0^\infty g(y_a, H_s, T_z) dH_s dT_z \tag{4.8}$$

This can be rewritten as,

$$g(y_a) = \int_0^\infty \int_0^\infty g(y_a | H_s, T_z) g(H_s) f(T_z | H_s) dH_s dT_z \tag{4.9}$$

Where the extreme significant wave height distribution is calculated using order statistics applied to the long-term significant wave height distribution:

$$\begin{aligned} &G(H_s) = F(H_s)^n \\ &\text{with} \\ &n = \frac{\text{return period} \times 365 \times 24}{T_{\text{short term}}} \end{aligned} \tag{4.10}$$

An example is given of the Weibull distribution for the Northern North Sea, see Bitner-Gregersen (1999). The 20-years significant wave height distribution is shown below.

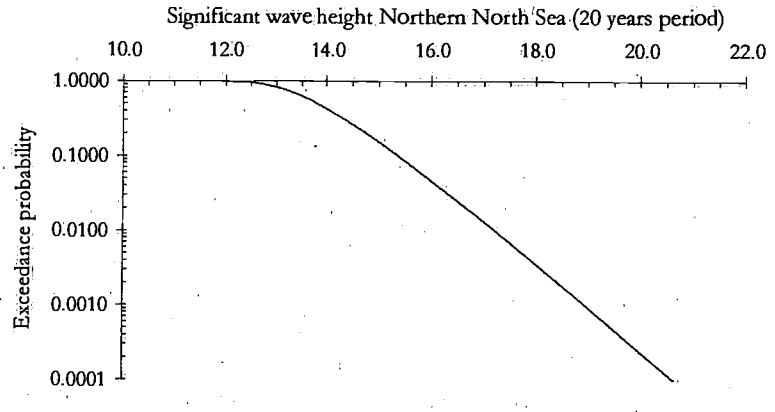

Figure 23 20-years significant wave height distribution for the Northern North Sea

Another approach to formulate a design storm was published by Winterstein et al (1993). They used an inverse FORM to establish environmental contour lines which corresponds to certain probabilities of occurrence, e.g. the 100-year value. The great advantage is that the environmental conditions are decoupled from the response model. But the same critical aspect holds here that the largest response does not necessarily have to occur in one of the conditions on the contour line but within the this area.

It is important to recognise that the procedure to restrict the analyses to the environmental conditions of a design storm is disputable as vessel dynamic effects are not appropriately accounted for. Maybe design storms are well applicable for offshore structures but for floating structures with or without forward speed the severest storm does not necessarily induce the largest responses. In the following a method is therefore presented, which does consider the dynamic behaviour properly and is suitable to reduce the full show of calculations of equation (4.3) to a limited amount of calculations.

Coefficient-of-Contribution method

A practical approach to identify the sea states and operational conditions, which have a significant contribution to the extremes, is by calculating the 'Coefficient-of-Contribution' (CoC), see e.g. Larsen and Passano (1991). A full linear approach, as described above, is conducted to calculate the expected lifetime linear extreme response. Next the contribution of every sea state is calculated to the total exceedance probability for this value. The formula for the CoC thus becomes,

$$CoC(H_s,T_z,\mu,V_s,L_c) = \frac{w_{H_s,T_z,\mu,L_c,V_s} Q_{ST}\left(Y_{lifetime}\middle|H_s,..,V_s\right) f(H_s,T_z) f\left(\mu,V_s\middle|H_s,T_z,L_c\right) f(L_c) dV_s d\mu dL_c dT_z dH_s}{Q_{LT}\left(Y_{lifetime}\right)} \tag{4.11}$$

By formulating a criterion, e.g. $CoC > a$, the scatter diagram and operational conditions can be reduced to a small subset of sea states and operational conditions, which is of most importance for the extreme responses. For this subset the amplitude distribution can be calculated using the same equation as (4.3) but with adjusted weigh factors and sea state probabilities. Thus equation (4.3) becomes,

$$F'_{LT}(y_a) = \int\int\int\int_{CoC>a} w'_{H_s,T_z,\mu,L_c,V_s} F_{ST}\left(y_a\middle|H_s,T_z,\mu,L_c,V_s\right) f'(H_s,T_z) \; f'\left(\mu,V_s\middle|H_s,T_z,L_c\right) f'(L_c) dV_s d\mu dL_c dT_z dH_s \tag{4.12}$$

The sea state, operational and loading condition probabilities have to be changed such that their integration becomes one, otherwise $F'_{LT}(y_a)$ will not yield unity.

$$f'(H_s,T_z)=\frac{f(H_s,T_z)}{\iint\limits_{CoC>a} f(H_s,T_z)dH_s dT_z} \tag{4.13}$$

$$f'(\mu,V_s|H_s,T_z,L_c)=\frac{f(\mu,V_s|H_s,T_z,L_c)}{\iint\limits_{CoC>a} f(\mu,V_s|H_s,T_z,L_c)dV_s d\mu} \tag{4.14}$$

$$f'(L_c)=\frac{f(L_c)}{\int\limits_{CoC>a} f(L_c)dL_c} \tag{4.15}$$

Lastly, the average period for this subset is different from the average period of the whole scatterdiagram thus the weigh factors should be changed accordingly.

$$\frac{1}{\bar{T}_2'}=\int\iiint\limits_{CoC>a}\iint \frac{1}{T_2|H_s,T_z,\mu,L_c,V_s} f'(\mu,V_s|H_s,T_z,L_c)f'(H_s,T_z)f'(L_c)dV_s d\mu dL_c dT_z dH_s \tag{4.16}$$

With the resulting amplitude distribution from equation (4.12) the extreme distribution can be calculated by applying order statistics with the number of cycles in this subset during the lifetime of the vessel given by,

$$n'_{LT}=\frac{T_{lifetime}\iint\limits_{CoC>a} f(H_s,T_z)f(\mu,V_s|H_s,T_z,L_c)f(L_c)dV_s d\mu dL_c dT_z dH_s}{\bar{T}_z'} \tag{4.17}$$

The resulting extreme distribution becomes then,

$$g'_{LT}(y_a)=n'_{LT}\cdot f'_{LT}(y_a)\cdot\left[F'_{LT}(y_a)\right]^{n'_{LT}-1} \tag{4.18}$$

The procedure to reduce the amount of sea states in a scatterdiagram to a small subset was investigated by Sagli (2000) for the calculation of lifetime expected extremes. She showed with a case-study for the vertical bending moment in the S-175 containership that the error in the expected lifetime extreme was small when considering a subset of the scatterdiagram. Even considering only one sea state, corresponding to the sea state with the maximum CoC, resulted in an error of only 10%.

EMLER implementation

The next step is to introduce the EMLER technique. The basic assumption of the response conditioning technique is that the linear model is a good identifier of extreme events. Thus the nonlinear extreme is a correction of the linear extreme. When using the CoC method the same assumption is applied; based on the linear model the amount of calculations is reduced to a small subset. The implementation of the EMLER technique in a CoC reduced calculation scheme would thus be a logical procedure. Different approaches are possible to do this.

Option 1
Having established a subset of sea states and operational conditions one can discretise this set and for every case an EMLER calculation can be applied. Next the integration of equation (4.12) is carried out with the linear amplitude distribution, $F_{ST}\left(y_a \middle| H_s, T_z, \mu, L_c, V_s\right)$, transformed to the nonlinear distribution by using equation (2.50).

Option 2
With the CoC approach a scatter diagram is reduced to a subset of sea states for a given operational condition. Instead of conducting EMLER calculations for all the sea states one can simplify this by conducting only once an EMLER calculation for one sea state within the subset. With this calculation the linear-nonlinear functional relationship is obtained, which is subsequently used to transform the linear distribution for all the sea states within the subset. The question is of course: Which sea state should be chosen from this subset? One can select the sea state with the maximum CoC or one can calculate the expected sea state from the subset. Of course intermediate solutions are possible as well. For example for every 4 sea states one EMLER calculation is conducted.

Volterra model implementation

The application of the Volterra model is quite simple as well. In principal a nonlinear approximate Volterra model is identified for a specific speed, heading and loading condition but can be applied for all significant wave heights and periods. Thus for every subset of the scatterdiagram the Volterra model can be applied.

4.2 Reliability based seakeeping performance assessment

Seakeeping performance is the ability for a ship to succeed in carrying out its voyage or mission. An important precondition is deduced from this, namely it should be known what defines the success of a voyage or mission and what the criteria are. Traditionally the success is defined as a performance percentage which is simply the sum of the

performances of all the responses having an influence on the performance, where the responses have all an equal influence.

As presented in the introduction a number of observations from the standard seakeeping assessments can be made.

- Criteria are defined as hard-clipped criteria with uncertain values.
- Only the expected seakeeping performance for a voyage or mission is dealt with.
- The effect of the mutual influence of responses on the total seakeeping performance is known only for the contribution to the expected performance not regarding their correlations and the influence on the performance variance.

The first point is a crude approach, which can easily be circumvented by modelling the criterion with a probability function thus the hard-clipped characteristic is eliminated while any uncertainty of the criterion value can be modelled. The second point is quite logical as the higher the expected performance the better, but the variance is also of importance and should be minimal as possible. For example, it is of interest how often a vessel, sailing on a fixed route and a fixed schedule, cannot make its arrival time or departure and with what delay. Another important application is the heavy lift transport. In this case one single trip is planned and design values for accelerations are to be defined for the lashing of the cargo and operational assistance. This information is of greater use than a single expected performance. The third point mentioned can be of importance in the design process where design changes are possible. In this phase it can be helpful to know what the effect is of the various responses on the performance and their mutual correlation. In order to overcome these difficulties a new seakeeping performance assessment technique is presented. The basic characteristics are a probabilistic formulation of the response criteria and a voyage/mission simulation approach. A large number of simulations give sufficient statistical information to calculate the total and system performance probability functions, correlations and sensitivity factors.

4.2.1 Probabilistic response criteria

Consider a ship in a short-term sea state for which the seakeeping performance is of interest. Following the standard approach for calculating a system performance the response value is compared with the criterion. If the response value is larger, the system is supposed to be unavailable and if the response value is lower than the criterion the system is 100% available. A few examples can demonstrate that this is a rather crude approach. Consider the availability of the Vertical Launch System (VLS) on a frigate for air defence purposes. Suppose the criterion states that the VLS is available if the root mean square (RMS) of the vertical acceleration is less than 0.70. If in some sea state this value is exceeded there are still periods of time for which the RMS value is less than 0.70. If the VLS is used within such a period the system will work properly. The same reasoning can be applied for a helicopter landing operation. The landing procedure starts with the approach of the helicopter until it is next to the heli-deck. Then it moves

sidewards until it is above the deck after which it descends and is put on the deck. The time from the moment it is next to the deck until it is has landed is approximately 15 to 20 seconds. When calculating the standard deviation of the heave motion for 15 seconds periods a probability function is obtained and sketched in Figure 24. This figure was constructed for the MO-2015 frigate, see paragraph 6.2, in a short-term sea state (H_s=2.8 [m], T_z=7.4 [s]) in head waves condition at 15 knots. The standard deviation for this response is exactly 0.70 [m], so it is equal to the criterion. But from this figure we see that in 60% of the cases the standard deviation is less than the criterion and in 30% of the cases the response is even less than 70% of the criterion. Two other landing periods are shown as well to demonstrate the influence of the time period on the uncertainty. Even for a time period of one minute significant lower response values can be encountered than the average value for this sea state.

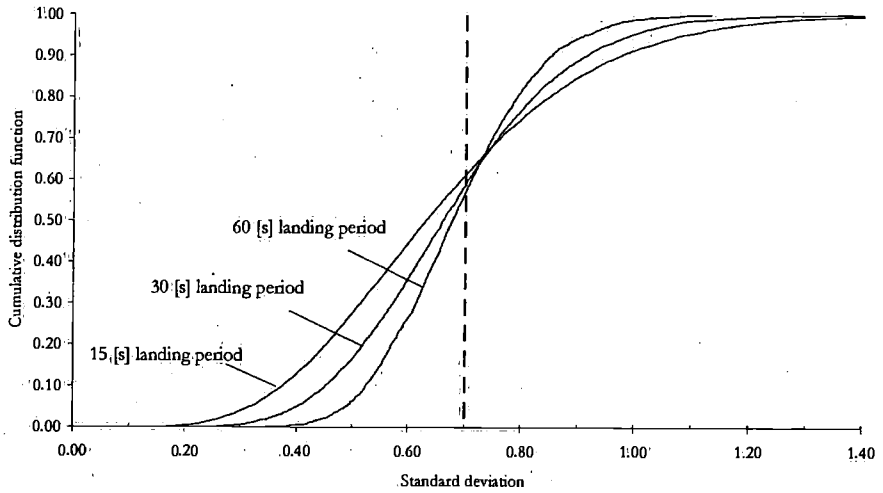

Figure 24 Probability function of std. dev. of vert. displ. at heli-deck for short time periods

Another motivation for the probabilistic modelling is also applicable. The uncertainty of the criteria values is quite large, because it is a very difficult task to define what the limiting response is. Is it 0.70 or 0.80? To take account of this uncertainty the criterion is given an uncertainty. Still it is a difficult task to formulate the criteria probability functions or criteria uncertainty. In this study no attempt has been made to establish the criteria probability functions, but arbitrary uncertainties are specified. The absolute effect of the probabilistic modelling is thus not known but with this approach it is at least possible to study the effect.

The procedure to specify criteria uncertainty distributions is as follows. First, realistic criteria, as presently used in seakeeping performance assessments, are taken and assumed

to be the mean value of the criterion distribution. Next, uncertainty is introduced by specifying a coefficient of variation,

$$CoV = \frac{\sigma_{criterion}}{\mu_{criterion}} \tag{4.19}$$

With this, the Gaussian distribution for the criterion is completely known. In the following figure a criterion probability function is pictured with a given response value. In fact two interpretations can be given. Either one can speak of availability or one speak of performance. This means the system is x% of time available or the system performs at x% of its maximum performance respectively.

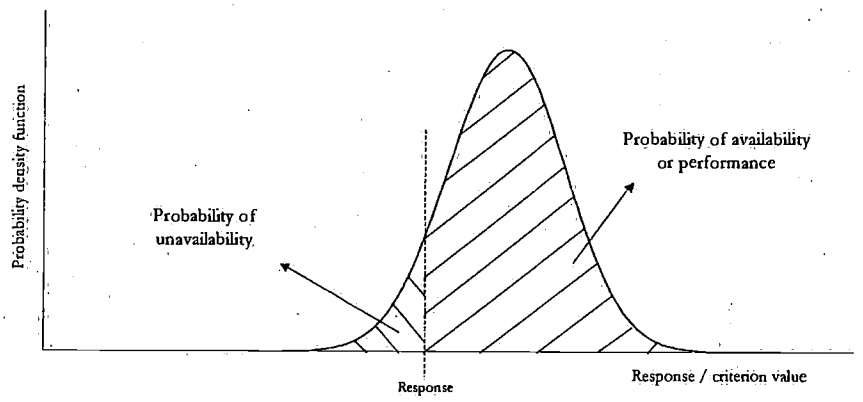

Figure 25 Ship response criterion probability function

The standard procedure to calculate the seakeeping performance is mathematically given by,

$$P = \sum_{j=1}^{N_{H_s}} \sum_{l=1}^{N_{T_z}} \sum_{m=1}^{N_{\mu}} \sum_{n=1}^{N_{system}} p_j \cdot p_l \cdot p_m \cdot w_n \cdot P\left(n \middle| H_s, T_z, \mu\right)$$

$$\text{with} \tag{4.20}$$

$$P\left(n \middle| H_s, T_z, \mu\right)_n = 100\% \quad \text{if response} < \text{criterion}$$

$$P\left(n \middle| H_s, T_z, \mu\right)_n = 0\% \quad \text{if response} > \text{criterion}$$

in case of a discrete formulation, e.g. when a scatterdiagram is used. The continuous case is given by,

$$P = \sum_{n=1}^{N_{system}} \int_{H_s} \int_{T_z} \int_{\mu} f(H_s, T_z, \mu) \cdot w_n \cdot P\left(n \middle| H_s, T_z, \mu\right) d\mu dT_z dH_s$$

$$\text{with} \qquad (4.21)$$

$$P\left(n \middle| H_s, T_z, \mu\right)_n = 100\% \quad \text{if response} < \text{criterion}$$

$$P\left(n \middle| H_s, T_z, \mu\right)_n = 0\% \quad \text{if response} > \text{criterion}$$

This can be extended by incorporating different operational modes, like Anti Air Warfare, Anti Surface Warfare etc. for warships and different ship conditions, like fully laden, ballast etc. for trading vessels. In this formula the probabilities, p_j, p_l, p_m, are known. The probabilities w_n are the weigh factors for all the systems onboard. If all systems are treated equally, this probability equals $\frac{1}{N_{system}}$. Often this is applied but is in fact not realistic. Consider the case of a combatant under air attack. It is of more importance that the air defence radars, missile control and launchers work properly than that a part of the crew is seasick. The question is of course how to estimate these weigh factors.

When applying probabilistic criteria the system performances are no longer 0% or 100% but become values between 0 and 100 percent as depicted in Figure 25. This may change the seakeeping performance.

4.2.2 Mission simulation

A mission is specified and simulated a large number of times. For every realisation of a mission the system and seakeeping performance are calculated, as explained in the next paragraph. The specification of a mission consists of the following information,

- Operation area,
- Wave spectrum type,
- Mission or voyage duration,
- Response criteria,
- Duration of short-term sea states,
- Maximum stepsize of successive significant wave heights,
- Number of mission/voyage simulation

The operation area defines the wave database. The mission or voyage duration together with the short-term sea state duration define the number of sea states per mission or voyage. The wave database can be a scatterdiagram or a mathematical description like a Weibull function for the significant wave height with a conditional log-normal distribution for the zero-crossing period. Key requirement is to be able to randomly

select sea states from the database. This is easily done when using a Weibull-conditional log-normal distribution. Randomly selecting a number, δ, between 0 and 1, the corresponding significant wave height is determined by,

$$H_s = \gamma + \alpha \left[\ln\left(\frac{1}{1-\delta} \right) \right]^{\frac{1}{\beta}} \tag{4.22}$$

While the conditional wave period is numerically determined from the following integral equation with a new random number,

$$\delta = \int_{-\infty}^{T_z} \frac{1}{\sigma_{T_z} T_z \sqrt{2\pi}} e^{-\frac{1}{2}\left(\frac{\ln(T_z)-\mu}{\sigma_{T_z}} \right)^2} dT_z \tag{4.23}$$

Here the mean and standard deviations, μ_{T_z} and σ_{T_z}, are depending on the significant wave height. As the severity of the sea is a continuous process the sequence of significant wave heights cannot randomly be chosen. In the present model a simple solution is applied. A maximum difference is specified for the significant wave height between two successive short-term sea states. The combination of a significant wave height and period gives a wave spectrum. From this point two options can be chosen, either a linear or a nonlinear path. For the linear case the wave spectrum can be used in combination with all the system transfer functions to calculate the system responses and thus the system performances. For the nonlinear case a time-domain approach is followed. An irregular wave is constructed from the wave spectrum with non-equidistant step-sizes for the frequencies. The procedure to establish these wave components is shortly explained.
The square root of the wave spectral values is integrated and the resulting area is then normalised. This normalised function is now treated as a probability density function and integrated to get the cumulative distribution function. The range of this function, 0 to 1, is divided into equidistant step-sizes. The inverse of the cumulative distribution function gives the corresponding wave frequencies. Subsequently wave amplitudes are determined for these frequencies. With this approach more wave components are modelled around the peak of the wave spectrum and no repetition of the wave signal is obtained.
A time-domain simulation is now conducted for this irregular wave using the nonlinear approximate Volterra models for the system responses and equation (3.29). The time-series are statistically post-processed to obtain the response statistics. The statistics together with the criteria distributions determine the system performances and their weighed sum the total seakeeping performance in that sea state. By averaging these performances, after all the short-term sea states for a mission or voyage have been simulated, the mission seakeeping performance is obtained.
In case of a combatant the mission duration is to be specified or in case of a merchant ship the voyage duration.

4.2.3 Reliability based mission performance assessment

The seakeeping performance as calculated according to the standard approach is one single value: the expected performance. Indeed the main goal is to optimise this to achieve a highest performance possible. But a ship's lifetime consists of voyages or in case of a warship of missions. All these voyages and missions have there own seakeeping performance and together their average will be in the long run equal to the expected performance from a standard approach. In case of warships the seakeeping performance must be high as lives can be at stake. Hence the seakeeping performance should be as high as possible for every mission. In order to study this, equation (4.21) can be applied to calculate the system performances for a mission realisation j of a given mission and the total seakeeping performance for mission j is then formulated by,

$$P_j = \sum_{n=1}^{N_{system}} w_n \cdot P_{j,n} \tag{4.24}$$

Thus the system performances $P_1 ... P_N$ become stochastic variables having a marginal distribution and range from 0 to 100 percent. The seakeeping performance distribution $F(P)$ can be calculated by integration of the joint probability function $F(P_1,...,P_N)$, which is to be determined.

$$F(P) = \int_{P_1+...} \cdots \int_{...+P_N \le P} f(P_1,...,P_N)\, dP_1 ... dP_N \tag{4.25}$$

The marginal distributions of the stochastic quantities $P_1 ... P_N$ are not known a priori nor are their correlations. But these can be determined by simulations and the joint distribution $F(P_1,...,P_N)$ therefore as well. This approach is a typical example of *uncertainty analysis*. By simulating the mission a large number of times the marginal distributions are obtained as well as the total seakeeping performance distribution and other statistical properties as sensitivity factors and correlation coefficients. This simulation procedure circumvents thus the need to establish the joint probability function $F(P_1,...,P_N)$. Having established this technique the approach can be used for a *sensitivity analysis*. In sensitivity analyses the importance of the variables $P_1 ... P_N$ for the function $F(P_1,...,P_N)$ is examined individually for fixed values.

As said, different statistical quantities can be derived from the mission simulations. If the total number of mission simulations is $N_{mission}$ the mean and variance of the total seakeeping performance as well as system performances are given by,

$$E[P] = \frac{1}{N_{mission}} \sum_{j=1}^{N_{mission}} P_j \tag{4.26}$$

$$\sigma^2 = E\left[\left(P_j - E[P]\right)^2\right] = \frac{1}{N_{mission}} \sum_{j=1}^{N_{mission}} \left(P_j - E[P]\right)^2 \tag{4.27}$$

$$E[P_l] = \frac{1}{N_{mission}} \sum_{j=1}^{N_{mission}} P_{l,j} \qquad \textit{for system } l \tag{4.28}$$

$$\sigma_l^2 = E\left[\left(P_{l,j} - E[P_l]\right)\right] = \frac{1}{N_{mission}} \sum_{j=1}^{N_{mission}} \left(P_{l,j} - E[P_l]\right)^2 \qquad \textit{for system } l \tag{4.29}$$

If the criteria are given small coefficients of variation the result of equation (4.26) is equal to the standard approach following (4.20) and (4.21). From the mission simulation approach performance correlation coefficients can be derived,

$$\rho_{l,m} = E\left[\frac{\left(P_{j,l} - E[P_l]\right)\left(P_{j,m} - E[P_m]\right)}{\sigma_l \qquad \sigma_m}\right] = \frac{1}{\sigma_l \sigma_m} \sum_{j=1}^{N_{mission}} \left(P_{j,l} - E[P_l]\right)\left(P_{j,m} - E[P_m]\right) \tag{4.30}$$

These correlations can be useful when studying a system for which different criteria are formulated, like for example the heli-deck vertical motion, velocity and roll motion.

The seakeeping performance variance, equation (4.27), can be evaluated further leading to,

$$\sigma^2 = \sum_{l=1}^{N_{system}} w_l^2 \sigma_l^2 + \sum_{l=1}^{N_{system}} \sum_{m=1}^{N_{system}} \rho_{l,m} w_l w_m \sigma_l \sigma_m \tag{4.31}$$

Thus the seakeeping performance variance is the result of all the system performance variances and their correlated contributions. This variance defines the seakeeping performance uncertainty, i.e. the larger the variance the wider the confidence interval for the mission seakeeping performance. In order to increase the performance reliability this variance should be reduced. By using equation (4.31) the influence of every system on the seakeeping performance uncertainty can be formulated in terms of sensitivity factors. To obtain one single sensitivity factor for every system the correlated parts should be divided up. The most reasonable approach is to weigh the joint sensitivity factors by their contributions, i.e. $w_l \sigma_l$ and $w_m \sigma_m$. This results in the following sensitivity factors,

$$\alpha_j^2 = w_j^2\left(\frac{\sigma_j}{\sigma}\right)^2 + \sum_{\substack{l=1 \\ l\neq j}}^{N_{system}} 2\rho_{j,l}w_j w_l \frac{\sigma_j\sigma_l}{\sigma^2}\left(\frac{w_j\sigma_j}{w_j\sigma_j + w_l\sigma_l}\right) \tag{4.32}$$

But how to interpret the resulting seakeeping performance probability functions for the individual systems and the total performance? Consider a ASW mission for a frigate. Basically there are two results possible: either the submarine is hit or not. This seems in contrast with the stochastic performance as presented here. But this is not the case, because a performance less than 100%, does not rule out that the submarine is not hit. During every mission there is a chance that the submarine is hit, even in severe conditions. The resulting seakeeping performance for that mission quantifies the likelihood that a submarine can be hit under those specific conditions. By combining all the mission simulations the quantification of hitting the submarine is obtained for the mission to be carried out.

5 Numerical application of presented methods compared with existing procedures

The first two chapters presented detail theoretical aspects of the response conditioning technique and the approximate Volterra modelling technique. The (E)MLER technique can be used to calculate expected nonlinear extreme responses or the amplitude or extreme response distributions, while the nonlinear approximate Volterra modelling technique is suitable for nonlinear response simulations and subsequently their statistical properties.

Both methods are now applied to different cases in order to evaluate their characteristics. It is not the purpose of the thesis to fully investigate the long-term assessment, although discussed in the previous chapter. The two novel techniques of the first chapters need to be applied and evaluated furthermore and then gradually be applied in full assessments. Key questions to study in this chapter are,

- How well can the response conditioning technique, MLER method, predict expected extremes?
- Moreover, how well can the extended conditioning technique, EMLER method, predict the amplitude and extreme probability functions?
- How accurate are the approximate Volterra models in reproducing nonlinear statistics?
- What are the characteristics of the reliability based seakeeping assessment technique?

First the response conditioning technique will be investigated by two cases studies. The hull girder bending moment in a FPSO and a frigate are subject of interest. Additionally the directional version of the response conditioning technique is applied to the vertical bending moment in a containership in a cross sea.

The second paragraph gives a detailed study on the identification and simulation aspects for both approximate Volterra models. The statistics of the vertical bending moment in a frigate are used as case-study.

The third paragraph deals with the seakeeping performance issue. A case is presented regarding the calculation of nonlinear roll motions using the response conditioning technique. Furthermore an application of the reliability based seakeeping performance assessment using nonlinear approximate Volterra models is presented. A simplified ASW mission for a frigate on the North Atlantic is used as case.

5.1 Extreme hull girder bending moment assessment

The vertical bending moments in a FPSO and a frigate are studied. For both cases a large amount of nonlinear simulations was conducted in order to obtain sufficient nonlinear statistical data. The MLER and EMLER approaches are used together with some existing techniques. These are first described after which both cases are presented.

5.1.1 Existing calculation procedures for nonlinear extreme responses

The (E)MLER method is numerically compared with several existing procedures. First of all the linear frequency domain approach is applied as described in paragraph 2.3. Secondly, two fitting procedures are applied. The first one is based on a Hermite polynomial expansion of the standard Gaussian variable. The great benefit of this approach is that it only needs estimates of the first four statistical moments. Subsequently estimates are obtained for the nonlinear amplitude and extreme probability distributions. The second fitting technique is the Gumbel distribution for the extreme value distribution. The last technique applied is the use of regular design waves for quick estimates of expected nonlinear extremes. A short summary is given below of these procedures.

Hermite transformation model

The Hermite model, as first introduced by Winterstein (1988), assumes that a nonlinear response process $y(t)$ can be described by a Hermite polynomial series of a standard Gaussian process $U(t)$. This functional relationship is modelled as,

$$y = g(U) = \bar{y} + \sigma_y \kappa \left[U + c_3 \left(U^2 - 1 \right) + c_4 \left(u^3 - 3u \right) \right]$$

with (5.1)

$$\kappa = \frac{1}{1 + 2c_3^2 + 6c_4^2}$$

In this formulation the coefficients c_3 and c_4 depend on the skew and kurtosis of the nonlinear response. The functional relationship must be monotone increasing function. The same condition was applied to the functional relationship as established with the EMLER method, see paragraph 2.4. Two matching procedures for the coefficients c_3 and c_4 were used. Torhaug (1996) presented matching results based on an unpublished report by Winterstein et al (1994). These formulations were based on an empirical fit:

$$c_4 = \frac{1 + 1.25\sqrt[3]{\alpha_4 - 3} - 1}{10} \left[1 - \frac{1.43\alpha_3^2}{(\alpha_4 - 3)} \right]^{1 - 0.1\alpha_4^{0.8}}$$

$$c_3 = \frac{\alpha_3}{6} \left[\frac{1 - 0.015|\alpha_3| + 0.3\alpha_3^2}{1 + 0.2(\alpha_4 - 3)} \right] \tag{5.2}$$

Mansour and Jensen (1995) presented exact, numerically computed results,

$$c_4 = \frac{\sqrt{1 + \frac{3}{2}(\alpha_4 - 3)} - 1}{18} \qquad c_3 = \frac{\alpha_3}{4 + 2\sqrt{1 + \frac{3}{2}(\alpha_4 - 3)}} \tag{5.3}$$

With the knowledge of the first four statistical moments of the nonlinear process the statistics of the response can be calculated using the Hermite transformation model as the statistics of the Gaussian process is known.

Gumbel extreme value distribution

Often initial distributions can be written in a general form,

$$F(y_a) = 1 - e^{-q(y_a)} \tag{5.4}$$

With $q(y_a)$ a positive real-valued function. When applying order statistics, as described in paragraph 2.3, to this initial distribution function the Gumbel extreme value distribution is obtained, Gumbel (1958).

$$G(Y_n) = e^{-e^{-\alpha_N(Y_N-u_N)}}$$

with

$$\alpha_N = \frac{\pi/\sqrt{6}}{\sqrt{E\left[\left(Y_N - E[Y_N]\right)^2\right]}} \qquad u_N = E[Y_n] - 0.5772\frac{\sqrt{6}}{\pi}\sqrt{E\left[\left(Y_N - E[Y_N]\right)^2\right]} \tag{5.5}$$

Thus we need estimates of the expected extreme as well as the variance of the extreme response. This implies that a number of simulations are required to get a reasonable estimate of these statistical moments. McTaggart (1999) applied the Gumbel distribution to the roll motion of frigates and concluded that at least 10 simulations were required to obtain a reasonable estimates of the mean and the variance.

Regular design wave

By simulating a regular wave with a nonlinear program an estimate of the expected nonlinear extreme can be obtained at low computational costs. Two approaches are used in the cases, which are subsequently presented. The first one starts by calculating a linear expected extreme. By dividing this value by the peak value of the transfer function a wave amplitude is obtained. Next this wave amplitude is simulated with the wave frequency of the transfer function peak as a regular wave. Henceforth this approach is called *Regular wave I.* The second approach calculates the expected extreme wave amplitude of the wave spectrum, which is simulated as a regular wave with the wave spectral peak frequency. This procedure is called from now on *Regular wave II.*

5.1.2 Vertical wave bending moment in a FPSO tanker

The vertical bending moments at st. 10 and st. 15 in a 100.000 dwt. FPSO tanker have been studied as first case to evaluate the (E)MLER technique. Bitner-Gregersen et al (1995) presented for the Northern North Sea a 3 parameter Weibull function for the significant wave height with a conditional log-normal distribution for the wave period. Using this information the 20 years storm was calculated and modelled by a JONSWAP spectrum. The peak-enhancement factor was set to 3.3. The table below presents the spectral characteristics for two other return periods as well.

Return period	Significant wave height [m]	Zero-crossing period [s]
20-years	13.5	11.2
50-years	14.3	11.5
100-years	14.8	11.6

Table 3 Storm conditions Northern North Sea

As the tanker is turret-moored the prevailing wave heading will be head waves. This situation was therefore adopted for this case and the vessel was free to heave and pitch with the turret forces not influences the first order motions or the global loads.

A total of 200 nonlinear simulations of 1-hour (ocean data) were conducted with the programs from appendix B.2 and B.3. Every hour another realisation of the spectrum was generated. This gives a large amount of data, which provides accurate predictions of statistical moments, expected 1-hour extremes and probability functions. It should be noted that the comparison of the Hermite models in this case-study is not completely fair as they use the first four statistical moments as calculated from the entire data-set of 200 hours. In a real application only a short simulation of say 3 hours will be done to get estimates of these statistical moments. The same reasoning can be applied to the Gumbel fit as this fit is based on the mean and variance of the 200 1-hour extremes.

First the calculation of the expected extreme to occur in 1 hour is studied. In the chart below the various methods are listed horizontally while their expected extreme estimates are vertically shown. The average of the 200 estimates from the irregular simulations is set to one and the others are correspondingly normalised. The linear predictions give large underestimated values. The linear frequency domain result is equal to the time domain result. This was done to check for the expected extreme formulation from equation (2.45). The other methods all perform well except for the *Regular wave II* approach.

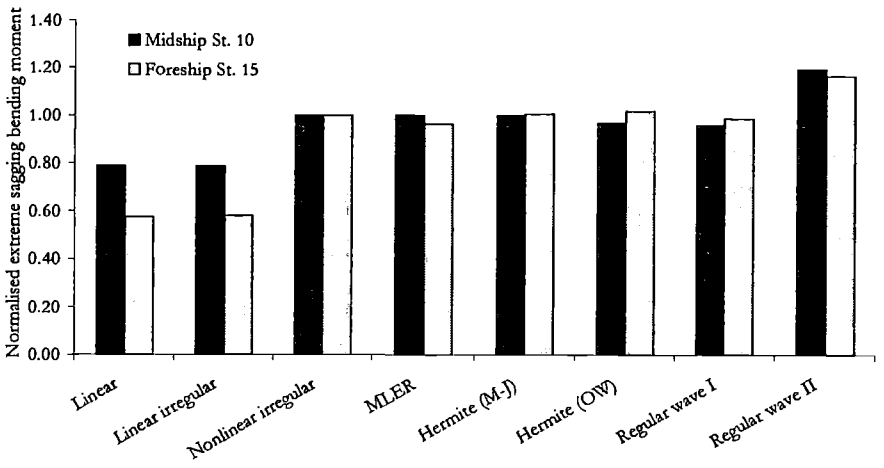

Figure 26 Expected 1-hour extreme sagging bending moment

Secondly the amplitude probability distributions are calculated with the EMLER method and the Hermite models. Below these are compared with the curves from the 200

irregular simulations. All three methods perform well with only a slight difference for the Hermite models for the foreship bending amplitude distribution.

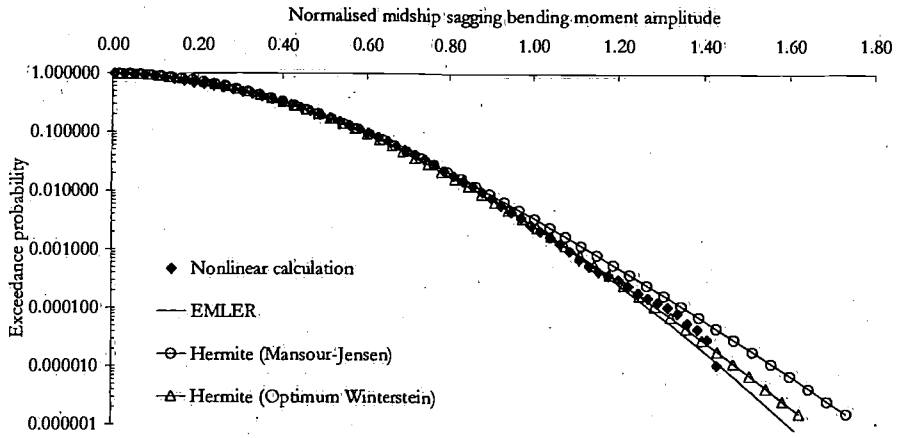

Figure 27 FPSO midship sagging bending moment amplitudes

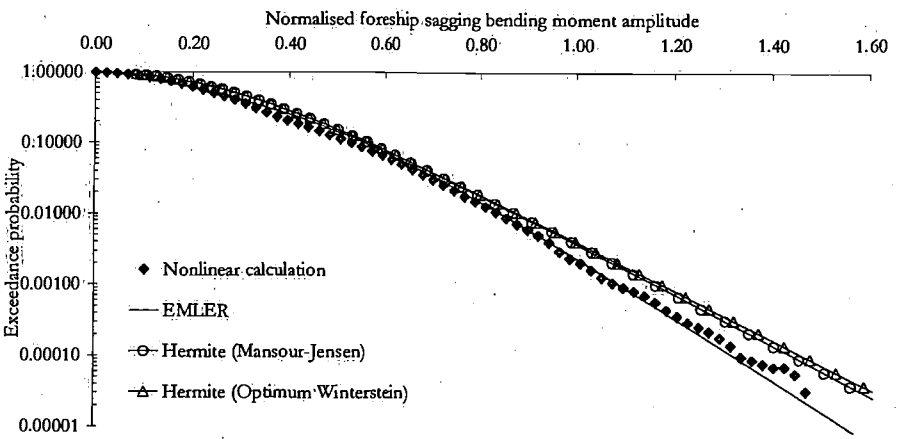

Figure 28 FPSO foreship sagging bending moment amplitudes

From the 200 1-hour extremes an estimate is made of the 1-hour extreme probability distribution, which is compared with the EMLER method, Hermite model and a Gumbel fit. Good results are obtained for the EMLER and Gumbel fit. Both Hermite fits perform somewhat less but the trend is good.

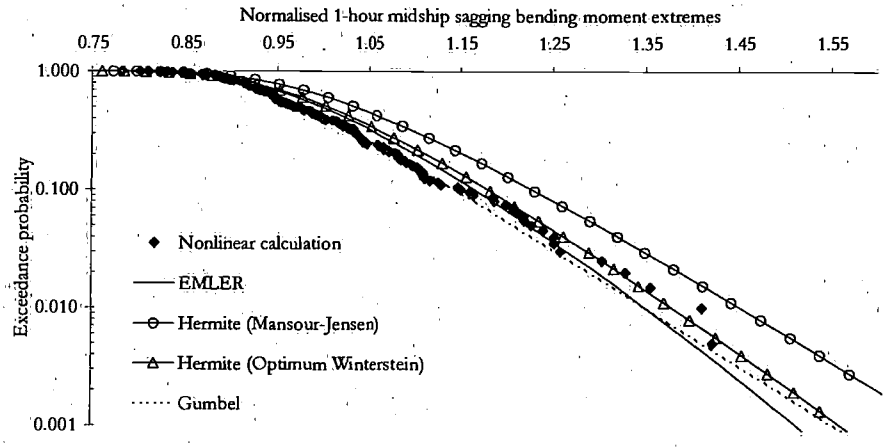

Figure 29 FPSO midship sagging bending moment extremes

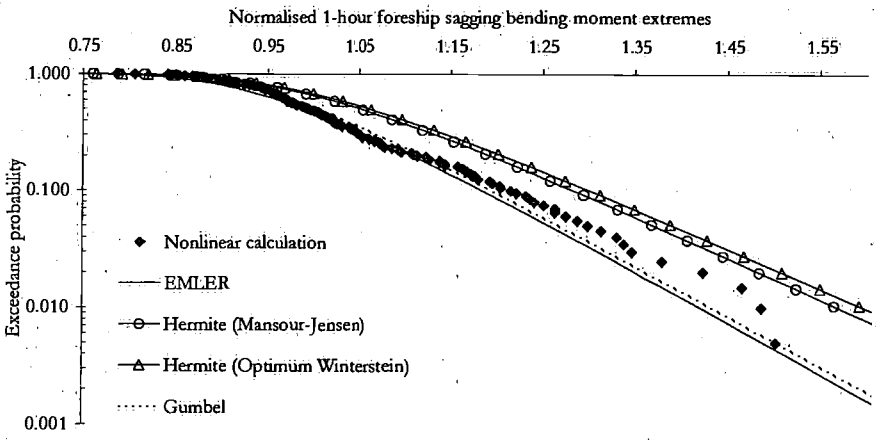

Figure 30 FPSO foreship sagging bending moment extremes

In offshore engineering often a 50 or 100-years storm is modelled as a design sea state. This originates from the application to fixed platforms as there the largest wave causes the largest load. The spectral parameters are listed in Table 3. These two storm conditions have been used here as well with the MLER technique and their expected extremes for the midship bending moment are shown in the figure below. Logically these values are somewhat larger than the lifetime expected extreme but not much. From a point of safety it does add only a few percent safety margin. But actually the safety is

defined by the overlap of the tail of the load distribution and the distribution of the ultimate hull girder capacity. The argumentation to conduct calculations or experiments in a 100-years storm is therefore weak.

In addition an extra curve is plotted based on the technique as presented in paragraph 4.1. The extreme significant wave height to occur in 20 years is modelled as a stochastic variable. The extreme responses become 5 to 10% larger.

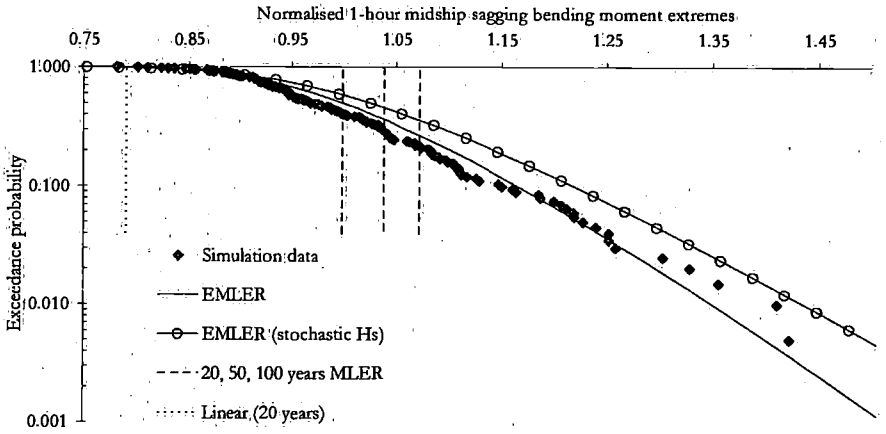

Figure 31 FPSO midship sagging bending moment extremes

More appropriate than modelling expected extreme storms is to confine the calculations to those sea states which contribute significantly to the extreme responses. By calculating the coefficient of contribution such a region can be established as described in paragraph 4.1. As an example the difference between the coefficient of contributions for the 20-years expected extreme wave amplitude and extreme bending moment are calculated. The contourplots for these two cases are shown below together with the design sea states of Table 3 and the steepness limit as proposed by DNV (2000). Clearly are different contours visible, from which we can conclude that it is indeed more appropriate to define design sea states using the coefficient of contribution approach for the response. Moreover the three design sea states are critical considering the steepness limit.

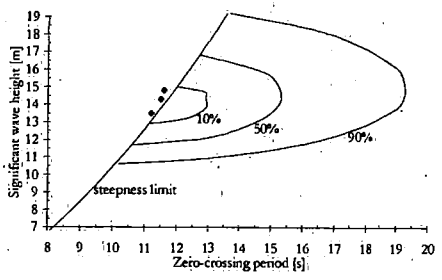

Figure 32 Contourplot of CoC for extreme wave

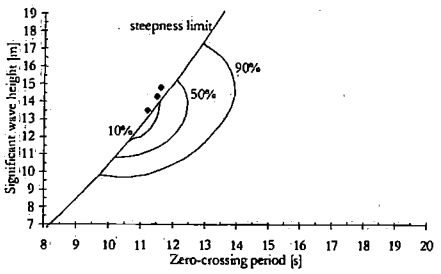

Figure 33 Contourplot of CoC for extreme bending moment

5.1.3 Vertical wave bending moment in a navy frigate

The case with the FPSO as described in the previous paragraph was a moderate test-case as the amount of nonlinear behaviour was mild although the differences between the linear and nonlinear expected extremes were considerable. The present paragraph presents therefore a test-case with a frigate in a severe sea state. The amount of bow flare is larger and the vessel has forward speed. Consequently the nonlinearities become more important.

The vessel under investigation is a frigate with a deplacement of 3400 tons. It sails at 18 knots in head waves of sea state 5, described by STANAG 4194. This sea state is modelled by a modified Pierson-Moskowitz spectrum with a significant wave height of 4.3 [m] and a zero-crossing period of 7.4 [s].

For this case a total of 100 nonlinear simulations of 1-hour (ocean data) were conducted. First we assess the expected 1-hour extreme predictions. The chart shows the predictions for the midship and foreship for various methods. Again the bars are normalised by the average of the 100 extreme values from the irregular simulations. The MLER method performs well. Both Hermite fits give also good predictions. Though *Regular wave I* performed well for the FPSO it does not for the foreship of the frigate. Also in contrast to the FPSO is the performance of *Regular wave II*, which gives good results for the midship and reasonable results for the foreship.

The reason that the *Regular wave I* approach shows a rather unpredictable behaviour is most likely caused by the shape of the transfer functions. In Figure 35 the vertical bending moment transfer functions for the frigate are shown. Both are normalised by their maximum values because of confidentiality reasons. The foreship transfer function has a much wider character than the midship transfer function. And although one can identify a maximum around 0.90 [rad/s] it is not a clear peak and other frequencies will

contribute significantly to the response spectrum. Thus it makes sense that the expected extreme, thus calculated, is far too low.

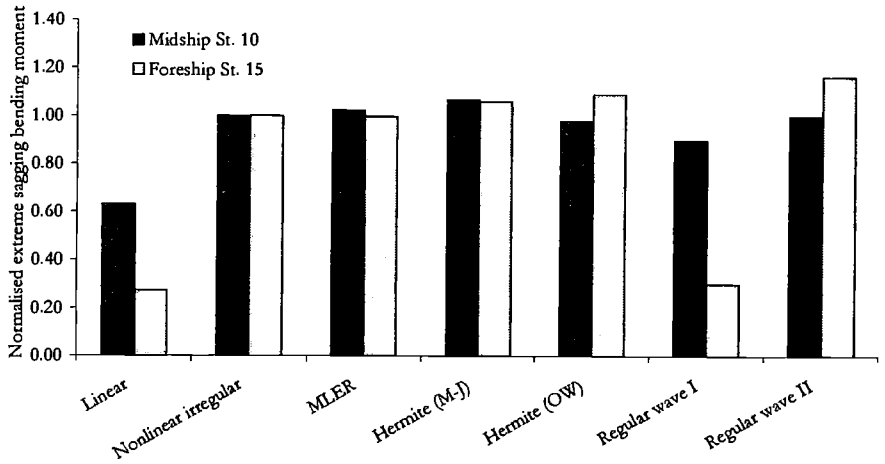

Figure 34 Frigate expected 1-hour extreme sagging bending moment

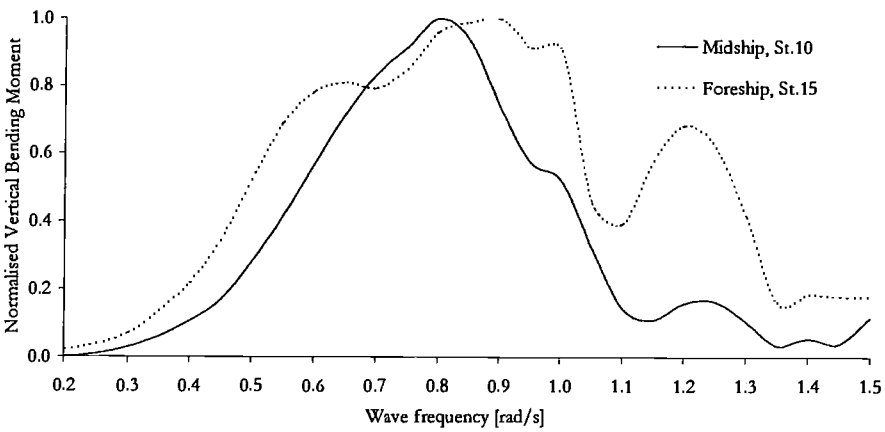

Figure 35 Normalised bending moment transfer function

The amplitude distributions are shown hereafter and show considerable different result than for the FPSO case. Despite the fact that the Hermite models gave good expected extreme predictions they fail to predict the tail of the amplitude distribution. For

responses larger than the expected extreme a pronounced bend is seen in the amplitude distribution curves. These bends are very well predicted by the EMLER method.

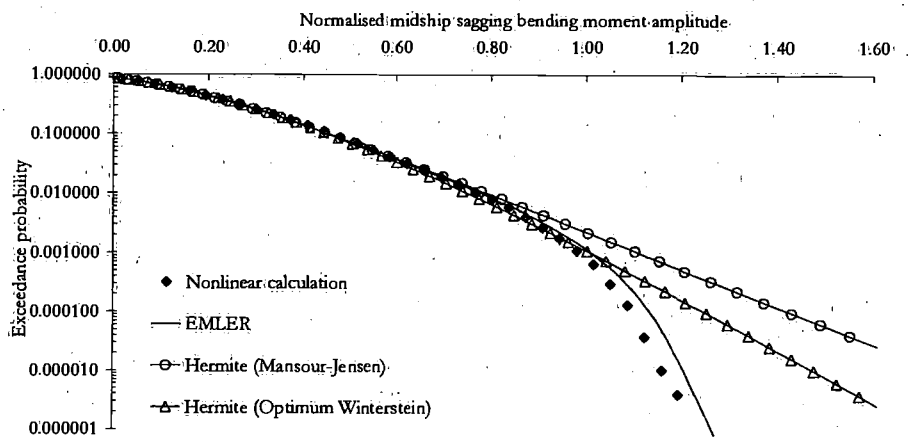

Figure 36 Frigate midship sagging bending moment amplitudes

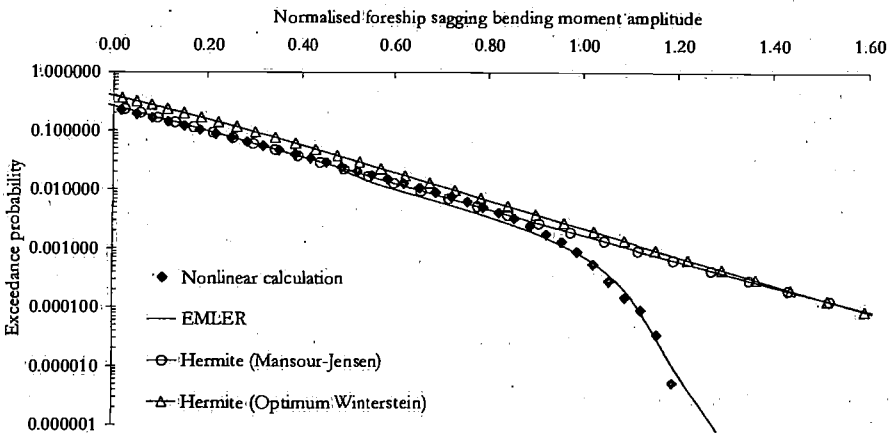

Figure 37 Frigate foreship sagging bending moment amplitudes

As the tail of the amplitude distribution showed such a pronounced bend the extreme probability function will be affected by this very much. This is clearly seen in the two next figures. The Hermite models fail to predict the behaviour of the extreme response. We can conclude that the sole possession of the first four statistical moments is not

sufficient to predict the extreme distributions. Again the EMLER method performs well and so does the Gumbel fit. And it is obvious that the Gumbel distribution is a fit technique as it does not capture the shape of the data correctly.
Of course it is important to realise that this a numerical case-study and it is to be seen how well the nonlinear program can predict the behaviour of the ship in these extreme cases.

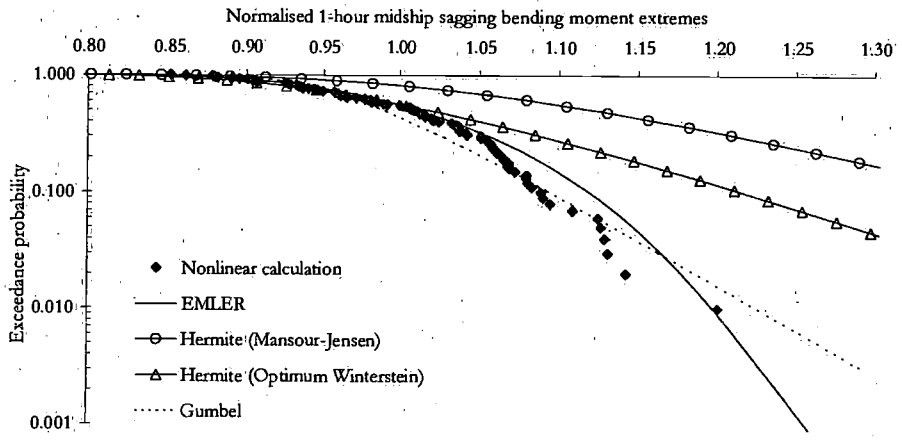

Figure 38 Frigate midship sagging bending moment extremes

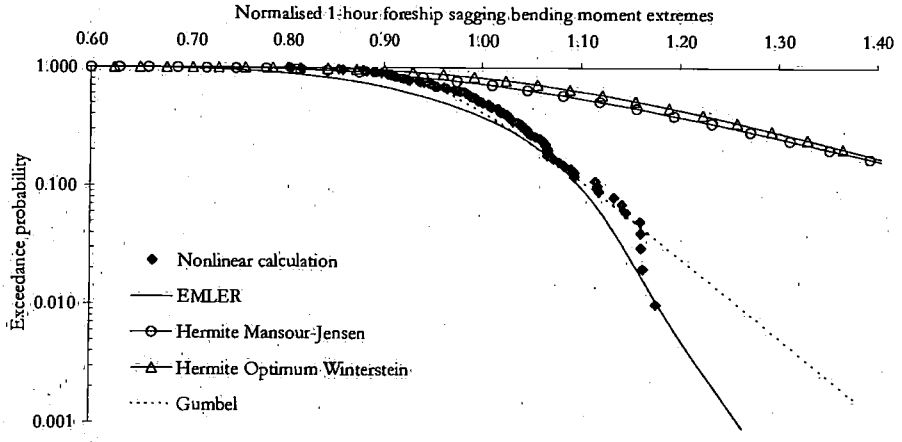

Figure 39 Frigate foreship sagging bending moment extremes

5.1.4 Vertical wave bending moment in a containership in a cross-sea

A directional sea has been modelled to assess the theoretical model of the Directional EMLER method. A containership of 270 metres long and a deplacement of 63.000 tons was used to study the sagging bending moments in waves coming from distinct directions, i.e. 180 and 150 degrees (head and bow waves). For both directions a Modified Pierson-Moskowitz spectrum was modelled with a significant wave height of 5.0 metres and a wave period of 9.5 seconds. A nonlinear irregular simulation of 1 hour and 45 minutes was conducted with the 3D nonlinear DNV-SWAN code, see Adegeest (2000). From this the sagging amplitude probability function was derived. Next the program was used in its linear mode to calculate the linear transfer functions. With these functions the linear amplitude distribution was calculated as well. Secondly these transfer functions were used to construct a directional conditioned incident wave using the Directional MLER technique, as outlined in paragraph 2.5. A total of 7 conditioned simulations were done and used to transform the linear distribution to a nonlinear distribution. The results are shown in Figure 40. For such a strong directional case the Directional EMLER result can be considered remarkably good.

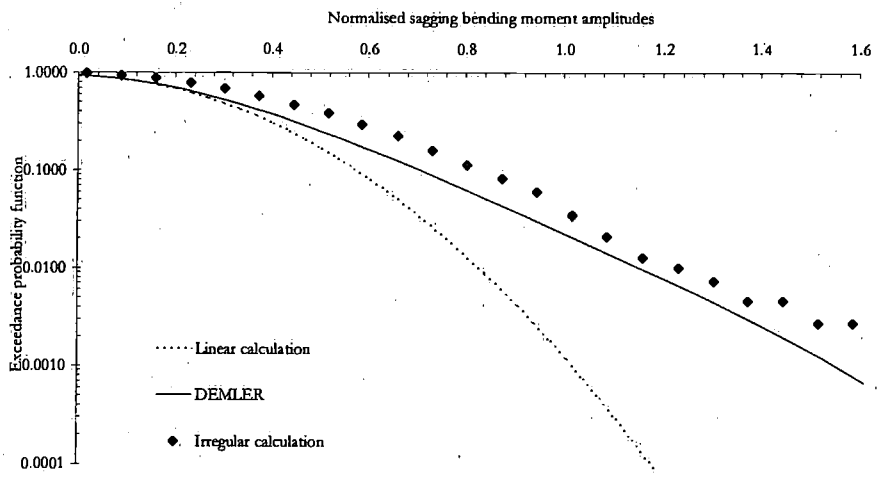

Figure 40 Sagging amplitude distribution in a cross-sea

5.2 Numerical case-study of both Volterra models

In order to assess the characteristics of both nonlinear approximate Volterra models a numerical case-study is performed. Both the identification and the simulation of the models is investigated and described in subsequent paragraphs. For the case-study the

midship vertical bending moment in a frigate is used. The vessels sails in head waves at 12 knots. Other details of the frigate are described in paragraph 6.2.

5.2.1 Identification assessment of the nonlinear approximate Volterra models

The identification of both nonlinear approximate Volterra models is investigated by varying several identification aspects. The assessment of the identification process is done with respect to the following criteria.

- Stability of the identification process
  With stability is meant that a change of the identification process does not dramatically change the identified transfer functions. The identification process should be robust.
- Uniqueness of the identified transfer functions
  If different input is given the output transfer function should be more or less identical.
- Efficiency of the identification process
  The identification should be easy and preferably be designed as a 'black-box for a convenient application of the technique. The application of the technique will be hampered if considerable expertise is required. Secondly, only limited computational costs are allowed for identification in order to benefit most of the low computational costs of the Volterra model simulation.

In order to assess these criteria a case-study is conducted and several aspects have been varied. The variations comprise,

- Spectral analysis variation for the Model I identification.
  The spectral identification procedure for Model I uses Welch's averaged periodogram method, see Welch (1967). A short description is given in appendix C.1. For the present case three window sizes have been used, 256, 512 and 1024 datapoints. While the sampling frequency was 10 [Hz].
- Sea state variation for Model I identification
  Three sea states have been simulated to obtain 3 hours irregular data. These sea states are of the modified Pierson-Moskowitz type with the following characteristics:
  Sea State I: Hs=2.5 [s], T_z=7.5 [s]
  Sea State II: Hs=3.7 [s], T_z=7.5 [s]
  Sea State III: Hs=5.5 [s], T_z=7.5 [s]
- Wave amplitude variation for Model II identification
  Three series of regular waves have been simulated with the following amplitudes, 2.0, 2.5 and 3.0 [m]. The wave frequencies range from 0.15 to 1.31 [rad/s] with a stepsize of 0.02 [rad/s].

- Volterra order variation for Model II identification
  The Volterra model II is identified for 2nd, 3rd, 4th and 5th order.

Model I identification

The Volterra kernels $A_1(\omega), A_2(\omega), A_3(\omega)$ are identified for the three sea states and for the three window sizes. The resulting kernels are pictured in Figure 42 to Figure 50. The x-axes are differently chosen as the second and third kernel act on the squared and cubic wave. The wave spectrum and the spectra of the squared and cubic wave are shown in the following figure. From this it is clearly seen that the ranges are different. The maximum encounter frequency in the wave train is 2.31 [rad/s]. Thus the second and third order maximum frequencies are 4.62 and 6.93 [rad/s] respectively.

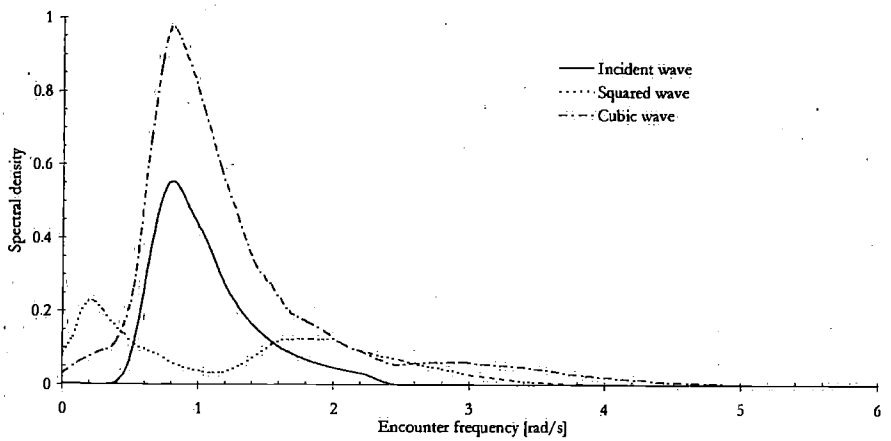

Figure 41 Incident, squared and cubic wave spectrum for H_s=2.5 [m], T_z=7.5 [s]

When studying the first order kernel, $A_1(\omega)$, the differences between the three sea states and between the windows is not large and they are quite similar to the linear transfer function. The smallest window size does give a smooth function but it is also wider, especially between 0.40 and 0.80 [rad/s]. For the second kernel major differences are seen both for the three sea states as well as for the window sizes. A window size of 1024 datapoints does not give a smooth transfer function prediction. But for the smaller window sizes the transfer function is still not uniquely determined between 0.60 and 1.60 [rad/s]. Maybe this is due to the fact that the squared wave spectrum does not have much energy in this frequency band. Outside this band $A_2(\omega)$ is consistently determined. For the third kernel the window size of 1024 datapoints is also too large. No smooth transfer function is obtained. Nor do the other window sizes give consistent transfer function predictions for the frequency range from 0.00 to 2.40 [rad/s]. The

pronounced hump around 2.80 [rad/s] is well predicted by the three applied window sizes.

The identification procedure for Model I is quite burdensome and is not a simple black-box procedure. First of all the irregular simulations require quite some computation time. In the present case a 3 hours simulation was conducted but less can be acceptable as Figure 51 to Figure 53 demonstrate. For the first kernel a simulation of 60 minutes is sufficient but for the second kernel quite large changes are seen for the frequency range of 0.60 to 1.60 [rad/s]. Equally the third kernel is not uniquely determined for the range of 0.00 to 2.40 [rad/s].

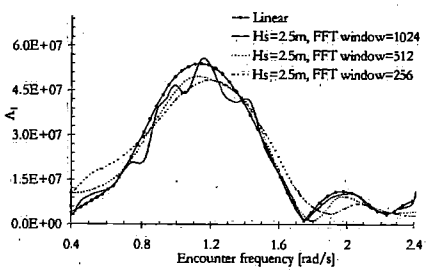

Figure 42 $A_1(\omega)$, Sea state I

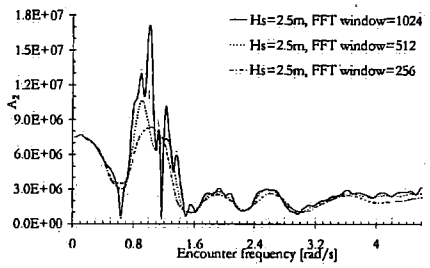

Figure 45 $A_2(\omega)$, Sea state I

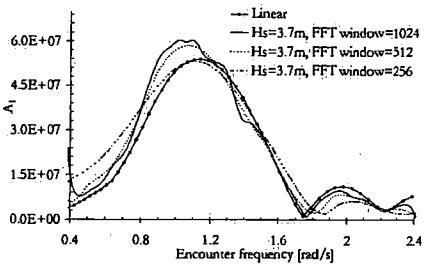

Figure 43 $A_1(\omega)$, Sea state II

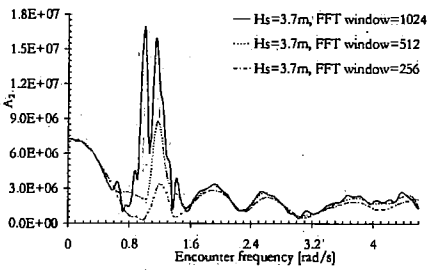

Figure 46 $A_2(\omega)$, Sea State II

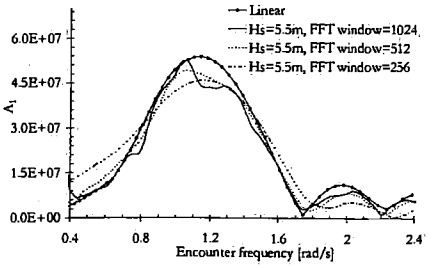

Figure 44 $A_1(\omega)$, Sea State III

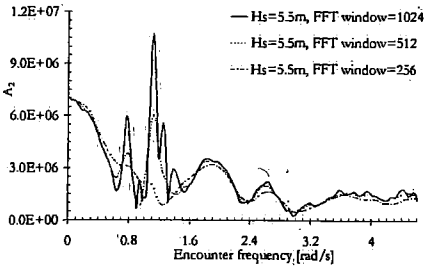

Figure 47 $A_2(\omega)$, Sea State III

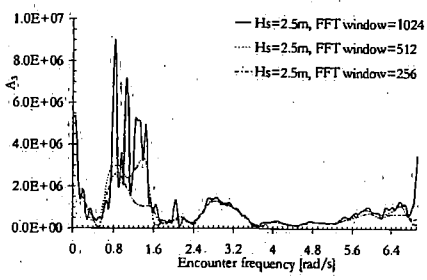

Figure 48 $A_3(\omega)$, Sea State I

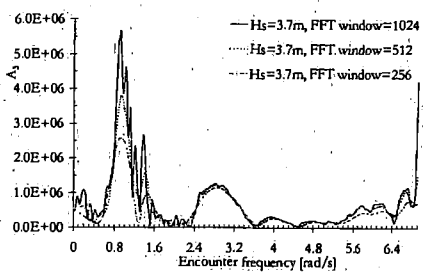

Figure 49 $A_3(\omega)$, Sea State II

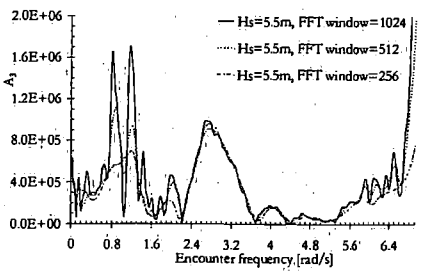

Figure 50 $A_3(\omega)$, Sea State III

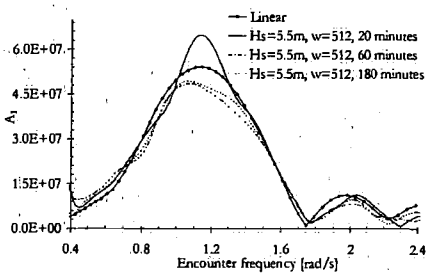

Figure 51 $A_1(\omega)$, simulation time variation

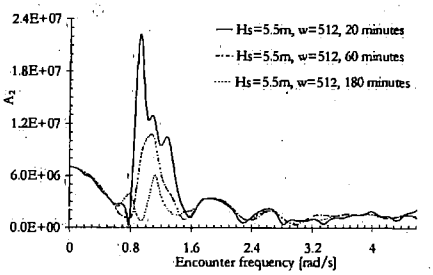

Figure 52 $A_2(\omega)$, simulation time variation

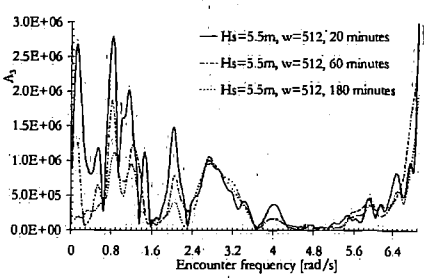

Figure 53 $A_3(\omega)$, simulation time variation

Model II identification

The Volterra kernels $B_1(\omega), B_2(\omega), B_3(\omega), B_4(\omega), B_5(\omega)$ are identified for the three series of regular waves and for the four order assumptions. The resulting kernels are pictured in Figure 54 to Figure 62. For these kernels the x-axes are all the same since they all act on the incident wave spectrum. The first order kernel is well predicted for a first order analysis but deviates for a 3rd and 5th order analysis. The transfer function peak shifts to lower frequencies and becomes larger. The second order kernel shows quite

good resemblance for a 2nd and 4th order analysis. The 4th order analysis gives a somewhat less smooth function. The same trend is seen for the 3rd order kernel, good agreement for a 3rd and a 5th order assessment but a slightly less smooth function for the 5th order analysis. The fourth and fifth order kernels are not smooth.

When comparing the three regular wave series it is seen that the differences in transfer functions are small. But one has to bear in mind that these transfer functions act on the wave and subsequently have to be squared, cubed etc. Thus a 10% difference in the third order kernel gives a 33% difference in 3rd order response!

The identification process for Model II is straight forward and can easily be done. Moreover the computational costs for the regular wave simulations are small. For every regular wave simulation the computation time can be adjusted in order to encounter a fixed number of waves for all frequencies.

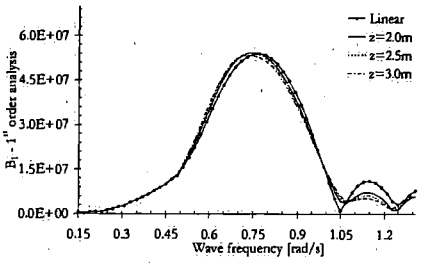

Figure 54 $B_1(\omega)$, 1st order analysis

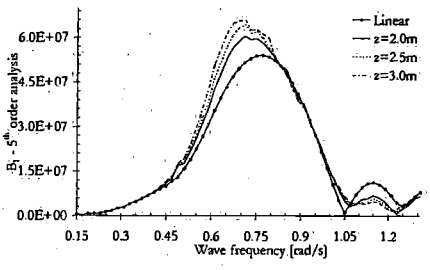

Figure 56 $B_1(\omega)$, 5th order analysis

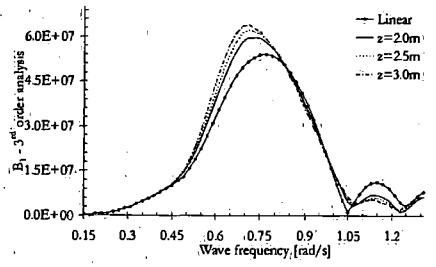

Figure 55 $B_1(\omega)$, 3rd order analysis

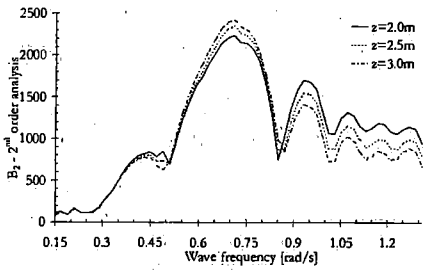

Figure 57 $B_2(\omega)$, 2nd order analysis

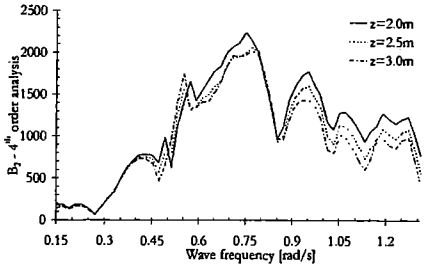

Figure 58 $B_2(\omega)$, 4th order analysis

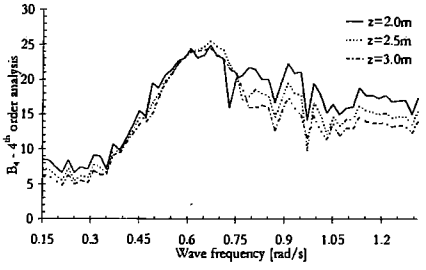

Figure 61 $B_4(\omega)$ 4th order

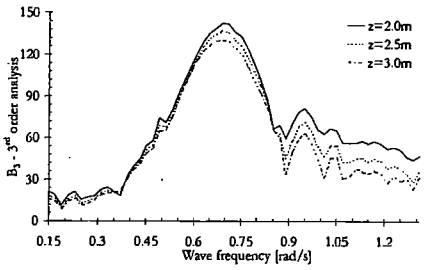

Figure 59 $B_3(\omega)$, 3rd order analysis

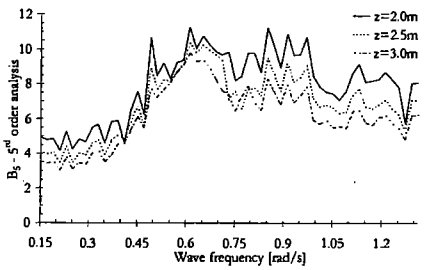

Figure 62 $B_5(\omega)$, 5th order

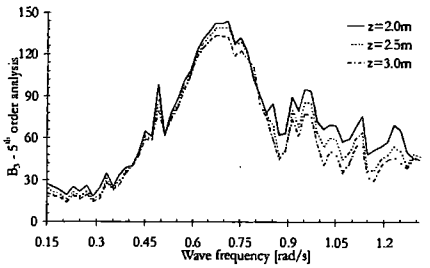

Figure 60 $B_3(\omega)$, 5th order

5.2.2 Simulation assessment of the nonlinear approximate Volterra models in irregular waves

The proof of the pudding is in the eating hence the different identified models have to be compared on the basis of irregular simulations. The criteria of importance are,

- Accuracy of the simulated output

How well the models predict the nonlinear response is of great importance. Hence the statistical moments and amplitude distributions of the simulations are compared as well as time series.

- Stability of the simulation procedure
  In order to benefit of the low computational costs of the Volterra model it should be applicable to different seas state after a single identification process. Thus the models should be accurate for different wave spectra and thus be more or less stable in the output.
- Efficiency of the simulation procedure
  Simulations should be conducted easily and with computational costs as low as possible.

To evaluate the above criteria three wave spectra have been modelled and simulated with the nonlinear program. The characteristics are defined according to STANAG 4194,

- Sea State 4: modified Pierson-Moskowitz, H_s=2.5 [s], T_z=6.5 [s]
- Sea State 5: modified Pierson-Moskowitz, H_s=4.3 [s], T_z=7.4 [s]
- Sea State 6: modified Pierson-Moskowitz, H_s=5.5 [s], T_z=7.8 [s]

From the nonlinear simulations the basic statistical moments are calculated, i.e. the standard deviation, skew and kurtosis.

$$\sigma = \sqrt{\frac{1}{N}\sum_{j=1}^{N}\left(y_j - E[y]\right)^2} \qquad \alpha_{3,4} = \sqrt[3/4]{\frac{1}{N}\sum_{j=1}^{N}\left(\frac{y_j - E[y]}{\sigma}\right)^{3/4}} \tag{5.6}$$

Secondly, the crest and trough probability distribution functions are derived. All the different Volterra models have simulated these spectra and the response statistical properties are compared subsequently.

In Figure 63 to Figure 71 the three statistical moments are presented for all models, where the light gray bars correspond with Model I while the dark bars correspond with Model II. The result from the nonlinear simulation is set to 100%. For the standard deviation quite good results are obtained for all models. Only Model I, derived from sea state I, gives significant overpredictions for sea state 5 and 6. The skew parameter is considerably underpredicted by all models, only Model I derived from sea state III gives good agreement. The kurtosis is reasonably predicted by Model II variations and good predicted by Model I derived from sea state I and III. Overall we can see a stable result for Model II but large fluctuations between the Model I variations. Moreover an unexpected trend is seen for Model I. One would expect a monotone behaviour of Model I, derived from sea state I,II and III. But instead the model derive from sea state II does not fit between the other two especially for the kurtosis coefficient.

In Figure 72 to Figure 80 the amplitude distributions are presented of the Model I simulations in comparison with the nonlinear and linear results. Overall we can conclude that the influence of different window sizes is small to very small.

- Sea state 4
  Hogging amplitudes are well predicted as well as the sagging except for the models derived from sea state III.
- Sea state 5
  Hogging is well predicted by the models derived from sea state II and III but not the one derived from sea state I. Sagging is well predicted by the model derived from sea state III but underpredicted by the model derived from sea state II and overpredicted by the model derived from sea state I.
- Sea state 6
  Hogging is well predicted by the models derived from sea state II and III but not from sea state I. Sagging is well predicted by the model derived from sea state III but underpredicted by the model derived from sea state II and overpredicted by the model derived from sea state I.

In Figure 81 to Figure 89 the amplitude distributions are presented of the Model II simulations in comparison with the nonlinear and linear results. The differences between the various order assessments is for most of the curves small especially for the hogging results.

- Sea state 4
  Hogging is reasonably predicted for the model derived from the first smallest regular wave series. The hogging results for the other two are poor, only the second order assessment is good. Sagging is well predicted with the second order assessment poorest.
- Sea state 5
  Hogging is reasonably predicted. Sagging is best predicted for the model derived from the largest regular waves, while the model, derived from the series with the smallest waves, gives poorest results.
- Sea state 6
  Hogging is reasonably well predicted. Equally as for sea sate 5 are the sagging amplitudes best predicted for the model derived from the largest regular waves, while the model, derived from the series with the smallest waves, gives poorest results.

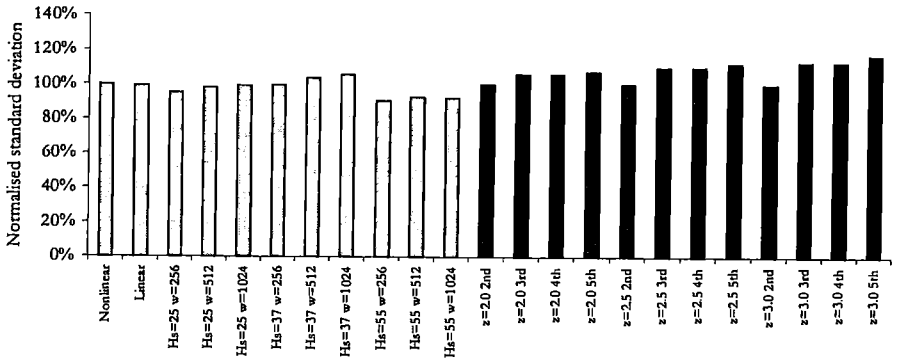

Figure 63 Standard deviation, sea state 4

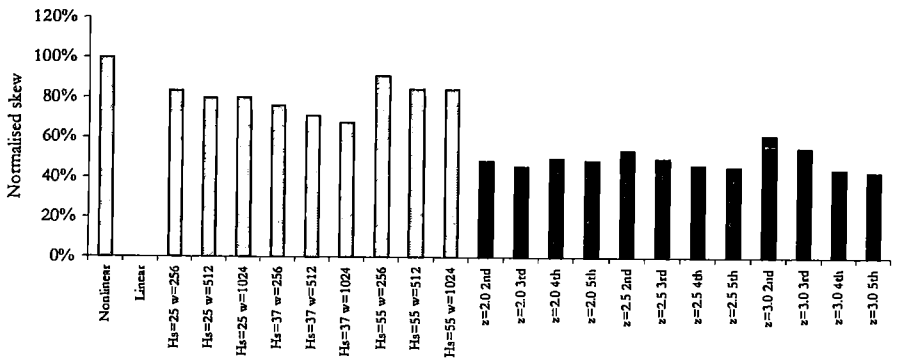

Figure 64 Skew, sea state 4

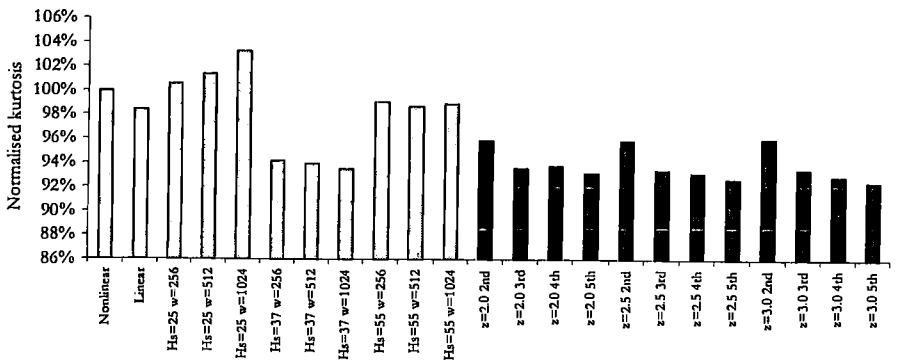

Figure 65 Kurtosis, sea state 4

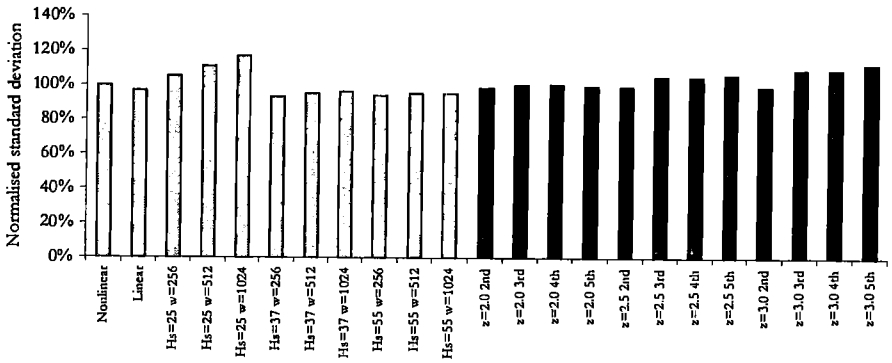

Figure 66 Standard deviation, sea state 5

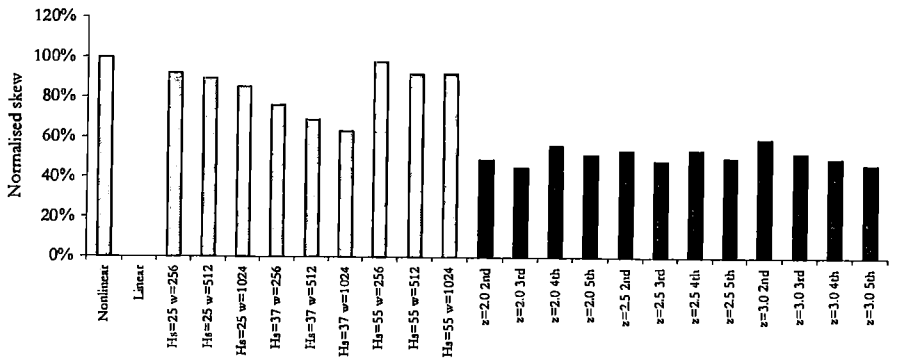

Figure 67 Skew, sea state 5

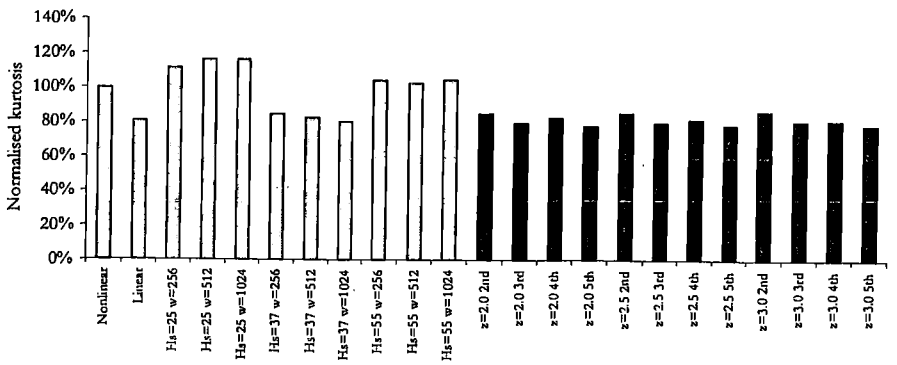

Figure 68 Kurtosis, sea state 5

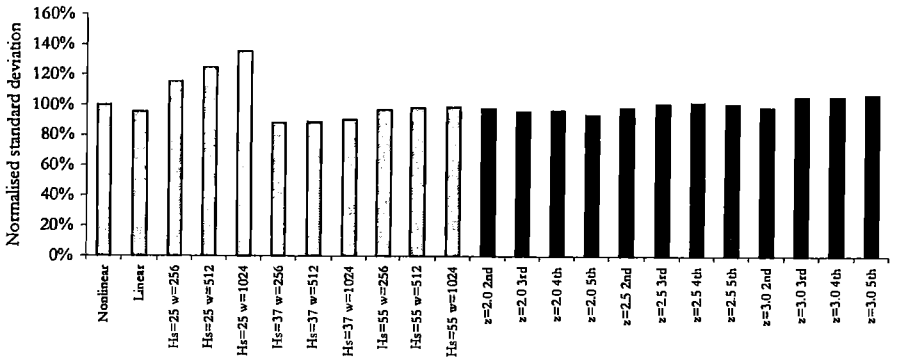

Figure 69 Standard deviation, sea state 6

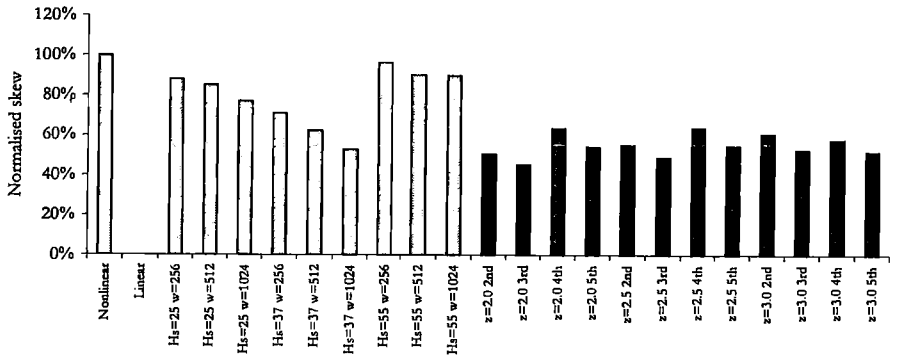

Figure 70 Skew, sea state 6

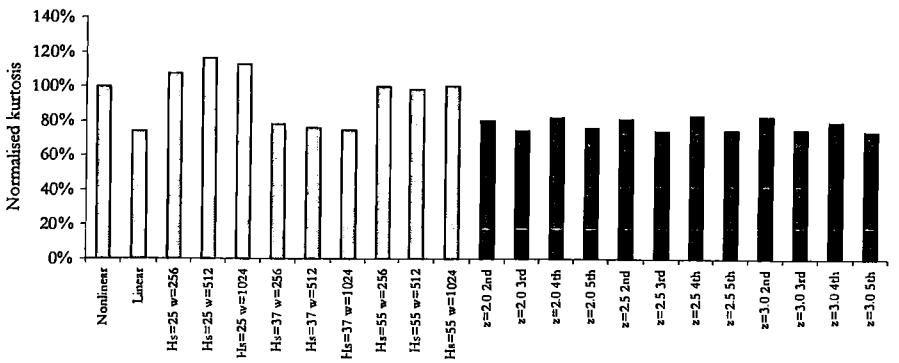

Figure 71 Kurtosis, sea state 6

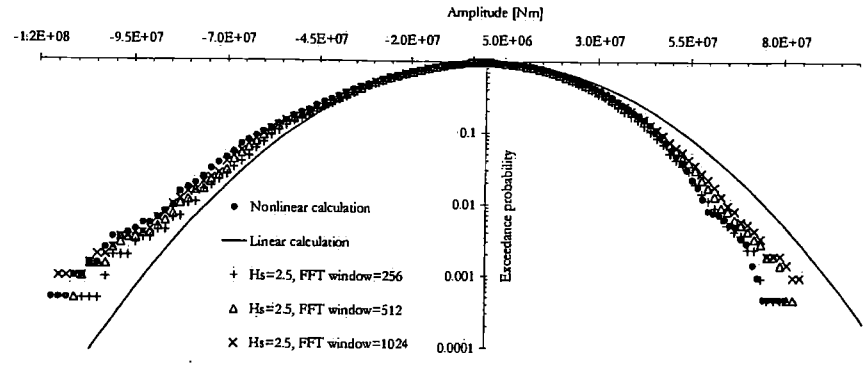

Figure 72 Amplitudes of Model I derived from sea state I, sea state 4

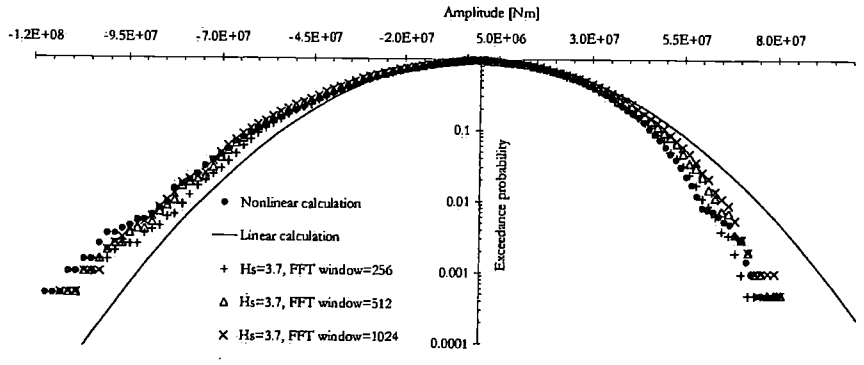

Figure 73 Amplitudes of Model I derived from sea state II, sea state 4

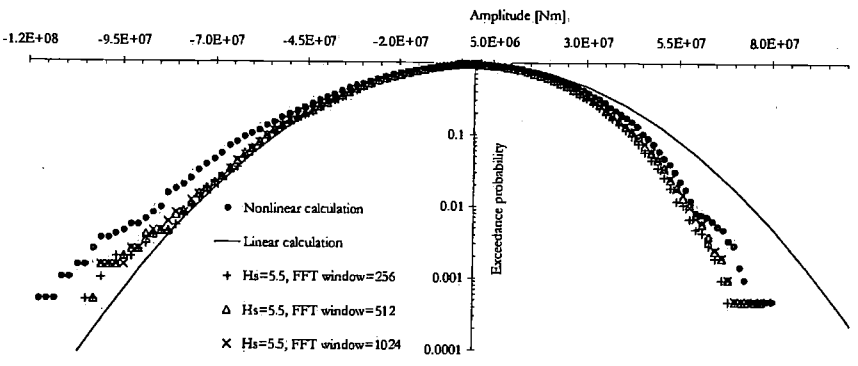

Figure 74 Amplitudes of Model I derived from sea state III, sea state 4

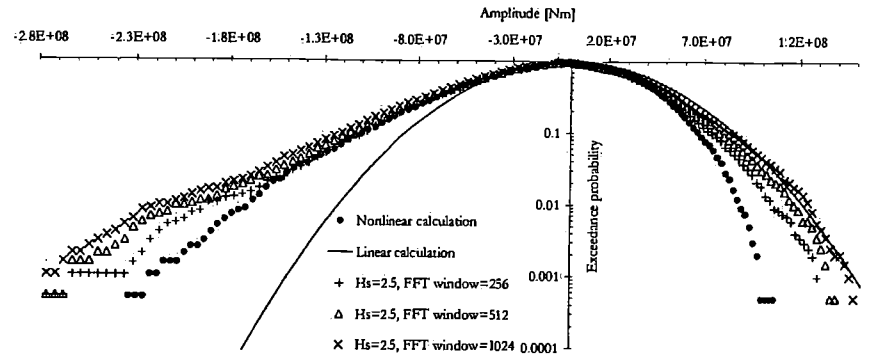

Figure 75 Amplitudes of Model I derived from sea state I, sea state 5

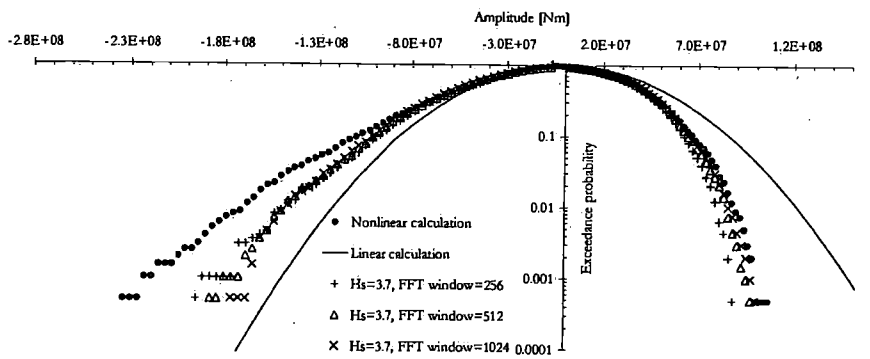

Figure 76 Amplitudes of Model I derived from sea state II, sea state 5

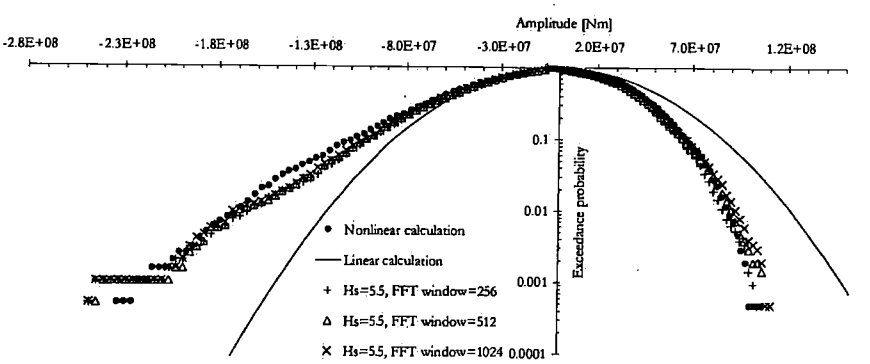

Figure 77 5.5 Amplitudes of Model I derived from sea state III, sea state 5

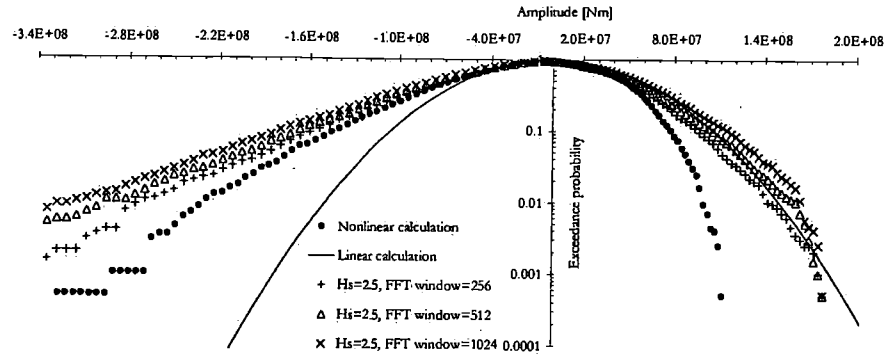

Figure 78 2.5 Amplitudes of Model I derived from sea state I, sea state 6

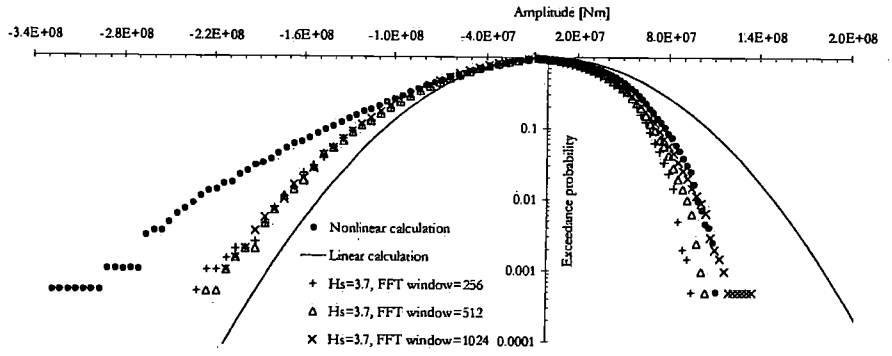

Figure 79 3.7 Amplitudes of Model I derived from sea state II, sea state 6

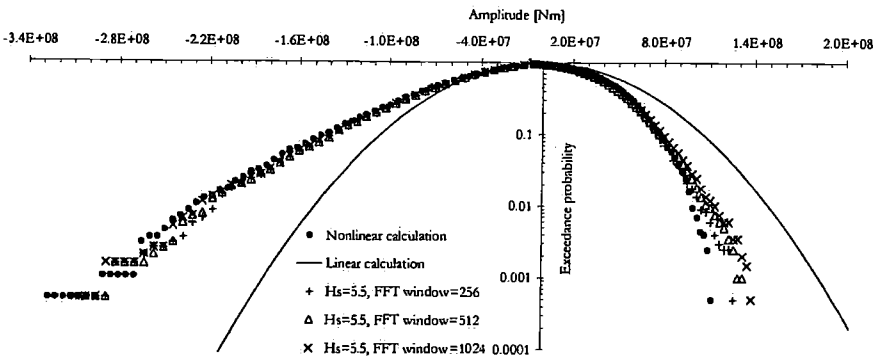

Figure 80 5.5 Amplitudes of Model I derived from sea state III, sea state 6

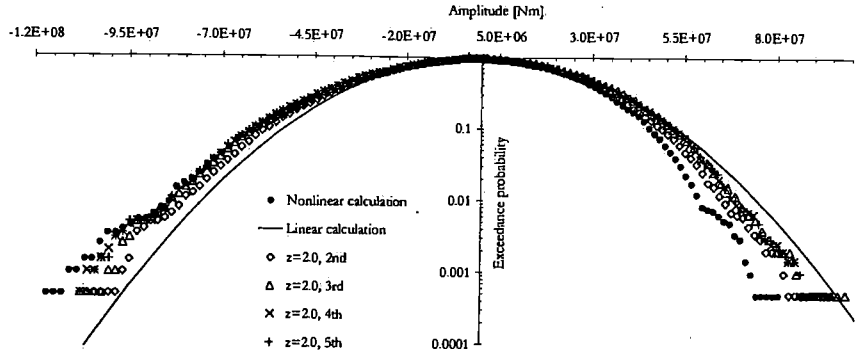

Figure 81 Amplitudes of Model II derived from regular wave series I, sea state 4

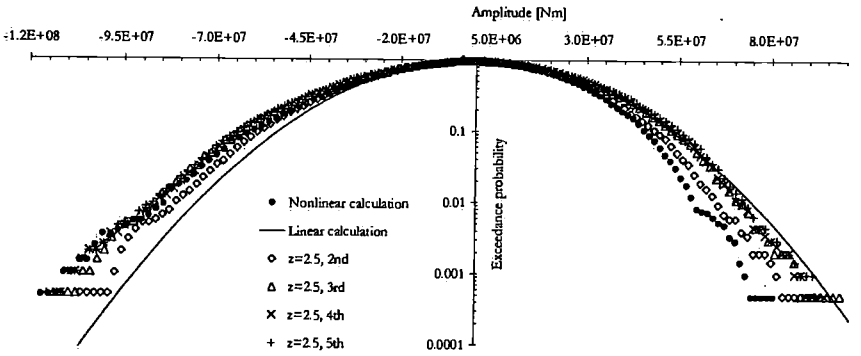

Figure 82 Amplitudes of Model II derived from regular wave series II, sea state 4

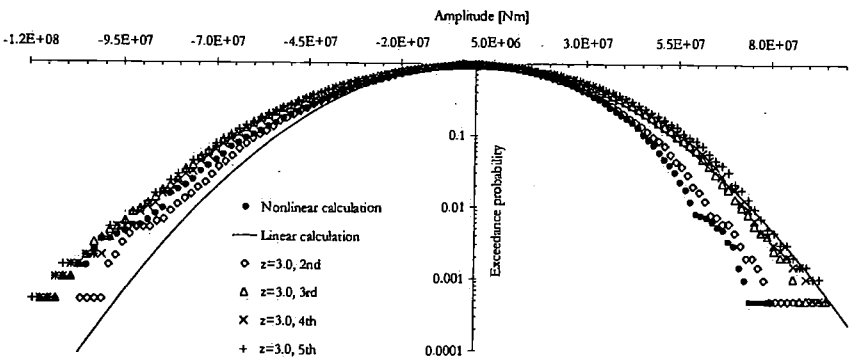

Figure 83 Amplitudes of Model II derived from regular wave series III, sea state 4

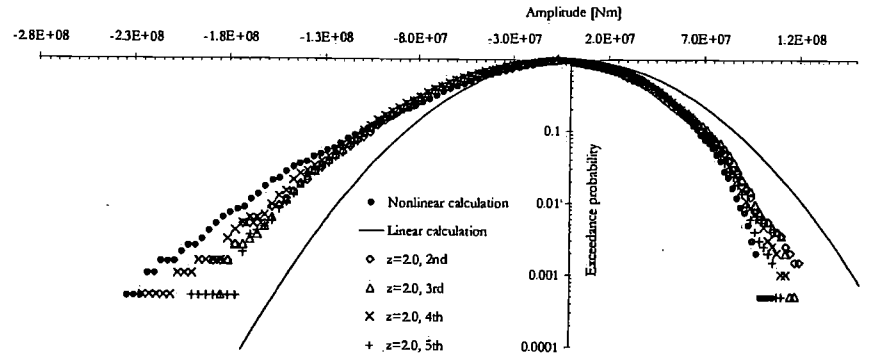

Figure 84 Amplitudes of Model II derived from regular wave series I, sea state 5

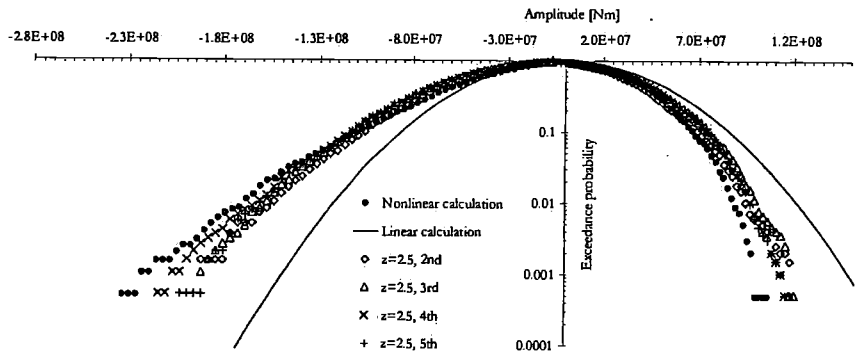

Figure 85 Amplitudes of Model II derived from regular wave series II, sea state 5

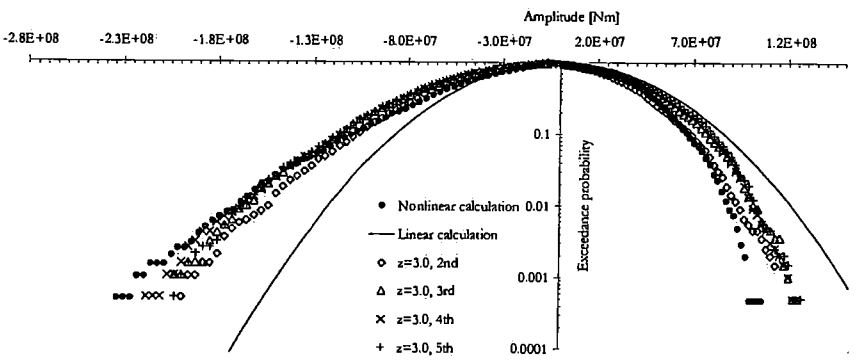

Figure 86 Amplitudes of Model II derived from regular wave series III, sea state 5

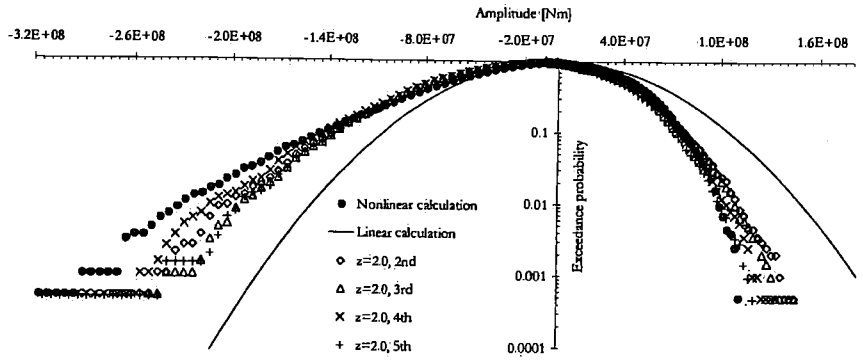

Figure 87 Amplitudes of Model II derived from regular wave series I, sea state 6

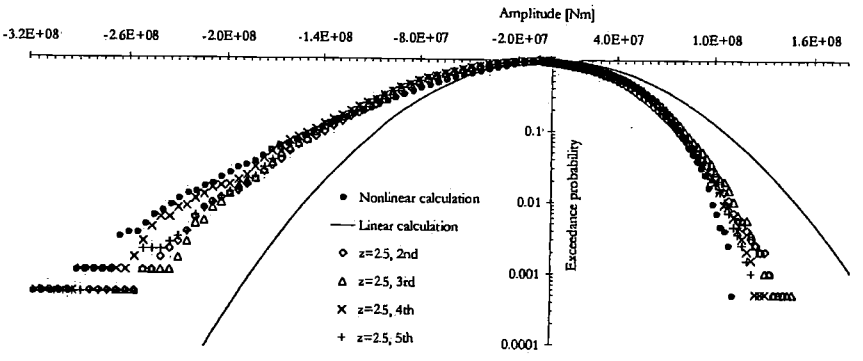

Figure 88 Amplitudes of Model II derived from regular wave series II, sea state 6

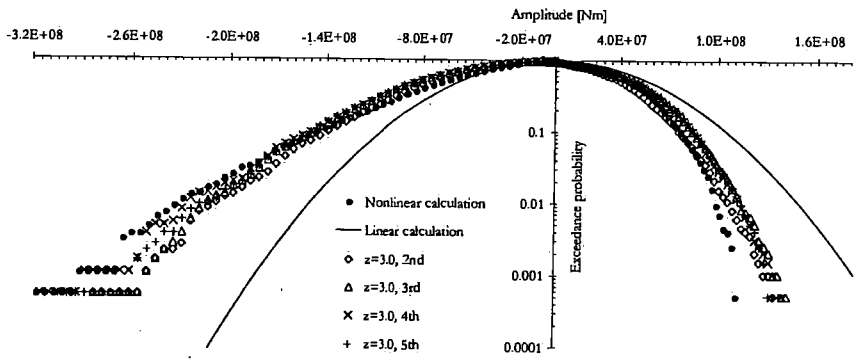

Figure 89 Amplitudes of Model II derived from regular wave series III, sea state 6

The last comparison is done for a MLER calculation. The expected 1-hour extreme in Sea State 6 is calculated by applying the MLER technique as formulated in paragraph 2.3. The following figure pictures the encountered response conditioned incident wave.

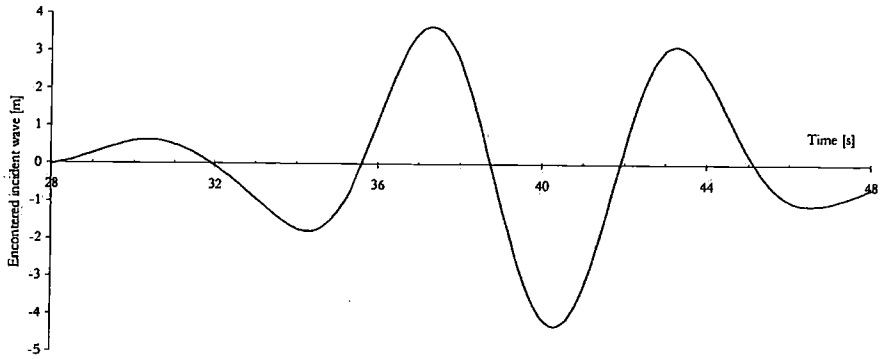

Figure 90 Response conditioned wave for expected extreme in Sea State 6

Simulations are conducted with both Volterra models. Model I is based on the identification from the simulation in Sea State III (H_s=5.5 [m]) and model II is based on the 4th order identification from the regular waves with amplitudes of 3.0 [m]. The response output for Model I and for the 4th order Model II are shown in the two subsequent figures. Model I depicts a shift in time but gives a reasonable to poor prediction of the crests and troughs. Model II performs much better and without a time shift. Figure 93 shows all the different orders for the Volterra model. No large differences are seen. Even a single second order model gives good results.

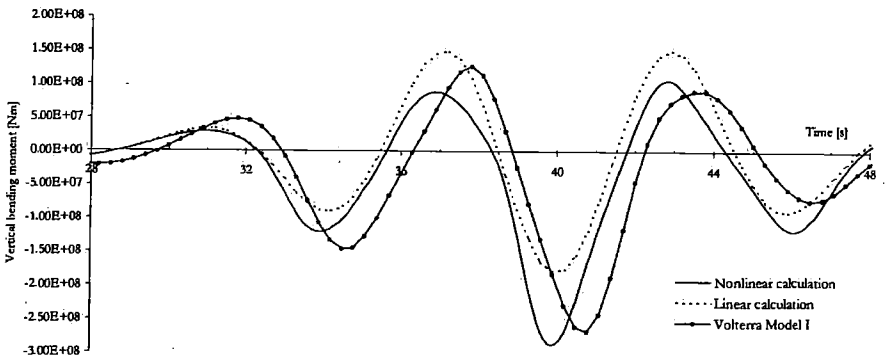

Figure 91 MLER calculation with Volterra model I

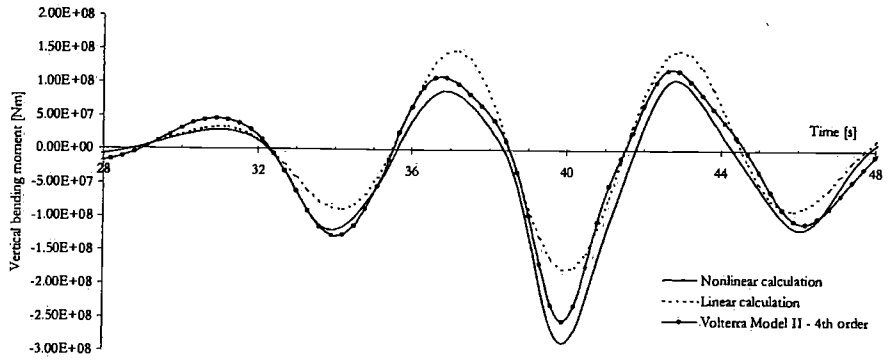

Figure 92 MLER calculation with 4th order Volterra model II

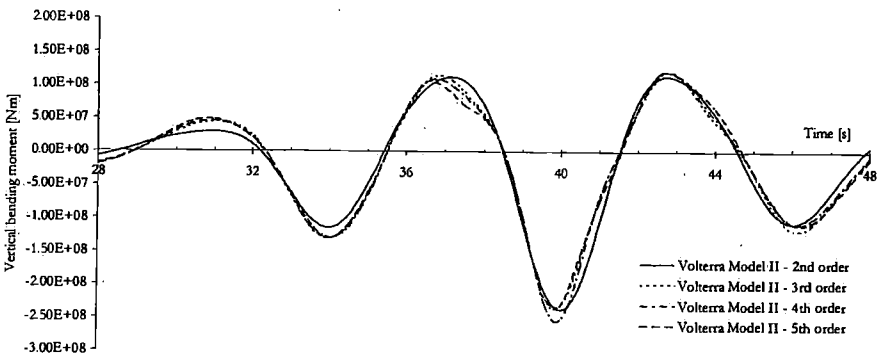

Figure 93 MLER calculation with different orders of Volterra model II

How the different orders contributed to the total Volterra model output is shown in Figure 94 and Figure 95. When comparing these figures we see that the different order contributions differ considerably. The first order responses from Model I and Model II differ in amplitude from 20 to 40%, while the third order parts differ even in sign! From both models it is seen that the second order parts for both models and the fourth order part for Model II, account for a major part in the decrease of hogging amplitudes and the increase of the sagging amplitudes.

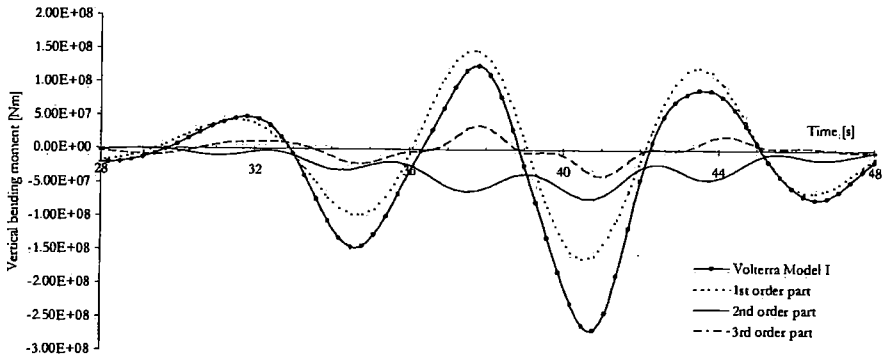

Figure 94 1st, 2nd and 3rd order contributions of Volterra model I

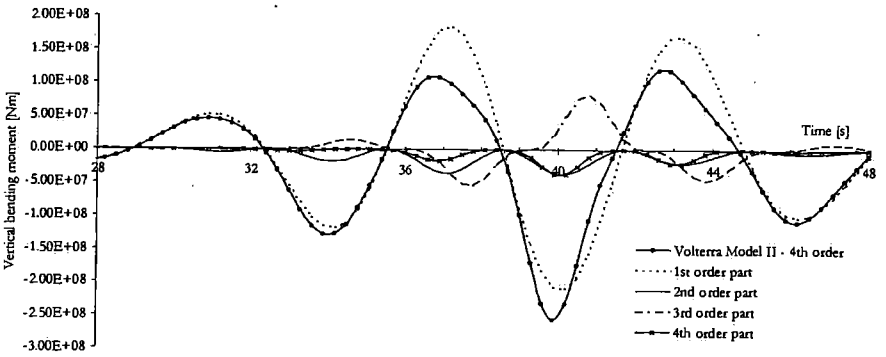

Figure 95 1st, 2nd , 3rd and 4th order contributions of Volterra model II

5.2.3 Case-study conclusions

Considering the stability of the identification process it is concluded that both approximate models are reasonably stable. Model I suffers particularly from instable results for the higher order functions in the wave frequency region. For the uniqueness of the kernels it is obvious that this can never be fulfilled entirely because a nonlinear Volterra model can never capture a nonlinear effect if it has not been simulated. For example if strong bow flare starts some meters above the waterline, the Volterra model can not model the effect of this if it is not entering the water during simulation. But comparing the figures the kernels are quite the same for different input sea states for both models. Considering the efficiency of the identification there's a clear preference for Model II. The identification process is simple and does not require special expertise

while Model I does require experience in spectral identification techniques while the amount of simulation time is also somewhat larger.

When studying the simulation performance of both models it becomes clear that Model II is favourite. Although both models give for some sea states similar accuracy Model II is much more stable and can therefore be used reliably for different sea states, which is doubtful for Model I. Moreover the efficiency of Model II is also greater as the computational costs are less.

Consequently there's a preference for Model II, based on this case-study. Of course this is not a general conclusion as different nonlinear behaviour might give different results regarding the applicability of both models.

If more accuracy is required a complete higher order Volterra model can be used but this is only attractive if the nonlinear program is very computationally demanding to justify the burden of the identification and simulation process of a complete nonlinear Volterra model. An alternative option is to increase the accuracy of Model II by using a series of regular waves with different amplitudes.

5.3 Seakeeping performance assessment

The motions of a ship are of importance with respect to vessel safety and seakeeping performance. Of paramount importance is the roll behaviour of ships in critical conditions. The prediction of capsize risks is a difficult process. A robust 6 DOF nonlinear ship motion program is required with realistic modelling of the manoeuvrability characteristics. Additionally a large amount of nonlinear simulations are to be conducted. It is therefore attractive to apply the response conditioning technique. No comprehensive study is conducted but a preliminary case is presented in the first paragraph together with a discussion on the applicability and the critical aspects involved.

The second paragraph presents a seakeeping performance assessment for a simple ASW mission of a frigate on the North Atlantic by using the reliability based approach as outlined in the previous chapter. Moreover the nonlinear approximate Volterra modelling technique has been used in order to assess the motions nonlinearly.

5.3.1 Short-term statistics of the roll motion of a navy frigate

The roll motion behaviour of vessels in following and stern quartering waves is an important aspect in order to design ships with sufficient dynamic stability. Different physical phenomena can cause extreme roll angles or even capsizing. Some are strongly or entirely nonlinear dominated. For instance parametric roll is a fully nonlinear phenomena and a first estimate of parametric roll behaviour is not predictable with a linear model. Consequently the response conditioning technique is not applicable. But

when studying the capsizing probability due to loss of stability it might be that a linear model can already identify extreme roll motion events and thus the response conditioning technique might be an appropriate technique. A preliminary case is shown here for a frigate in waves coming from astern (60 degrees). Calculations were done with the DNV-WASIM code. The frigate is a small frigate of 3030 tons. In order to model nonlinear damping a linear kappa-curve was specified.

$$\kappa = \kappa_1 + \kappa_2 \phi_a \tag{5.7}$$

Here κ_1 is additional linear damping while κ_2 is nonlinear damping. The values of these kappa parameters were chosen arbitrarily and were not calibrated with model test. The forward speed of the vessel was 8 knots and the waves were modelled by a modified Pierson-Moskowitz spectrum with a significant wave height of 4.0 meters and a period of 9.0 seconds. Below the negative roll amplitude exceedance probability function is shown. The response conditioning technique can predict the nonlinear amplitude distribution reasonably well. Especially the shape is well predicted but the EMLER curve shows a slight shift even for small roll angles.

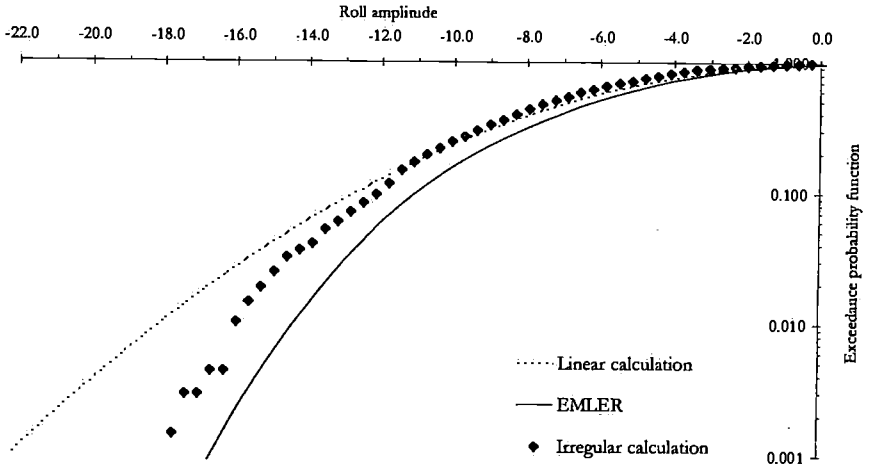

Figure 96 Roll motion of frigate in 60 degrees waves

The two figures below show the response conditioned simulation carried out for a conditioned linear extreme of 29.7 degrees. The resulting nonlinear amplitude is 20 degrees. As seen the horizontal motions are small up to t=60 [s], which is the incident of the extreme event. It is likely that because of this the response conditioning technique works fine. But in case of more severe sea states the manoeuvring behaviour becomes an important aspect, which should be modelled correctly. A far too stiff autopilot, for example, will influence the roll behaviour significantly. Oosterhuis (2001) conducted some conditioned simulations in order to get a first impression on the application of the

EMLER technique in more severe sea states and different headings. Remarkably, very good results were obtained for the case with waves coming from 15 degrees. It was expected that for this heading situation the horizontal motion control and the possibility of broaching would be a threat to the application of the EMLER technique. More simulations and different cases should shed more light on the applicability of the EMLER method for the prediction of nonlinear roll motion statistics.

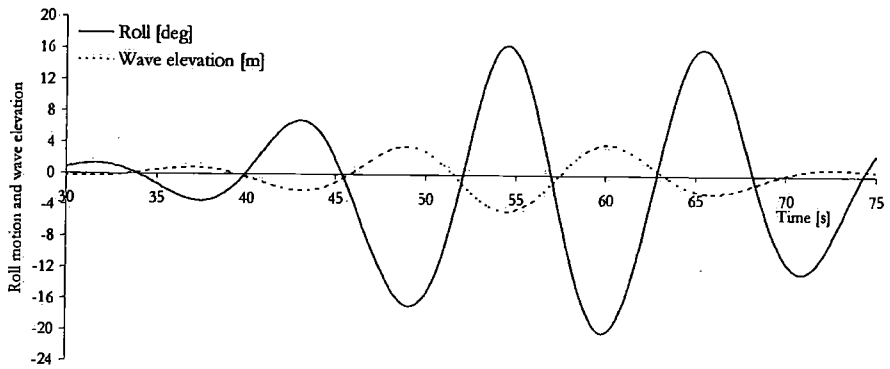

Figure 97 Roll motion and wave elevation of roll conditioned simulation

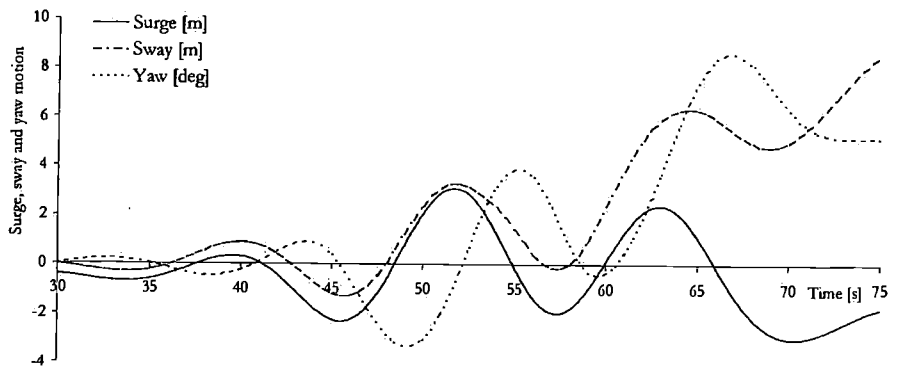

Figure 98 Horizontal motions of roll conditioned simulation

5.3.2 Seakeeping performance assessment of a navy frigate

The reliability based seakeeping performance assessment technique, as outlined in paragraph 4.2, is studied in this paragraph. The main objective is to investigate the

characteristics of the reliability based approach in comparison with the standard approach.

A navy frigate was chosen to study the seakeeping performance for a simplified ASW mission. Details of the vessel are given in paragraph 6.2. For the present case-study only one forward speed, 15 knots, and heading, head waves, was modelled. The response criteria that were chosen are listed in the following table with the criteria as used in a conventional seakeeping performance assessment procedure. These criteria were modelled by Gaussian distributions with the listed values as mean values and a coefficient of variation of 15%.

Name	Response	Criterion
Sonar dome emergence	Relative displacement	24/hr
Bridge	Vertical acceleration	0.25g [m/s²] RMS
Heli-deck	Vertical velocity	1.00 [m/s] RMS
Heli-deck	Vertical displacement	0.70 [m] RMS

Table 4 Main particulars of the MO-2015 frigate

A mission of 5 days was formulated at the North Atlantic. The long-term wave description was given by a Weibull conditional log-normal distribution as given by DNV (2000). The wave spectra were based on the modified Pierson-Moskowitz spectrum. The short-term sea state duration was 3 hours with a maximum stepsize from one sea state to the next of 1.0 [m]. This mission was simulated 250 times after which the statistical post-processing was done. All the responses were equally weighed. The cumulative distribution functions of these response seakeeping performances and the total seakeeping performance are shown in the next figure. The sonar dome emergence and the heli-deck vertical velocity have a similar performance behaviour while the heli-deck displacement performs much worse while the bridge vertical acceleration performs much better. The expected total seakeeping performance is 81% but the variance is large. The sensitivity factors, both uncorrelated and correlated show the contribution of every response to the total seakeeping performance variance in Table 5. These values confirm the impression of Figure 99, with the heli-deck vertical displacement being dominant. The performance correlation coefficients are shown in Table 6. All the coefficients are positive and high, which is not surprising. For most responses it is valid to state that the more severe the sea state the less the performance. Thus the correlations coefficients are also high and positive. The correlation coefficient between the two heli-deck responses is 086. Thus a worse performance of the vertical velocity means mostly a worse vertical displacement performance as well.

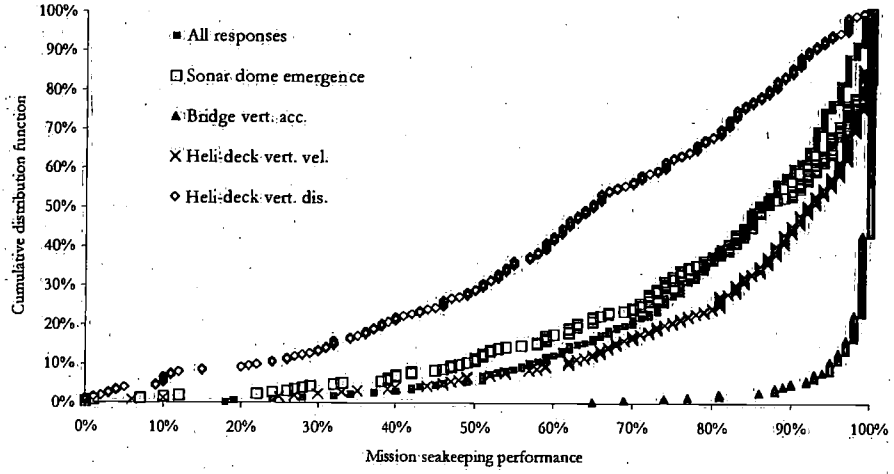

Figure 99 Seakeeping performance distributions

Name	Sensitivity factor (uncorrelated)	Sensitivity factor Eq. (4.32)
Sonar dome emergence	10%	33%
Bridge	1%	2%
Heli-deck velocity	7%	25%
Heli-deck displacement	15%	40%
Joints	67%	0%

Table 5 Squared sensitivity factors, α_j^2

Name	Total	Sonar dome emergence	Bridge	Heli-deck velocity	Heli-deck displacement
Total	1.00	0.99	0.75	0.97	0.96
Sonar dome emergence	-	1.00	0.73	0.97	0.93
Bridge	-	-	1.00	0.83	0.57
Heli-deck velocity	-	-	-	1.00	0.86
Heli-deck displacement	-	-	-	-	1.00

Table 6 Correlation coefficients

Linear versus nonlinear simulation

When comparing a linear and nonlinear assessment for this frigate hardly differences are seen. This is not so surprising as the hullform is rather slender and does not have excessive flare. Secondly nonlinearities are not as pronounced in motions and velocities as they are in accelerations. Consider the case of a regular time domain displacement decomposed in its Fourier components. The time derivatives show that the relative contribution of higher harmonics compared to the first harmonic is larger for the accelerations than for the displacements.

$$\begin{bmatrix} y(t) \\ \dot{y}(t) \\ \ddot{y}(t) \end{bmatrix} = \begin{bmatrix} 1 & 1 & 1 & 1 \\ i\omega & 2i\omega & 3i\omega & 4i\omega \\ -\omega^2 & -4\omega^2 & -9\omega^2 & -16\omega^2 \end{bmatrix} \cdot \begin{bmatrix} y_1(t) \\ y_2(t) \\ y_3(t) \\ y_4(t) \end{bmatrix} \tag{5.8}$$

And there's a third explanation, which is related to the criteria formulation. Many criteria are given as limit values for response RMS values. But a nonlinear response with larger crests and smaller troughs than the linear response can have an equal RMS value. For example the bridge vertical acceleration. A linear and nonlinear assessment hardly differ but if we look at the crest amplitude probability function a large difference with a linear approach is seen. If the criteria would be formulated in terms of a maximum number of exceedances of a given positive value a difference would be obtained. To illustrate this the criterion is reformulated. A maximum of 10 exceedances of 0.5g is allowed. Figure 101 shows the seakeeping performance for the bridge with this new criterion formulation and this demonstrates the difference between a linear and a nonlinear approach.

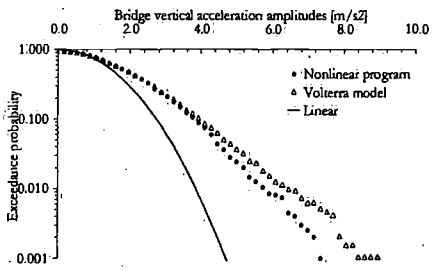

Figure 100 Bridge vert. Accelerations, sea state 6

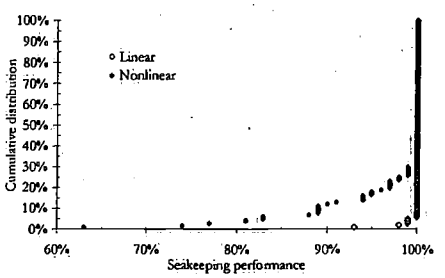

Figure 101 Seakeeping performance bridge

Influence of mission duration

If the mission duration becomes longer the confidence interval for the mission seakeeping performance becomes smaller. This is logical as the uncertainty of the encountered wave environment during a mission becomes smaller. To study this effect the mission duration is varied and the 90% confidence interval is determined as a function of the mission duration. For this case the same vessel was used but for winter time North Atlantic and a higher speed, namely 18 knots. As seen below the size of the confidence interval is still quite large (30%) for missions of 30 days.

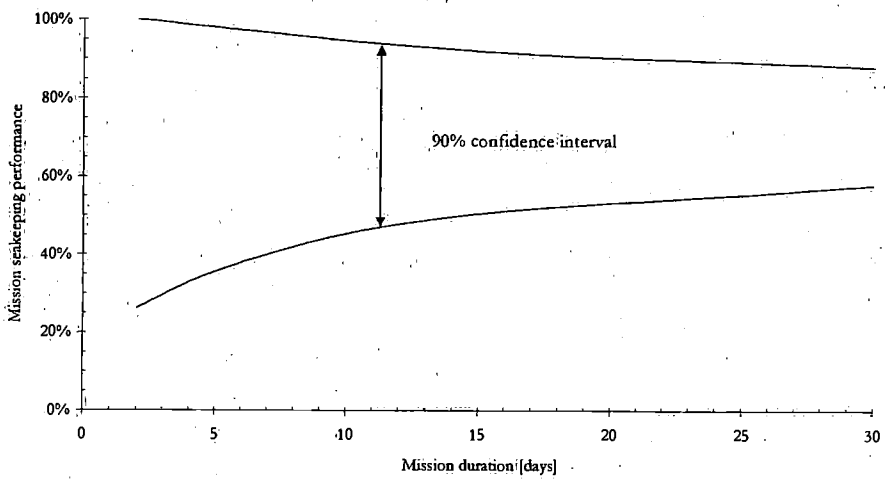

Figure 102 Mission seakeeping performance as a function of mission duration

Influence of criterion uncertainty

The criteria are modelled by Gaussian distributions with arbitrary coefficients of variation. No attempt is made to establish realistic criterion probability functions. To study the effect of the size of the coefficient of variation three values were modelled, 5, 50 and 75 %. For these three values the sonar dome emergence criterion probability function has been plotted in Figure 103. Clearly is seen that a value of 50% is already very extreme. But as the next figure shows, the effect of this on the seakeeping performance is quite small. For this case all four responses were modelled with the mentioned coefficients of variation.

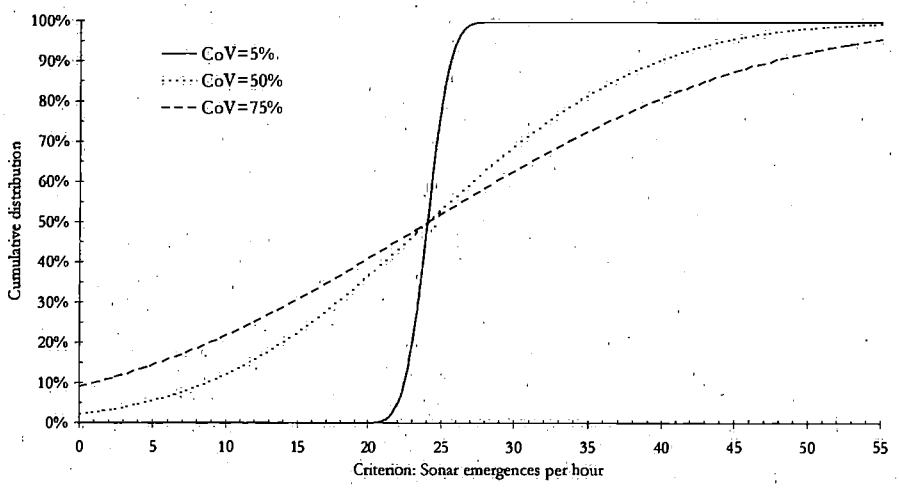

Figure 103 Criterion distribution for various CoV's

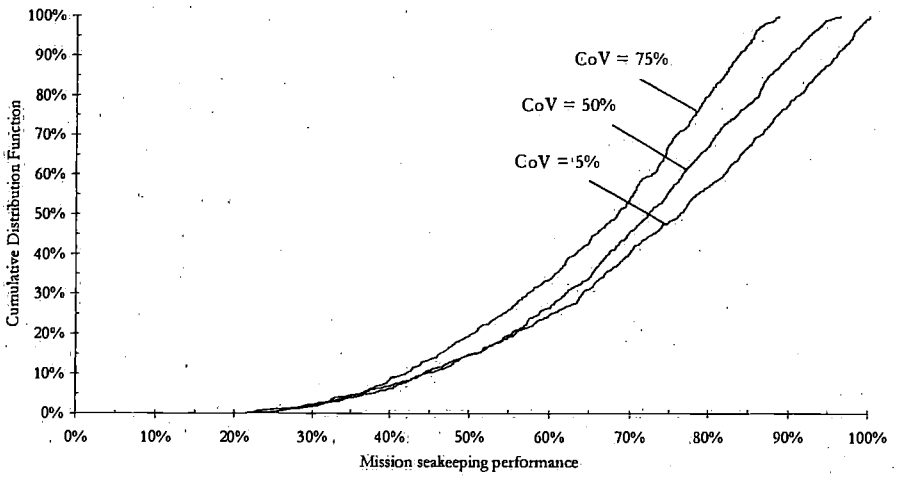

Figure 104 Mission seakeeping performance for various criteria CoV's

Influence of weigh factors

In the previous case all four responses were equally weighed but it is very plausible that this is not realistic. From equation (4.24) it is obvious that the influence of these weigh factors is large and consequently the sensitivity factors, equation (4.32), as well.

6 Model experiments

The numerical cases to verify the MLER and EMLER method showed good results and support the application of the technique. Especially for the calculation of the extreme probability function an enormous reduction in computation time is gained. Still the nonlinear programs that were used do not account for all the nonlinearities present. Phenomena like slamming and green water are not taken into account in the cases. For example the amplitude distributions of the sagging bending moments in the frigate show a remarkable bend. It is rather doubtful whether this is true or not. In these cases large amounts of green water and slamming will occur. Consequently the next step in the research is to verify the response conditioning technique more accurately, which is possible in a towing tank. Hence an experimental program was set-up with the main objectives:

- Validate the EMLER method
- Increase the knowledge of this technique,
- Improve the confidence in the application.

Besides these aims, other side-objectives have been formulated as well:

- Investigate the feasibility of experimental response conditioned testing
- Compare experiments with numerical predictions

Key requirement for this testing is to be capable of generating response conditioned waves. This demands a careful control of the wavemaker. The first paragraph of this chapter gives an in-depth description of the generation of these specific wave profiles. The response, which is used for the response conditioned testing, is the midship vertical bending moment in a frigate. The details of the hullform and the experiments are given in the second paragraph. The last paragraph gives an analysis of the experiments and compares the results with numerical predictions. Part of the measurements are presented in this thesis. For details on the measurements one is referred to the data report, see Pastoor (2001).

6.1 Experimental generation of response time conditioned waves

As said above, the accurate generation of response conditioned waves is a dominant precondition for the experimental verification of the EMLER method. Several problems have to be dealt with before this testing can be done:

- Develop a model to calculate the control signal for the wavemaker
  A response conditioned wave is a transient wave, which occurs at some time-step at some place in the towing tank. Moreover the different harmonic components in the wave train progress at different speeds. Taking this into account and applying a wavemaker transfer function the wavemaker control signal can be calculated.
- Investigate the accuracy of the generated waves.
  If the desired response conditioned waves cannot be experimentally generated with good accuracy tests with a model would not be done.
- Investigate wave profile scaling by scaling the wavemaker control signal
  The EMLER technique is based on a series of MLER runs with scaled response conditioned wave profiles. It would make the testing much more convenient if scaling of the control signal results in identical but scaled wave profiles.
- Investigate the reproducibility of the generated waves
  The generation of the conditioned waves should be a stable process, thus the conditioned wave profiles should be reproducible.
- Solve the wave-model synchronisation problem
  If the conditioned wave occurs at some time-step at some place in the tank the model has to be on that spot, on that time-step and with the correct speed. This requires an advanced control mechanism of the carriage.

A wavemaker model for response conditioned waves

The MLER method determines the incident wave profile, which induces a prescribed most likely extreme response profile. This incident wave is calculated as a series of regular wave components, each with its own amplitude and phase angle. By prescribing that this conditioned wave occurs at a specific location in the towing tank and developing a model for the wavemaker action and for the propagation of the waves through the tank it is possible to calculate the control signal for the wavemaker.

Figure 105 shows the system of axes used to develop a control signal for the wavemaker in order to generate response conditioned waves in the towing tank. The vessel starts in the origin of the $x_0y_0z_0$ reference frame and travels a distance D_1 until the moment of the MLER event. The waves in this earth-fixed reference frame are defined by,

$$\zeta(x_0,t)=\sum_{j=1}^{N}\zeta_{a,j}\cos\left(\omega_j t+\varepsilon_{\zeta,j}+k_j x_0\right) \tag{6.1}$$

This wave formulation is transformed to the wavemaker reference frame XYZ, by introducing a distance D_2.

$$X=-x_0+(D_1+D_2)=-x_0+D \tag{6.2}$$

Hence the waves are defined as,

$$\zeta(X,t)=\sum_{j=1}^{N}\zeta_{a,j}\cos\left(\omega_j t+\varepsilon_{\zeta,j}-k_j X+k_j D\right) \tag{6.3}$$

By incorporating the phase shift $k_j D$ in the wave phase angle the wave profile at the moment of the extreme response is formulated as,

$$\zeta(X,t_{MLER,1})=\sum_{j=1}^{N}\zeta_{a,j}\cos\left(\omega_j t+\varepsilon_{\zeta,j}-k_j X\right) \tag{6.4}$$

This wave profile has to be fully developed in the towing tank. While this profile is easily prescribed in a numerical program, in the towing tank the group velocity has to be taken into account. This group velocity is smallest for the shortest waves in the wave profile. Therefore a distance, D_3, is introduced. The shortest wave in the wave train should have advanced up to this point. This requirement prescribes a minimum time duration of,

$$t_{MLER,2}=\frac{D_3}{c_g}=\frac{2kD_3}{\omega}\frac{\sin kh}{\sin kh+2kh} \tag{6.5}$$

Thus all harmonic components in the wave train are fully developed in the extreme response wave profile as long as D_3 is sufficiently larger than D_2. This results in revised phase angles $\varepsilon_{\zeta,j,2}$ by equating,

$$\sum_{j=1}^{N}\zeta_{a,j}\cos\left(\omega_j t_{MLER,1}+\varepsilon_{\zeta,j,1}-k_j X\right)=\sum_{j=1}^{N}\zeta_{a,j}\cos\left(\omega_j t_{MLER,2}+\varepsilon_{\zeta,j,2}-k_j X\right) \tag{6.6}$$

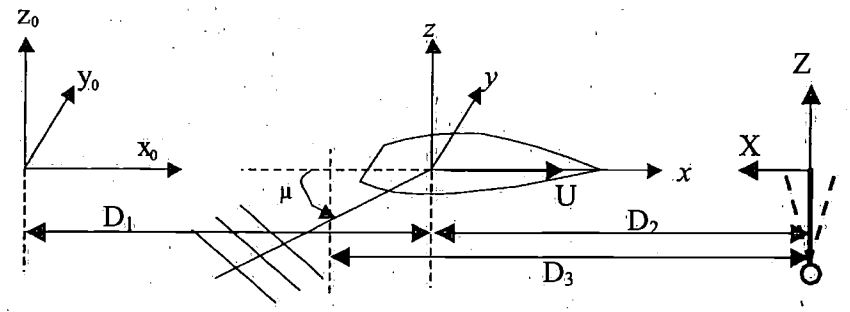

Figure 105 System of axes for towing tank conditioned waves formulation

The resulting wave amplitudes, frequencies and phase angles can now be used to generate the wavemaker control signal. For this purpose the wavemaker transfer function was determined by measuring the sinusoidal control signal and the wave elevation at 30 meters from the wavemaker. This showed a nonlinear behaviour in the determined phase transfer. The following figure shows the wavemaker transfer function phase angles as a function of wave steepness for different wave frequencies.

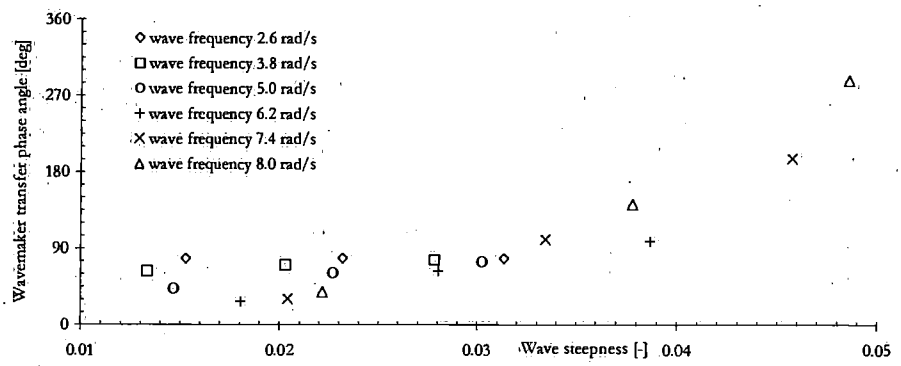

Figure 106 Wavemaker transfer function phase angle as a function of wave steepness

The larger the frequency the larger the differences in phase angles. The best way to investigate this effect is to measure the wavemaker flap position. It is possible that the wavemaker hydraulics introduce a time delay, which could depend on wave amplitude and frequency. A physical explanation is also possible. If for short waves large amplitudes are generated the flap amplitude cannot be assumed small compared to the

wavelength. Hence the assumption of a wave crest at the neutral position of the wavemaker at the instance of a positive stroke is doubtful. Another explanation can be sought in nonlinear physical behaviour of the waves.

In order to overcome this nonlinear problem a quasi-linear transfer function was established. The phase transfer was determined from a series of regular wave tests with average steepnesses of 0.03, see Figure 107.

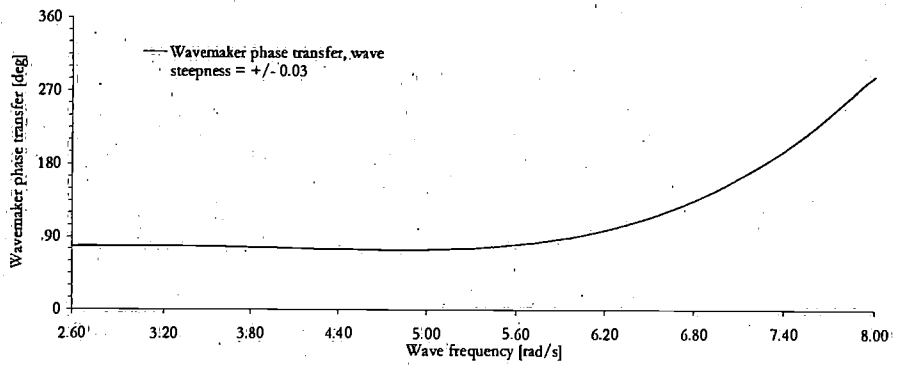

Figure 107 Wavemaker transfer function phase angle

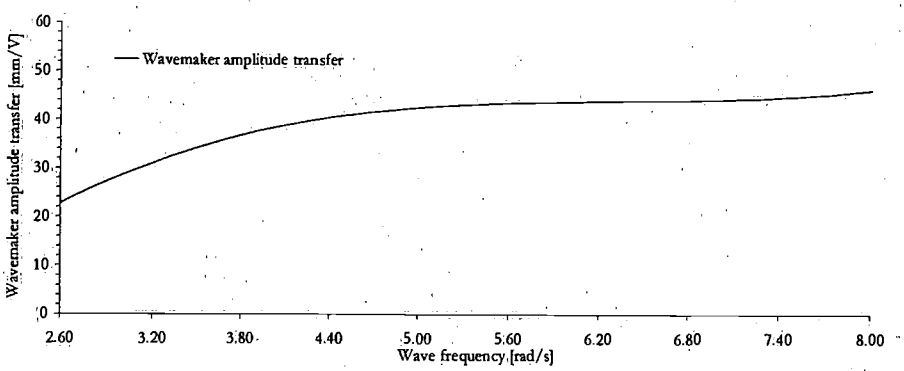

Figure 108 Wavemaker transfer function amplitude

Thus the wavemaker control signal, consisting of voltage amplitudes, $U_{a,j}$, and phase angles, $\varepsilon_{U,j}$, are determined from the following equation.

$$\zeta(X=0;t)=\sum_{j=1}^{N}\zeta_{a,j}\cos\left(\omega_j t+\varepsilon_{\zeta,j;2}\right)=\sum_{j=1}^{N}\left|H_{wm}(\omega)\right|U_{a,j}\cos\left(\omega_j t+\varepsilon_{U,j}+\varepsilon_{wm}\right) \quad (6.7)$$

The figure below shows the wavemaker control signal, which was used for the conditioned waves as pictured in Figure 112 and Figure 113. This signal corresponds with the wavemaker flap motion and it illustrates how different the flap motion is compared with the resulting conditioned wave at the MLER location. This conditioned wave evolves from a low wave profile with many crests to a large profile with only a few crests.

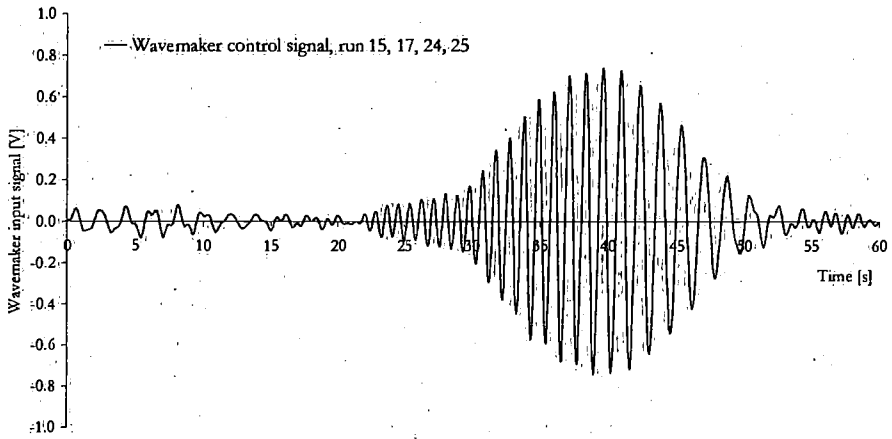

Figure 109 Example wavemaker control signal

In the previous derivation the minimum travel distance, D_3., for the shortest waves was introduced. By experimental testing a distance of 10 meters beyond the MLER location was found sufficient. For this case the wavefront of the longest waves is somewhere near the end of the tank. Consequently no reflection problems are encountered. See Figure 110 for an example of the wave profile in the towing tank at the incidence of an MLER event. This figure is calculated according to linear theory as described above.

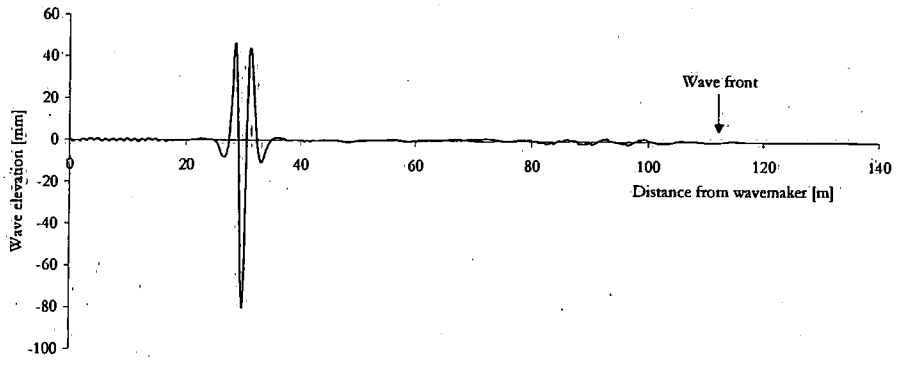

Figure 110 Typical wave profile in towing tank at timestep of MLER event

Preliminary tests with response conditioned waves

A preliminary test series studied the feasibility of generating response conditioned waves. All the details of these experiments can be found in Pastoor (2000B). Response conditioned waves were prescribed to occur at 30.0 meter from the wavemaker. At this location a wave probe was placed and two probes were placed 1.5 meters in front and aft of this centre probe. Three aspects were to be investigate from these preliminary series:

- Accuracy of the generated wave profiles,
- Reproducibility of the wave profiles, both shape and time,
- Scaling of the wave profiles by scaling the wavemaker control signal

The first aspect was satisfactorily answered as good agreement was obtained between the prescribed and the generated wave profiles. The second aspect was also not a problem. Equal profiles were measured for equal test conditions. The following figures demonstrates these aspects. The first figure shows that the shape reproducibility is very good. The differences between the four tests are very small and they fit quite well with the desired profile especially between 67 and 70 seconds. This is the most important region as in case of an experiment with a vessel this part account for the inswing into the extreme event. Consequently, it is not a problem that the wave profiles do not agree satisfactorily after the crest at 70 seconds, because the extreme event has already occurred when the vessel encounters this part. The second figure shows that the time reproducibility is good. The measured profiles lie within one-tenth of a second. Part of this difference can be contributed to the manually, simultaneously starting of the measurement and the wavemaker.

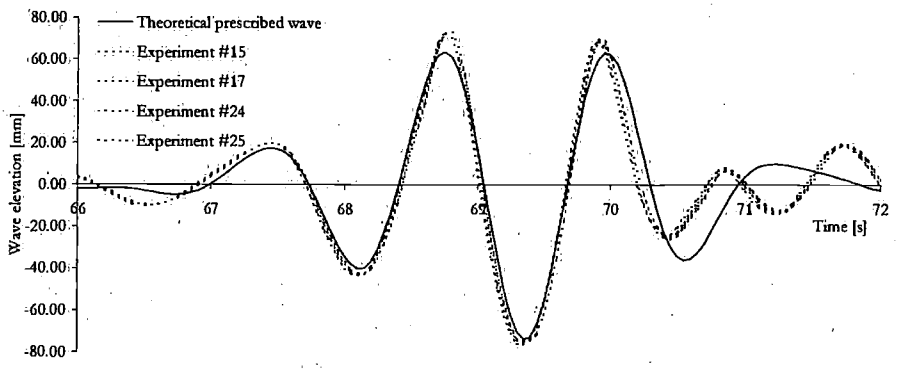

Figure 111 Accuracy and shape reproducibility of response conditioned waves

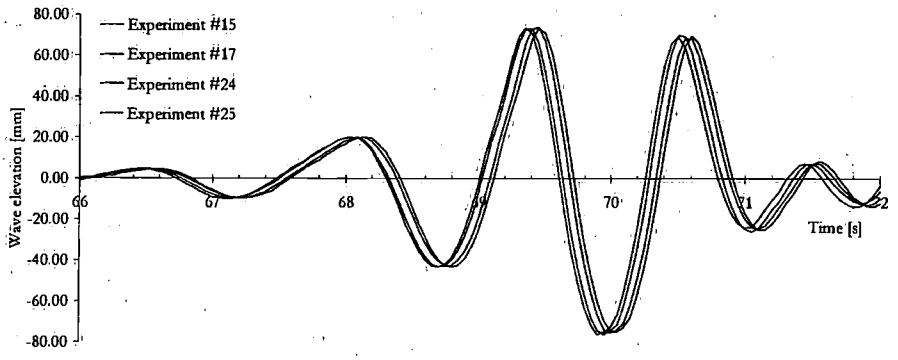

Figure 112 Time reproducibility of response conditioned waves

The third aspect, generating scaled wave profiles, is troublesome as a scaled wavemaker control signal does not reproduce the prescribed wave profile fully satisfactorily. See the two figures below. It is difficult to derive from these results what causes the scaling to be unsatisfactorily. Maybe the scaled profile does occur but is shifted in position or the nonlinear behaviour of the wavemaker phase transfer is causing the discrepancy. If the profile does occur but is shifted in position it can be taken into account by tuning the arrival time of the model. Consequently this is then an important precondition for the carriage control program.

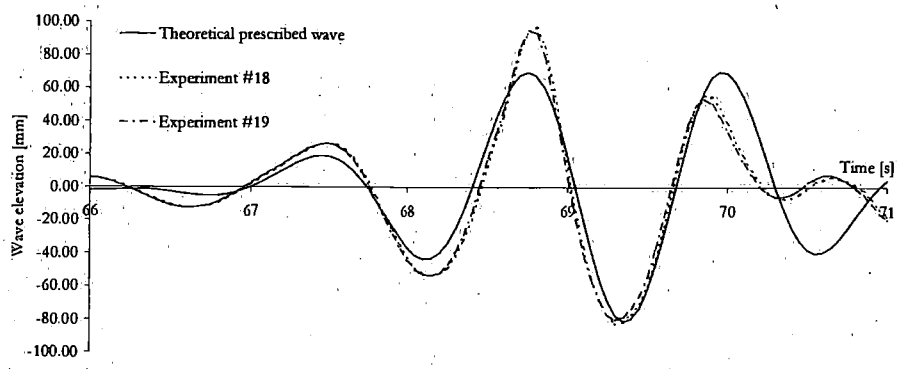

Figure 113 Response conditioned wave profile with scaled wavemaker signal, scale factor = 1.10

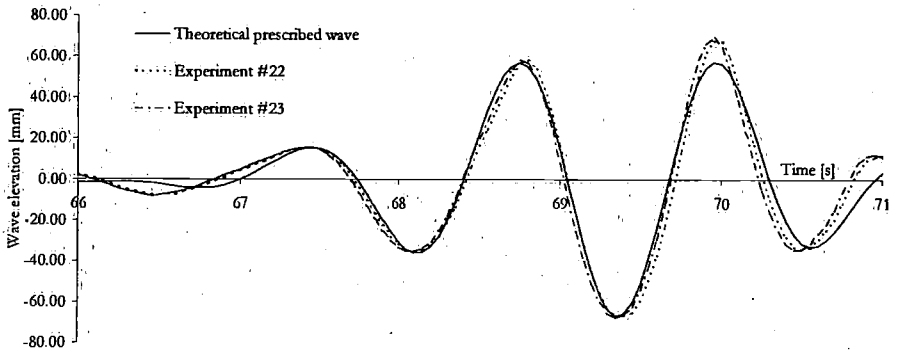

Figure 114 Response conditioned wave profile with scaled wavemaker signal, scale factor = 0.90

Overall we can conclude that the application of linear wave theory reproduces the desired wave profiles sufficiently accurately. If nonlinearities would be stronger a nonlinear simulation program could be used, see for instance Westhuis (2001). He showed that a nonlinear potential code could well predict nonlinear behaviour of bi-harmonic waves in a towing tank. Such a program should be used inversely by specifying the desired wave profile and fluid velocities and the location of it and calculating backwards to determine the required wavemaker motions.

Synchronisation of response conditioned wave generation and a moving carriage

As the response conditioned wave occurs at some location in the tank a difficult requirement for the carriage control arises as the model has to be on that spot, at that timestep and with the correct forward speed. Moreover a tuning requirement was put forward from the preliminary feasibility experiments. In order to overcome these

difficulties a control program was developed, which controlled the speed of the carriage and incorporated a simultaneous start of the wavemaker. Before every run the carriage was placed at the MLER location, 30 meters from the wavemaker. The carriage was driven backwards while the computer measured the distance. When the carriage was stopped the desired arrival time and the desired arrival speed were given to the control program. With these parameters and the measured distance the control program can accurately drive the carriage up to the MLER location and arrive at the correct MLER timestep with the correct speed. The tuning requirement was possible by varying the arrival time with small time quantities. With this tuning possibility scaling became much better as the next paragraph demonstrates.

6.2 Description of the model experiments

A description is given of the hullform as well as the experimental lay-out.

The MO-2015 frigate model

A modern frigate hullform was chosen for an experimental study of the EMLER technique. This hullform was used by the Royal Netherlands Navy and MARIN as a Point Design in several studies, see for instance Kapsenberg and Brouwer (1998). The scale factor was 48. The main particulars are summarised in the following table. The hullform is shown in Figure 115.

Name	Symbol	Value (full scale)
Length between perpendiculars	L_{pp}	120.00 [m]
Beam on waterline	B_{wl}	15.76 [m]
Depth	D	10.20 [m]
Draft	T	4.60 [m]
Displacement	∇	4137.4 [m^3]
Vertical centre of gravity	KG	8.12 [m]
Block coefficient	C_b	0.4765
Midship section coefficient	C_m	0.7593

Table 7 Main particulars of the MO-2015 frigate

The hullform is a typical modern frigate hullform with rather flat lines in the aft ship and with bow flare. A moderate bow flare angle was chosen in order to circumvent extreme slamming incidents. It was thought that a successful testing of the EMLER would stimulate new experiments with stronger nonlinear behaviour. In that case increased bow flare is an option for further testing.

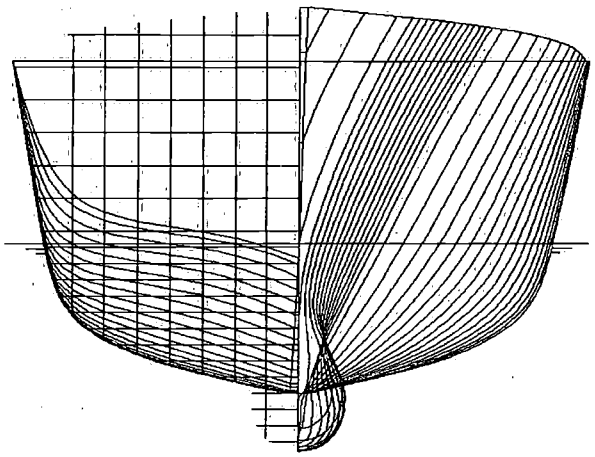

Figure 115 Body plan of the MO-2015 frigate

The model was made of wooden slats, which were attached to transverse frames. Next the hull was divided in two parts in order to measure the vertical bending moment and vertical shear force. This cut was placed at the midship at ordinate 10. In both parts a honey-cumb bulkhead was placed and a force-transducer was placed between these two bulkheads. The centre of the force transducer was placed at the same vertical position as the centre of gravity. The hull was made watertight again by putting flexible rubber over the cut.

The individual centres of gravity, masses and mass moment of inertias were calibrated for both parts separately. The properties are listed in the table.

	Aft module	**Fore module**	**Total hull**
Mass	2276.0 [ton]	1964.8 [ton]	4240.8 [ton]
x_{cog} (from A_{pp})	36.0 [m]	82.8 [m]	57.68 [m]
z_{cog} (from A_{pp})	8.12 [m]	8.12 [m]	8.12 [m]
k_{yy}	18.75 [m]	18.97 [m]	30.00 [m]

Table 8 Mass properties of the MO-2015 frigate

The stiffness of the model was tested in calm water by hitting the model with a hammer to determine the first eigenfrequency. This resulted in a value of 12.4 [Hz], while the

highest encounter frequency of the wave spectra was 2.42 [Hz]. Thus the eigenfrequency was large enough to prevent severe interference of hull vibrations with the higher harmonics due to nonlinear wave induced loads.

Experimental lay-out

The vessel was placed under the carriage and kept in position by two rods. The first one was connected on the fore part with a hinge and was free to heave. The second rod was placed aft to prevent the vessel from sway and yaw but was free to surge and heave. The hinge of the forward rod was placed at the same height as the vertical centre of gravity. This forward rod towed the vessel forward.
A total of 7 measurement channels were used. Two wave probes were placed to measure the wave elevation. One probe was placed in front of the model to measure the undisturbed incident wave and one was placed aside of the model at the same longitudinal position as the centre of gravity. These probes were of the electric wire type. The relative wave motion was also measured using an electric-wire type probe. This probe was placed at ordinate 18 and at 15 [mm] from the hull surface. The heave and pitch motions were measured with an optical motion measurement system. A force transducer between the two parts measured the vertical shear force and vertical bending moment.

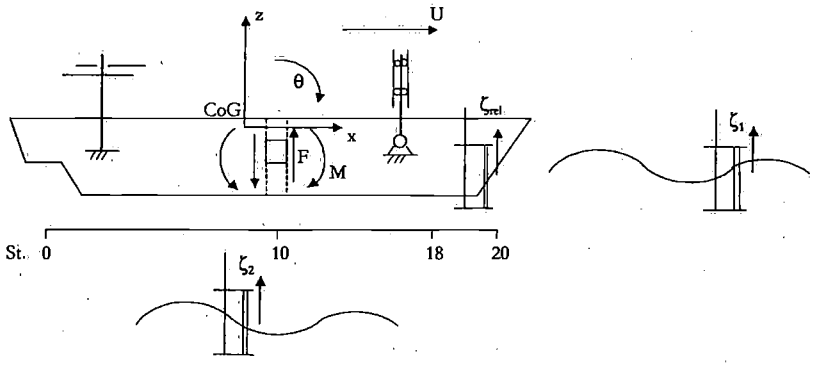

Figure 116 Experimental set-up and sign convention of measurement channels

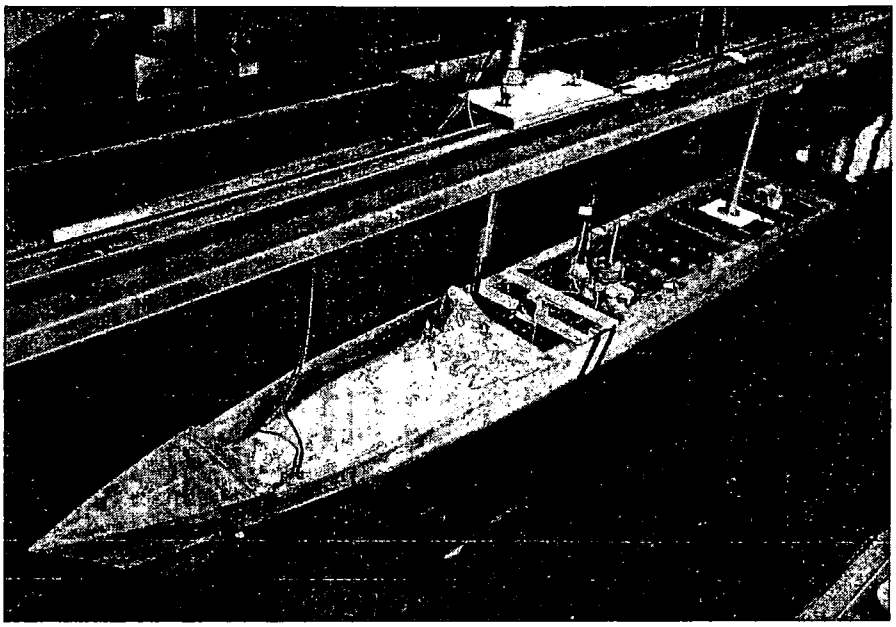

Figure 117 Divided frigate model under towing tank carriage

6.3 Results and analysis of model experiments

The modeltest program comprised regular, irregular and response conditioned wave experiments. The following analyses are derived from the tests,

- Linear transfer function versus numerical prediction
- Modeltest response statistics from irregular tests versus model test response statistics from EMLER conditioned tests
- Modeltest response conditioned tests versus numerical simulation
- Modeltest response statistics from irregular tests versus numerical predictions
- Analysis of average wave profiles around crests and troughs from experiments and compare with numerical prediction
- Expected extreme prediction from experiments and numerical simulation
- Towing tank feasibility assessment of response conditioned testing

6.3.1 Regular wave experiments

The transfer function of the midship vertical bending moment was required for the generation of response conditioned waves. In order to investigate the EMLER technique

as accurate as possible this transfer function was obtained from experiments. A second objective was to get more validation of the ship motion program as formulated in appendix B.2. Regular wave experiments were conducted with small wave amplitudes, for a large set of frequencies and for two speeds, 12 and 15 knots. These correspond with Froude numbers of 0.18 and 0.22 respectively. The resulting transfer functions are shown below together with the numerical predictions. The linear program is a 3D Green function panel program solving both the radiation and the diffraction problem. The zero-forward speed Green function is used, thus high speed is consistently accounted for. As base flow the double-body flow is used and the body boundary conditions for the radiation problem incorporate the full m-terms. Forces are obtained by integrating the pressures over the hullform. The potential derivatives are calculated using the Green function derivatives instead of a Stokes formulation. To suppress irregular frequency phenomena a panel lid was placed in the hull at the waterline level. More details and calculation variations of this program are given in appendix B.2.

For the 12 knots case the bending moment is reasonably predicted while for 15 knots the result is good. The shear force is poor predicted for both speeds. For the lower frequencies the transfer function is under predicted while for larger frequencies the transfer function is over predicted. The relative wave motion is under predicted for the 12 knots case and this is even somewhat worse for the 15 knots case. Most likely the contribution due to radiation and diffraction causes this discrepancy between the experiments and the calculations, as these are not incorporated in the program. Heave and pitch are well predicted for both speeds.

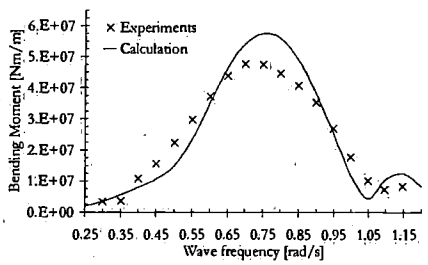

Figure 118 Bending moment, 12 knots, head waves

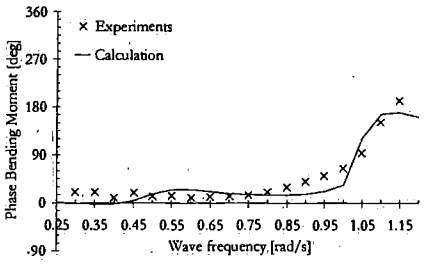

Figure 119 Phase bending moment, 12 knots

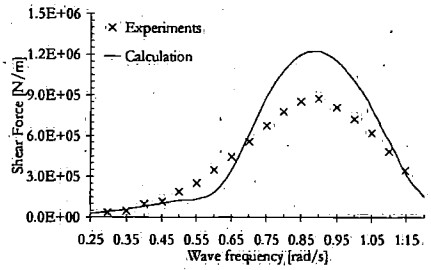

Figure 120 Shear force, 12 knots

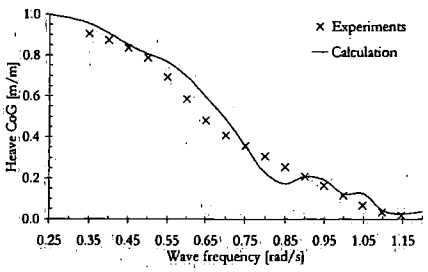

Figure 124 Heave motion CoG, 12 knots

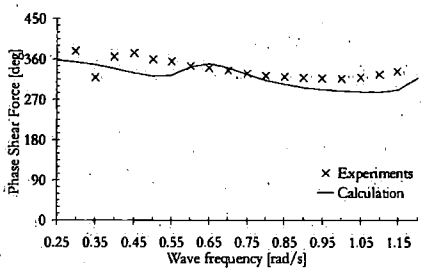

Figure 121 Shear force phase, 12 knots

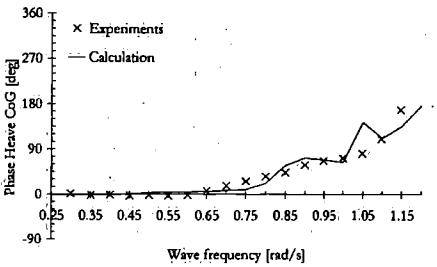

Figure 125 Heave motion CoG phase, 12 knots

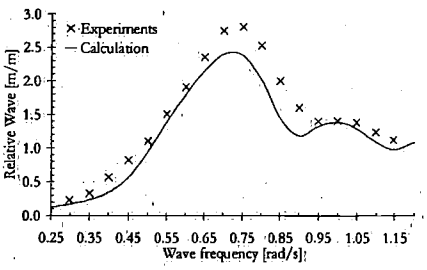

Figure 122 Relative wave motion, 12 knots

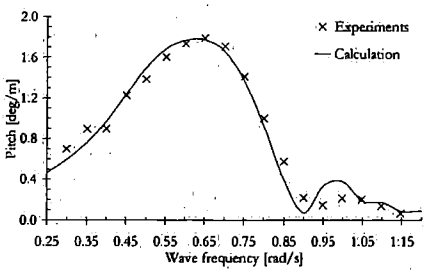

Figure 126 Pitch motion, 12 knots

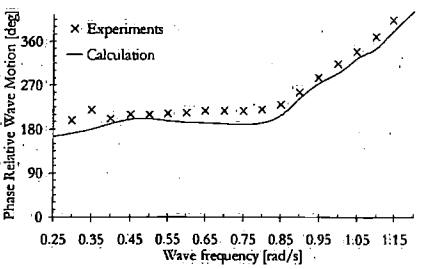

Figure 123 Relative wave motion phase, 12 knots

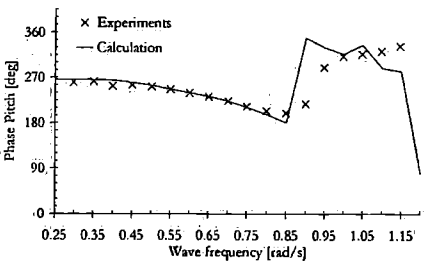

Figure 127 Pitch motion phase, 12 knots

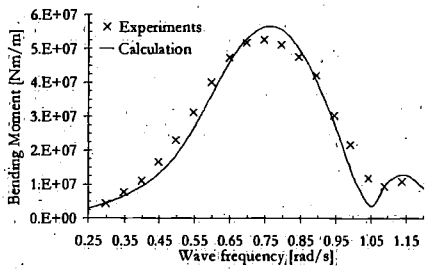

Figure 128 Bending moment, 15 knots

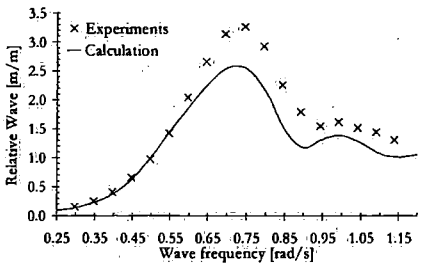

Figure 132 Relative wave motion, 15 knots

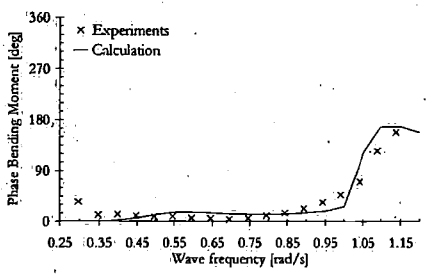

Figure 129 Bending moment phase, 15 knots

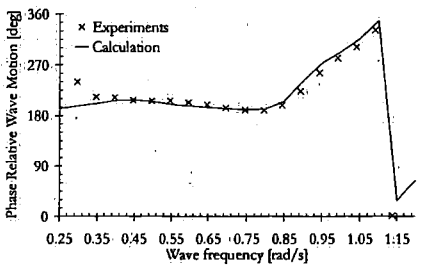

Figure 133 Relative wave motion phase, 15 knots

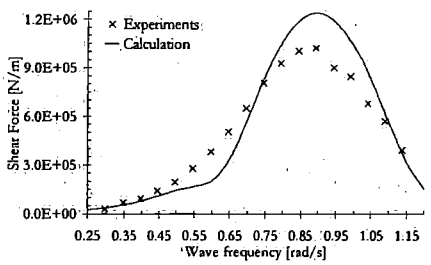

Figure 130 Shear force, 15 knots

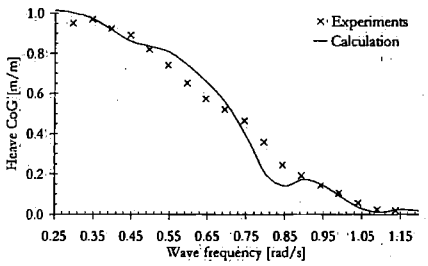

Figure 134 Heave motion CoG, 15 knots

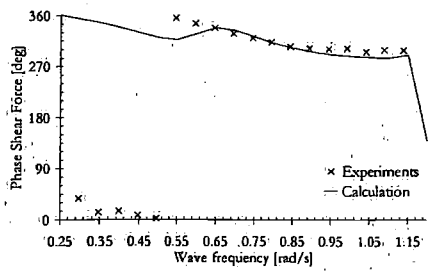

Figure 131 Shear force phase, 15 knots

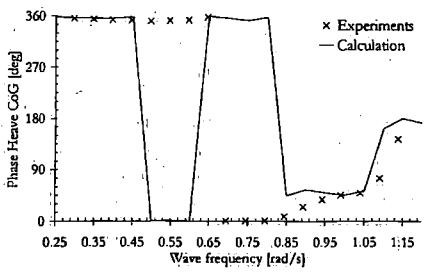

Figure 135 Heave motion CoG phase, 15 knots

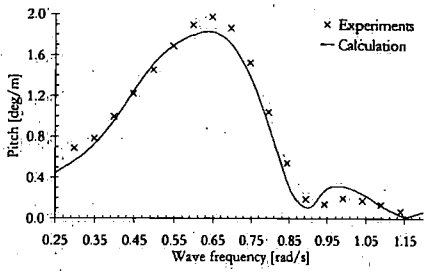

Figure 136 Pitch motion, 15 knots

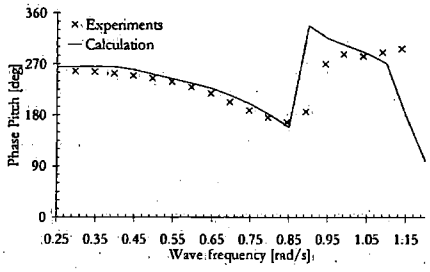

Figure 137 Pitch motion phase, 15 knots

6.3.2 Irregular wave experiments

Two irregular sea states have been tested in the tank. These irregular wave spectra are listed in the table below and are given by the following modified Pierson-Moskowitz formulation, see DNV (2000).

$$S_{\zeta\zeta}(\omega) = \alpha_s \frac{g^2}{\omega^5} \cdot e^{-\frac{5}{4}\left(\frac{\omega_p}{\omega}\right)^4} \cdot \gamma_s^{e^{-\frac{1}{2}\left(\frac{\omega-\omega_p}{\beta_s\omega_p}\right)^2}}$$

where

$$\alpha_s = \frac{5}{16}\left(\frac{H_s^2\omega_p^4}{g^2}\right)\cdot(1-0.287\cdot\ln\gamma_s) \qquad (6.8)$$

$$\beta_s = 0.07 \quad if\ \omega \le \omega_p$$

$$\beta_s = 0.09 \quad if\ \omega > \omega_p$$

Sea State	Spectrum	H_s	T_z
4	Modified Pierson-Moskowitz	2.5 [m]	6.5 [s]
5	Modified Pierson-Moskowitz	4.3 [m]	7.4 [s]

Table 9 Irregular wave spectral properties according to STANAG 4194

The wave frequency range was limited from 0.30 to 1.15 [rad/s]. This was done because of physical limitations of the wavemaker. In order not to lose wave energy the wave amplitudes were enlarged such that the prescribed significant wave height was correct according to,

$$H_s = 4\sqrt{m_0} \qquad and \qquad m_0 = \sum_{j=1}^{N} \frac{1}{2}\zeta_{a,j}^2 \tag{6.9}$$

Response conditioned experiments

Response conditioned waves have been calculated with the use of the experimentally determined transfer functions for the midship vertical bending moment and the wave spectra. With the procedure as outlined in paragraph 6.1 the control signal for the wavemaker was formulated. For both wave spectra, which have been tested, response conditioned experiments have been conducted at different scales. Sea state 4 does not induce situations with severe green water or slamming effects. Hence for this case it is expected that the EMLER method should work well. By scaling the wavemaker control signal and tuning the arrival time scaled response conditioned waves could be generated. These tests were used to transform the linear exceedance probability function to the nonlinear exceedance probability function. Below the resulting prediction is shown. As seen the conditioned experiments give a good prediction of the tail of the sagging exceedance probability function.

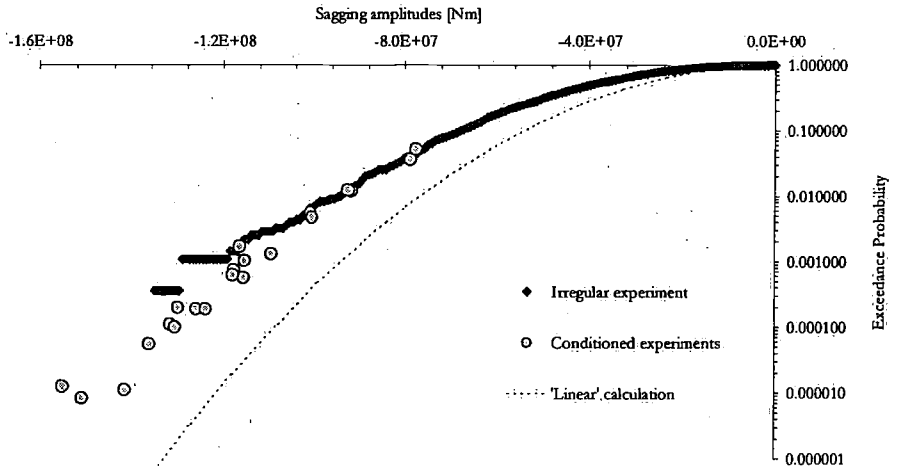

Figure 138 Sagging probability function, 15 kn, SS-4

For sea state 5 the situation is different as large amounts of green water are shipped over the bow and slamming is also present. A total of 33 conditioned experiments were conducted and used to calculate the sagging amplitude exceedance probability function. Figure 139 shows the result. Again a good prediction is obtained. The key assumption of the EMLER method is that the linear model should identify extreme events. While green water and slamming are not present in the linear model the method performs very well for this case.

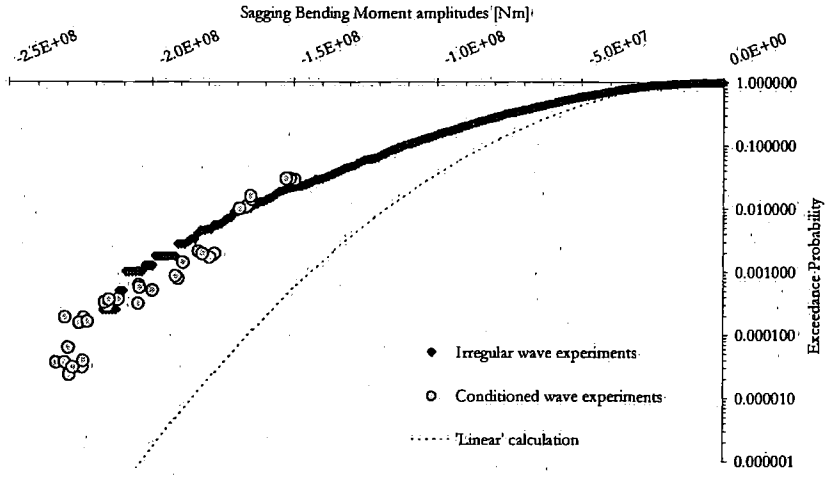

Figure 139 Sagging probability function, 12 kn, SS-5

In order to let this method work properly in the towing tank it is of importance that the theoretically prescribed response conditioned waves are well produced in the tank. By tuning the arrival time this could well be established and several examples are presented hereafter. The encounter incident wave, the bending moment response and the relative wave motion are shown. For both responses the nonlinear numerical prediction are given as well.

The nonlinear Froude-Krylov program as described in appendix B.3 was used to simulate the response conditioned waves and the time series are compared with some experiments, see Figure 140 to Figure 148. The results for three scale factors are shown, 0.72, 1.05 and 1.22. These scale factors refer to the incident wave, where a scale factor of 1.0 corresponds to the wave, which induces the expected 1-hour extreme bending moment. The encountered waves corresponds well with only a slight difference for the simulation with the largest scale factor. The differences after 18-19 seconds are not important as the extreme event has already occurred. The calculated bending moment sequence for the smallest scale factors fits very well with the experiment, while the relative wave motions shows a strong nonlinear peak around t=14 [s] in the experiments, which cannot be calculated by the program. Moreover the relative wave troughs are underpredicted. The results for the scale factor being 1.05 show that the nonlinear program overpredicts the sagging extreme and a slam induces a whipping response of the hull. Both the relative wave crests and troughs reach their maxima, which is the constraint of the relative wave probe. The third simulation shows even a greater difference in the sagging extreme.

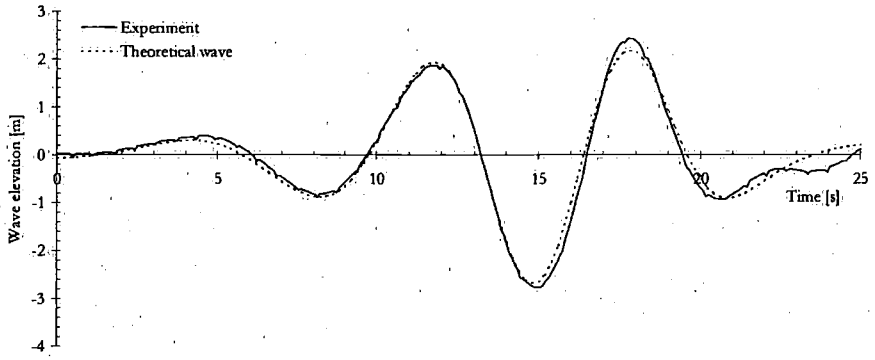

Figure 140 Encounter wave elevation, MLER scale=0.72, 12kn

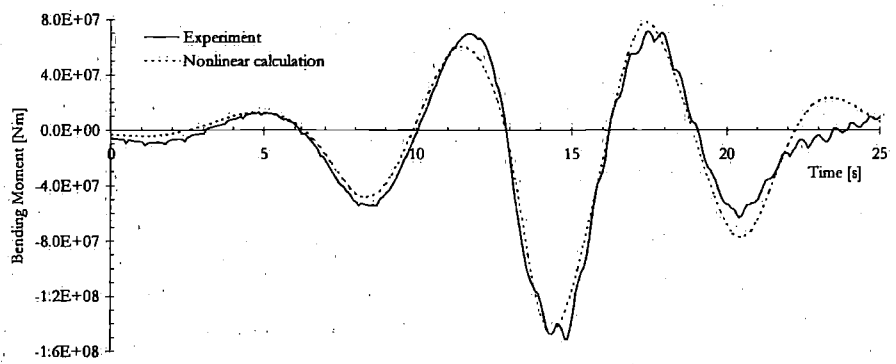

Figure 141 Bending moment, MLER scale=0.72, 12kn

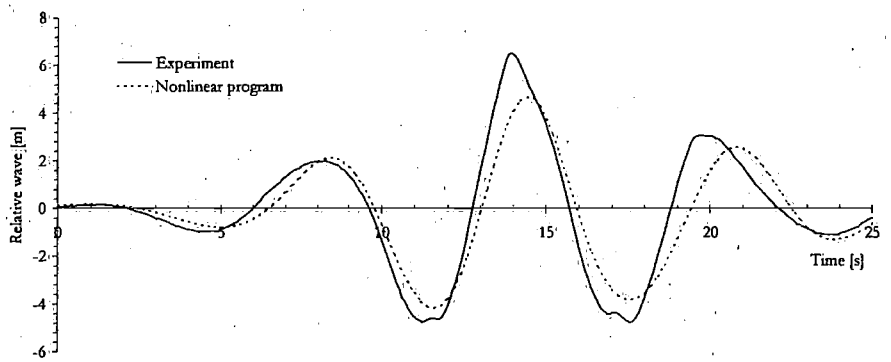

Figure 142 Relative wave, MLER scale=0.72, 12kn

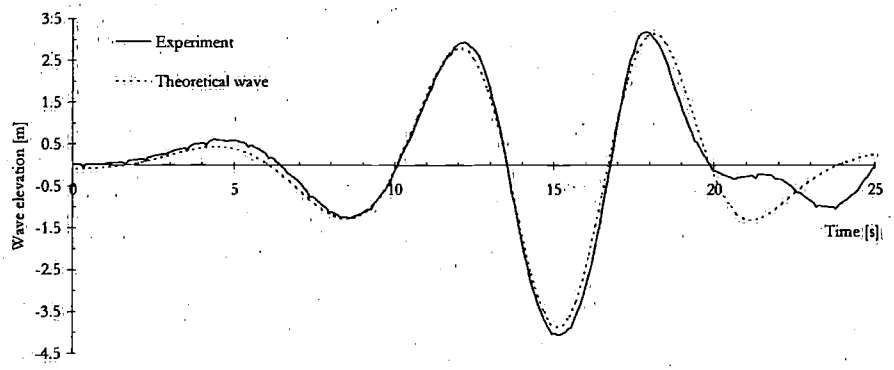

Figure 143 Encountered wave, MLER scale=1.05, 12kn

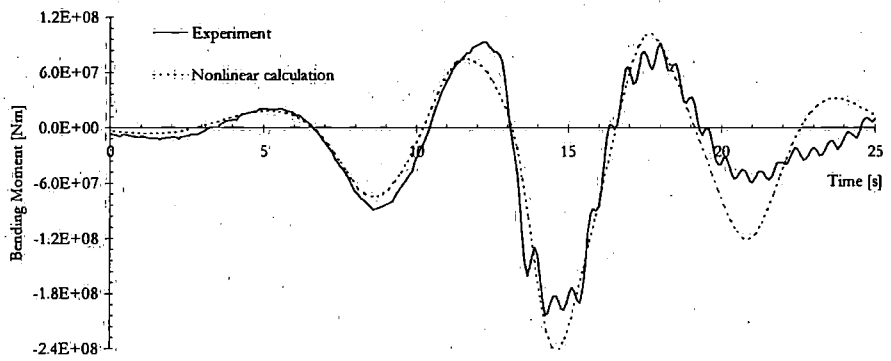

Figure 144 Bending moment, MLER scale=1.05, 12kn

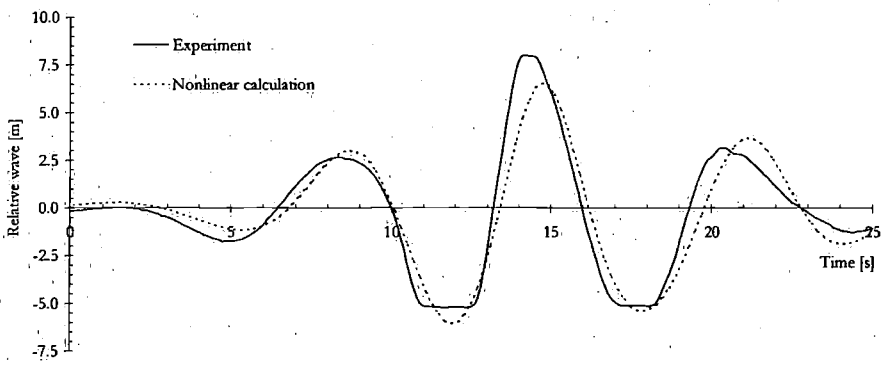

Figure 145 Relative wave, MLER scale=1.05, 12kn

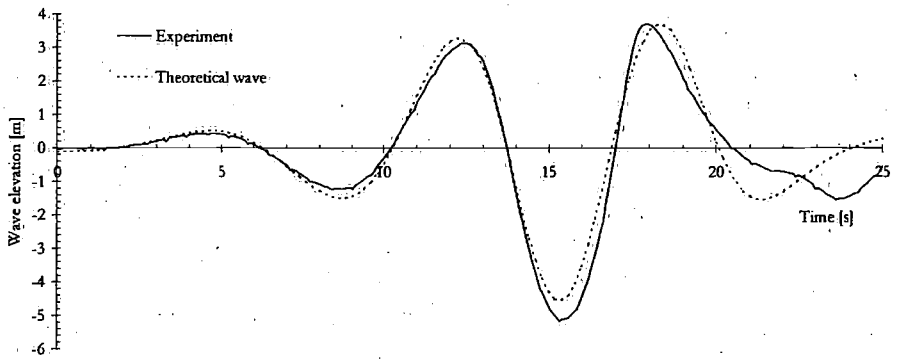

Figure 146 Encountered wave, MLER scale=1.22, 12kn

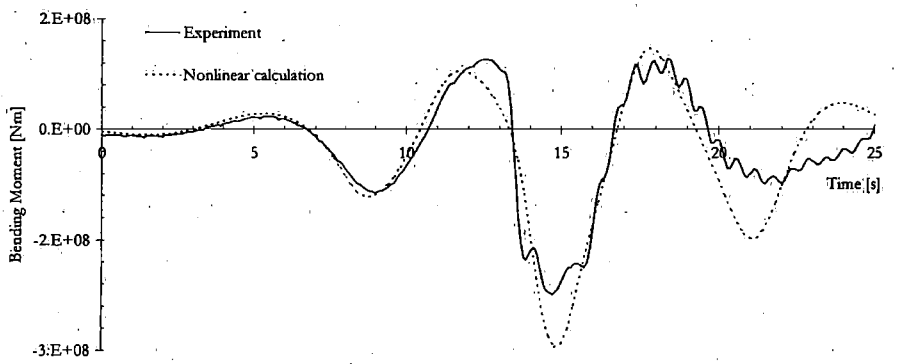

Figure 147 Bending moment, MLER scale=1.22, 12kn

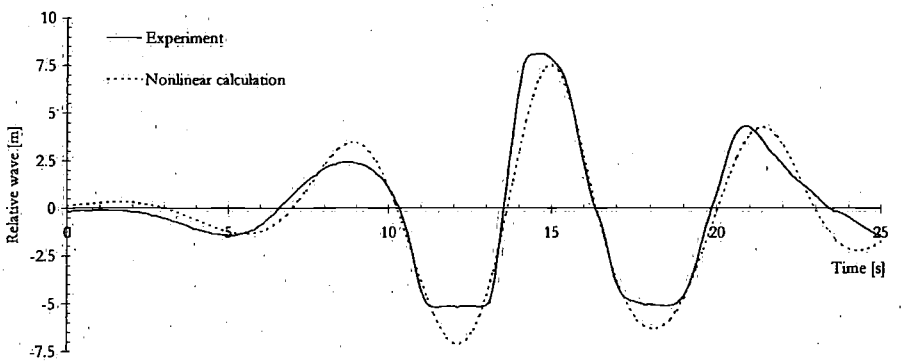

Figure 148 Relative wave, MLER scale=1.22, 12kn

Expected 1-hour extreme bending moment in sea state 5

Several techniques are available if the expected extreme is required, either for design purposes or as a characteristic value in a LRFD approach. A comparison is made between them in this section. In addition to the irregular experiments and the conditioned experiments regular design waves were tested. The techniques discussed in the previous part are all applied and in addition a series of regular wave experiments have been conducted. The frequency of the bending moment transfer function peak was generated as a regular wave and varied with different amplitudes. See Figure 149 for the results. By dividing the calculated expected linear extreme by the transfer function peak a wave amplitude is obtained and this figure subsequently provides the corresponding nonlinear extreme. Besides these experimental methods a series of mathematical approaches are applied, namely:

- 3-parameter Weibull fit
- Hermite transformation model
- Nonlinear program irregular simulation
- Nonlinear program MLER
- Nonlinear program regular design waves

The expected 1-hour extreme sagging amplitude, as derived from the irregular tests, was set to 100% and all the other methods are accordingly scaled. The predictions are plotted in Figure 150. The best prediction is given by the conditioned experiments with also a good result from the regular experiments and the Weibull fit. Both the Hermite fit and the nonlinear program predictions are 8% too high, while the two remaining calculations give overpredictions of 17% and 28% respectively.

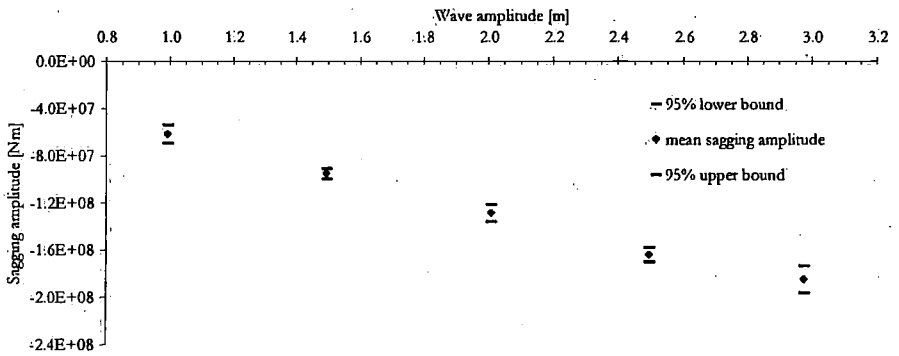

Figure 149 Averaged sagging amplitudes in experimental regular waves, 12 knots

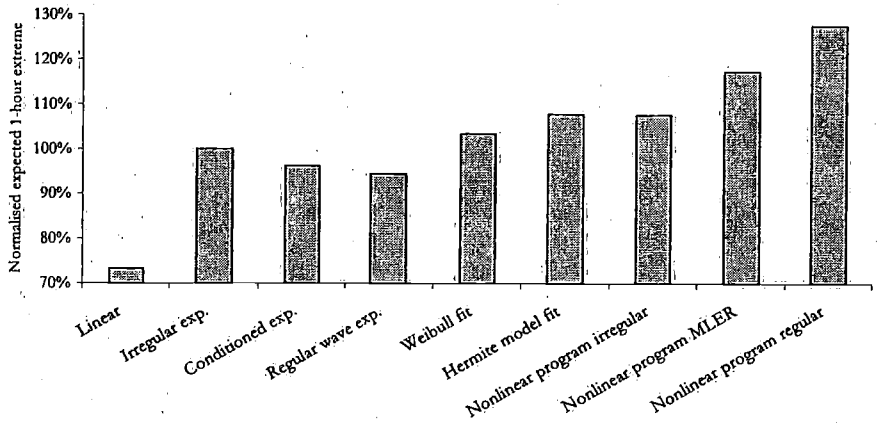

Figure 150 Expected 1-hour extreme sagging amplitude

Irregular experiments versus numerical predictions

First a comparison is made between the irregular data for all measured signals and the nonlinear program.

Irregular waves were constructed from the measured wave spectra as generated in the towing tank and used to simulate the motions and loads with the nonlinear Froude-Krylov program. The resulting crest and trough probability functions are plotted together with the irregular experiments in Figure 151 to Figure 174. In addition the linear Rayleigh probability function are given as well. These have been calculated by using the experimental determined transfer functions and the measured wave spectra. Therefore 'Linear' is placed between quotation marks. The wave amplitudes are well predicted for sea state 4 and show a slight difference for sea state 5. The hogging amplitudes are underpredicted for sea state 4 but are excellent predicted for sea state 5. The sagging amplitudes are well predicted for both sea states except for the largest sagging responses in sea state 5. The program gives here overpredicted values. It seems that the program cannot predict the 'bend' in the probability curve. The shear force positive amplitudes are overpredicted for both sea states with only a small difference in sea state 5. The negative amplitudes are very good predicted in sea state 4 and reasonably predicted for sea state 5. This is quite remarkable as the prediction of the linear transfer function was severe overpredicted for the 15 knots case, which was used in sea state 4. The relative wave crests are well predicted up to exceedance probabilities of 0.001 for sea state 4 but are underpredicted for sea state 5. For the relative wave troughs it is even worse. Underpredictions of more than a meter are seen. This can partly be explained because the nonlinear program does not incorporate the contributions from radiated and diffracted waves but another part is explained by studying video recordings of the bow

motions in waves. The relative wave probe was placed directly after the sonar dome, which acts as a bulb as well. The transient effect of the bulb was quite strong. If the bulb moved upwards and approached the water surface a large trough behind the sonar dome was seen. This can explain as well why the relative wave troughs are underpredicted. The sharp cut downwards of the relative wave troughs probability function around 5.0 [m] is due to the fact that the probe ends there. As the relative wave motion and the midship bending are strongly related it looks somewhat strange to have good predictions of the bending moments and poor relative wave motions predictions. But the bending moment is the result of the integrated water pressures and the inertia effects and it is very well possible that locally the predictions might be troublesome but globally not. The positive heave motion amplitudes are slightly overpredicted while the negative amplitudes are slightly underpredicted. For sea state 4 the nonlinear prediction agrees well with the measurements. Both the positive and negative pitch amplitudes are slightly underpredicted for sea state 4. This is somewhat strange as the irregular experiments follow the linear curve perfectly while the linear transfer function was very well predicted. For sea state 5 the positive pitch amplitudes were excellent predicted while the negatives ones slightly underpredicted.

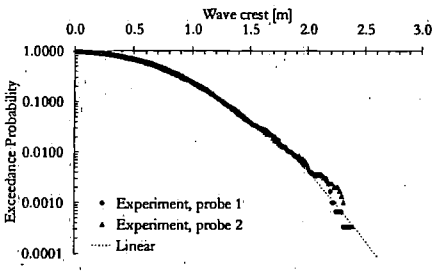

Figure 151 Wave crests, SS-4, 12 knots

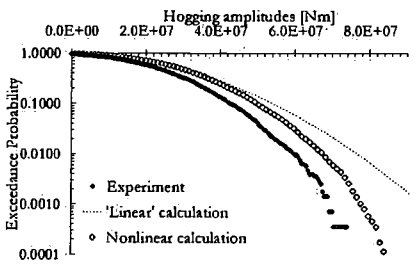

Figure 153 Hogging, SS-4, 12 knots, head

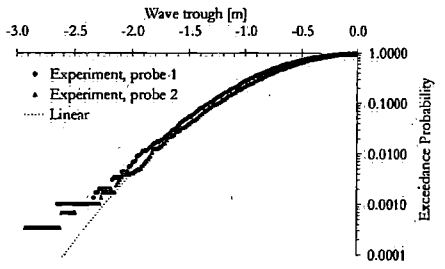

Figure 152 Wave troughs, SS-4, 12kn

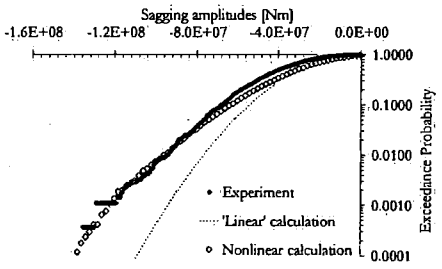

Figure 154 Sagging, SS-4, 12kn

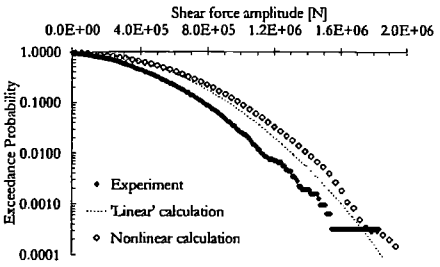

Figure 155 Shear force crests, SS-4, 12kn

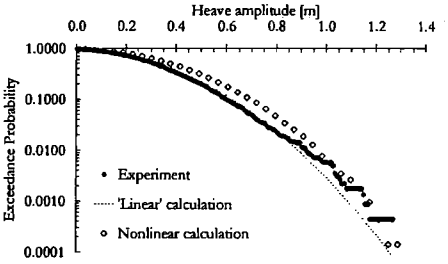

Figure 159 Heave CoG crests, SS-4, 12 kn

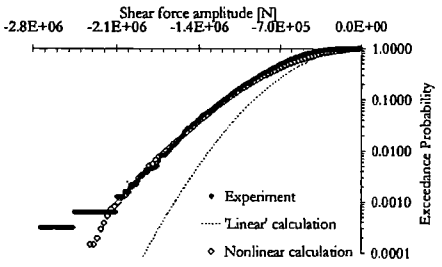

Figure 156 Shear force troughs, SS-4, 12kn

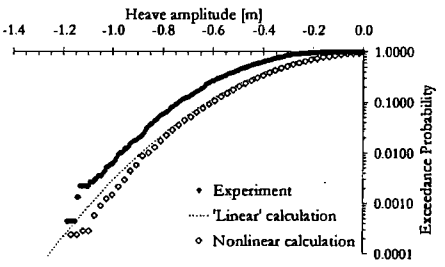

Figure 160 Heave CoG troughs, SS-4, 12kn

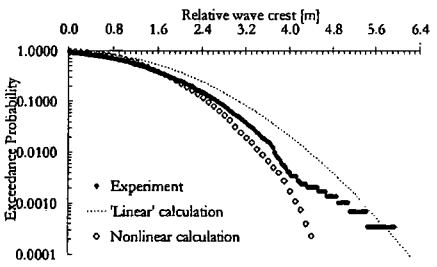

Figure 157 Relative wave crests, SS-4, 12kn

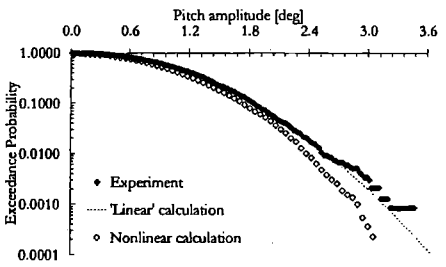

Figure 161 Pitch crests, SS-4, 12kn

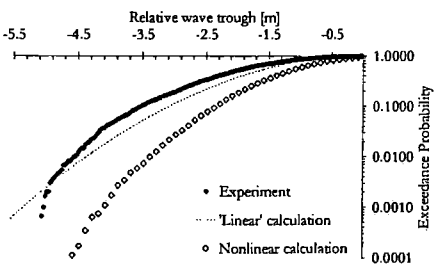

Figure 158 Relative wave troughs, SS-4, 12kn

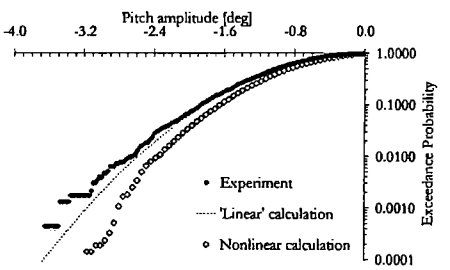

Figure 162 Pitch troughs, SS-4, 12kn

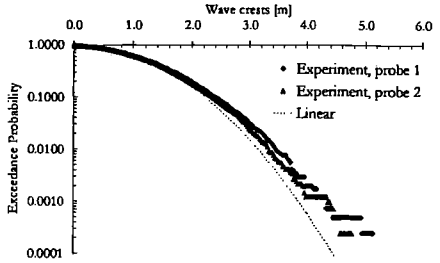

Figure 163 Wave crests, SS-5, 12 knots

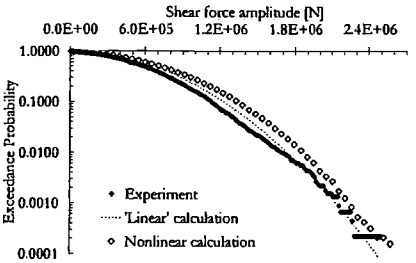

Figure 167 Shear force crests, SS-5, 12kn

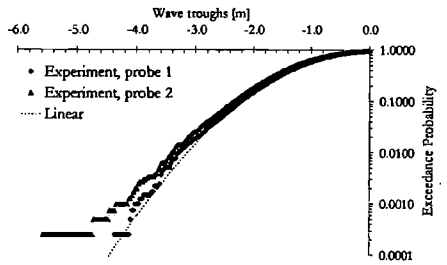

Figure 164 Wave troughs, SS-5, 12kn

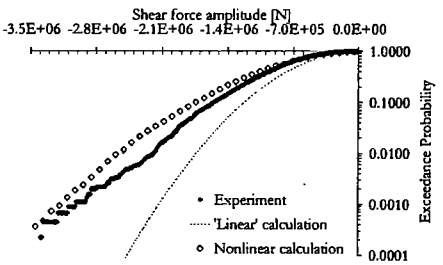

Figure 168 Shear force troughs, SS-5, 12kn

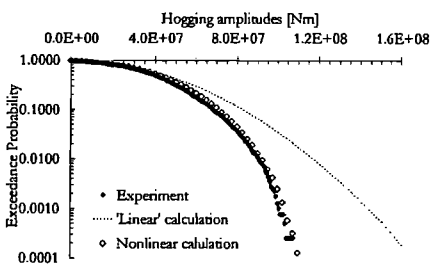

Figure 165 Hogging, SS-5, 12 knots, head

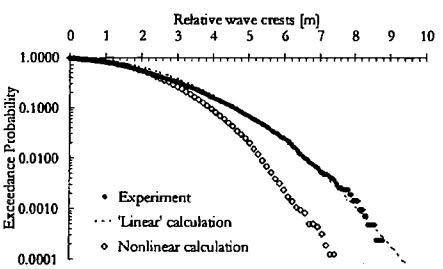

Figure 169 Relative wave crests, SS-5, 12kn

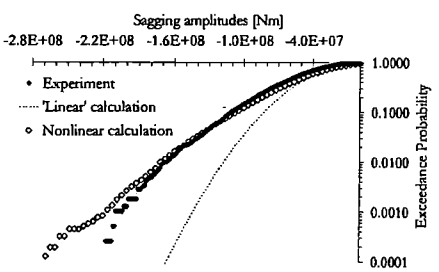

Figure 166 Sagging, SS-5, 12kn

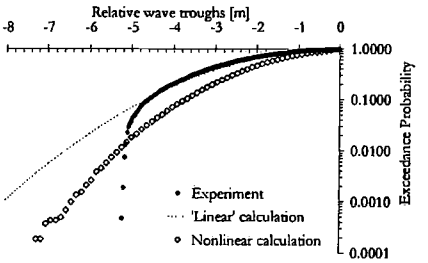

Figure 170 Relative wave troughs, SS-5, 12kn

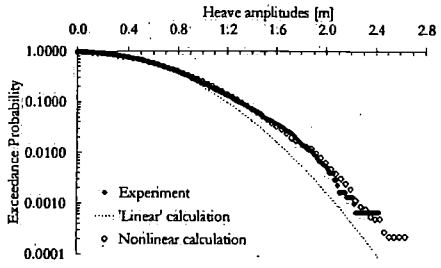

Figure 171 Heave CoG crests, SS-5, 12 kn

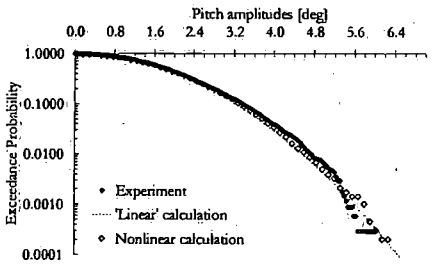

Figure 173 Pitch crests, SS-5, 12kn

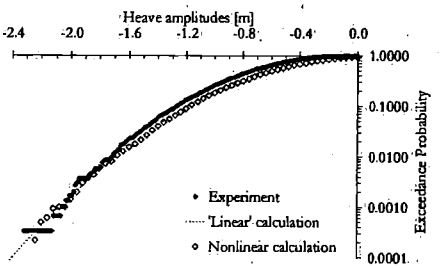

Figure 172 Heave CoG troughs, SS-5, 12kn

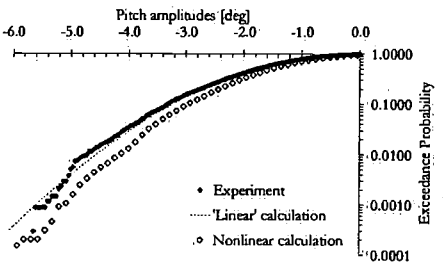

Figure 174 Pitch troughs, SS-5, 12kn

Hermite transformation model and 3-parameter Weibull fitting

It is common practice to apply a mathematical fit on short-term statistics obtained with an irregular simulation. In the previous part mathematical fit methods were already applied to the irregular data to estimate the expected 1-hour extreme. Many different models can be used. Wang (2001) has studied three models for different ships; a Generalised Gamma distribution, a Generalised Pareto distribution and a three-parameter Weibull distribution and concluded that the Weibull model was most suitable. In this study the three-parameter Weibull is also used and fitted to the experiments for one hour of the data and for the entire set (6 ½ hours). Additionally the Hermite transformation technique, as applied in the previous chapter, is used as well. In the figure below both are shown. From this figure it is easily seen that the difference in the prediction of the expected extreme in 3 hours is not large but the tails of the amplitude distributions are significantly different. Moreover the conditioning technique clearly shows one of the important advantages, namely the ability to calculate extreme behaviour with small exceedance probabilities. If by irregular experiments the same exceedance level was to be obtained, 69 hours of irregular data would be necessary. This equals three weeks of continuous testing. When calculating the 3-hour extreme sagging distribution by applying order statistics to these amplitude distributions we get Figure 176. As the structural hull girder reliability is defined by the overlap of the extreme load distribution

and the ultimate capacity distribution we can conclude form this figure that significant differences in the reliability index will be obtained. To illustrate this the expected maximum sagging bending moment in 1 out of 10.000 ships is determined. These values are compared with the expected 1-hour extremes as previously presented. In Figure 177 these extreme values are presented normalised by the linear values. For the conditioned experiments the increase is smaller for the maximum extreme in 10.000 ships than for the 1-hour extreme. The Weibull fit presents a larger increase and the Hermite model shows a much larger increase. Care is to be taken to interpret the results in this form as this is a short term sea state and not the maximum severity the vessel must withstand.

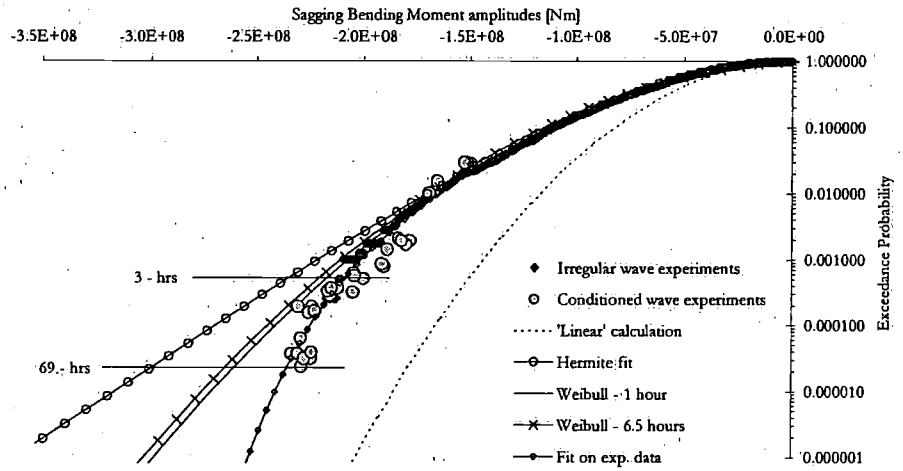

Figure 175 Sagging amplitude probability functions, 12 kn, SS-5

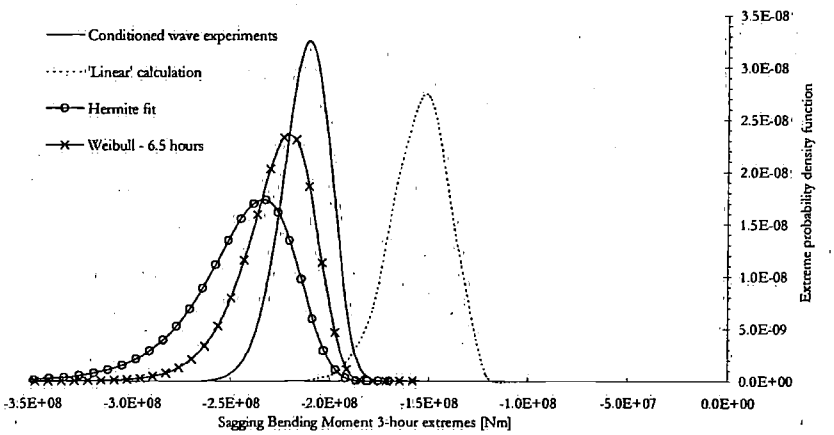

Figure 176 Sagging extreme probability density function, 12 kn, SS-5

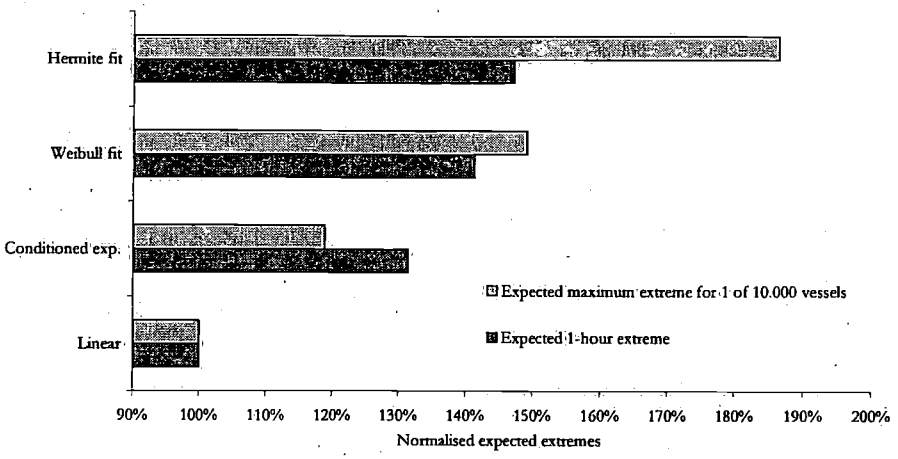

Figure 177 Expected 1-hour extreme and maximum expected extreme for 10.000 ships

Average wave profiles around large wave and response amplitudes

The response conditioning technique predicts the most likely profile around a large crest or trough and calculates subsequently the incident wave causing this specific response profile. The irregular measurements have been used to validate both steps. The average profile around the 10% largest wave crests and troughs have been used and these are compared with the theoretical prediction, namely the Tromans formulation. These three profiles are shown in Figure 178. From this it is concluded that the Tromans formulation fits well with the experimentally derived profiles. The second test was done by identifying large sagging bending moments and average the encountered wave profile around the time-step of these sagging responses. If the response conditioning technique performs well, the theoretical conditioned wave should fit this profile. Figure 179 shows this profile together with the theoretical profile and the average profile around large wave troughs. It is seen that the average wave profile around large sagging amplitudes corresponds well, especially the inswing, with the theoretical conditioned wave. Moreover the most likely profile around large wave troughs has a different character, from which the conclusion can be drawn that the extreme responses do not necessarily occur with the most likely extreme wave. These two figures therefore support the ideas behind the theoretical derivation of the response conditioning technique.

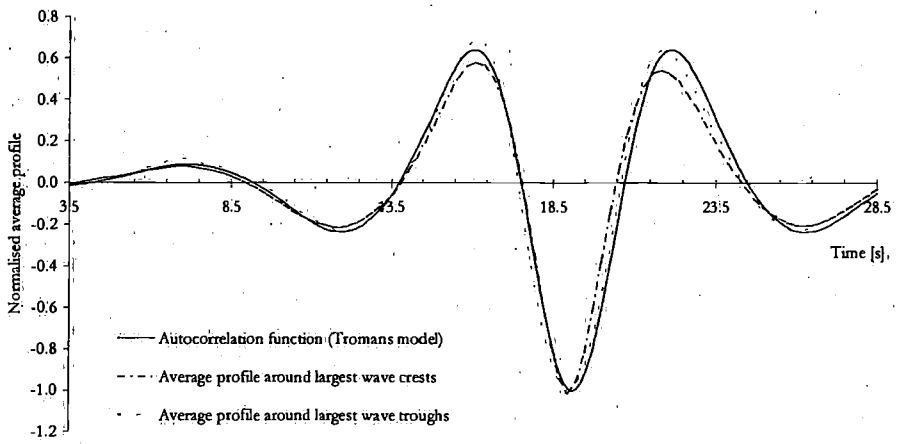

Figure 178 Average wave profile around large wave amplitudes, sea state 5

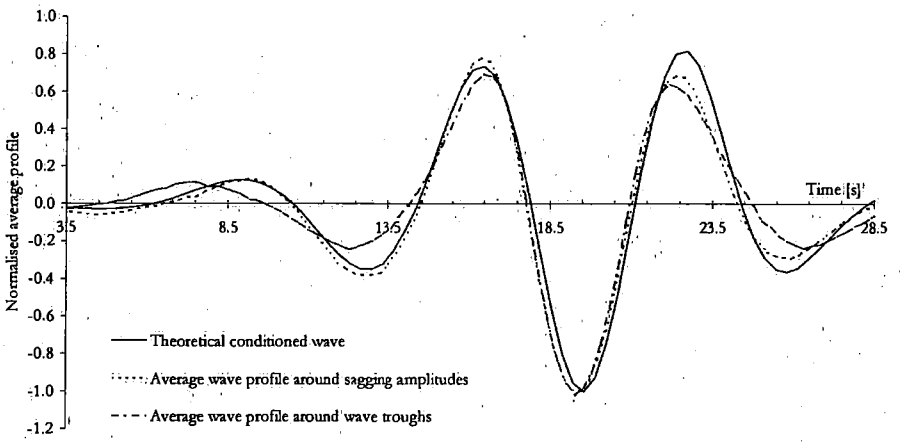

Figure 179 Average wave profile around large sagging amplitudes, sea state 5

7 Conclusions and recommendations

First the objectives as formulated in the introduction are shortly dealt with after which the conclusions are presented, which can be drawn from the research as presented in this thesis. The second paragraph presents a series of research objectives for the future, based on a discussion of the present research.

7.1 Conclusions

The introduction of the thesis states three research questions, from which the thesis objectives were formulated:

1. Develop and study advanced techniques to calculate nonlinear ship response statistics efficiently and accurately.
2. Evaluate these techniques and discuss how to implement these in existing assessments strategies for extreme hull girder loads and seakeeping performance.
3. Develop a seakeeping performance assessment method with stochastic treatment of the performance and gradual performance degradation.

The first objective is met by the study and further development of the response conditioning technique (chapter 1) and the approximate Volterra modelling technique (chapter 1). Chapter 1 presented options how the response conditioning technique can be used in long-term assessments. Secondly a reliability based seakeeping performance assessment is formulated in chapter 1 as well. The evaluation of the response conditioning and Volterra modelling technique is conducted in chapter 1 together with a case-study of the seakeeping performance of a frigate applying the reliability based seakeeping performance assessment technique in a nonlinear way. In addition to the numerical evaluations of chapter 1 a detailed evaluation of the response conditioning technique is conducted in chapter 1 by modelexperiments.

Based on this study the following conclusions are drawn:

- The most likely profile around large response amplitudes can well be predicted by the autocorrelation function scaled by the amplitude.

- The systematic association between amplitudes and periods is not an important aspect to take into account when predicting the most likely profile around large response amplitudes.
- The MLER method can predict expected nonlinear extreme responses and is very efficient and accurate. The MLER method saves computational costs by a factor of ± 300 in comparison with a 3-hours irregular simulation.
- The EMLER method can predict nonlinear amplitude and extreme distributions and is very efficient and accurate compared to other techniques. The EMLER method saves computational costs by a factor of ± 60 in comparison with a 3-hours irregular simulation. But when predicting the 3-hours extreme probability distribution a computational saving factor of 6000 is obtained when assuming that 100 simulations of 3-hours are enough to estimate the extreme distribution.
- Modelexperiments have shown that response conditioned wave profiles could well be generated in the towing tank based on linear wave theory and a linear model for the wavemaker.
- The response conditioned waves show a highly transient behaviour, which demands an accurate control mechanism to force the model at the correct position with the correct speed and at the correct timestep. It was shown that this could be achieved very well.
- The average result of measured wave profiles for large sagging responses shows a very good resemblance with the theoretical prescribed profile from the MLER approach, moreover this profile is different from the average result of measured wave profiles for large wave amplitudes.
- A few response conditioned experiments could well predict the sagging bending moment amplitude distributions up to very small exceedance probabilities. A total of 20 days continuous testing would be required when this exceedance level is to be obtained by irregular testing. In these extreme cases a large part of the bow exceeds the water surface and a large amounts of green water floods on the deck.
- Mathematical fit methods for amplitude distributions are unreliable when extrapolation is carried out to small exceedance probabilities.
- By modelling nonlinear ship responses with a nonlinear approximate Volterra model enormous reductions in computational costs can be obtained. The accuracy of the models is good but not as reliable as the MLER method.
- The kernels of the first Volterra model are more difficult to identify and is less accurate than the second model. For this second model a series of regular wave simulations suffice and the identification is very simple.
- For the presented cases the fourth order Volterra model (model II) gave best results. A fifth order model did not give any improvements. The results can become even worse as the identification procedure changes the first and third order kernel.
- It was further shown that a second order model captures already quite a large portion of the nonlinear behaviour.

- A reliability based seakeeping assessment technique is presented, which simulates a prescribed mission a large number of times. Thus probabilistic information is obtained on the seakeeping performance of all the responses, their combined result, their influence on the total performance variance and their mutual correlation. This technique offers therefore more information to the designer compared to traditional approach and secondly it can very well be fitted in a Simulation Based Design tool. Furthermore a nonlinear seakeeping assessment can be carried out when utilising nonlinear approximate Volterra models.
- The probabilistic modelling of response criteria does not lead to significant different results in seakeeping performance.
- A linear ship motion program utilising a zero-forward speed Green function and a double-body base flow can predict the motions and loads with reasonable to good accuracy. Still the accuracy is comparable with strip theory results and it is believed that only a consistent forward speed formulation for the free surface boundary condition as well can overcome this. The pressure integrations can be done using a direct formulation or using a Stokes variant. From the calculations we can conclude that the direct formulation gives best results.
- The nonlinear Froude-Krylov program can predict the nonlinear hull girder loads with reasonable to good accuracy. For the extreme cases the program is not accurate as slamming and green water are not taken into account.

7.2 Discussion and recommendations for further research

The MLER and EMLER method have been applied to several cases but need to be validated for other responses as well as for other headings. When this is conducted with good result the application to a long-term assessment is to be investigated. In chapter 1 the procedure to do so is already outlined. The important advantage is that the long-term extreme response distribution can be calculated without the need for extrapolation as the EMLER approach calculates the behaviour in the extreme cases with small exceedance probabilities. As the computational costs for such long-term nonlinear assessments are small the opportunity is there to study variations and uncertainties of the stochastic models for the wave environment and the operational scenarios. For example the effects of a careful master avoiding rough weather and a fearless one, ordering 'full ahead', can be studied.

The fundamental assumption of the response conditioning technique is that the nonlinear extreme is a correction of the linear extreme. When large linear sagging bending moments occur a large relative wave motion is present at the bow. This gives large probabilities for slamming and green water. It is thus not so surprising that the technique works well for the experimental cases where the foreship comes out of the water and large amounts of green water are shipped over the bow. But when exploring the application of the technique to other responses this assumption should be validated.

One application, which would be interesting, is the roll motion of ships for which a case was presented in chapter 1. It will be of great importance to model the manoeuvring characteristics of the vessel correctly as rudder actions influence the roll motion directly and secondly the rudder induced sway and yaw motions can lead to a different encountered incoming wave as prescribed by the MLER method.

Hull girder bending moments have been studied numerically in this studied without modelling the elastic behaviour of the hullform, slamming and green water. From the modeltests it was observed that slamming occurred as the hull started to vibrate although the slamming loads are probably not large as the average deadrise angle of the bow is 65 degrees. Large amounts of green water were shipped over the bow during the experiments. It is believed that the slamming and green water loads need to be modelled in the program for a better prediction of extreme hull girder bending moments. It is expected that the green water loading is probably responsible for less severe sagging responses. But with increasing bow flare it can very well be that slamming loads become much more important and less green water is shipped thus sagging will increase even more.

Furthermore we have seen that the nonlinear Froude-Krylov program could not predict the nonlinear motion behaviour of an advanced frigate hullform, see appendix B.4. The discrepancy between measurements and calculations might be due to nonlinear damping. Oscillation tests and calculations with other programs, like consistent three dimensional forward speed nonlinear programs, could be helpful in determining the effects, which cause the significant nonlinear behaviour of basic motions in moderate sea states.

This thesis presents a reliability based seakeeping performance assessment, which should be further evaluated within the design practice. Only then the technique can be judged on its merits. The seakeeping performance assessment depends very much on the criteria, mainly their absolute value but also their type definition. More discussion is therefore required on the criteria definitions as was shown in this thesis that linear and nonlinear simulations can give equal RMS values for vertical accelerations although nonlinear positive amplitudes are significantly larger than the linear values, but the negative amplitudes are smaller. The weigh factors for the responses can have a great influence on the total performance and its uncertainty. The actual values of these weigh factors are not known and a discussion between ship designers and operators is required to establish these values or specify at least a range. This gives subsequently the opportunity to study their effect.

References

Adegeest, L.J.M. (1995) 'Nonlinear hull girder loads in ships', Ph.D. thesis, Ship Hydromechanics Laboratory, Delft University of Technology.

Adegeest, L.J.M., Braathen, A., Løseth, R. (1998) 'Use of non-linear sea-loads simulations in design of ships', Proceedings PRADS conference, Ed. M.W.C.Oosterveld & S.G. Tan, pp. 53-58.

Adegeest, L.J.M., Braathen, A., Vada, T. (1998) 'Evaluation of methods for estimation of extreme non-linear ship responses based on numerical simulations and model tests', 21st Symposium on Naval Hydrodynamics, Office of Naval Research.

Adegeest, L.J.M., Vada, T. (2000) 'DNV-SWAN - The new hydrodynamic tool for ship structures', Report No. 2000-0349, Det Norske Veritas, Oslo.

Andrews, D. (2001) 'Adaptability - the key to modern warship design', RINA Conference Warship 2001, London.

Bales, N.K. (1980) 'Optimising the seakeeping performance of destroyer-type hulls', Proceedings of the 13th Symposium on Naval Hydrodynamics.

Barltrop, N.D.P., Adams, A.J. (1991) 'Dynamics of fixed marine structures', Published by Butterworth-Heinemann, 3rd edition.

Beck, R.F., Løken, A.E. (1989) 'Three-dimensional effects in ship relative-motion problem', Journal of Ship Research, Vol.33, No. 4, pp.261-268.

Beck, R.F., Magee, A.R. (1990) 'Time-domain analysis for predicting ship motions', Dynamics of marine vehicles and structures in waves, pp. 49-64.

Beck, R.F., Cao, Y., Lee, T.H. (1993) 'Fully nonlinear water wave computations using the desingularized method', Proceedings of the 6th International Conference on Numerical Ship Hydrodynamics, pp. 3-20.

Bendat, J.S. (1990) 'Nonlinear system analysis & identification', John Wiley & Sons.

Bishop, R.E.D., Price, W.G. (1978) 'On the truncation of spectra', International Shipbuilding Progress, Vol. 25, No.281

Bitner-Gregersen, E.M., Cramer, E.H., Løseth, R. (1995) 'Uncertainties of load characteristics and fatigue damage of ship structures', Marine Structures, Vol. 8, pp. 97-117.

Blok, J.J., Beukelman, W. (1984) 'The high-speed displacement ship systematic series hull forms - Seakeeping characteristics', SNAME Transactions, Vol. 92, pp. 129-150.

Brard, R. (1972) 'The representation of a given ship form by singularity distributions when the boundary condition on the free surface is linearized', Journal of Ship Research, Vol. 16, pp. 79-92.

Bunnik, T. (1999) 'Seakeeping calculations for ships, taking into account the non-linear steady waves', Ph.D. thesis, Delft University of Technology, Department of Mathematics.

Cartwright, D.E., Longuet-Higgins, M.S. (1956) 'The statistical distribution of the maxima of a random function', Proceedings of the Royal Society London, Vol. A-237, pp.212-232.

Cavanié, A., Arhan, M.K., Ezraty, E. (1976) 'A statistical relationship between individual heights and periods of storm waves', Proceedings Conference on the Behaviour of Offshore Structures, Vol. 2, pp. 354-360.

Chang, M.S. (1977) 'Computation of three-dimensional ship motions with forward speed', Proc. of the 2nd International Conference on Numerical Ship Hydrodynamics, Univ. of Berkeley, pp. 124-135.

Chen, X.B., Malenica, S. (1996) 'Uniformly valid solution of the wave-current-body interaction problem', Proc. 11th International Workshop on Water Waves and Floating Bodies, Hamburg.

Cummins, W.E. (1962) 'The impulse-response function and ship motions', Schiffstechnik 9, Vol. 47, pp. 101-109.

Dallinga, R.P. (1992) 'Selection on Seakeeping', Proceedings of MARIN workshops, Hydrodynamics: Computations, Model test and Reality, Elsevier, pp. 165-186.

Dalzell, J.F. (1975) 'The applicability of the functional polynomial input-output model to ship resistance in waves', Technical Report SIT-DL-75-1794, Stevens Institute of Technology.

Dalzell, J.F. (1982) 'An investigation of the applicability of the third degree functional polynomial model of nonlinear ship motion problems', Technical Report SIT-DL-82-9-2275, Stevens Institute of Technology.

DNV (2000) ' Environmental conditions and environmental loads', Det Norske Veritas, Classification Notes No. 30.5.

Friis-Hansen, P. (1994) 'Reliability analysis of a midship section', Ph.D. thesis, Technical University of Denmark.

Friis-Hansen, P., Nielsen, L.P. (1995) 'On the New Wave model for the kinematics of large ocean waves', Proc. OMAE, Vol. I-A, pp. 17-24.

Fritts, M., Comstock, E., Lin, W.C., Salvesen, N. (1990) 'Hydro-numeric design: Performance prediction and impact on hull design', SNAME Transactions, Vol. 98, pp. 473-493.

Fujino, M., Yoon, B.S. (1986) 'A practical method of estimating ship motions and wave loads in large amplitudes waves', International Shipbuilding Progress, Vol. 33, No. 382, pp. 159-172.

Gerritsma, J., Beukelman, W. (1967) 'Analysis of the modified strip theory for the calculations of ship motions and wave bending moments', Journal of Ship Research, Vol. 14, No. 156, pp. 7-24.

Griethuyzen van, W.J., Bucknall, R.W.G., Zhang, J.W. (2001) 'Trimaran design - choices and variants for surface warship applications', RINA Conference Warship 2001, London.

Guedes Soares, C., Trovão, N.F.S. (1991) 'Influence of wave climate modelling on the long-term prediction of wave induced responses of ship structures', Dynamics of Marine Vehicles and Structures in Waves, (ed. Proce, W.G., Temarel, P., Keane, A.J.), Elsevier Science Publishers, pp. 1-10.

Guedes Soares, C., Moan, T. (1991) 'Model uncertainty in the long-term distribution of wave-induced bending moments for fatigue design of ship structures', Marine Structures, Vol. 4, pp. 295-315.

Guedes Soares, C. (1996) 'On the definition of rule requirements for wave induced vertical bending moments', Marine Structures, Vol. 9, pp. 409-425.
Guedes Soares, C., Schellin, T. (1996) 'Long term distribution of non-linear wave-induced vertical bending moments on a containership', Marine Structures, Vol. 9, pp. 333-352.

Guevel, P., Bougis, J. (1982) 'Ship motions with forward speed in finite depth', International Shipbuilding Progress, No. 29, pp. 103-117.

Gumbel, E.J. (1958) 'Statistics of extremes', Columbia University Press, New York.

Harland, L.A., Vugts, J.H., Jonathan, P., Taylor, P.H. (1996) 'Extreme responses of non-linear dynamic systems using constrained simulations', Proceedings OMAE, Vol. I, pp.193-200.

Huang, Y.F. (1997) 'Nonlinear ship motions by a Rankine panel method', Ph.D. thesis, MIT.

Huijsmans, R.H.M. (1996) 'Mathematical modelling of the mean wave drift force in current', Ph.D. thesis, Delft University of Technology.

Inglis, R.B., Price, W.G. (1981) 'A three dimensional ship motion theory - comparison between theoretical prediction and experimental data of hydrodynamic coefficients with forward speed', RINA Transactions, Vol. 124, pp. 141-157.

Jensen, J.J., Pedersen, P.T. (1979) 'Wave-induced bending moments in ships - a quadratic theory', RINA Transactions, Vol. 121, pp. 141-157.

Jensen, J.J., Pedersen, P.T. (1981) 'Bending moments and shear forces in ships sailing in irregular waves', Journal of Ship Research, Vol. 25, No. 4, pp. 243-251.

Jensen, J.J. (1990) 'Fatigue analysis of ship hulls under non-Gaussian wave loads', Marine Structures, Vol. 4, pp. 279-294.

Jensen, J.J., Dogliani, M. (1996) 'Wave-induced ship hull vibrations in stochastic seaways', Marine Structures, Vol. 9, pp. 353-387.

Jensen, J.J., Beck, R.F., Du, S., Faltinsen, O.M., Fonseca, N., Rizzuto, E., Stredulinsky, D., Watanabe, I. (2000) 'Extreme hull girder loading', Report of the Committee VI.1 on the 14th ISSC.

Jonathan, P., Taylor, P.H., Tromans, P.S. (1994) 'Storm waves at the northern North Sea', Proceedings of the BOSS conference, Vol. 2.

Journée, J.M.J., (2001) 'Theoretical Manual of SEAWAY (Release 4.19)', Delft University of Technology, Shiphydromechanics Laboratory, Report No. 1216a.

Journée, J.M.J., (2001), 'Trustworthiness Analyses of Measured Motions in Waves', Ship Hydromechanics Laboratory, Delft University of Technology, Report No.1295.

Kapsenberg, G.K., Brouwer, R. (1998) 'Hydrodynamic development for a frigate for the 21st century', PRADS conference, The Hague, pp. 555-566.

Keane, R.G., Sandberg, W.C. (1984) 'Naval architecture for combatants, a technical survey', Naval Engineers Journal, pp. 47-64.

Keuning, J.A. (1994) 'The nonlinear behaviour of fast monohulls in head waves', Ph.D. thesis, Ship Hydromechanics Laboratory, Delft University of Technology.

Kim, C.H. (1990) 'A method of time domain simulation of wave drift forces', Proc. of the Offshore Station Keeping Symposium, Vol.1, No.4, pg-1, nrpg-9, gr-14

Kim, M.H., Yue, D.K.P. (1991) 'Sum- and difference-frequency wave loads on a body in unidirectional Gaussian seas', Journal of Ship Research, vol.35, no.2, pp. 127-140.

King, B.K., Beck, R.F., Magee, A.R. (1988) 'Seakeeping calculations with forward speed using time-domain analysis', Proc. of the 17th Symposium on Naval Hydrodynamics, pp. 577-596.

Korsmeyer, T., Klemas, T., White, J., Phillips, J. (1999) 'Fast hydrodynamic analysis of large offshore structures', Proceedings ISOPE conference, Brest.

Korvin-Kroukovsky, B.V., Jacobs, W.R. (1957) 'Pitching and heaving motions of a ship in regular waves', SNAME Transactions, 65, pp. 590-632.

Kring, D., Huang, Y.F., Sclavounos, P. (1996) 'Nonlinear motions and wave-induced loads by a Rankine method', Proceedings of the 21st Symposium on Naval Hydrodynamics, pp. 16-33.

Larsen, C.M., Passano, E. (1990) 'Extreme response estimation for marine risers', 14th WEGEMT School, Trondheim.

Lin, W.M., Yue, D. (1990) 'Numerical solutions for large-amplitude ship motions in the time-domain', Proc. of the 18th Symposium on Naval Hydrodynamics, pp. 41-66.

Lin, W.M., Meinhold, M., Salvesen, N., Yue, D. (1994) 'Large-amplitude motions and wave loads for ship design', Proc. of the 20th Symposium on Naval Hydrodynamics, pp. 205-226.

Lindgren, G., Rychlik, I. (1983) 'Wave characteristic distributions for Gaussian waves - wave-length, amplitude and steepness', Ocean Engineering, Vol. 9, No. 5, pp. 411-432.

Liu, D., Spencer, J., Itoh, T., Shigematsu, K. (1992) 'Dynamic load approach in tanker design', SNAME Transactions, Vol. 100, pp. 143-172.

Longuet-Higgins, M.S. (1975) 'On the joint distribution of the period and amplitude in sea waves', Journal of Geophysical Research, Vol. 80, No. 18, pp. 2688-2694.

Longuet-Higgins, M.S. (1983) 'On the joint distribution of wave periods and amplitudes in a random wave field', Proceedings of the Royal Society London, A 389, pp. 241-258.

Mansour, A.E., Jensen, J.J. (1995) 'Slightly nonlinear extreme loads and load combination', Journal of Ship Research, Vol. 39, No.2, pp. 139-149.

MacGregor, J.R., Black, F., Wright, D., Gregg, J. (1999) 'Design and construction of the FPSO vessel for the Schiehallion field', Issued by RINA for written discussion, w247.

McTaggart, K.A., Graham, R. (1993) 'SHIPOP: A program for computing ship operability in waves and wind', DREA, Technical Memorandum 93/202.

McTaggart, K., Kat de, J.O.(2000) 'Capsize risk of intact frigates in irregular seas', SNAME Transactions, Vol. 108, New York.

Medina, J.R., Anguilar, J., Diez, J.J. (1985) 'Distortions associated with random sea simulators', Journal of Waterway, Port, Coastal and Ocean Engineering, ASCE, Vol. 111, No. 4, pp. 603-628.

Myrhaug, D., Kvalsvold, J. (1992) 'Comparitive study of joint distributions of primary wave characteristics', Proceedings OMAE, Vol. II, pp. 291-299.

Myrhaug, D., Rue, H. (1998) 'Joint distribution of successive wave periods revisited', Journal of Ship Research, Vol. 42, No. 3, pp. 199-206.

Nakos, D.E. (1990) 'Ship wave patterns and motions by a three dimensional rankiine panel method, Ph.D. thesis, MIT.

Nakos, D.E., Kring, D., Sclavounos, P. (1993) Rankine panel methods for transient free surface flows', Proc. 6th International Conference on Numerical Ship Hydrodynamics, pp. 613-632.

Nitta, A., Aral, H., Magaino, A. (1992) 'Basis of IACS unified longitudinal strength standard', Marine Structures, Vol. 5, pp. 1-21.

O'Dea, J., Powers, E., Zselecsky, J. (1992) 'Experimental determination of nonlinearities in vertical plane ship motions', Proceedings of the 19th Symposium on Naval Hydrodynamics, pp. 73-91.

Ogilvie, T.F. (1964) 'Recent progress towards the understanding of and prediction of ship motions', Proceedings of the 5th Symposium on Naval Hydrodynamics', pp. 3-128.

Ogilvie, T.F., Tuck, E.O. (1969) 'A rational strip theory of ship motions: part 1', Report No. 013, Department of naval architecture and marine engineering, University of Michigan.

Ohmatsu, S. (1975) 'On the irregular frequencies in the theory of oscillating bodies in a free surface', Paper No. 48 of the Ship Research Institute, Tokyo, Japan.

Paik, I (1997) 'Application of higher order transfer functions in modeling nonlinear dynamic behavior of offshore structures', Int. Journal of Offshore and Polar Engineering, vol.7, no.4, pp. 301-308.

Pastoor, L.W. (2000A) 'Nonlinear extreme vertical hull girder bending moments in a North Sea FPSO', Proceedings NAV 2000 Conference, Vol. II, pp. 7.9.1-7.9.10

Pastoor, L.W. (2000B) 'Experimental generation of response conditioned waves (MLER method)', Delft University of Technology, Ship Hydromechanics Laboratory, report no. 1244.

Pastoor, L.W. (2001) 'Response conditioned model experiments with a divided frigate (Data report)', Delft University of Technology, Ship Hydromechanics Laboratory, report no. 1271-Data.

Pawlowski, J. (1992) 'A nonlinear theory of ship motions in waves', Proceedings of the 19th Symposium on Naval Hydrodynamics.

Petersen, J.B., Mamæs, L. (1989) 'Comparison of nonlinear strip theory predictions and model experiments', Proc. PRADS Conference, Varna, Bulgaria.

Pinkster, J.A. (1980) 'Low frequency second order wave exciting forces on floating structures', Ph.D. thesis, Delft University of Technology.

Rice (1944, 1945) 'Mathematical analysis of random noise', Bell System Tech. Journal, Vol. 23 & 24, pp. 282-332, pp.46-156.

RINA (2000) "R V Triton: Trimaran Demonstrator Project", RINA Conference.

Sagli, G. (2000) 'Model uncertainty and simplified estimates of long-term extremes of hull girder loads in ships', Ph.D. thesis, University of Trondheim.

Salvesen, N., Tuck, E.O., Faltinsen, O. (1970) 'Ship motions and sea loads', SNAME transactions, Vol. 78.

Schlachter, G. (1989) 'Hull girder loads in a seaway including nonlinear effects', Schiffstechnik, Vol. 36.

Schönknecht, R., Laue, U. (1990) 'Unkonventionelle Schiffe', Transpress, VEB Verlag für Verkehrswesen, Berlin.

Scorpio, S.M. (1997) 'Fully nonlinear ship-wave computations using a multi-pole accelerated, desingularised method', Ph.D. thesis, University of Michigan.

Sobey, R.J. (1992) 'The distribution of zero-crossing wave heights and periods in a stationary sea state', Ocean Engineering, Vol. 19, No.2, pp. 101-118.

Söding, H. (1982) 'Leckstabilität im Seegang', report 429 of the Institute für Schiffsbau, Hamburg.

Srokosz, M.A., Challenor, P.G. (1987) 'Joint distributions of wave height and period: a critical comparison', Ocean Engineering, Vol. 14, No.4, pp. 295-311.

Tayfun, M.A. (1993) 'Joint distribution of large wave heights and associated periods', Journal of Waterway, Port, Coastal and Ocean Engineering, Vol. 119, No.3, pp.261-273.

Taylor, P.H., Jonathan, P., Harland, L.A. (1995) 'Time domain simulation of jack-up dynamics with the extremes of a Gaussian process', Proceedings OMAE, Vol. I-A, pp.313-319.

Torhaug, R. (1996) 'Extreme response of nonlinear ocean structures: identification of minimal stochastic wave input for time-domain simulation', Ph.D. thesis, Dep. of. Civil Engineering, Stanford University.

Tromans, P.S., Anaturk, A.R., Hagemeijer, P. (1991) 'A new model for the kinematics of large ocean waves - application as a design wave', Proc. ISOPE conf., Vol. III, pp. 64-71.

Van 't Veer, A.P. (1998) 'Behaviour of catamarans in waves', Ph.D. thesis, Ship Hydromechanics Laboratory, Delft University of Technology.

Vassilopoulos, L.A. (1967) 'The application of statistical theory of nonlinear systems to ship motion performance in random seas', International Shipbuilding Progress, Vol. 14, No. 150, pp. 54-65.

Wang, H.T., Crouch, J.D. (1993) 'Accuracy of low-order models for simulations of random ocean waves, Journal of Waterway, Port, Coastal and Ocean Engineering, Vol. 199, No. 1, pp. 70-87.

Wang, M.L., Troesch, A.W., Maskew, B. (1996) 'Comparisons of two different mixed Eulerian-Lagragian schemes based on a study of flare-slamming hydrodynamics', Journal of Offshore and Arctic Engineering, Transactions ASME, Vol. 118, pp. 174-183.

Watanabe, I., Guedes Soares, C. (1999) 'Comparative study on the time-domain analysis of non-linear ship motions and loads', Marine Structures, Vol. 12, pp. 153-170.

Weems, K., Zhang, S., Lin, W.M., Bennet, J., Shin, Y.S. (1998) 'Structural dynamic loadings due to impact and whipping', Prads, pp. 79-85.

Weinblum, G.P., St.Denis, M. (1950) 'On the motions of ships at sea', SNAME Transactions, 58, pp. 184-248.

Welch, P.D. (1967) 'The use of fast fourier transform for the estimation of power spectra: a method based on time averaging over short, modified periodograms', IEEE transactions Audio and Electroacoustics, Vol. AU-15, pp. 70-73.

Winterstein, S.R. (1988) 'Nonlinear vibration models for extremes and fatigue', Journal of Eng. Mechanics, ASCE 114(10), pp. 1772-1790.

Winterstein, S.R., Ude, T.C., Cornell, C.A., Bjerager, P., Haver, S. (1993) 'Environmental parameters for extreme response: Inverse FORM with omission factors', Proceedings ICOSSAR, Innsbruck.

Winterstein, S.R., Lange, C.H., Kumar, S. (1994) 'FITTING: A subroutine to fit four moment probability distributions to data', Report RMS-14, Reliability of Marine Structures Program, Civil Eng. Dep., Stanford University.

Wolf, P.A. (2000) 'Conceptual design of warships', Ph.D. thesis, Technical University of Twente.

Wood, P. (1962) 'Lid method for suppression of irregular frequencies', Journal of Fluid Mechanics, Vol. 531.

A Derivation of response conditional probability functions

In paragraph 2.1 three models are presented for the most likely profile around a crest or trough of an irregular response process $y(t)$, which is Gaussian distributed with zero mean and with variance σ_y^2. This response is continuous and differentiable. A detailed derivation of the formulation as derived by Pastoor (2000A) is given below.

In order to obtain the Gaussian distribution of equation (2.15) the numerator and denominator are to be determined, these are respectively quadri- and tri-variate Gaussian distributions. For these distributions the covariance matrices are to be solved for and this is discussed hereafter. The denominator in equation (2.15) is written as,

$$f\left(y(t),\dot{y}(t),\ddot{y}(t)\right)=f\left(\bar{Y}\right)=\frac{1}{(2\pi)^{3/2}\cdot|\Sigma|^{1/2}}e^{-\frac{1}{2}\bar{Y}^T\Sigma^{-1}\bar{Y}} \tag{8.1}$$

with Σ the covariance matrix,

$$\Sigma=\begin{bmatrix}\sigma_{yy}^2 & \sigma_{y\dot{y}}^2 & \sigma_{y\ddot{y}}^2\\ \sigma_{y\dot{y}}^2 & \sigma_{\dot{y}\dot{y}}^2 & \sigma_{\dot{y}\ddot{y}}^2\\ \sigma_{y\ddot{y}}^2 & \sigma_{\dot{y}\ddot{y}}^2 & \sigma_{\ddot{y}\ddot{y}}^2\end{bmatrix}=\begin{bmatrix}m_0 & 0 & -m_2\\ 0 & m_2 & 0\\ -m_2 & 0 & m_4\end{bmatrix} \tag{8.2}$$

These covariances are determined by writing the response process as a summation of cosines and sines.

$$y(t)=\sum_{j=1}^{N}A_j\cos\omega_j t+B_j\sin\omega_j t \tag{8.3}$$

Differentiation of (8.3) gives $\dot{y}(t)$ and $\ddot{y}(t)$. The amplitudes A_j and B_j are statistically independent random variables with zero mean and variances given by,

$$E\left[A_j^2\right] = E\left[B_j^2\right] = \frac{1}{2} y_{a,j}^2 \tag{8.4}$$

Further more A_j and A_i are statistically independent as well as B_j and B_l. With these properties the covariances can be calculated. As an example $\sigma_{\dot{y}\ddot{y}}$ is derived.

$$\begin{aligned}
\sigma_{\dot{y}\ddot{y}} &= E\left[\dot{y}(t)\ddot{y}(t)\right] \\
&= E\left[\sum_{j=1}^{N}\left(-\omega_j A_j \sin\omega_j t + \omega_j B_j \cos\omega_j t\right)\sum_{l=1}^{N}\left(-\omega_l A_l \sin\omega_l t + \omega_l B_l \cos\omega_l t\right)\right] \\
&= \sum_{j=1}^{N}\sum_{l=1}^{N}\omega_j\omega_l E\left[A_j A_l\right]\sin\omega_j t \sin\omega_l t + \omega_j\omega_l E\left[B_j B_l\right]\cos\omega_j t \cos\omega_l t \\
&= \sum_{j=1}^{N}\omega_j^2 E\left[A_j^2\right]\sin^2\omega_j t + \sum_{j=1}^{N}\omega_j^2 E\left[B_j^2\right]\cos^2\omega_j t \\
&= \sum_{j=1}^{N}\omega_j^2 \frac{1}{2} y_{a,j}^2 = \sum_{j=1}^{N}\omega_j^2 S_{yy}(\omega_j)\Delta\omega = \int_0^{\infty}\omega^2 S_{yy}(\omega)\,d\omega = m_2
\end{aligned} \tag{8.5}$$

The numerator in equation (2.15) can also be written as a Gaussian distribution as in equation (8.1). The covariance matrix is,

$$\begin{aligned}
\Sigma &= \begin{bmatrix}
\sigma_{yy}^2 & \sigma_{y(t+\tau)\dot{y}(t)}^2 & \sigma_{y(t+\tau)\dot{y}(t)}^2 & \sigma_{y(t+\tau)\ddot{y}(t)}^2 \\
\sigma_{y(t+\tau)y(t)}^2 & \sigma_{yy}^2 & \sigma_{y\dot{y}}^2 & \sigma_{y\ddot{y}}^2 \\
\sigma_{y(t+\tau)\dot{y}(t)}^2 & \sigma_{y\dot{y}}^2 & \sigma_{\dot{y}\dot{y}}^2 & \sigma_{\dot{y}\ddot{y}}^2 \\
\sigma_{y(t+\tau)\ddot{y}(t)}^2 & \sigma_{y\ddot{y}}^2 & \sigma_{\dot{y}\ddot{y}}^2 & \sigma_{\ddot{y}\ddot{y}}^2
\end{bmatrix} \\
&= \begin{bmatrix}
m_0 & m_0\rho(\tau) & m_0\dot{\rho}(\tau) & m_0\ddot{\rho}(\tau) \\
m_0\rho(\tau) & m_0 & 0 & -m_2 \\
m_0\dot{\rho}(\tau) & 0 & m_2 & 0 \\
m_0\ddot{\rho}(\tau) & -m_2 & 0 & m_4
\end{bmatrix}
\end{aligned} \tag{8.6}$$

Directional response conditional probability function

In case of the directional MLER formulation, see paragraph 2.5, the probability distribution of equation (2.54) is to be calculated. The denominator is known but the

numerator has some unknown covariances. The covariance matrix of this tri-variate Gaussian distribution, $f\left(y_l(t+\tau), y(t), \dot{y}(t)\right)$, is,

$$\begin{aligned}\Sigma &= \begin{bmatrix} \sigma^2_{y_l y_l} & \sigma^2_{y_l(t+\tau)y(t)} & \sigma^2_{y_l(t+\tau)\dot{y}(t)} \\ \sigma^2_{y_l(t+\tau)y(t)} & \sigma^2_{yy} & \sigma^2_{y\dot{y}} \\ \sigma^2_{y_l(t+\tau)\dot{y}(t)} & \sigma^2_{y\dot{y}} & \sigma^2_{\dot{y}\dot{y}} \end{bmatrix} \\ &= \begin{bmatrix} m_{0,l} & m_{0,l}\rho_{y_l y_l}(\tau) & m_{0,l}\dot{\rho}_{y_l y_l}(\tau) \\ m_{0,l}\rho_{y_l y_l}(\tau) & m_0 & 0 \\ m_{0,l}\dot{\rho}_{y_l y_l}(\tau) & 0 & m_2 \end{bmatrix}\end{aligned} \tag{8.7}$$

The covariances of the response due to direction l and the total response or the total response time derivative can be determined in an equal fashion as done in the previous section by writing the total response and the response due to directions l as,

$$\begin{aligned} y(t) &= \sum_{j=1}^{N} A_j \cos\omega_j t + B_j \sin\omega_j t = \sum_{l=1}^{M} y_l(t) \\ y_l(t) &= \sum_{j=1}^{N} A_{l,j} \cos\omega_j t + B_{l,j} \sin\omega_j t \end{aligned} \tag{8.8}$$

In the derivations of the covariances the following expectations occur,

$$E\left[A_{l,j}A_j\right] \qquad E\left[B_{l,j}B_j\right] \tag{8.9}$$

These can be determined as follows. The sum of all the amplitudes are, for a given frequency,

$$A_j = \sum_{m=1}^{M} A_{m,j} \qquad B_j = \sum_{m=1}^{M} B_{m,j} \tag{8.10}$$

By multiplying both sides with $A_{l,j}$ and $B_{l,j}$ respectively and taking the expectation we get,

$$E\left[A_{l,j}A_j\right] = \sum_{m=1}^{M} E\left[A_{l,j}A_{m,j}\right] \qquad E\left[B_{l,j}B_j\right] = \sum_{m=1}^{M} E\left[B_{l,j}B_{m,j}\right] \tag{8.11}$$

Because the directions are mutually uncorrelated this results in,

$$E\left[A_{l,j}A_j\right]=E\left[A_{i,j}A_{i,j}\right]=\frac{1}{2}y_{a;l,j}^2 \qquad E\left[B_{l,j}B_j\right]=E\left[B_{l,j}B_{l,j}\right]=\frac{1}{2}y_{a;l,j}^2 \quad (8.12)$$

With this result the covariances in matrix (8.7) can be solved for.

Conditioning on two responses: slamming incidences

Some events are conditioned on more than one response. For example slamming is an event for which the bow should emerge from the water while the entrance velocity should exceed a critical value. Upon time conditioning of such an event both conditions should be taken into account. For the case of a slam this will be derived hereafter.

Consider the relative wave motion at the bow to be a Gaussian distributed zero mean process, which is continuous and differentiable. For the following derivation the relative velocity is simplified by assuming a small forward speed,

$$\frac{D\zeta_r}{Dt}=\dot{\zeta}_r-U\theta\approx\dot{\zeta}_r \quad (8.13)$$

Now we formulate the most likely relative wave profile conditional on a slam by,

$$E\left[\zeta_r(t+\tau)\middle|\zeta_r(t)=-T,\dot{\zeta}_r(t)=v_{cr}\right] \quad (8.14)$$

Solving this expectation we get,

$$E\left[\zeta_r(t+\tau)\middle|\zeta_r(t)=-T,\dot{\zeta}_r(t)=v_{cr}\right]=-T\rho_{\zeta\zeta}(\tau)+v_{cr}\dot{\rho}_{\zeta\zeta}(\tau)\frac{m_0}{m_2} \quad (8.15)$$

By discretising this and writing the relative wave motion as in equation (2.32) we can equate these two in order to obtain the conditioned incident wave amplitudes and phases as,

$$\zeta_{a,j}=\sqrt{\left(\frac{-T\zeta_{r,a,j}^2}{2m_0\left|H_r(\omega_j)\right|^2}\right)^2+\left(\frac{v_{cr}\omega_j\zeta_{r,a,j}^2}{2m_2\left|H_r(\omega_j)\right|^2}\right)^2} \qquad \varepsilon_{\zeta,j}=\arctan\left(\frac{v_{cr}m_0\omega_j}{-Tm_2}\right)-\varepsilon_{\zeta_r,j} \quad (8.16)$$

This approach gives thus the opportunity to condition slamming events with prescribed entry velocities.

B A solution for the linear and nonlinear ship motion problem

Three programs are used to calculate linear and nonlinear ship motions and loads in a seaway. The first program is called *Delflow* and solves the double-body flow and *m*-terms. The second program is called *Delspeed* and solves the linear ship motion problem using the *Delflow* pre-calculation results. The hydrodynamic coefficients and diffraction forces are subsequently submitted to *SIMMOLO*. This program simulates the motions and loads in the time domain by solving the motions and loads in an Eulerian frame and with nonlinear Froude-Krylov and hydrostatic forces. The basic mathematical modelling behind these three programs is described below. More details can be found in Pastoor (1999A & B)

B.1 Solving the double-body base flow and m-terms

We assume the fluid around the ship to be non-viscous, irrotational, homogenous and incompressible. Thus the fluid motions can be described by a potential function and this function must satisfy the Laplace equation.

$$\nabla^2 \Psi = 0 \tag{9.1}$$

This total velocity potential, defined in the steady moving reference frame, is separated into steady and unsteady components. The steady parts are the double-body flow potential and the steady wave potential. The steady wave perturbation is omitted as it is assumed small compared to the double-body flow. This assumption is valid for slender hulls. The total velocity potential becomes thus,

$$\Psi(\bar{x},t) = \Phi(\bar{x}) + \varphi(\bar{x},t) \tag{9.2}$$

The so-called double-body flow is obtained by copying the hull in the free surface and solve the potential flow around the hull. The double-body potential must satisfies the Laplace equation as well and the Neumann condition on the hull,

$$\Delta\Phi(x,y,z)=\Delta\Phi(\bar{x})=0 \qquad \frac{\partial\Phi(\bar{x})}{\partial n}=0 \tag{9.3}$$

We write the double-body potential as,

$$\Phi(\bar{x})=-Ux+\phi(\bar{x}) \tag{9.4}$$

The boundary condition is now formulated for the unknown perturbation potential,

$$\frac{\partial\phi(\bar{x})}{\partial n}=-U\cdot n_1(\bar{x}) \tag{9.5}$$

By applying Green's second identity a boundary integral equation is obtained with unknown source and dipole strengths distributed over the hull. By choosing the dipole strengths zero the following Fredholm equation of the second kind is obtained,

$$\begin{aligned}&\frac{\partial\phi(\bar{p})}{\partial n}=\frac{1}{2}\sigma_0(\bar{p})+\frac{1}{4\pi}\iint_S\sigma_0(\bar{x})\frac{\partial G}{\partial n}dS\\ &\text{with}\quad G(\bar{x},\bar{p})=-\frac{1}{r(\bar{x},\bar{p})}\end{aligned} \tag{9.6}$$

After discretisation of this integral equation the source strengths can be solved for, after which the perturbation velocities at every point can be calculated.

Next the m-terms are calculated, which were derived by Ogilvie and Tuck (1969). They are formulated as,

$$\begin{aligned}(m_1,m_2,m_3)&=-(n\cdot\nabla)\nabla\Phi\\ (m_4,m_5,m_6)&=-(n\cdot\nabla)(r\times\nabla\Phi)\end{aligned} \tag{9.7}$$

Thus we need second derivatives of the potential, which are rather difficult to calculate as we use flat quadrilateral panels with constant source distributions. Therefore another approach is used as published by Chen and Malenica (1998). Instead of the second derivatives of the Green's function a second boundary integral equation is formulated. In this equation the perturbation velocities are prescribed as potential values on the hull and thus treated as Dirichlet conditions.

$$\frac{\partial\phi(\bar{p})}{\partial x}=\iint_S \sigma_1(\bar{x})G(\bar{x},\bar{p})dS \quad ; \quad \frac{\partial\phi(\bar{p})}{\partial y}=\iint_S \sigma_2(\bar{x})G(\bar{x},\bar{p})dS \tag{9.8}$$

Second derivatives are subsequently calculated by,

$$\frac{\partial^2\phi(\bar{p})}{\partial x^2}=\iint_S \sigma_1(\bar{x})\frac{\partial G(\bar{x},\bar{p})}{\partial x}dS=\Phi_{xx}(\bar{p}) \tag{9.9}$$

$$\frac{\partial^2\phi(\bar{p})}{\partial x\partial y}=\iint_S \sigma_1(\bar{x})\frac{\partial G(\bar{x},\bar{p})}{\partial y}dS=\Phi_{xy}(\bar{p}) \tag{9.10}$$

$$\frac{\partial^2\phi(\bar{p})}{\partial x\partial z}=\iint_S \sigma_1(\bar{x})\frac{\partial G(\bar{x},\bar{p})}{\partial z}dS=\Phi_{xz}(\bar{p}) \tag{9.11}$$

$$\frac{\partial^2\phi(\bar{p})}{\partial y^2}=\iint_S \sigma_2(\bar{x})\frac{\partial G(\bar{x},\bar{p})}{\partial y}dS=\Phi_{yy}(\bar{p}) \tag{9.12}$$

$$\frac{\partial^2\phi(\bar{p})}{\partial y\partial z}=\iint_S \sigma_2(\bar{x})\frac{\partial G(\bar{x},\bar{p})}{\partial z}dS=\Phi_{xz}(\bar{p}) \tag{9.13}$$

$$\begin{aligned}\Phi_{yx}&=\Phi_{xy} & \Phi_{zx}&=\Phi_{xz}\\ \Phi_{zy}&=\Phi_{yz} & \Phi_{z}&=-\Phi_{xx}-\Phi_{yy}\end{aligned} \tag{9.14}$$

B.2 A linear solution for the three-dimensional ship motion problem for moderate forward speed

The previous paragraph solved the double-body flow potential in the total velocity potential. This leaves the unsteady potential to be unknown.

$$\Psi(\bar{x},t)=\Phi(\bar{x})+\varphi(\bar{x},t) \tag{9.15}$$

The linear ship motion problem is subdivided into the radiation and diffraction problem. The dynamic perturbation potential can therefore be separated in eight components, i.e. the known incident wave potential, the unknown diffracted wave potential and six unknown radiation potentials. These radiation potentials are normalised by the six body motions. The total potential becomes thus,

$$\Psi(\bar{x},t)=\Phi(\bar{x})+\left[\varphi_0(\bar{x})+\varphi_7(\bar{x})+\sum_{j=1}^{6}\xi_j(\bar{x})\varphi_j(\bar{x})\right]e^{i\omega_e t} \tag{9.16}$$

The incident wave potential read as,

$$\varphi(\bar{x},t)=\frac{i\zeta_a g}{\omega}\frac{\cosh k(h+z)}{\cosh kh}e^{-i(x\cos\mu+y\sin\mu)}e^{i\omega_e t} \tag{9.17}$$

The fluid motion problem is solved by a boundary integral formulation. Thus boundary conditions need to be prescribed for the diffraction and for the six radiation problems. The radiation condition and diffraction conditions on the hull surface read as,

$$\frac{\partial\varphi_j(\bar{x})}{\partial n}=i\omega_e n_j+m_j \qquad j=1...6 \tag{9.18}$$

$$\frac{\partial\varphi_7(\bar{x})}{\partial n}=-\frac{\partial\varphi_0(\bar{x})}{\partial n} \tag{9.19}$$

The m-terms follow from equation (9.7) or if the undisturbed incoming flow is used as base flow these are given by,

$$\begin{aligned} &m_j=0 \qquad j=1...4\\ &m_5=-Un_3\\ &m_6=Un_2 \end{aligned} \tag{9.20}$$

The ocean floor is assumed horizontal and the boundary condition is thus,

$$\frac{\partial\varphi_j(\bar{x})}{\partial z}=0 \qquad j=1,7 \tag{9.21}$$

When the double-body flow is used as base flow and the free surface boundary condition is linearised around the still water level the following condition is obtained, see Van 't Veer (1998),

$$\begin{aligned} &\varphi_{tt}+2\nabla\Phi\cdot\nabla\varphi_t+\nabla\Phi\cdot\nabla(\nabla\Phi\cdot\nabla\varphi)+\frac{1}{2}\nabla\varphi\cdot\nabla(\nabla\Phi\cdot\nabla\Phi)-\\ &\Phi_{zz}(\varphi_t+\nabla\Phi\cdot\nabla\varphi)-\frac{1}{2}(\varphi_{zz}+\varphi_{tz})(\nabla\Phi\cdot\nabla\Phi-U^2)+g\varphi_z=0 \end{aligned} \tag{9.22}$$

Substitution of $\Phi=(-Ux,0,0)$ gives the well-known Kelvin free surface condition,

$$\varphi_{tt} + 2U\varphi_{tx} + U^2\varphi_{xx} + g\varphi_z = 0 \tag{9.23}$$

And for zero forward speed the condition becomes,

$$\varphi_{tt} + g\varphi_z = 0 \tag{9.24}$$

Brard (1972) derives a boundary integral equation for the steady flow around a ship. This integral equation consists of a surface and line integral. The same procedure can be followed for the unsteady flow problem leading to,

$$\begin{aligned} 4\pi\varphi(\bar{p}) = &\iint_S \sigma(\bar{x})G(\bar{x},\bar{p}) + \mu(\bar{x})\frac{\partial G(\bar{x},\bar{p})}{\partial n}dS + \frac{2i\omega U}{g}\int_\Gamma \mu(\bar{x})G(\bar{x},\bar{p})dy \\ &\frac{U^2}{g}\int_\Gamma G(\bar{x},\bar{p})\left(\alpha_l\frac{\partial\mu(\bar{x})}{\partial l} + \alpha_m\frac{\partial\mu(\bar{x})}{\partial m} + \alpha_n\sigma(\bar{x})\right) + \mu(\bar{x})G_x(\bar{x},\bar{p})dy \\ &\textit{with } \bar{p} \textit{ in the fluid domain} \end{aligned} \tag{9.25}$$

Here $G(\bar{x},\bar{p})$ is the free surface Green function which gives the potential at a point $\bar{p}$ due to a unit source strength at point $\bar{x}$ while the free surface and sea bottom boundary conditions are satisfied. Furthermore $(\bar{l},\bar{m},\bar{n})$ is a local orthogonal system at the waterline with $\bar{l}$ tangent to the waterline curvature, $\bar{m}$ pointing upwards, $\bar{n}$ perpendicular to the waterline curvature and pointing into the fluid. Then the α coefficients are formulated as,

$$\begin{aligned} \alpha_l &= \cos(\bar{l}, Ox) \\ \alpha_m &= \cos(\bar{m}, Ox) \\ \alpha_n &= \cos(\bar{n}, Ox) \end{aligned} \tag{9.26}$$

Several option are possible to obtain a boundary integral equation, which can be solved. As we use Neumann boundary conditions for the potentials we can chose the potential inside the hull zero or we can set the dipole strength zero and arrive at a Fredholm equation of the second kind. The latter option is chosen here and hence the final boundary integral equation, which is used to solve the radiation and diffraction potentials, is,

$$\frac{\partial\varphi(\bar{p})}{\partial n} = \frac{1}{2}\sigma_j(\bar{p}) + \frac{1}{4\pi}\iint_S \sigma_j(\bar{x})\frac{\partial G(\bar{x},\bar{p})}{\partial n}dS + \frac{U^2}{4\pi g}\int_\Gamma \sigma_j(\bar{x})\frac{\partial G(\bar{x},\bar{p})}{\partial n}n_1(\bar{p})dy \tag{9.27}$$

As written above the Green function automatically satisfies the free surface condition, either (9.23) or (9.24). Thus the use of a free surface Green function implies that equation (9.22) cannot be satisfied. Thus it would be most consistent to satisfy the Kelvin free surface condition, (9.23), but in case of low forward speed, as is rather common for severe sea states, equation (9.24) could be used. The corresponding Green function is easier to calculate and considerably faster. Moreover it is intuitively felt that the fluid motion on the hull surface is more important as there the pressures are to be solved. Therefore we chose to use this option despite a mathematically inconsistent approach.

The hull is discretised into flat quadrilateral or triangular panels. This leads to a linear system of equations with the source strengths as unknowns. With the solution of these source strengths it is possible to calculate the perturbation potentials and derivatives in the fluid. Substitution of equation (9.15) in the Bernoulli equation and neglecting higher order terms we then get the linearised Bernoulli equation for the fluid pressure,

$$p(\bar{x},t) = p_0 - \rho\varphi_t - \frac{1}{2}\rho\left(\nabla\Phi\cdot\nabla\Phi + 2\nabla\Phi\cdot\nabla\varphi - U^2\right) - \rho gz \tag{9.28}$$

From this the hydrodynamic reaction forces and diffraction forces can be calculated by integrating the dynamic pressures over the hull. The hydrodynamic reaction forces are given by,

$$F_{jk} = \rho e^{i\omega_e t}\iint_S (i\omega_e + \nabla\Phi\cdot\nabla)\varphi_k\cdot\xi_k\cdot n_j dS = \left(\omega_e^2 a_{jk} - i\omega_e b_{jk}\right)\xi_k e^{i\omega_e t} \tag{9.29}$$

And the excitation force is given by,

$$F_j = \rho e^{i\omega_e t}\iint_S (i\omega_e + \nabla\Phi\cdot\nabla)(\varphi_0 + \varphi_7)\cdot n_j dS \tag{9.30}$$

As seen the formulations need derivatives of the perturbation potentials. By applying a variant of Stokes' theorem and assuming wall-sidedness of the hull at the mean waterline this part can be rewritten as,

$$\iint_S \nabla\Phi\cdot\nabla\varphi_k\cdot n_j dS = -\iint_S \varphi_k\cdot m_j dS \tag{9.31}$$

Hence the pressure formulation requires only the calculation of potential values and thus the Green function derivates do not have to be evaluated, which saves time.

Having calculated the hydrodynamic coefficients, excitation forces and spring terms the body motions can be solved from the equations of motions,

$$\sum_{k=1}^{6}\left\{-\omega_e^2\left[m_{jk}+a_{jk}\right]+i\omega\left[b_{jk}\right]+\left[c_{jk}\right]\right\}\xi_k = F_j \qquad for\ j=1,\ldots,6 \tag{9.32}$$

With the use of Bernoulli's equation first order pressures for every panel are calculated. By substitution of the potentials into equation (9.28) we can formulate first order complex pressure amplitudes for every panel as,

$$p(\bar{x}) = -i\omega_e\rho\left(\varphi_0+\varphi_7+\sum_{j=1}^{6}\xi_j\varphi_j\right)-\rho\nabla\Phi\cdot\nabla\left(\varphi_0+\varphi_7+\sum_{j=1}^{6}\xi_j\varphi_j\right)-\rho g\left(\xi_3+y\xi_4-x\xi_5\right) \tag{9.33}$$

Hull girder internal loads can now be calculated by solving the linearised equations of motion for every hull module. The external forces and moments are the result of the integration of the pressures together with a correction for the gravitational force for surge and sway forces due to the roll and pitch motions. The internal loads are the unknowns in the equations.

Suppressing of irregular frequencies

One disadvantage of the integral equation that forms the basis for the solution of the radiation and diffraction problem is it non-uniqueness for certain frequencies, so-called irregular frequencies. Different authors have studied this problem both for the two and three dimension. A practical approach was proposed by Wood (1962) for the two dimensional case. By applying a lid on the free surface in the vessel a closed surface was obtained for internal flow problem thereby forcing a unique solution for the source strengths. The justification of the method by Wood (1962) was given by Ohmatsu (1975) using Green's theorem. The validity was proved by numerical calculations. Huijsmans (1996) applied this method in three dimensions for zero speed and presented a comparison study. Both the method with and without free surface panels was used and the number of panels was varied both on the hull and the free surface. In general the lid method is an effective technique to remove most of the irregular frequency phenomena. The differences between original calculations and lid calculations are small, so the main disadvantage of the technique is the increased computational costs.

The basic idea of the lid method is to close the hull by adding fixed free surface panels in the hull. With a suitable boundary condition, $\frac{\partial\varphi_i(\bar{p})}{\partial n}=0$, for the interior flow a unique solution is obtained. The boundary integral equation becomes thus for a point p on the hull surface,

$$\frac{\partial \varphi_o(\bar{p})}{\partial n} = \frac{1}{2}\sigma_j(\bar{p}) + \frac{1}{4\pi}\iint_S \sigma_j(\bar{x})\frac{\partial G(\bar{x},\bar{p})}{\partial n}dS + \frac{1}{4\pi}\iint_{Sf}\sigma_j(\bar{x})\frac{\partial G(\bar{x},\bar{p})}{\partial n}dS + \frac{U^2}{4\pi g}\int_\Gamma \sigma_j(\bar{x})\frac{\partial G(\bar{x},\bar{p})}{\partial n}n_1(\bar{p})d\Gamma \tag{9.34}$$

and for a point p on the free surface,

$$\frac{\partial \varphi_i(\bar{p})}{\partial n} = \sigma_j(\bar{p}) + \frac{1}{4\pi}\iint_S \sigma_j(\bar{x})\frac{\partial G(\bar{x},\bar{p})}{\partial n}dS + \frac{1}{4\pi}\iint_S \sigma_j(\bar{x})\frac{\partial G(\bar{x},\bar{p})}{\partial n}dS + \frac{U^2}{4\pi g}\int_\Gamma \sigma_j(\bar{x})\frac{\partial G(\bar{x},\bar{p})}{\partial n}n_1(\bar{p})d\Gamma \tag{9.35}$$

Here φ_o is the potential for the outer domain and φ_i is the potential for the inner domain, inside the hull, and Sf is the free surface inside the hull.

This method has been implemented in the ship motion program and below two plots of the diagonal heave and pitch damping are shown. This calculation is for the frigate as described in paragraph 6.2 sailing in head waves at 15 knots. The number of panels on a half ship was 462 while the number of panels on the lid was 216. These plots show clearly that the lid method returns more smooth curves, which is of special importance when calculating the impulse response function as described in the next section.

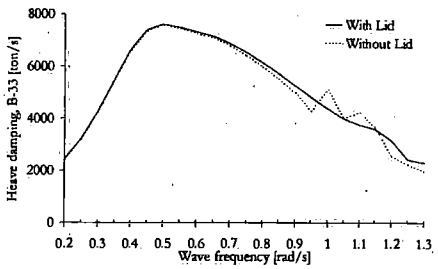

Figure 180 Heave added mass, Fn=0.20

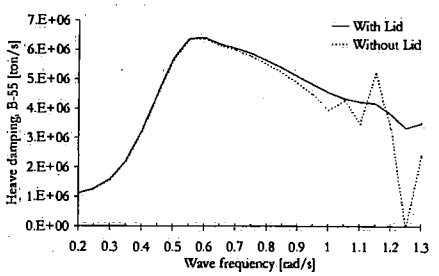

Figure 181 Heave damping, Fn=0.20

B.3 Nonlinear simulation of motions and loads

A first step towards the nonlinear simulation of ship motions and loads is possible by calculating the nonlinear Froude-Krylov force, nonlinear hydrostatics and solving the body motions in an Eulerian frame. The radiation and diffraction forces are still simulated linearly. The simulation program used in this study is called *SIMMOLO* and

was developed by Adegeest (1995). The program requires linear diffraction forces as frequency domain transfer functions while the radiation forces are to be prescribed as impulse response functions.

Following the formulations by Cummins (1962) and Ogilvie (1964) the radiation forces can be written in the time domain as,

$$F_{jk}(t) = -\mu_{jk}\ddot{\xi}_k(t) - \lambda_{jk}\dot{\xi}_k(t) - \gamma_{jk}\xi_k(t) - \int_0^t K_{jk}(t-\tau)\dot{\xi}_k(\tau)\,d\tau \tag{9.36}$$

The third term acts as a modification of the hydrostatic restoring force. As the steady wave potential is not solved for and thus neglected this term is omitted. The first and second term are the added mass and damping values for $\omega \to \infty$. The hydrodynamic coefficients are calculated by *Delspeed*. The tail of the added mass and damping curves are calculated for large frequencies. If numerical errors occur the tail can be extrapolated using an exponential function. This approach is used to estimate the damping term, λ_{jk}. Next the impulse response function is calculated by,

$$K_{jk}(t) = \frac{2}{\pi}\int_0^\infty \left(B_{jk}(\omega_e) - \lambda_{jk}\right)\cos(\omega_e t)\,d\omega_e \tag{9.37}$$

With this impulse response function the added mass can be calculated using,

$$A_{jk}(\omega) - \mu_{jk} = -\frac{1}{\omega}\int_0^\infty K_{jk}(\tau)\sin(\omega_e\tau)\,d\tau \tag{9.38}$$

By conducting this integration for a number of frequencies several estimates of the added mass term μ_{jk} are obtained, which are averaged.

The diffraction forces are calculated by *Delspeed* as a frequency domain transfer function. By interpolation the transfer function values are obtained and thus the diffraction force in the time domain is,

$$F_{7k}(t) = \sum_{j=1}^{N}\left|H_{7k}(\omega_{e,j})\right| \cdot \zeta_{a,j}\cos\left(\omega_e t + \varepsilon_{\zeta j} + \varepsilon_{7k}\right) \tag{9.39}$$

The Froude-Krylov force is calculated by integrating the undisturbed wave pressure over the instantaneous wetted hull. If a point on the hull is wet or dry is defined by the instantaneous orientation and position of the hull and the undisturbed incident wave elevation. If a point is wet and below the still water surface the pressure is calculated by

applying linear wave theory. With reference to an earth-fixed reference frame with origin in the still water surface the pressure is given by,

$$p(\bar{x}_0,t) = -\rho g z_0 + \rho g \sum_{j=1}^{N} \zeta_{a,j} e^{k_j z_0} \cos\left(\omega t + \varepsilon_{\zeta,j} + k_j\left(x_0 \cos\mu + y_0 \sin\mu\right)\right) \qquad (9.40)$$

If a point is wet and above the still water surface the pressure is modelled hydrostatically,

$$p(\bar{x}_0,t) = \rho g\left(\zeta(\bar{x}_0,t) - z_0\right) \qquad (9.41)$$

These hydromechanic forces and the gravitational force are all formulated in the body-fixed reference frame and used to solve the body motions. The governing equations for the motions are,

$$\begin{aligned} m\dot{\bar{v}} + \bar{\omega} \times m\bar{v} &= \bar{F} \\ I\dot{\bar{\omega}} + \bar{\omega} \times I\omega &= \bar{M} \end{aligned} \qquad (9.42)$$

In this equation $\bar{v} = (u,v,w)^T$ is the translation and $\bar{\omega} = (p,q,r)^T$ the rotational velocity vector of the centre of gravity. Structural loads are calculated by assuming a rigid hull and solving thus the connection forces and moments. The equations for a hull module defined in it's local co-ordinate system are,

$$\begin{aligned} \left[m\dot{\bar{v}} + \bar{\omega} \times m\bar{v}\right]_{\text{module j}} &= \bar{F}_j + \bar{Q}_{j-1} - \bar{Q}_j \\ \left[I\dot{\bar{\omega}} + \bar{\omega} \times I\omega\right]_{\text{module j}} &= \bar{M}_j + B_{j-1} - B_j - \bar{Q}_{j-1} \times \bar{r}_{j-1} + \bar{Q}_j \times \bar{r}_j \end{aligned} \qquad (9.43)$$

In this equation the connection forces and moments are given by $\bar{Q}$ and $\bar{B}$. The vectors $\bar{r}$ define the points where the connecting forces are calculated with reference to the local centres of gravity of every module. For the most aft and most forward module the connection forces and bending moments are zero and hence solutions for the connection forces and moments between the modules can be found.

B.4 Comparison of calculations with experiments

Calculations with the ship motion programs were carried out to study the accuracy of the mathematical model. In paragraph 6.3.1 some results were already shown, but here different hullforms are assessed and different mathematical formulations in the program are evaluated.

Wigley-I

The first hull discussed here is a Wigley. The main particulars are described in the following table.

Name	Symbol	Value (full scale)
Length between perpendiculars	L_{pp}	3.00 [m]
Beam on waterline	B_{wl}	0.30 [m]
Draft	T	0.1875 [m]
Displacement	∇	9.46E-2 [m^3]
Pitch radius of inertia	k_{yy}	0.75 [m]
KG	KG	0.170 [m]

Table 10 Main particulars of the MO-2015 frigate

The model has been tested at the Delft Ship Hydromechanics Laboratory, see Journée (1992). Oscillation, excitation and free running model experiments were conducted. The hydrodynamic coefficients, excitation forces and the heave and pitch motion are given in Figure 180 to Figure 195. The panel model has 400 panels per half ship, 40 in length and 10 in height. Four different calculation schemes of the linear program have been used:

- Direct
  The potential derivatives in the pressure formulations are calculated using Green function derivatives. The base-flow is the undisturbed incoming flow and the simplified m-terms are used.
- Direct & double-body
  The potential derivatives in the pressure formulations are calculated using Green function derivatives. The base-flow is the double-body flow and the complete m-terms are used.
- Stokes
  The potential derivatives, as used in the pressure formulations, are eliminated using Stokes' theorem. The base-flow is the undisturbed incoming flow and the simplified m-terms are used.
- Stokes & double-body
  The potential derivatives, as used in the pressure formulations, are eliminated using Stokes' theorem. The base-flow is the double-body flow and the complete m-terms are used. If these are correctly calculated and the hull is wall-sided this calculation scheme should be equal to the direct formulation with a double-body base flow.

In addition to these four curves strip theory results are presented as well. This program is based on the ordinary strip theory, see Journée (2001).

When studying the prediction of the hydrodynamic coefficients we see besides significant differences also different shape predictions. The differences between the calculations with and without a double-body calculation are small except for the Direct calculation. The Wigley is wall-sided and the *m*-terms have been correctly calculated as both calculation schemes with the double-body pre-calculation are equal. We can conclude from these curves that the double-body calculations do not consistently offer better accuracy compared with the calculations using the undisturbed incoming flow and simplified *m*-terms. To increase the reliability of the modeltest data-set and the linear approach Journée (2001) showed that the measured coefficients and excitation forces for this Wigley and this speed give equal motions as were measured during the free running tests in waves. Therefore the discrepancies between predicted pitch motions and measured values can be attributed to the numerical methods.

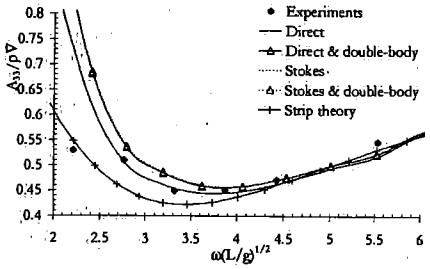

Figure 182 Heave added mass

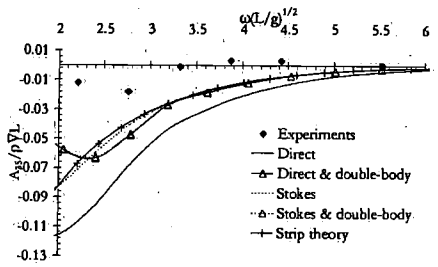

Figure 184 Pitch to heave added mass

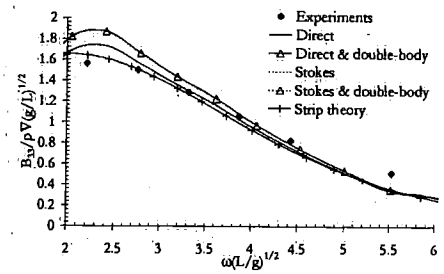

Figure 183 Heave damping

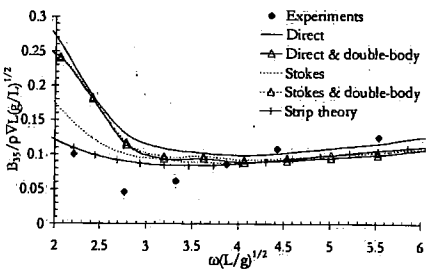

Figure 185 Pitch to heave damping

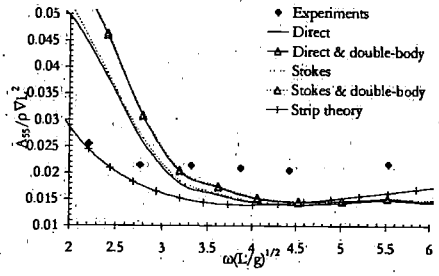

Figure 186 Pitch added mass

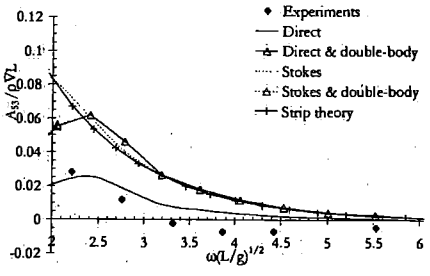

Figure 188 Heave to pitch added mass

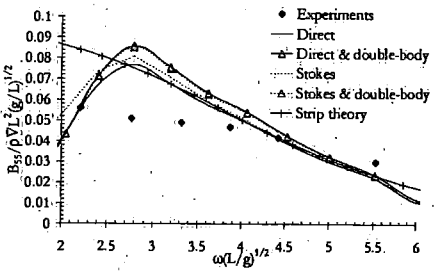

Figure 187 Pitch damping

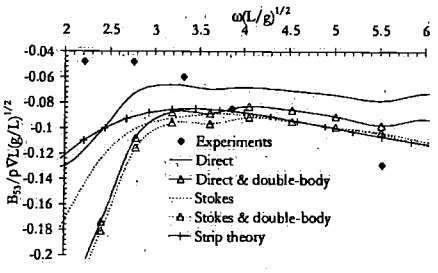

Figure 189 Heave to pitch damping

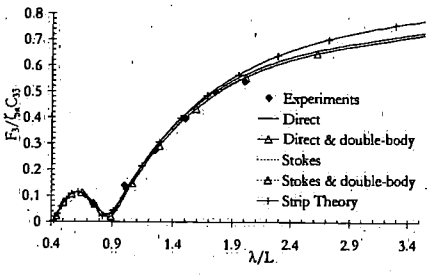

Figure 190 Heave excitation

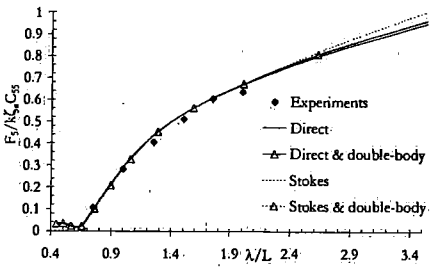

Figure 191 Pitch excitation

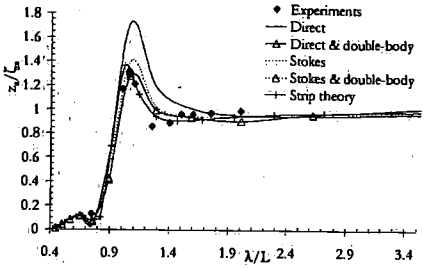

Figure 192 Heave motion

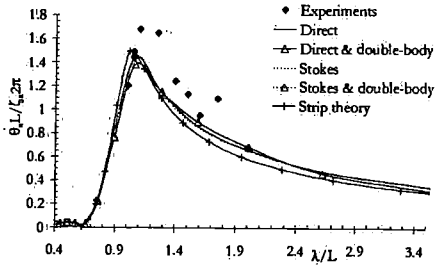

Figure 194 Pitch motion

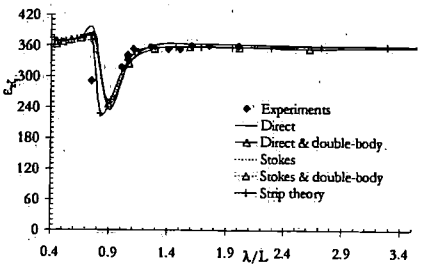

Figure 193 Heave phase

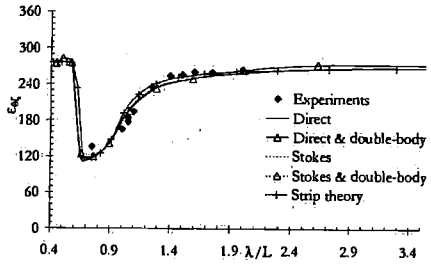

Figure 195 Pitch phase

MO-2015 frigate

In paragraph 6.3.1 calculation results were shown for the MO-2015 frigate. In addition to these the four calculation schemes as used for the Wigley are applied for this vessel as well. The following figures show the results for the 12 knots case, which corresponds to a Froude number of 0.18. Overall we can conclude that the differences between the Stokes formulations and the Direct formulations are small except for the shear force where both Stokes formulations give different results and differ also considerably from the Direct formulations.

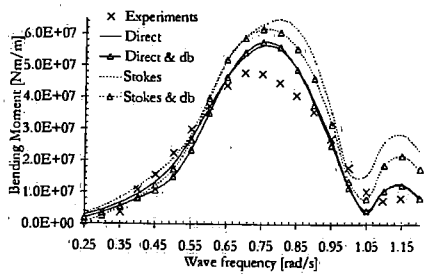

Figure 196 Vertical bending moment

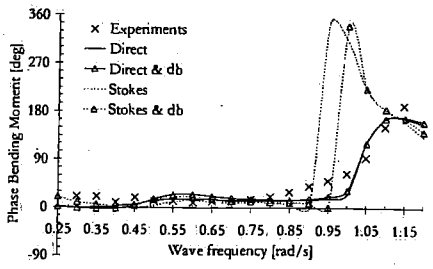

Figure 197 Vertical bending moment phase

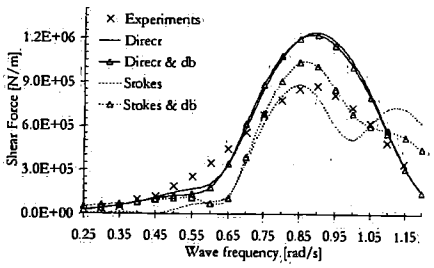

Figure 198 Shear force

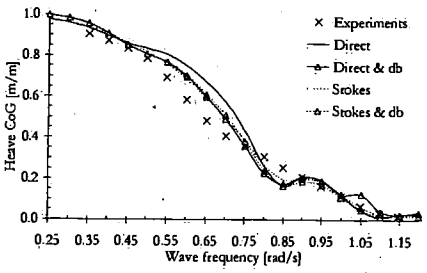

Figure 202 Heave motion

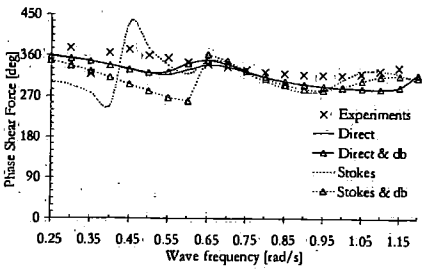

Figure 199 Shear force phase

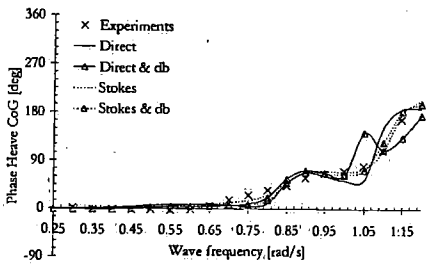

Figure 203 Heave phase

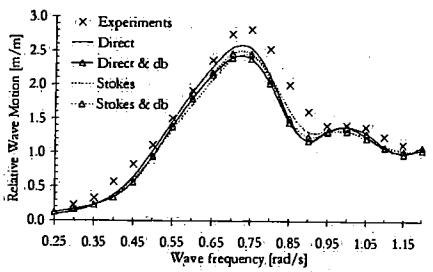

Figure 200 Relative wave motion

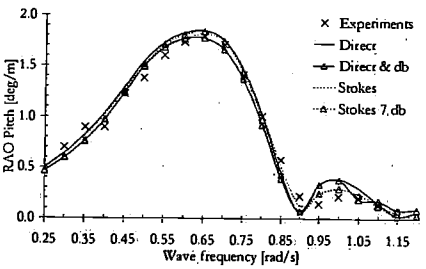

Figure 204 Pitch motion

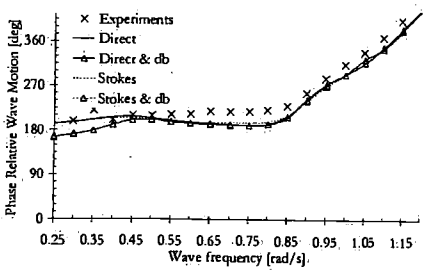

Figure 201 Relative wave motion phase

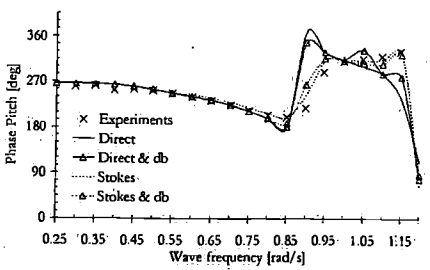

Figure 205 Pitch phase

COFEA hullform

A joint research project between the Royal Netherlands Navy and the MARIN was conducted to study advanced monohull concepts. Part of this research was published by Kapsenberg and Brouwer (1998). One advanced concept was tested and the results showed the shortcomings of linear prediction tools. This hullform was named COFEA, which stands for 'Coefficient Of Floatation Extreme Aft'. The particulars of the vessel are listed in the table while the bodyplan is shown in the subsequent figure. Due to the large bulbous bow and wide aft-body the LCB-LCF separation is large, which influences the heave-pitch coupling strongly. The objective was to minimise the vertical motions over the ship length despite a possible increase in the midship region. As the experiments showed significant nonlinear behaviour even in moderate seas states. An attempt is made to predict the behaviour using the nonlinear Froude-Krylov program as this program gave good results for the MO-2015 frigate experiments. Figure 207 and Figure 208 show the normalised heave and pitch response respectively. Different wave amplitudes were simulated with the program giving significantly different results. The heave resonance shifts for the simulations in larger waves, which fits better with the experiments. But the absolute values are much larger than the experimental values. Possibly nonlinear damping could cause this discrepancy. Therefore a linear calculation was conducted with and increased draft, 1.2 [m]., with equal mass and inertia as the original configuration. This calculation confirms the resonance shift and also shows a considerable positive effect of the increased draft. The measured sinkage and trim of the vessel were very small and can thus not have an effect on the nonlinear behaviour.

Thus the conclusion is that the nonlinear Froude-Krylov program is not appropriate to simulate the motions of this advanced vessel with strong 3 dimensional shapes both in length and vertical direction.

Name	Symbol	Value (full scale)
Length between perpendiculars	L_{pp}	120.00 [m]
Beam on waterline	B_{wl}	18.26 [m]
Draft	T	4.60 [m]
Displacement	∇	4139 [m^3]
Pitch radius of inertia	k_{yy}	30.0 [m]
KG	KG	8.12 [m]

Table 11 Main particulars of the MO-2015 frigate

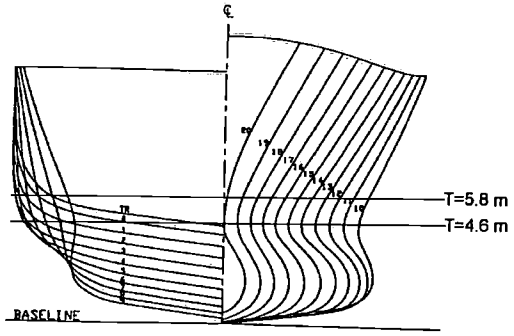

Figure 206 Bodyplan COFEA hullform

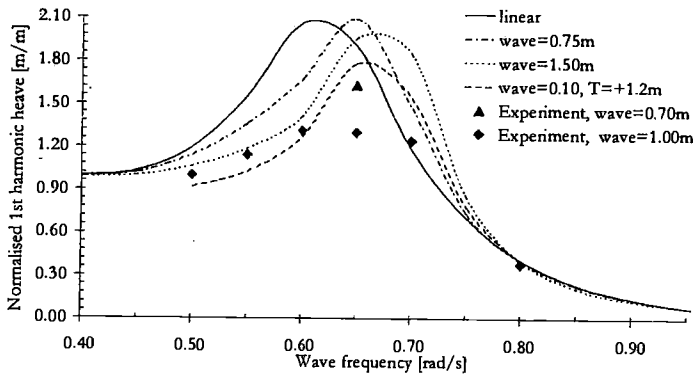

Figure 207 Normalise heave motion

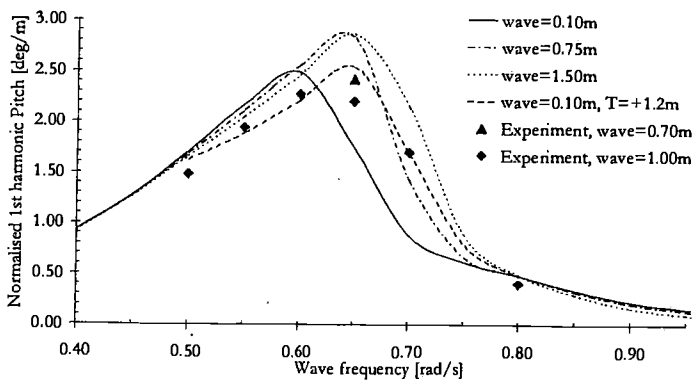

Figure 208 Normalised pitch motion

B.5 Conclusions and discussion

From the calculations in paragraph 6.3 and this appendix some general conclusions can be drawn on the performance of the three programs, i.e. the double-body program, the linear and the nonlinear program.

The accuracy of motion and load predictions by the linear program is satisfactory for conventional hullforms like the MO-2015 frigate and the Wigley. It was thought that a double-body pre-process calculation could give improved results despite the fulfilment of the zero-forward speed free surface condition. But the results show that it offers only little improvement. The zero-forward speed free surface boundary condition should therefore preferably be replaced by a consistent linearised forward speed condition. This implies the use of a free surface Rankine program instead of a free surface Green function. Several authors have shown that this approach gives improved results over strip theory, see for instance Nakos (1990) and Van 't Veer (1998). The benefit of the present approach is that it is straight forward applicable for all headings and only the hull needs to be distributed with panels. Moreover a free surface Rankine program requires special care of the open-boundaries and in case of the critical speed, $\frac{U\omega_e}{g} = \frac{1}{4}$.

The nonlinear program takes account of the nonlinear Froude-Krylov force, nonlinear hydrostatic force and the equations of motion are solved in an Eulerian frame. For the MO-2015 frigate these nonlinearities show to be sufficient as the nonlinear bending moments are well predicted. Differences occur when large amounts of green water are present. But the calculations for the COFEA hull prove that the program is not capable to assess this hullform although it gives improvements over a linear approach. Perhaps nonlinear damping causes the discrepancies. A full nonlinear potential model could give better results but is yet not practically feasible. In order to retain a practical nonlinear simulation approach a 2D strip theory approach can be used, where different hydrodynamic coefficients are used depending on the position, velocity and acceleration with reference to the wave. See for instance Schlachter (1989). A difficulty arises because it is not known a priori which frequency dependent hydrodynamic coefficient should be used. A solution for this was presented by Söding (1982). He has formulated, based on the relative motion principle, an approach to replace the added mass and damping by frequency independent coefficients.

C Derivations for nonlinear Volterra modelling

Several formulations are given, which are used for the Volterra modelling technique as described in chapter 1.

C.1 Spectral density function

Consider the stationary ergodic random process $x(t)$, for which the Fourier pair is defined as,

$$X(\omega)=\int_{-\infty}^{\infty} x(t)e^{-i\omega t}dt \qquad x(t)=\frac{1}{2\pi}\int_{-\infty}^{\infty} X(\omega)e^{i\omega t}d\omega \tag{10.1}$$

Consider now the integral to calculate the mean square value of the realisation over a range $2T$,

$$\overline{x^2(t)}=\lim_{T\to\infty}\frac{1}{T}\int_{-\infty}^{\infty} x(t)\left\{\frac{1}{2\pi}\int_{-\infty}^{\infty} X(\omega)e^{i\omega t}d\omega\right\}dt \tag{10.2}$$

By reversing the integrations we get,

$$\overline{x^2(t)}=\int_{-\infty}^{\infty}\lim_{T\to\infty}\frac{1}{2T}\left|X(\omega)\right|^2 d\omega=\int_{-\infty}^{\infty} G(\omega)d\omega \tag{10.3}$$

Here $G(\omega)$ is the two-sided spectral density function. In ocean engineering it is more common to use the one-sided energy spectrum, which is simply formulated as,

$$S_{xx}(\omega)=2\cdot G_{xx}(\omega) \tag{10.4}$$

And in discrete notation for an ocean wave spectrum this is formulated as,

$$S_{\zeta\zeta}(\omega)\Delta\omega = \frac{1}{\pi T}\left|X(\omega)\right|^2 \Delta\omega = \frac{1}{\pi T}\left|X(\omega)\right|^2 \frac{2\pi}{T} = \frac{2}{T^2}\left|X(\omega)\right|^2 = \frac{1}{2}\zeta_a^2 \qquad (10.5)$$

Since,

$$X(\omega_0) = \int_{-T/2}^{T/2} (\zeta_a \cos\omega_0 t) e^{-i\omega t} dt = \zeta_a \int_{-T/2}^{T/2} \cos^2\omega_0 t - i\cos(\omega_0 t)\sin(\omega_0 t)\, dt = \frac{1}{2} T\zeta_a \qquad (10.6)$$

Although the definition of spectral density is quite simple their accurate derivation requires careful attention. For the determination of auto- or cross-spectral densities Welch's averaged periodogram method is used in this thesis. This method divides a record into overlapping sections. Every section is windowed by a Hanning window and the spectral density is determined. By averaging all these densities the resulting spectral density is obtained. By keeping the window size as large as possible spectral peaks are preserved. But the smaller the window size the smoother the spectrum becomes. Hence there's a trade-off between peak identification and leakage.

C.2 Wiener-Khintchine theorem

The autocorrelation function is defined as follows and the Fourier transform is taken,

$$R_{xx}(\tau) = \frac{1}{T}\int_{-\infty}^{\infty} x(t)x(t-\tau)\,dt = \frac{1}{T}\int_{-\infty}^{\infty} x(t-\tau)\frac{1}{2\pi}\int_{-\infty}^{\infty} X(\omega)e^{i\omega t}\,d\omega\,dt \qquad (10.7)$$

By changing the integrations we get,

$$\begin{aligned} R_{xx}(\tau) &= \frac{1}{2\pi T}\int_{-\infty}^{\infty} X(\omega)\int_{-\infty}^{\infty} x(t-\tau)e^{i\omega(t-\tau)}e^{i\omega\tau}\,dt\,d\omega \\ &= \frac{1}{2\pi T}\int_{-\infty}^{\infty} X(\omega)X^*(\omega)e^{i\omega\tau}\,d\omega = \int_{-\infty}^{\infty} G_{xx}(\omega)e^{i\omega\tau}\,d\omega = \int_0^{\infty} S_{xx}(\omega)\cos\omega\tau\,d\omega \end{aligned} \qquad (10.8)$$

Inversely this results in,

$$S_{xx}(\omega) = \frac{2}{\pi}\int_{-\infty}^{\infty} R_{xx}(\tau)\cos\omega\tau\,d\tau \qquad (10.9)$$

C.3 Zero-memory squarer and cuber

Consider a zero-memory squarer operating on input $x(t)$ with output $y(t)$. The input is written as,

$$x(t)=\int_{-\infty}^{\infty}\delta(\tau_1)x(t-\tau_1)d\tau_1 \tag{10.10}$$

The output is then written as,

$$y(t)=x^2(t)=\int_{-\infty}^{\infty}\int_{-\infty}^{\infty}\delta(\tau_1)\delta(\tau_2)x(t-\tau_1)x(t-\tau_2)d\tau_1 d\tau_2 \tag{10.11}$$

Thus if we formulate the input output relation of the squarer as a second order Volterra model,

$$y(t)=\int_{-\infty}^{\infty}\int_{-\infty}^{\infty}h(\tau_1,\tau_2)x(t-\tau_1)x(t-\tau_2)d\tau_1 d\tau_2 \tag{10.12}$$

we see that the time domain second order transfer function $h_2(\tau_1,\tau_2)=\delta(\tau_1)\delta(\tau_2)$, which only exists for $\tau_1=\tau_2=0$. Therefore the frequency domain transfer function is,

$$H_2(\omega_1,\omega_2)=\int_{-\infty}^{\infty}\int_{-\infty}^{\infty}\delta(t_1)\delta(t_2)e^{-i(\omega_1 t_1+\omega_2 t_2)}dt_1 dt_2=1 \tag{10.13}$$

And the Fourier transform of the output is,

$$Y(\omega)=\frac{1}{2\pi}\int_{-\infty}^{\infty}X(\omega_1)X(\omega-\omega_1)d\omega_1 \tag{10.14}$$

The same derivation can of course be followed for a cuber and leads to,

$$Y(\omega)=\frac{1}{4\pi^2}\int_{-\infty}^{\infty}\int_{-\infty}^{\infty}X(\omega_1)X(\omega_2-\omega_1)X(\omega-\omega_2)d\omega_1 d\omega_2 \tag{10.15}$$

D Videos and photos of model experiments

The enclosed CD contains a small selection of videos of the conditioned experiments, corresponding with Figure 140 to Figure 148, and a recording of an irregular experiment. The photos give an overview of the model and the measurement lay-out.

Samenvatting

Het gedrag van schepen in golven is een belangrijk onderwerp daar de bewegingen en belastingen een sterke invloed hebben op de veiligheid, economische aspecten en de operationele prestatie van een schip. Door schepen met nieuwe rompvormen, hogere vaarsnelheden en offshore constructies die in diep water en ruige zeecondities geexploiteerd worden zijn verbeterde analyses voor zeegang en golfbelastingen meer en meer noodzakelijk. Een toenemend belang van veiligheid en betrouwbaarheid geeft bovendien dat niet alleen een nauwkeuriger predictie van de bewegingen en belastingen noodzakelijk is maar ook de voorspelling van de respons statistiek en de beoordeling daarvan. Alleen dan, kunnen uitspraken gedaan worden over onderwerpen als veiligheid, risico en prestatie betrouwbaarheid. Hoewel in de afgelopen tijd niet-lineaire scheepshydrodynamische programma's ontwikkeld zijn, voor een nauwkeuriger predictie van scheepsresponsies, is de praktische toepassing daarvan nog steeds een lastige taak. Lineaire predictie methoden hebben het grote voordeel van eenvoudige beoordelingstechnieken zoals het frequentiedomein en spectral-analytische methoden. Niet-lineaire tijdsdomein programma's zijn tijdrovend en hebben geen snelle, direct toepasbare beoordelingsmethoden. Desondanks is de noodzaak voor niet-lineaire beoordelingsmethoden onvermijdelijk omdat lineaire technieken niet betrouwbaar zijn wanneer het geavanceerde schepen, hoge vaarsnelheden en ruige omstandigheden betreft. Deze studie richt zich daarom op de ontwikkeling van precitie en met name beoordelingsmethoden voor niet-lineaire scheepsbewegingen en belastingen.

De conditionering van extreme responsies is bestudeerd als een praktische techniek om niet-lineaire extreme responsies efficiënt te berekenen. Met de aanname dat een lineair model adequaat is om extreme gebeurtenissen te identificeren kan een onregelmatige inkomend golfveld zo geconditioneerd worden dat een voorgeschreven lineaire extreme respons optreedt op een voorgeschreven tijdstip en met een voorgeschreven respons profiel. Dit profiel is het zogenaamde 'meest-waarschijnlijke respons profiel' rond grote respons amplitudes. Vervolgens wordt deze korte, geconditioneerde inkomende golf in een niet-lineair programma gesimuleerd en de corresponderende niet-lineaire extreme wordt aldus verkregen. Verschillende mathematische modellen om dit meest-waarschijnlijke profiel te voorspellen zijn geëvalueerd. Twee modellen nemen de

systematische associatie tussen amplitudes en periodes in rekening, maar er is aangetoond dat een derde, meest simpel, model het beste resultaat gaf voor grote amplitudes. Een belangrijke extensie van de respons conditioneringstechniek is ontwikkeld om de amplitude of extreme kansverdeling te berekenen. Door een korte serie van conditionerings simulaties te doen voor verschillende lineaire extremen wordt een functioneel verband verkregen tussen lineaire en niet-lineaire responsies. Deze relatie wordt gebruikt om de lineaire amplitude of extreme kansverdeling te transformeren naar de niet-lineaire distributie. Dit betekent een enorme tijdwinst met name als de extreme kansverdeling berekend wordt. Verder is een formulering opgesteld om de tijdconditioneringstechniek toe te passen in een kortkammig golfveld.

Een tweede techniek, die bestudeerd is, is de modellering van niet-lineaire scheepsresponsies door een niet-lineair benaderend Volterra modellen. Door dit te doen is een niet-lineair scheepbewegingenprogramma enkel en alleen nodig om de Volterra overdrachtsfuncties te bepalen, waarna het Volterra model gebruikt kan worden om respons statistiek te generen in een willekeurige zeetoestand. De basis van de twee niet-lineaire benaderende Volterra modellen is de vervanging van de hogere orde overdrachtsfuncties door geheugen-vrije operatoren en een lineaire overdrachtsfunctie. Daardoor wordt een deel van het niet-lineaire gedrag weg gelaten, maar eenvoudige identificatie en simulatie procedures worden verkregen. Een validatie van de identificatie en simulatie van beide modellen laat goede resultaten zien.

De integratie van de respons conditioneringstechniek en de Volterra modellering in een lange-termijn analyse voor de berekening van extreme responsies en voor zeegangsinzetbaarheidstudies is gepresenteerd. Bovendien is een nieuwe zeegangsinzetbaarheidsmethode ontwikkeld. Deze methode, gebaseerd op een betrouwbaarheidsaanpak, bestaat uit een missie simulatie methode met een probabilistische modellering van de respons criteria. Door een gespecificeerde missie een groot aantal malen te simuleren kan de zeegangsinzetbaarheid van alle responsies en hun gecombineerde resultaat verkregen worden in de vorm van een kansverdeling. Dit geeft de mogelijkheid om de onzekerheid in zeegangsinzetbaarheid te bestuderen en om een betrouwbaarheidsinterval te specificeren voor de missie zeegangsinzetbaarheid. Tevens worden gevoeligheidsfactoren en correlatie coefficiënten verkregen. De gevoeligheidsfactoren beschrijven de invloed van alle individuele responsies op de totale inzetbaarheid variantie, terwijl de correlatie coefficiënten een quantificering geven van de inzetbaarheid degradatie correlatie tussen onderlinge responsies.

Verschillende numerieke studies zijn verricht voor verschillende schepen en deze bewijzen dat de respons conditioneringstechniek een nauwkeurige techniek is die grote winst geeft in rekentijd. De Volterra modellering is ook een erg snelle rekentechniek maar is niet zo nauwkeurig. Toch biedt deze techniek veelbelovende mogelijkheden wanneer deze wordt toegepast in de zeegangsinzetbaarheidsstudies gebaseerd op een betrouwbaarheidsaanpak. Deze nieuwe zeegangsinzetbaarheidsmethode is een krachtige techniek als ondersteuning van het ontwerpproces en de exploitatie van schepen daar het

meer informatie verschaft over de zeegangsinzetbaarheid en de respons relaties in vergelijking tot bestaande technieken.

Modelproeven zijn uitgevoerd met een gedeeld fregat om de respons conditioneringstechniek uitgebreider te onderzoeken. De geconditioneerde inkomende golven konden goed gegenereerd worden en de synchronisatie van het veranderende golfprofiel met het varende model kon uitstekend afgestemd worden met een regelprogramma voor de sleepwagen. Een serie van geconditioneerde proeven in zware condities met veel groen water zijn uitgevoerd en hiermee kon de amplitude distributie van de doorbuigende rompmomenten erg goed voorspeld worden. Een vergelijking met bestaande technieken laat zien dat de extrapolatie van een geschatte mathematische functie een kritische aanpak is daar de staart van de respons kansverdeling foutief voorspeld kan worden. Het is juist deze staart die van groot belang is wanneer het op veiligheid en betrouwbaarheid aankomt. Het grote voordeel van de respons conditioneringstechniek is dat de methode het gedrag van het schip in die extreme condities, welke de staart opbouwen, expliciet berekend of beproefd.

Curriculum Vitae

De auteur werd geboren in 1973 te Assen, alwaar hij ook zijn jeugd doorbracht. In 1991 behaalde hij aan het Christelijk Scholengemeenschap Assen het VWO diploma. Direct hierna is de schrijver begonnen aan de studie Maritieme Techniek aan de Technische Universiteit Delft. Hij behaalde het Scheepsbouwkundig Ingenieursdiploma in 1997 met het predikaat 'lof'. Dit afstudeerwerk betrof de berekening van hydrodynamische belastingen op een FPSO-tanker voor vermoeiingsanalyses. Voor dit afstudeerwerk werd de Afstudeerprijs van het Universiteitsfonds Delft in ontvangst genomen. Na zijn studie is de schrijver in dienst getreden bij de Technische Universiteit Delft waar hij vier jaar als promovendus op het vakgebied Scheepshydromechanica werkzaam was. Per januari 2002 werkt de schrijver als consulent hydromechanica bij Det Norske Veritas in Oslo.

Acknowledgement

In the past four years that I worked at the Ship Hydromechanics Laboratory my enthusiasm for the field has only increased. With great pleasure I look back at this period and would like to thank all my colleagues for their contribution to a good atmosphere, their interest and their support for my research and especially for the experiments. I want to express my gratitude to Jo Pinkster and Lex Keuning, promotor and co-promotor, who gave me the freedom and the support to carry out this research.

Thanks to the financial support of the Royal Netherlands Navy I was able to conduct four years of research and I am very grateful for that. Especially I want to thank the department Bureau Militaire Maritieme Technologie for their support and for their help when I studied at their offices in the first period of the Ph.D. study.

The Maritime Research Institute Netherlands was also involved in this research. A number of people have assisted me during the years. Their interest and assistance is very much appreciated.

In addition I would like to thank Bluewater Engineering for providing necessary information regarding the case-study of the FPSO in chapter 5.

Furthermore I am grateful to Det Norske Veritas for my guest period there during the summer of 2000 and for their support for the model experiments. In particular I'd like to thank Leon Adegeest very much for his help. I enjoyed my time at Det Norske Veritas very much and I am looking forward to a new working period in Oslo.

The interest for the field was 'boosted' during a student trainee period at Bluewater Engineering, where Max Krekel and Mirek Kaminski gave me not only the self confidence and interest for naval architecture but also the interest for research and the application of it. This trainee period has been of great influence on my career and on my choice to start a Ph.D. study after graduation. These two colleagues should therefore not be neglected in a word of thanks in this Ph.D. thesis.

The front cover was created by Wilbert Blom, for which I am grateful as well as for his assistance with modifying the video recordings of the experiments.

Furthermore I'd like to thank all my friends, inside and from outside the university, who gave me pleasure and distraction during the past years.

Of course I'd like to thank my father, mother and brother for their love and support during my years in Delft. Since long they have observed that it were ships, that fascinated me. When reading chapter 6, I hope they look back with pleasure on my first 'modelexperiments' with a self-made frigate in 1986.

Well above all the pleasure and joy of the naval architectural and shiphydrodynamics discipline are two people. Thank you very much, Véronique, for all the love, comfort, care and pleasure! The last month working on this thesis were the best, not because the end was near, but becoming father of a lovely son: Pelle!

Wouter Pastoor
Delft, november 2001

Stellingen

behorend bij het proefschrift

"On the Assessment of Nonlinear Ship Motions and Loads"

door

Louis Willem Pastoor

1. Slechts het berekenen van een enkele, meest waarschijnlijke extreme scheepsrespons, is niet voldoende voor het veilig ontwerpen van een zeegaande constructie, want niets kan gezegd worden over de kans dat een grotere responsie zal optreden en dus de kans op falen.

2. De veiligheid en betrouwbaarheid van zeegaande constructies vragen om een integrale probabilistische aanpak van scheepshydrodynamica en constructieleer met medeneming van alle relevante kansverdelingen.

3. De extrapolatie van amplitude kansverdelingen om extreme waarden te bepalen op basis van een korte onregelmatige simulatie is geen betrouwbare techniek. Daarom geldt voor de amplitude kansverdeling van hydrodynamische belastingen: 't venijn zit 'em in de staart'.

4. Het ontwikkelen van tijdbesparende reken- en analysetechnieken geeft naast de gewenste tijdbesparing tevens meer inzicht in de onderliggende fysische processen.

5. Zeeganginzetbaarheidstudies moeten een integrale plaats innemen in ontwerpsimulatiestudies.

6. Het heeft geen zin om de maximale belastingen in een scheepsdoorsnede te berekenen wanneer het effect van zowel groen water als slamming wordt verwaarloosd.

7. Hoe meer onzekerheid gemodelleerd wordt hoe groter de nauwkeurigheid van de berekening.

8. De ambitie van de TU Delft om een top-universiteit te zijn die wereldwijd als een uitmuntende onderzoeksuniversiteit te boek staat, getuigt van weinig affectie met de behoefte van de Nederlandse industrie.

9. De beloning en stimulering van excellente studenten op de universiteit is equivalent te omschrijven als het negeren van de grote groep 'gewone' studenten.

10. De nadruk ligt bij de functie hoogleraar vaak meer meer op 'hoog' dan op 'leraar'.

11. Een sportduiker moet beoordeeld worden op zijn duiktechniek en respect voor het onderwaterleven en niet, zoals te vaak gebeurt, op zijn lidmaatschap van een specifieke duikorganisatie.

12. Een promotieonderzoek is een evolutieproces met hopelijk aan het eind een Big Bang.

13. In de praktijk blijkt 'vernieuwingsdrang' maar al te vaak slechts 'veranderingsdrang' en geen 'verbeteringsdrang'.

14. Het is een gelukkige bijkomstigheid dat de benaming "Betuwelijn" ook buitengewoon goed klinkt voor een aantrekkelijke NS-dagtocht.

15. Wanneer wordt gekeken naar het aantal telefonische klachten over geluidsoverlast ten gevolge van Schiphol is het belangrijk de explosieve stijging van het aantal mobiele telefoons mee te nemen in de beoordeling. Tenslotte is een telefoontje, zittend vanuit de tuin, snel gemaakt.

16. Dat extreem-rechts de stelling: "Nederland is vol", identiek blijft propageren, is een duidelijk bewijs van het weinig intelligente vermogen van deze groepering aangezien de Nederlandse bevoling in de afgelopen 15 jaar met meer dan 10% is gegroeid. (Bron: CBS)